IS-T--1441

DE91 000610

Fundamental Investigations of Supported Monometallic and Bimetallic Catalysts by Proton Magnetic Resonance Spectroscopy

by

Wu, Xi

PHD Thesis submitted to Iowa State University

Ames Laboratory, U.S. DOE

Iowa State University

Ames, Iowa 50011

Date Transmitted: September 21, 1990

PREPARED FOR THE U.S. DEPARTMENT OF ENERGY

UNDER CONTRACT NO. W-7405-Eng-82.

DISCLAIMER

Fundamental investigations of supported monometallic and bimetallic catalysts by proton magnetic resonance spectroscopy

Xi Wu

Under the supervision of Dr. Terry S. King
From the Department of Chemical Engineering
Iowa State University

Proton magnetic resonance spectroscopy, or nuclear magnetic resonance (NMR) of hydrogen, has been applied to investigate silica-supported Group VIII monometallic and Group VIII-Group IB bimetallic catalysts and alumina- and silica-supported platinum-rhenium bimetallic catalysts. A number of other techniques such as volumetric chemisorption by hydrogen, thermogravimetric analysis, X-ray fluorescence, and model reaction studies were also used to assist the investigations on these catalysts.

Two adsorbed states of hydrogen, i.e., irreversible and reversible hydrogen, on the surfaces of monometallic Ru, Pt, and Cu particles and bimetallic Ru-Group Ib, Pt-Group Ib, and Pt-Re particles were observed directly via proton NMR. The same amounts of the irreversible hydrogen adsorbed on pure Ru catalysts were measured by both proton NMR and the volumetric technique. This strongly chemisorbed hydrogen was used to

determine the dispersion of Group VIII monometallic catalysts and the overall dispersion of the Ru-Cu and Pt-Cu bimetallic catalysts. A metal-to-metal hydrogen spillover phenomenon was observed on Group VIII-Cu bimetallic catalysts. Also, the weakly adsorbed hydrogen could spill over from the metal surfaces onto the support and exchange with the OH group.

The electronic environments on surfaces of monometallic catalysts are sensitive to changes in metal dispersion, state of adsorbed hydrogen, and residual chlorine. Hydrogen tends to bond more strongly with smaller metal particles containing more defect-like sites but adsorbs more weakly on chlorine-contaminated ruthenium surfaces. Minor perturbations of the valence electrons were inferred on Ru-Cu and Pt-Cu bimetallic systems. Strong electronic interactions between Pt and Re were found in the Pt-Re bimetallic catalysts.

Surface compositions for the Ru-Cu and Pt-Cu bimetallic catalysts were determined by NMR of adsorbed hydrogen. The Group Ib elements segregate strongly to the surfaces of Group VIII metal particles. Copper has the strongest tendency to form bimetallic particles with a Group VIII element among the Group Ib metals. Platinum is miscible with Re in the bulk but selectively segregates to the bimetallic surfaces. The catalytic activity of cyclohexane dehydrogenation was much higher on Pt-Re bimetallic catalysts than on Pt catalysts.

Fundamental investigations of supported monometallic and bimetallic catalysts by proton magnetic resonance spectroscopy

by

Xi Wu

A Dissertation Submitted to the
Graduate Faculty in Partial Fulfillment of the
Requirements for the Degree of
DOCTOR OF PHILOSOPHY
Major: Chemical Engineering

Approved:

_____
In Charge of Major Work

_____
For the Major Department

_____
For the Graduate College

Iowa State University
Ames, Iowa

1990

TABLE OF CONTENTS

SECTION III

SECTION IV

DEDICATION

To my beloved mother and father

GENERAL INTRODUCTION

Supported Bimetallic Catalysts

Highly dispersed supported monometallic and bimetallic catalysts have many applications in industrial chemical processes involving catalytic reactions of hydrocarbons. One example is alumina supported platinum catalysts (Pt/Al_2O_3) and platinum-rhenium ($Pt-Re/Al_2O_3$) bimetallic catalysts. They both have been widely used in the process of catalytic reforming to produce gasoline of high octane number from petroleum naphtha fractions (1, 2). The platinum-rhenium bimetallic catalysts are typically 3 to 4 times more active and much more stable in activity than the platinum catalysts. The reason for the superior performance of the $Pt-Re/Al_2O_3$ bimetallic catalysts over the Pt/Al_2O_3 catalysts is not well understood, neither are the detailed mechanisms in various hydrocarbon reactions occurring on these catalysts. In order to understand the catalytic phenomena, we must be able to investigate these catalysts on a microscopic level.

In general, two types of supported bimetallic catalysts have been investigated. The first type consists of two Group VIII elements, e.g., the Pt-Ir bimetallic catalyst (also a useful reforming catalyst). The second type consists of one Group VIII element and one element from Group IB or other groups of metallic elements (The Ru-Cu bimetallic catalyst is

an example). The two metallic elements in a bimetallic pair may be miscible, partially miscible, or immiscible in the bulk state (3). The first type of bimetallic catalysts is difficult to investigate by conventional techniques such as hydrogen chemisorption and model reaction studies since both elements have similar chemisorptive properties and comparable catalytic properties for certain reactions. In contrast, the second type of bimetallic catalysts is relatively simple to investigate if the non-Group VIII element is inert to adsorbates such as hydrogen or inactive for a certain model reaction. However, exceptions do exist. For example, copper is relatively inactive for ethane hydrogenolysis compared to ruthenium in the Ru-Cu bimetallic catalyst (1, 4). But Cu maintains the activity for cyclohexane dehydrogenation (1) and is capable of adsorbing hydrogen at room temperature (5). In this case, investigations on the Ru-Cu bimetallic catalyst are equally as difficult as those on a bimetallic catalyst belonging to the first type. It is hoped that successful investigations on the simpler, second type of bimetallic system will lead to a much improved understanding of the catalytic phenomena occurring in the first type of bimetallic system.

The bimetallic systems investigated by the author have included only the first type. The work on silica-supported monometallic Ru and Cu and bimetallic Ru-Group Ib (Cu, Ag, or

Au) catalysts is detailed in the first three sections of this dissertation. Section IV reports the work on the effect of chlorine contamination on Ru/SiO_2 and $Ru-Cu/SiO_2$ catalysts. The work on Pt/SiO_2 monometallic catalysts and $Pt-Cu/SiO_2$ and $Pt-Ag/SiO_2$ bimetallic catalysts is reported in detail in Section V. Finally, the work on monometallic Re/SiO_2 and Re/Al_2O_3 catalysts and bimetallic $Pt-Re/SiO_2$ and $Pt-Re/Al_2O_3$ catalysts is detailed in Section VI.

Catalyst Characterization Techniques

Catalyst characterization is the key to fundamental understanding of supported mono- and bimetallic catalysts. The methods of catalyst characterization may be categorized into chemical and physical methods. Chemical methods such as selective hydrogen chemisorption are useful in measuring the total number of active chemisorption sites in bimetallic catalysts but may not be suitable for determining the amount of each individual metallic element. Some physical methods such as X-ray photoelectron spectroscopy (XPS) and extended X-ray absorption fine structure (EXAFS) may provide valuable information such as binding energy and average coordination of metal atoms, but the techniques are usually not sensitive to only the top metal layer. Electron microscopy is one of the most powerful instrumental techniques available today and is capable of providing useful information such as the metal

particle size of supported metal catalysts. But the method is limited by its inability to resolve the two components separately in bimetallic particles. Infrared spectroscopy is widely used to monitor adsorbates such as CO and NO on metal surfaces. However, the technique is not very quantitative and is restricted to those adsorbed species with an electric dipole moment. As one can see, all catalyst characterization techniques have their advantages and restrictions. Detailed descriptions of these techniques for characterization of mono- and bimetallic catalysts can be found elsewhere (1, 6, 7). The application of solid state NMR to heterogeneous catalysis in general is also described (7).

Application of Proton NMR to Supported Metal Catalysts

In recent years, solid state nuclear magnetic resonance (NMR) spectroscopy has emerged as a useful tool in studying adsorption and catalytic phenomena occurring on surfaces of supported metal catalysts. NMR enables us to probe catalysts on an atomic level. In comparison with other spectroscopic techniques, NMR is a relatively low-powered and non-invasive technique that does not perturb the catalyst system being studied. Although NMR by itself is not a surface technique, it can be made to probe the surface effectively when combined with other methods such as adsorption. NMR can be applied to study either catalyst particles directly by doing experiments

on an NMR active element (e.g., ^{195}Pt) or indirectly by doing experiments on an adsorbate bound to the surfaces of metal particles. The latter is exclusively a surface technique provided that the adsorbate does not penetrate into the metal particles. The latter technique is of particular interest since it has the potential in elucidating the fundamental catalytic processes taking place on surfaces of catalyst particles.

The author does not intend to repeat the basic concepts and principles of solid state NMR in this dissertation. They have been described in great detail in a number of textbooks (8, 9). Also, the application of NMR in the investigation of small molecules adsorbed on metal surfaces has recently been reviewed (10, 11). However, since this dissertation deals with application of proton magnetic resonance (PMR), or NMR of adsorbed hydrogen, the author would like to mention the advantages and disadvantages of the technique as it is applied to supported metal catalysts. In addition, some methods for improving the technique will be discussed.

A proton has the second highest sensitivity among all the NMR active nuclei due to its large value of gyromagnetic ratio. It has a natural abundance of 99.98%. Both facts contribute to the superior sensitivity of protons over other NMR active nuclei such as ^{13}C and ^{195}Pt. When dealing with small metal particles, the Knight shift interaction of the

metal conduction electrons with the adsorbed hydrogen can result in a shift roughly one order of magnitude greater than normal chemical shifts. This large shift distinguishes the hydrogen adsorbed on metal surfaces and avoids interference from the strong OH resonance from the support. Since in most cases the adsorbed hydrogen does not penetrate into the metal particles at ambient temperature, NMR of hydrogen adsorbed on the metal particles is truly a surface-sensitive technique. The electronic environment at metal surfaces may be probed directly by the adsorbed hydrogen.

Due to the small energy differences for nuclear spin transitions, NMR is inherently an insensitive technique and the NMR signals are susceptible to thermal noise. This is not a serious problem when a pure compound is used as the sample. But in supported metal catalysts, the small metal particles are diluted in the support and the total metal surface area is small. A typical supported metal catalyst can adsorb only about 10^{20} protons per gram of catalyst sample. Aside from poor sensitivity, the NMR resonance may be broadened by various internal interactions (one or more of the H-H dipole, chemical shift anisotropy, or Knight shift interactions). Magnetic susceptibility variations due to different metal particle sizes can also cause NMR line broadening. Furthermore, the number of protons in the OH group in the catalyst support is usually about two orders of

magnitude larger than the number of hydrogen atoms adsorbed on metal particles. This large resonance tends to obscure other, weaker resonances.

In recent years, high field superconducting magnets have become available. The improvements in both sensitivity and resolution of NMR spectra can be achieved with the use of a high magnetic field. Also, physical line-narrowing methods such as multiple pulse experiments, magic angle spinning (MAS), and the combination of the two (CRAMPS) (8) have come to play an important role in improving the resolution of NMR spectra. However, these physical methods are not very useful for ^1H NMR on supported metal catalysts because of excessive line broadening and non-uniform metal particle size. But other, simpler techniques can be used to improve sensitivity. For instance, data acquisition with extensive NMR signal averaging can increase the signal-to-noise ratio. Due to a much longer spin-lattice relaxation time, T_1, for the OH resonance from the support, selective T_1 saturation can be used to reduce the intensity from the OH group resonance. In addition, a novel chemical method of support deuteration has been applied in this work to greatly reduce the OH resonance intensity. The deuteration method for platinum-containing catalysts is described in detail in Section V and Section VI.

The application of proton NMR to investigations of supported bimetallic catalysts was a pioneering work carried

out by the author. In addition to proton NMR, other methods such as selective hydrogen chemisorption, X-ray fluorescence, and thermogravimetric analysis were also applied to study the supported mono- and bimetallic catalysts. The results from these techniques were correlated with the NMR results. Also, a study of the cyclohexane dehydrogenation reaction was carried out on Pt-Re/SiO_2 bimetallic catalysts. The reaction was monitored by proton NMR and the results are reported in Section VI.

Explanation of Dissertation Format

The entire dissertation contains six separate sections. Each section was written by the author in a form suitable for submission for publication in a technical journal. The first three sections have been published in recent issues in the Journal of Catalysis. Each section details original work carried out by the author. The project was a collaborative effort with Professor Bernard C. Gerstein of the Chemistry Department at Iowa State University, who kindly shared his expertise in solid state NMR.

SECTION I

CHARACTERIZATION OF SILICA-SUPPORTED RUTHENIUM CATALYSTS BY HYDROGEN CHEMISORPTION AND NMR OF ADSORBED HYDROGEN

CHARACTERIZATION OF SILICA-SUPPORTED RUTHENIUM CATALYSTS BY HYDROGEN CHEMISORPTION AND NMR OF ADSORBED HYDROGEN

Xi Wu[1]

Bernard C. Gerstein[2]

Terry S. King[1]

[1]Department of Chemical Engineering and Ames Laboratory

231 Sweeney Hall

Iowa State University

Ames, Iowa 50011

[2]Department of Chemistry and Ames Laboratory

229 Spedding Hall

Iowa State University

Ames, Iowa 50011

ABSTRACT

Adsorbed hydrogen on four different silica-supported ruthenium catalysts was measured quantitatively by the method of nuclear magnetic resonance (NMR) of hydrogen, or proton magnetic resonance (PMR). The PMR technique revealed two distinct adsorbed states of hydrogen on Ru: reversible and irreversible. The results from PMR and those from the traditional hydrogen chemisorption measurements were compared directly. The observed discrepancy between the PMR and the volumetric technique in the case of total adsorption is attributed to spillover of the reversibly adsorbed hydrogen from ruthenium onto the silica support. Good agreement was obtained between the two techniques in the case of strong hydrogen adsorption. The relatively narrow line of PMR spectra on the reversibly adsorbed hydrogen indicates rapid motion for this state of hydrogen on ruthenium surfaces. The variation of spectral lineshift and of the spin-lattice relaxation times for the adsorbed hydrogen with ruthenium particle size suggests a stronger interaction between the adsorbed hydrogen and defect-like ruthenium adsorption sites. The results from PMR intensity measurements also suggest that the reversibly bound hydrogen is at least in part associated with the defect-like ruthenium adsorption sites.

INTRODUCTION

Dissociative chemisorption of hydrogen on Group VIII transition metal surfaces is well known and is the basis for the volumetric method of selective hydrogen chemisorption on these supported metal catalysts. This technique has been used to measure the ruthenium dispersion (fraction of Ru atoms at the metal surface) in Ru/SiO_2 (1-4), Ru/Al_2O_3 (5, 6), and Ru/Y (6-8) catalysts. The basic assumptions involved in obtaining the dispersion by this method include (i) a specific stoichiometry between the adsorbed hydrogen atoms and the ruthenium atoms at the surface, and (ii) no hydrogen spillover from ruthenium onto the support. Using total hydrogen adsorption, Dalla Betta (1), Kubicka (2), Taylor (5), and Goodwin (6) estimated the stoichiometric ratio $H/Ru_{(s)}$ to be in the range of 1.1 to 1.5, although $H/Ru_{(s)}$ = 1.0 was recommended by some of these researchers.

However, there are indications of two adsorbed states of hydrogen on ruthenium powder (9), Ru/SiO_2 (10), and Ru/Y (7) catalysts, namely, the strongly (or irreversibly) adsorbed hydrogen and the weakly (or reversibly) adsorbed hydrogen. The irreversible adsorption may be attributed to strong chemisorption of hydrogen on ruthenium. The reversibly adsorbed hydrogen is known to be readily removed under high vacuum at ambient temperature, and it may be attributed to either multiple adsorption of hydrogen on ruthenium alone

or both multiple adsorption and hydrogen spillover onto the support. But there is no convincing evidence in previous literature to support or exclude the possibility of hydrogen spillover in supported ruthenium catalysts. Some evidence of hydrogen spillover onto the support at ambient temperature in silica and zeolite-supported platinum catalysts has been found by hydrogen chemisorption measurements (11, 12), which showed an enhanced adsorption of hydrogen (H/Pt > 1.0) in these catalysts. If this is true, hydrogen spillover could occur in silica-supported ruthenium catalysts as well.

There is an additional complication in characterizing supported ruthenium catalysts when $RuCl_3$ nH_2O is used as a precursor in preparing the catalysts. Recent studies (13-16) showed that chlorine cannot be effectively removed from the surface of ruthenium particles at usual temperatures (573-773 K) for reduction and that it inhibits adsorption of hydrogen on ruthenium. Since chlorine-contaminated ruthenium catalysts were used in most of the previous studies (1-5), the results obtained from these catalysts may be questionable and are worth reexamining.

Nuclear magnetic resonance (NMR) of hydrogen atoms, or proton magnetic resonance (PMR) has been applied to measure the resonance linewidth and lineshift of hydrogen adsorbed on silica- and alumina-supported platinum catalysts (17-19). Also, PMR has been applied to measure the lineshift values of

hydrogen adsorbed on ruthenium in Ru/SiO_2 catalysts (19, 20), although the lineshift may have been influenced by the Cl impurity. In fact, marked changes in the lineshift of the hydrogen adsorbed on ruthenium due to the chlorine residue have been observed (21). In addition, previous intensity measurements (19) on the upfield peak, which corresponds to resonance of hydrogen adsorbed on ruthenium, could account for only 70% of the total adsorbed hydrogen by volumetric measurements. The discrepancy may be due to some inherent experimental errors and/or hydrogen spillover onto the silica support.

The objective of the present study was to examine the validity of hydrogen chemisorption in determining ruthenium dispersion on chlorine-free Ru/SiO_2 catalysts by the method of proton magnetic resonance and to investigate the nature of the reversibly adsorbed hydrogen in these catalysts. PMR offers a great advantage in discerning between the reversibly adsorbed hydrogen on ruthenium and the spiltover hydrogen on the silica support.

EXPERIMENTAL METHODS

Catalyst Preparation

All catalysts were prepared by the incipient wetness impregnation of a ruthenium impregnating solution with a dried Cab-O-Sil HS5 silica (300 m^2/g BET surface area) as the support. The impregnating solution was made by dissolving an appropriate amount of the metal salt $Ru(NO)(NO_3)_3$ (AESAR) in distilled water. Approximately 2.2 ml of the impregnating solution per gram of support was needed to achieve incipient wetness. The slurries obtained after impregnation were dried for 24 hours at room temperature and 4 hours in air at 383 K. Catalysts with ruthenium loadings of 1, 4, 8, and 12% by total weight of Ru metal plus dry support were prepared for the present study.

Adsorption Apparatus

The apparatus used for adsorption in this study was a multiport high-vacuum Pyrex glass manifold with a measured volume of 127.3 cm^3 in connection with a turbo-molecular pump (Balzers, Model TPH 050) backed by a forepump trap and a two-stage mechanical pump. A detailed diagram of the apparatus is shown in Figure 1. High-vacuum greaseless, bakeable stopcocks (Ace Glass) with Teflon plugs and FETFE O-ring seals were employed to manipulate gas storage, dosage, or

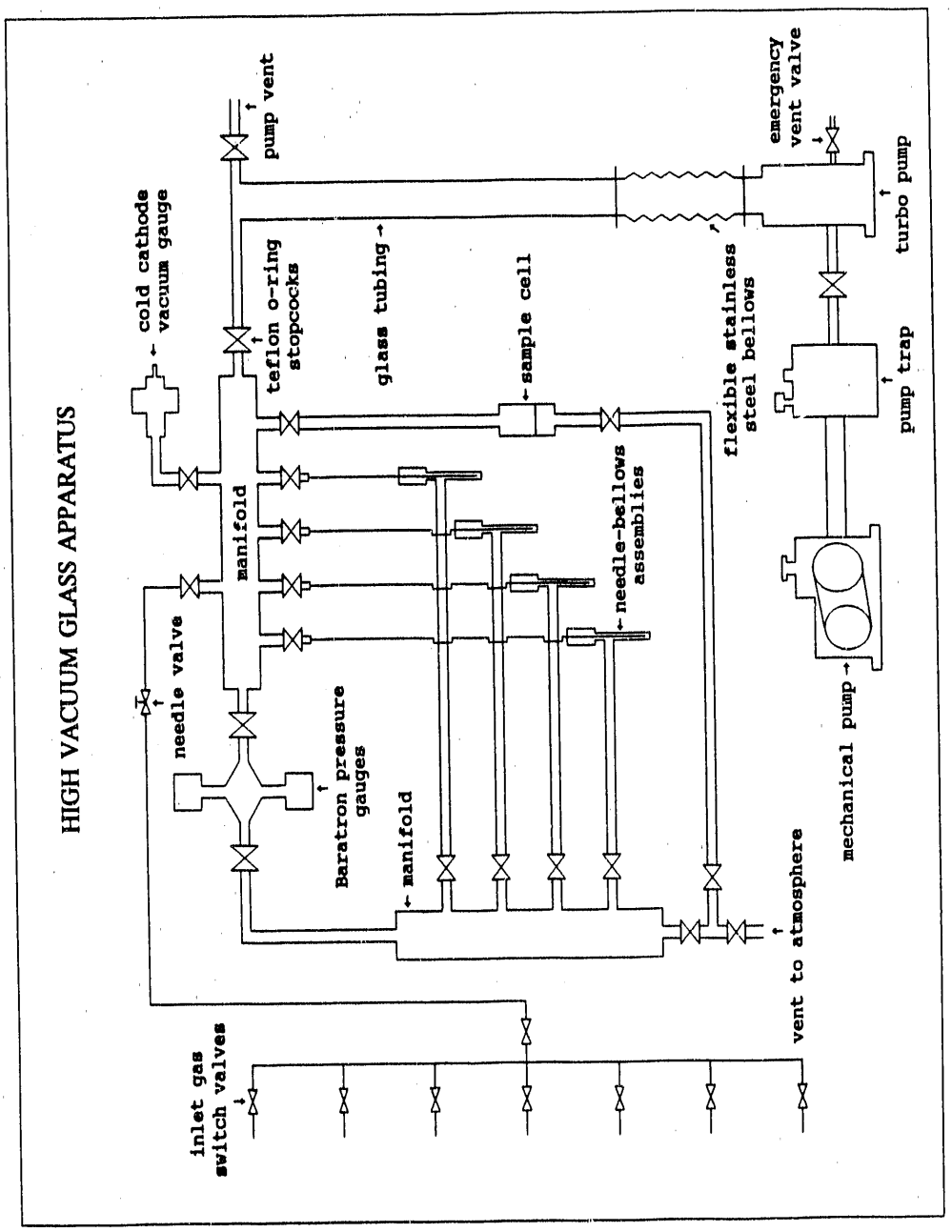

Figure 1. A schematic diagram of a high vacuum adsorption apparatus. Each component is labeled as indicated in the figure

both and to minimize hydrocarbon impurities in the manifold. The manifold was capable of a vacuum better than 10^{-7} Torr (1 Torr = 133.3 Pa) after bakeout. Pressures below 10^{-2} Torr were monitored by a cold cathode gauge (Varian Model 860A). Pressures from 10^{-2} to 10^{3} Torr were measured by two Baratron absolute pressure gauges (MKS Instruments).

Catalyst samples were held in a Pyrex cell by a coarse frit with an average pore diameter of 35 μm. A small furnace was used to heat the cell. The temperature of the furnace was controlled to within ±1 K by a temperature controller (Omega Engineering).

Catalyst Reduction and Adsorption

All catalyst samples were treated inside the Pyrex cell. Approximately one gram of sample was loaded into the cell, which was then attached to one of the sample ports of the manifold. While helium was allowed to flow through the cell, the temperature of the furnace surrounding the cell was raised to 423 K. Then helium was replaced by hydrogen gas at a flow rate of 50 cm^3 /min, and reduction proceeded for 1 hour at that temperature before it was raised at 10 K/min to 723 K. Further reduction was carried out for an additional 2 hours at 723 K. Helium (99.999%) and hydrogen (99.8%) gas (Liquid Air Co.) were used as received. After reduction, a two-hour evacuation period at 723 K was followed to remove

traces of water and surface hydrogen.

Hydrogen used for adsorption was purified by passing it through a catalytic hydrogen purifier (Engelhard Deoxo) in series with a gas purifier with Drierite and 5-Å molecular sieve (Alltech) to remove traces of oxygen and moisture. Hydrogen adsorption experiments were performed at ambient temperature (294 K). The total hydrogen adsorption isotherm was measured in the pressure range 0-30 Torr. The reversible hydrogen adsorption isotherm was collected under the same conditions after a ten-minute evacuation period to 10^{-6} Torr following the total adsorption. The irreversible uptake was obtained by taking the difference between the extrapolated values of these two isotherms at zero pressure. A period of 4 hours and 1 hour for equilibration were used for the first dose and for subsequent doses, respectively.

NMR Sample Treatment

A specially designed needle-bellows assembly (shown in Figure 2), which was made of stainless steel, was used for direct reduction of a catalyst sample in flowing hydrogen inside a 5 mm NMR tube. The syringe needle (18 gauge) was capable of moving vertically by more than 6 cm through proper adjustable compression and extension of the bellows. Good vacuum-tight connections were made between the NMR tube and the needle-bellows assembly as well as between the assembly

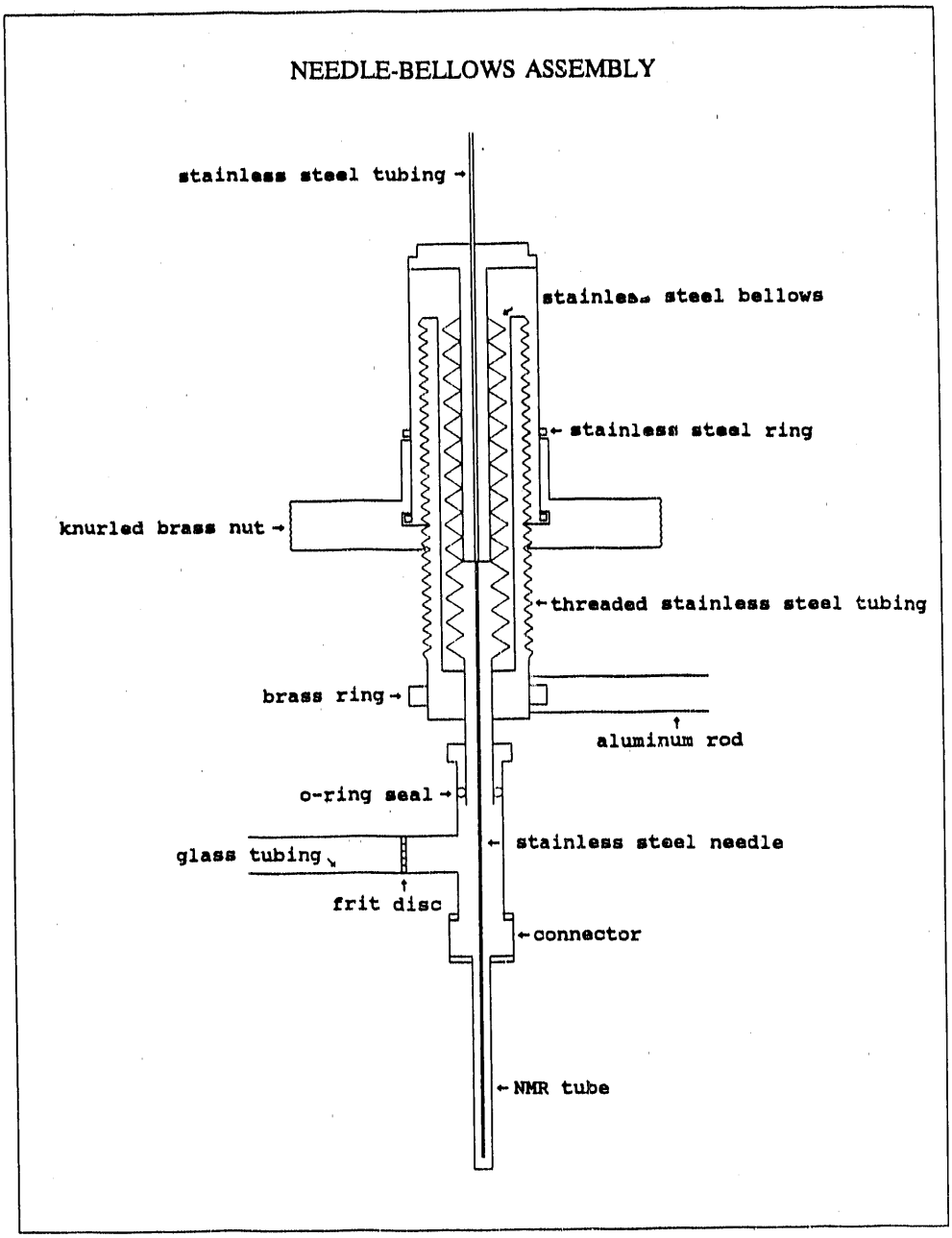

Figure 2. A detailed drawing of a needle-bellows assembly. Each part of the device is labeled as indicated in the figure

and the manifold. In addition, a small cylindrical furnace provided uniform heating around the NMR tube and the furnace temperature was controlled to better than ±1 K.

With helium gas flowing through the needle, the needle was lowered down to the bottom of the NMR tube, which was loaded with approximately 60 mg of catalyst sample. The reduction procedure was the same as previously described, with a hydrogen flow rate of 15 cm^3/min. After reduction, the needle was lifted out of the sample, and evacuation proceeded for 2 hours at the reduction temperature before the sample was cooled to ambient temperature. Up to four samples could be reduced simultaneously. Then purified hydrogen was dosed through the needle to each sample separately and was allowed to equilibrate for 4 hours. The samples were then immersed in a water bath and the NMR tube was sealed off with a micro-torch. Sample weights were measured after the NMR tubes were sealed by subtracting the weight of the empty tube.

For the deuterium exchange experiment, deuterium gas (Linde, 99.5%) instead of hydrogen was dosed to a ruthenium catalyst sample in an NMR tube immersed in liquid nitrogen. The NMR tube was sealed and the sample was temporarily stored in liquid nitrogen to inhibit the exchange until the sample was brought to room temperature at the onset of the exchange experiment.

NMR Experiments

The home-built NMR spectrometer (22) used in the present study was operated at 220 MHz for proton resonance. A probe (free of protons) with a doubly wound coil was used for all the NMR measurements. The probe quality factor Q was set at 100 for sufficient sensitivity and low ringdown time. A detailed description of the spectrometer's receiving system was given elsewhere (20).

The spectrometer was capable of detecting 10^{17} protons, while the number of hydrogen atoms adsorbed on ruthenium in a typical catalyst sample was around 5×10^{18}. The recycle time between 90° pulses was set between 0.2 and 0.3 second to suppress selectively the strong intensity of the resonance corresponding to protons in the silanol group that have a relatively long spin-lattice relaxation time T_1 (on the order of seconds). The recycle rate given above avoids saturation of T_1 for the peak corresponding to hydrogen adsorbed on ruthenium. The total number of scans for data acquisition on each sample was 10,000 unless noted otherwise. The inversion recovery pulse sequence (180°-τ-90°) was applied to measure the spin-lattice relaxation times of the silanol protons (in the time domain) and the hydrogen adsorbed on ruthenium (in the frequency domain). A pure water sample was used as the reference standard for the observed lineshifts. For the purpose of intensity measurements, the water sample was doped

with $FeCl_3$ to yield a resonance of a comparable linewidth with the observed resonances. In addition, the doped water was sealed in a capillary tube with the same length as the catalyst sample in the NMR tube to offset errors due to B_1 inhomogeneity of the coil. All NMR measurements were done at ambient temperature (294 ± 1 K).

RESULTS

PMR spectra of 1, 4, 8, and 12% Ru catalyst samples under 5 Torr hydrogen are shown in Figure 3. As can be seen, two well-resolved resonance lines are clearly displayed in all spectra. The peak near the reference shift is designated the downfield peak and the peak on the right-hand side the upfield peak. The downfield peak is assigned to the terminal silanol protons (Si-OH) in the silica support since spectra for samples of these catalysts with no gaseous hydrogen added and a sample of pure silica under 5 Torr hydrogen all display only this peak. Note that the lineshift of the downfield peak moves slightly from 5 to 3 ppm and the linewidth (full width at half-maximum) increases from 3.3 to 4.5 kHz as the ruthenium loading increases. The upfield resonance has been assigned to hydrogen adsorbed on ruthenium (19, 20). The linewidth of the upfield peak decreases from 7.5 to 5.9 kHz with an increase in the ruthenium loading. There is also a noticeable change in the lineshift of the upfield resonance toward downfield. Lineshift data for the upfield peak are shown later.

The downfield peak is symmetric and can be well fitted by a Lorentzian line. The upfield resonance is asymmetric, especially for high ruthenium loadings. The area under the upfield peak can be obtained precisely by integrating the spectrum from which the downfield peak has been subtracted.

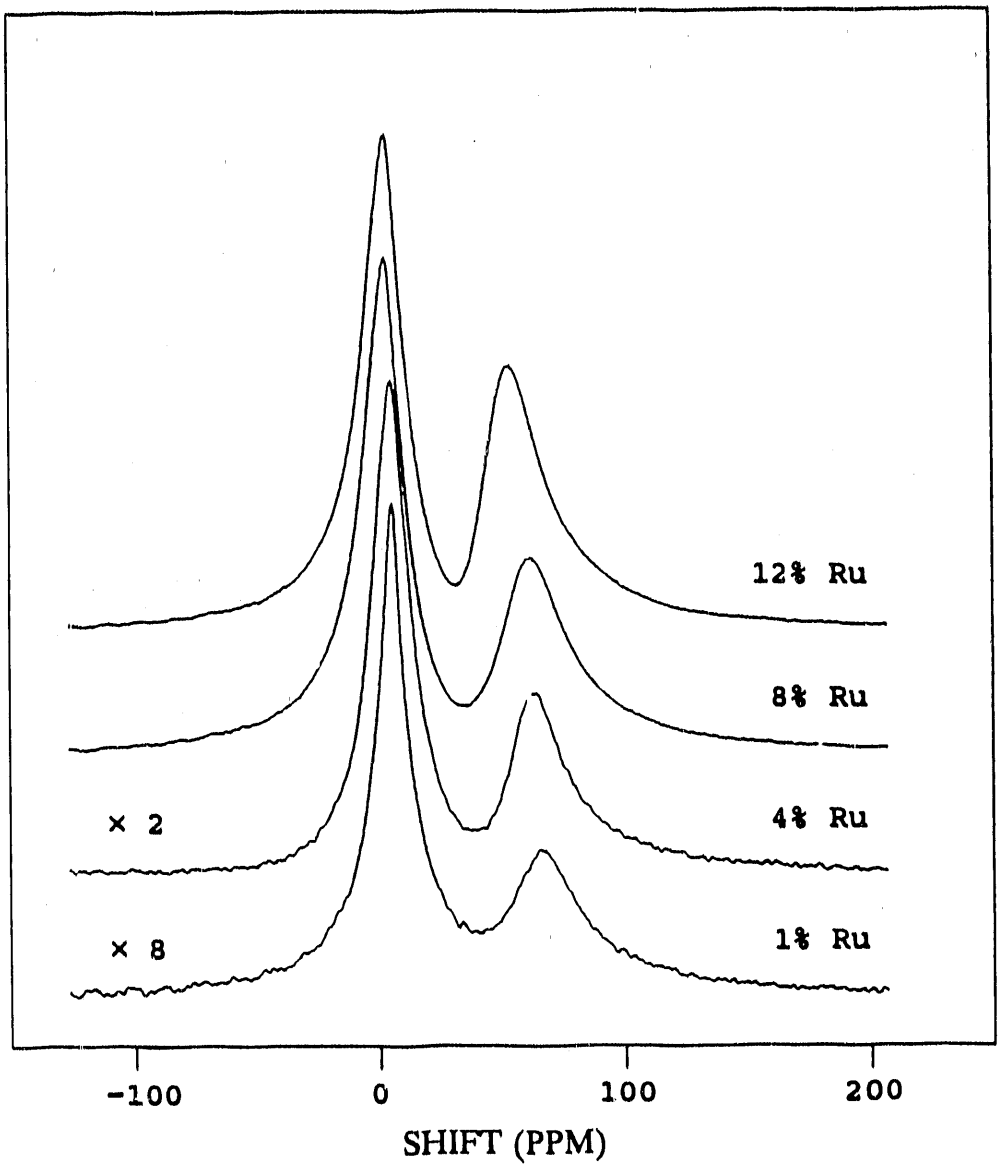

Figure 3. PMR spectra of adsorbed hydrogen on Ru/SiO_2 catalysts. All catalyst samples are under 5 Torr hydrogen. Ruthenium weight loadings are as indicated. Water is used as reference for the lineshift

The upfield peak location is calculated by the first moment of the subtracted spectrum.

The total hydrogen adsorption isotherms measured by both the volumetric technique and PMR for 1 and 8% Ru catalysts are shown in Figure 4. For the PMR measurements, all data points are obtained from the upfield peak intensity only. All isotherms are extrapolated to zero hydrogen pressure to obtain the values for H/Ru ratio. In both cases, the H/Ru value measured by total hydrogen adsorption is greater than that measured by PMR. In fact, this is true for all the catalysts, as will be shown.

In the hydrogen pressure range 5 to 30 Torr, the slope of the total adsorption isotherm is slightly greater than that of the PMR isotherm. The difference may be due in part to physisorbed hydrogen on SiO_2. However, the amount of physisorbed hydrogen on pure SiO_2 in this pressure range is less than 1% of the total hydrogen uptake on a supported catalyst sample. Extrapolation of the isotherm measured on SiO_2 yields zero hydrogen uptake, indicating that physisorbed hydrogen on SiO_2 makes no contribution to the measured H/Ru values.

The strong hydrogen uptake is the difference between the total hydrogen uptake and the reversible hydrogen uptake. The irreversible hydrogen adsorption isotherms for 1 and 8% ruthenium catalysts, which are derived from the corresponding

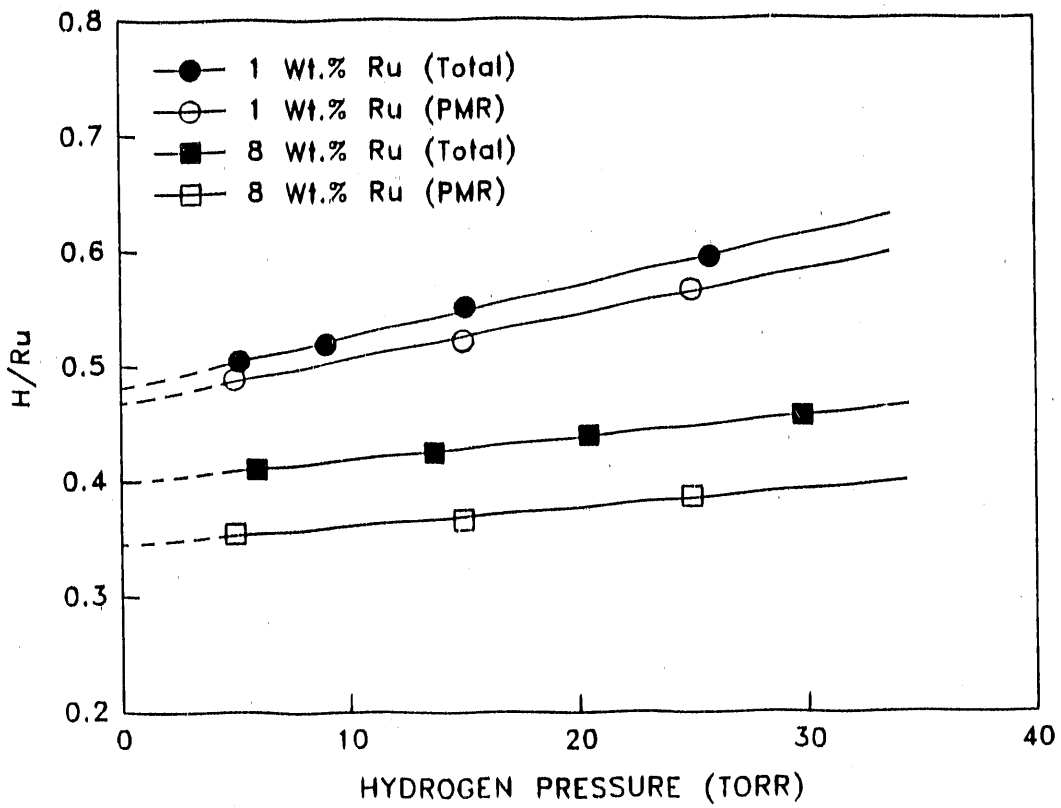

Figure 4. Total hydrogen adsorption isotherms measured by both the volumetric technique and PMR on 1 and 8% Ru/SiO_2 catalysts at 294 K. The dashed lines represent extrapolation of the isotherms to zero hydrogen pressure

total and reversible isotherms, are shown in Figure 5. The values for irreversible hydrogen measured by PMR are also shown in the same figure for comparison. For measurements from PMR, all samples were evacuated to 10^{-6} Torr for 10 min after they were equilibrated with 5 Torr hydrogen and only the intensity of the upfield peak, which corresponds to the irreversibly adsorbed hydrogen on ruthenium, was measured.

For both the 1% and the 8% ruthenium catalysts, portions of the irreversible isotherms obtained by the volumetric technique at hydrogen pressures below about 3 Torr probably do not represent the true equilibrium since adsorption at these low pressures require much longer time to achieve equilibrium. Portions of the isotherms at hydrogen pressures beyond 3 Torr are nearly horizontal. This may be interpreted as formation of a complete monolayer of strongly chemisorbed hydrogen on Ru surfaces. The horizontal portions of the isotherms are extrapolated to zero pressure to obtain values of the H/Ru ratio. As can be seen, the results from the PMR measurements are close to those from the measurements by volumetric adsorption.

The total and irreversible H/Ru values measured by both techniques on all four Ru catalysts are shown in Figure 6. The agreement between the two techniques is good for the irreversible hydrogen. However, noticeable discrepancies are observed for the total hydrogen adsorption, especially for

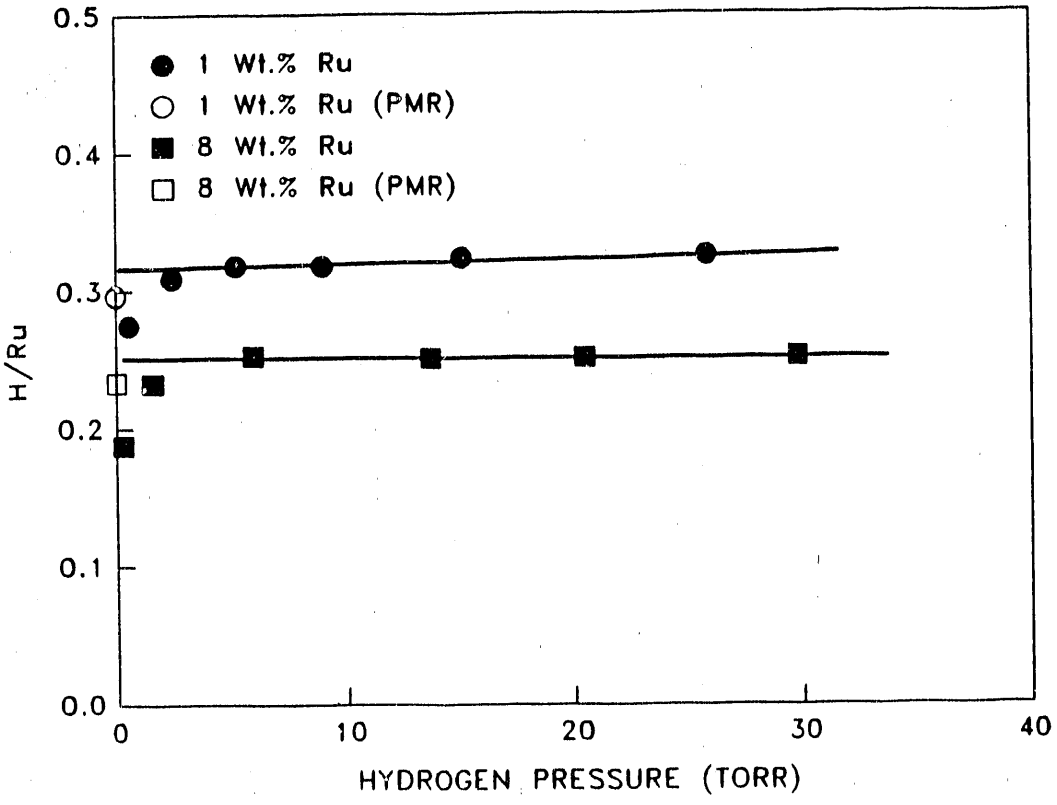

Figure 5. Irreversible hydrogen adsorption isotherms obtained by the difference between the total and the reversible hydrogen adsorption isotherms on 1 and 8% Ru/SiO_2 catalysts at 294 K. The horizontal portion of the isotherms is extrapolated to zero hydrogen pressure. The amount of irreversibly adsorbed hydrogen on ruthenium measured by PMR is also shown for comparison

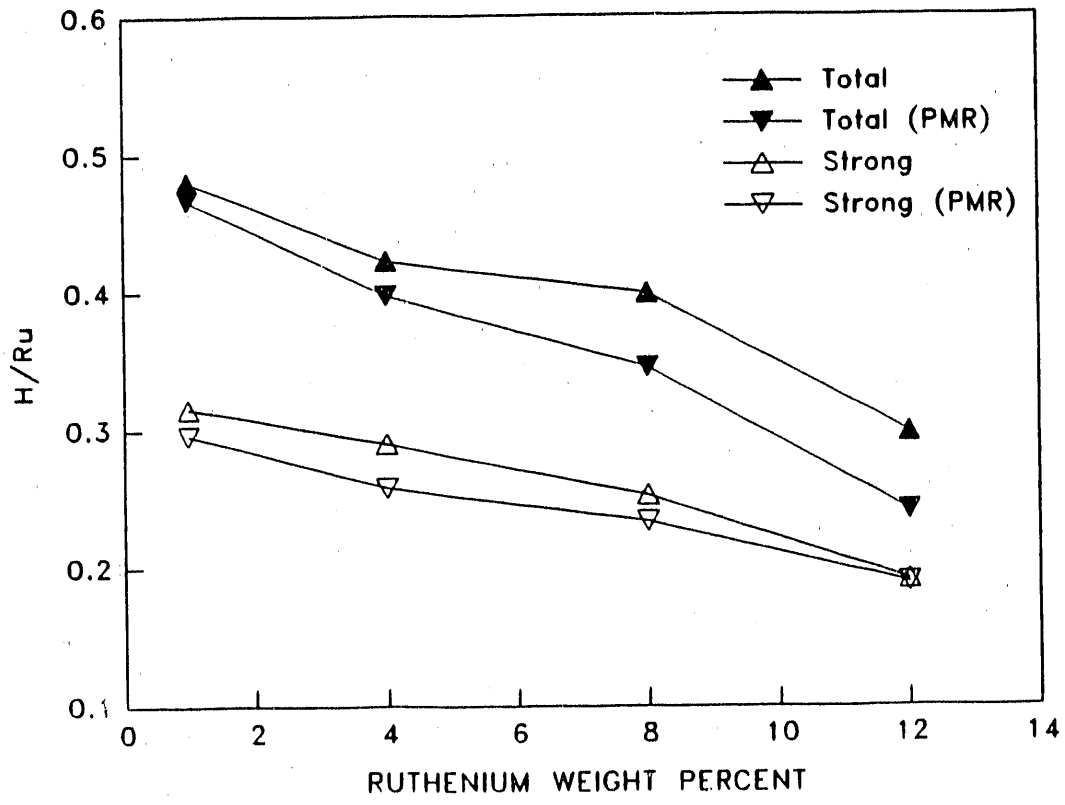

Figure 6. The H/Ru ratios for both the total and the irreversible adsorption of hydrogen with variation in the ruthenium loading. Results from measurements by both the volumetric technique and PMR are shown for comparison

catalysts with high ruthenium loadings. One may argue that these discrepancies are only due to experimental errors. However, for high ruthenium loadings both the total amount of hydrogen adsorption and the PMR signal intensity are higher, which should lead to smaller experimental errors. Thus, a reasonable explanation is that hydrogen spillover from Ru onto the silica support is the main cause for the observed discrepancies. This point will be discussed in more detail later.

The correlations between the total amount of reversible hydrogen on Ru and the total amount of surface Ru and between the total amount of spiltover hydrogen and the total amount of surface ruthenium are illustrated in Figure 7, where one gram of SiO_2 is used as the common basis. The amount of reversible hydrogen on Ru was computed from the difference between the H/Ru ratio for the total hydrogen and that for the irreversible hydrogen measured by PMR. The amount of spiltover hydrogen was obtained by taking the difference between the total H/Ru ratio measured by hydrogen adsorption and that measured by PMR. The amount of surface ruthenium was calculated from the dispersion obtained from the H/Ru value for the irreversible hydrogen determined by PMR (see Figure 6), assuming one irreversibly adsorbed hydrogen atom for every surface Ru atom, i.e., $H/Ru_{(s)} = 1$. As shown in the plot, both the total amount of reversible hydrogen on

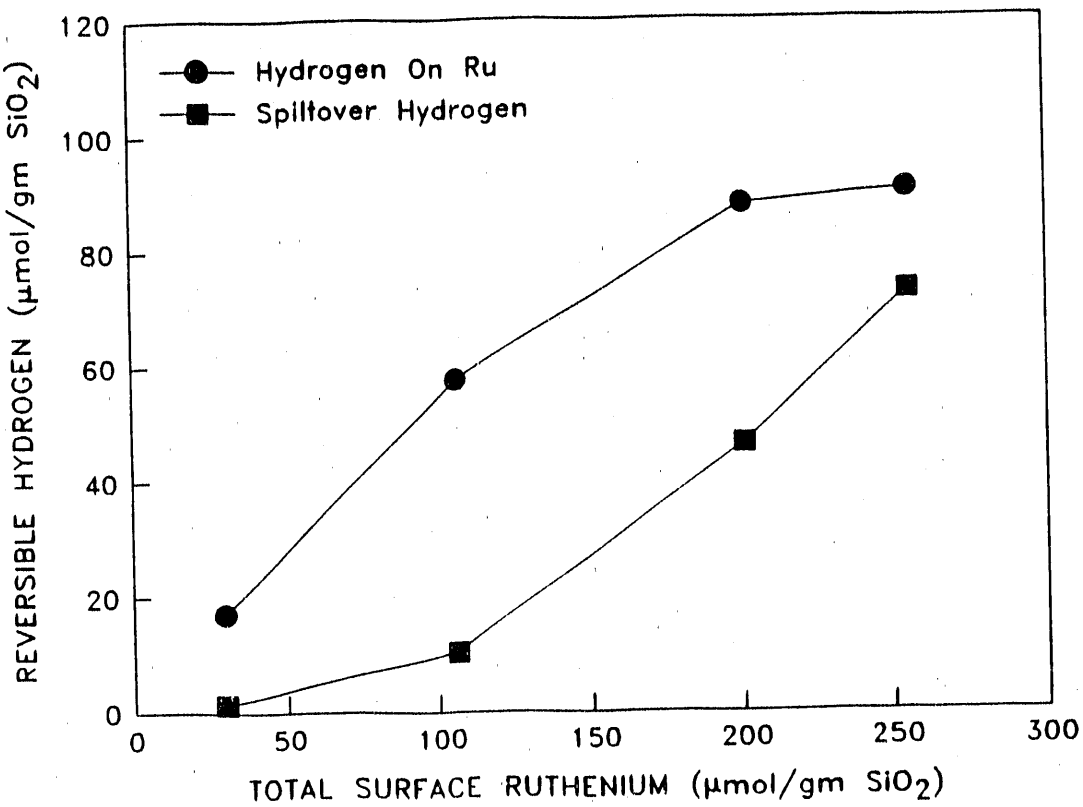

Figure 7. Correlation among the reversible hydrogen on ruthenium (circles), the spiltover hydrogen (squares), and surface ruthenium. The total amounts of these two states of hydrogen are plotted as a function of the total amount of ruthenium at the surface

ruthenium and that of spiltover hydrogen increase with the increasing total amount of surface ruthenium.

Figure 8 shows the spectra for the irreversibly adsorbed hydrogen on ruthenium for both the 1% and the 8% ruthenium catalysts. The dotted resonance lines drawn on top of the upfield peaks are portions of the spectra corresponding to the same ruthenium catalyst under 5 Torr hydrogen pressure (which have been shown in Figure 3). Since no significant change in the position of the upfield peak is found under the two conditions of hydrogen adsorption, it is appropriate to subtract one spectrum from the other to obtain spectral features of the reversibly adsorbed hydrogen. Here the difference spectra between a sample under 5 Torr hydrogen and that under vacuum after hydrogen adsorption are shown in Figure 8 underneath the composite spectra as the spectra for the reversibly adsorbed hydrogen on ruthenium.

Spectra shown in Figure 8 clearly indicate that there are two adsorbed states of hydrogen on ruthenium surfaces, the irreversible hydrogen and the reversible hydrogen. The irreversibly adsorbed hydrogen shows an asymmetric resonance lineshape, while the reversibly adsorbed hydrogen displays a relatively symmetric lineshape. The linewidths for the irreversible hydrogen are 8.7 and 11.8 kHz, and those for the reversible hydrogen are 3.8 and 5.6 kHz for the 8 and 1% ruthenium catalysts, respectively. Also, the resonance

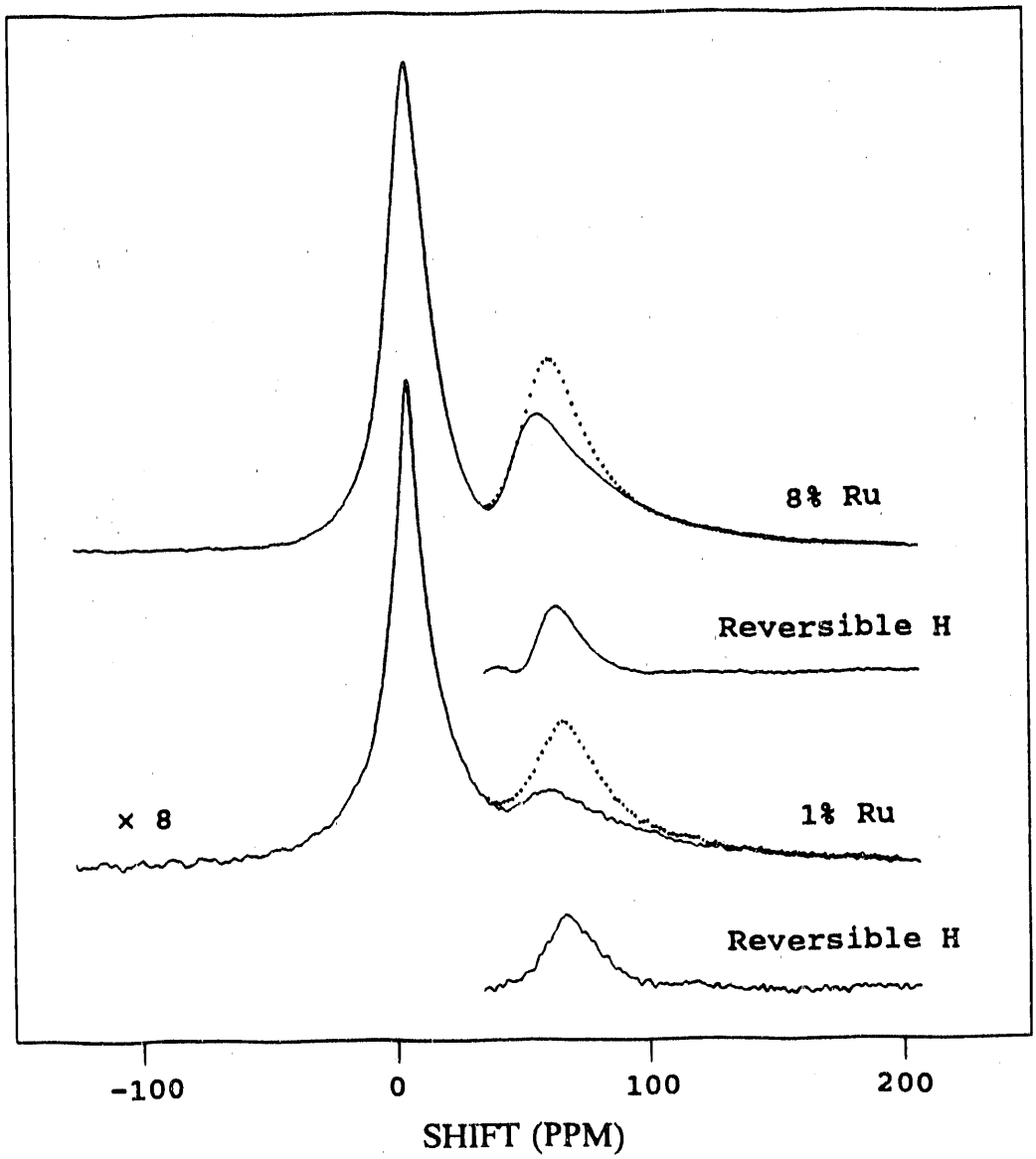

Figure 8. Spectra of 5 Torr hydrogen, irreversibly adsorbed hydrogen, and reversibly adsorbed hydrogen on ruthenium for 1 and 8% Ru/SiO_2 catalysts. The spectra under 5 Torr hydrogen are shown as dotted lines. The spectra of reversible hydrogen, which are the difference spectra between 5 Torr hydrogen and irreversible, are shown underneath the composite spectra

lineshifts of the reversible hydrogen are farther upfield than those of the irreversible hydrogen. The differences in lineshape, linewidth, and lineshift imply that these two adsorbed states of hydrogen are experiencing different local environments on the surfaces of ruthenium particles. This is the first time the irreversibly adsorbed hydrogen and the reversibly adsorbed hydrogen on the surfaces of ruthenium particles are identified separately by the method of proton magnetic resonance.

Shifts of the first moment of the upfield peak for 5 Torr hydrogen, the irreversible hydrogen, and the reversible hydrogen on ruthenium are shown in Figure 9 as functions of the ruthenium loading. Obviously, a gradual decreasing trend with increasing ruthenium loading is present for all the lineshifts. In all cases, the lineshifts for the reversible hydrogen are farther upfield than the those for the strongly bound hydrogen. The difference in the lineshifts of these two adsorbed states of hydrogen decreases with increasing ruthenium loading.

Note that lineshifts reported in the present study are farther upfield than those reported in previous studies (19, 20) on ruthenium catalysts of similar metal loadings and under similar experimental conditions, even when the shifts of different reference standards are taken into account. We believe that such a disagreement is caused by some residual

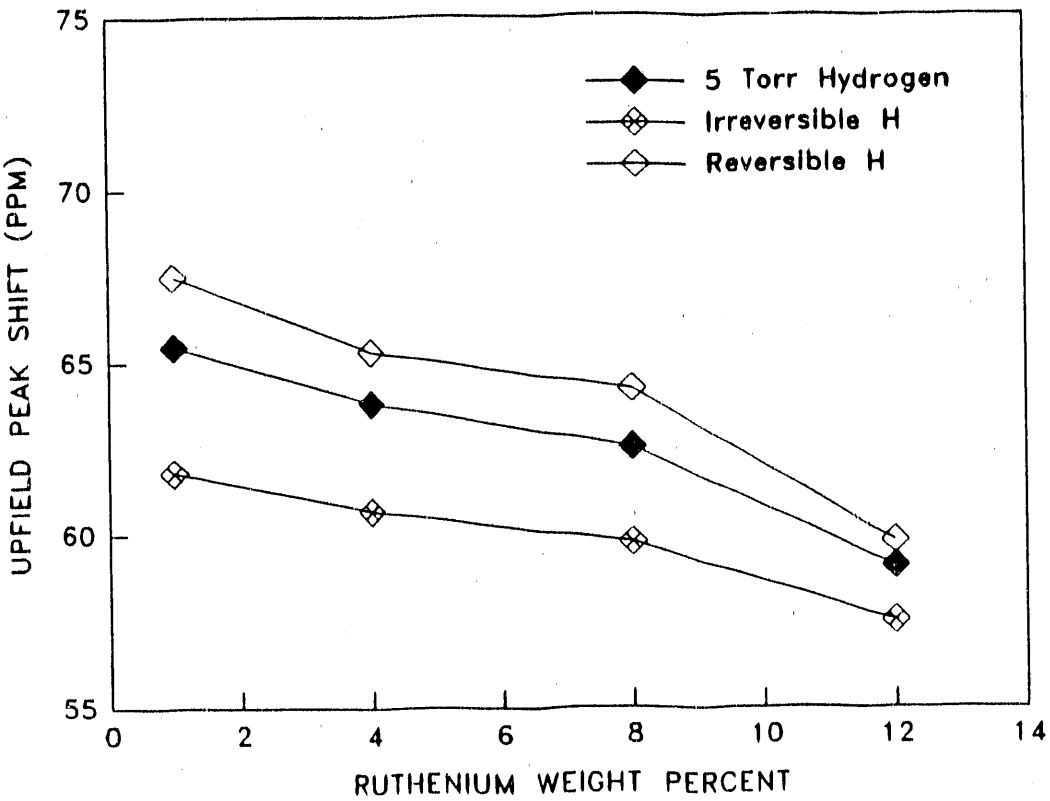

Figure 9. Variation of the upfield resonance shift with the ruthenium loading. Shifts corresponding to 5 Torr hydrogen, irreversible hydrogen, and reversible hydrogen are shown

chlorine on the surface of ruthenium particles in catalysts used in previous studies. Preliminary results (21) indicate that chlorine on the surface of ruthenium particles tends to move the upfield peak toward downfield.

The upfield peak shifts and spin-lattice relaxation times as functions of the hydrogen pressure for both the hydrogen adsorbed on ruthenium and the silanol proton are listed in Table 1. The lineshift of the upfield peak varies only slightly as the hydrogen pressure increases from 5 to 60 Torr. The small variation may be due to saturation of the ruthenium surface by the reversibly adsorbed hydrogen or exchange between this adsorbed state of hydrogen with gaseous hydrogen. This result agrees with observations by Sheng and Gay (19) that showed lack of variation of the upfield peak position with hydrogen coverage in Ru/SiO_2 catalysts. Note that considerable variation of the upfield peak position with hydrogen pressure does occur in some other systems such as supported Rh catalysts. A trend toward the direction of upfield in the resonance position of the adsorbed hydrogen with increasing hydrogen coverage was reported for Rh/SiO_2 catalysts (19). On Rh/TiO_2 catalysts, the resonance of the adsorbed hydrogen shifts downfield with increasing hydrogen pressure (23). The discrepancy associated with the rhodium catalysts may be attributed to many factors such as residual chlorine on the metal surface, possible interaction between

Table 1. Effects of hydrogen pressure on a 4% Ru/SiO_2 catalyst

Hydrogen pressure (Torr)	Upfield peak shift (ppm)	Spin-lattice relaxation time T_1(s)	
		Upfield peak	Downfield peak[a]
0[b]	61	0.026	5.4
5	64	0.021	3.2
30	62	0.018	2.8
60	61	0.018	2.4

[a]The spin-lattice relaxation time of the silanol proton in a pure SiO_2 sample was 31.6 s and that in a 4% Ru/SiO_2 sample under vacuum (not hydrogen dosed) was 16.9 s.

[b]The catalyst sample was outgassed to 10^{-6} Torr for 10 min after adsorption of hydrogen.

metal and support, and varied rates of exchange between the reversibly bound hydrogen on the metal and the hydroxyl protons in the supports or hydrogen in the gas phase. These complications are absent for the Ru/SiO_2 catalysts prepared for the present study.

The effect of pressure on the spin-lattice relaxation

times associated with the upfield and downfield peaks is also given in Table 1. As listed in the first two entries in the table, the spin-lattice relaxation time of the irreversibly adsorbed hydrogen on ruthenium is longer than that of the reversibly adsorbed hydrogen, considering the fact that the observed value of T_1 on the sample under 5 Torr of hydrogen is the combined relaxation effect from both the irreversible and the reversible hydrogen. Further increase in hydrogen pressure has little effect on T_1 of the hydrogen adsorbed on ruthenium. However, there is a marked decrease in the spin-lattice relaxation time of the silanol proton when both the ruthenium and the hydrogen are introduced to the silica support. A T_1 of 31.6 seconds was observed for protons in the silanol group in a pure silica sample. There was no significant change of this value when the pure silica was under 30 Torr of hydrogen gas. For a sample of 4%Ru/SiO_2 that has been reduced, outgassed, and sealed under vacuum, T_1 of the silanol group decreased to 16.9 seconds. We attribute this decrease to additional relaxation effects caused by ruthenium, to trace amounts of iron impurities that are associated with the ruthenium, or both. A significant drop in the silanol group T_1 was observed when hydrogen gas was dosed onto the catalyst. Evacuation after hydrogen dosage resulted in only a small increase in the silanol group T_1, but it is still much lower compared to the catalyst sample

without hydrogen dosage.

Using an average area of 0.0817 nm^2 per surface Ru atom (1), we calculated the total ruthenium surface areas. The average ruthenium particle sizes, d, were calculated by use of the relationship $d = 6/(S\beta)$, where S is the surface area per gram of ruthenium and β the density of ruthenium. The estimated average Ru particle size and the corresponding Ru dispersion (measured by PMR of the irreversible hydrogen with an assumed stoichiometric ratio of $H_{(irr)}/Ru_{(s)} = 1$) are listed in Table 2. Note that the average ruthenium particle size does not increase very much with an increase in the ruthenium loading.

The spin-lattice relaxation times of hydrogen adsorbed on ruthenium and the silanol proton for all four ruthenium catalysts are also shown in Table 2. It is surprising to see a drastic decrease in the silanol group T_1 as the ruthenium loading increases. One may explain this by the increased iron impurity due to increasing Ru loading. No detectable amount of iron was found in pure silica. The iron impurities originated mainly from the ruthenium salt $Ru(NO)(NO_3)_3$. Less than 8 ppm of iron was detected in the 12% Ru/SiO_2 catalyst by atomic absorption spectroscopy. Even though the iron may have induced relaxation of silanol group protons, it cannot fully account for such a large decrease in the spin-lattice relaxation time. Like the 4% Ru/SiO_2 catalyst, other Ru

Table 2. Effects of metal loading on Ru/SiO_2 catalysts

Ruthenium metal loading (wt%)	Average ruthenium particle size (nm), (dispersion)	Spin-lattice relaxation time T_1 (s)			
		Upfield peak		Downfield peak	
		Total[a]	Strong[b]	Total	Strong
1	3.4 (0.30)	0.019	0.024	18.3	19.2
4	3.9 (0.26)	0.021	0.026	3.2	5.4
8	4.3 (0.23)	0.029	0.031	1.0	1.5
12	5.3 (0.19)	0.043	0.044	0.7	1.1

[a]The catalyst sample was dosed with 5 Torr hydrogen.

[b]The catalyst sample was outgassed to 10^{-6} Torr for 10 min after adsorption of hydrogen.

catalysts also exhibit a much longer T_1 of the silanol group proton when no hydrogen is dosed. It is therefore believed that the hydrogen adsorbed on ruthenium that has spilled over to the support is at least partially responsible for the sharp decrease in the spin-lattice relaxation time of the silanol proton.

On the basis of the measured iron content in the 12% ruthenium catalyst, we estimate that on the average each

ruthenium particle (about 10,800 atoms) contains less than one iron atom. If the trace amount of iron impurity is segregated to the surface of Ru particles during reduction of the catalysts, as one may expect from the thermodynamics of surface segregation, a decrease in T_1 of the hydrogen bound on ruthenium with increase in ruthenium particle size should be observed due to increased surface concentration of iron. However, as shown in Table 2, the spin-lattice relaxation time of the adsorbed hydrogen on the surface of ruthenium increases with an increase in the ruthenium particle size. This result may be an indication that the adsorbed hydrogen experiences many different structural environments on the surface of the ruthenium particles.

Figure 10 shows the PMR spectra, which indicate the progress of the hydrogen-deuterium exchange with time at ambient temperature on a 4% Ru/SiO_2 catalyst. The catalyst was under 5 Torr deuterium at the onset of the exchange experiment. Obviously, the exchange between the deuterium adsorbed on ruthenium (not detectable by PMR) and the silanol proton at room temperature is a very slow process. The half-life (with 50% deuterium exchanged) for the exchange process at 294 K is about 12 hours. This is much shorter than that reported by Sheng and Gay (19). The reason for the observed discrepancy seems to be the residual chlorine present in the Ru/SiO_2 catalysts used by these researchers. If chlorine can

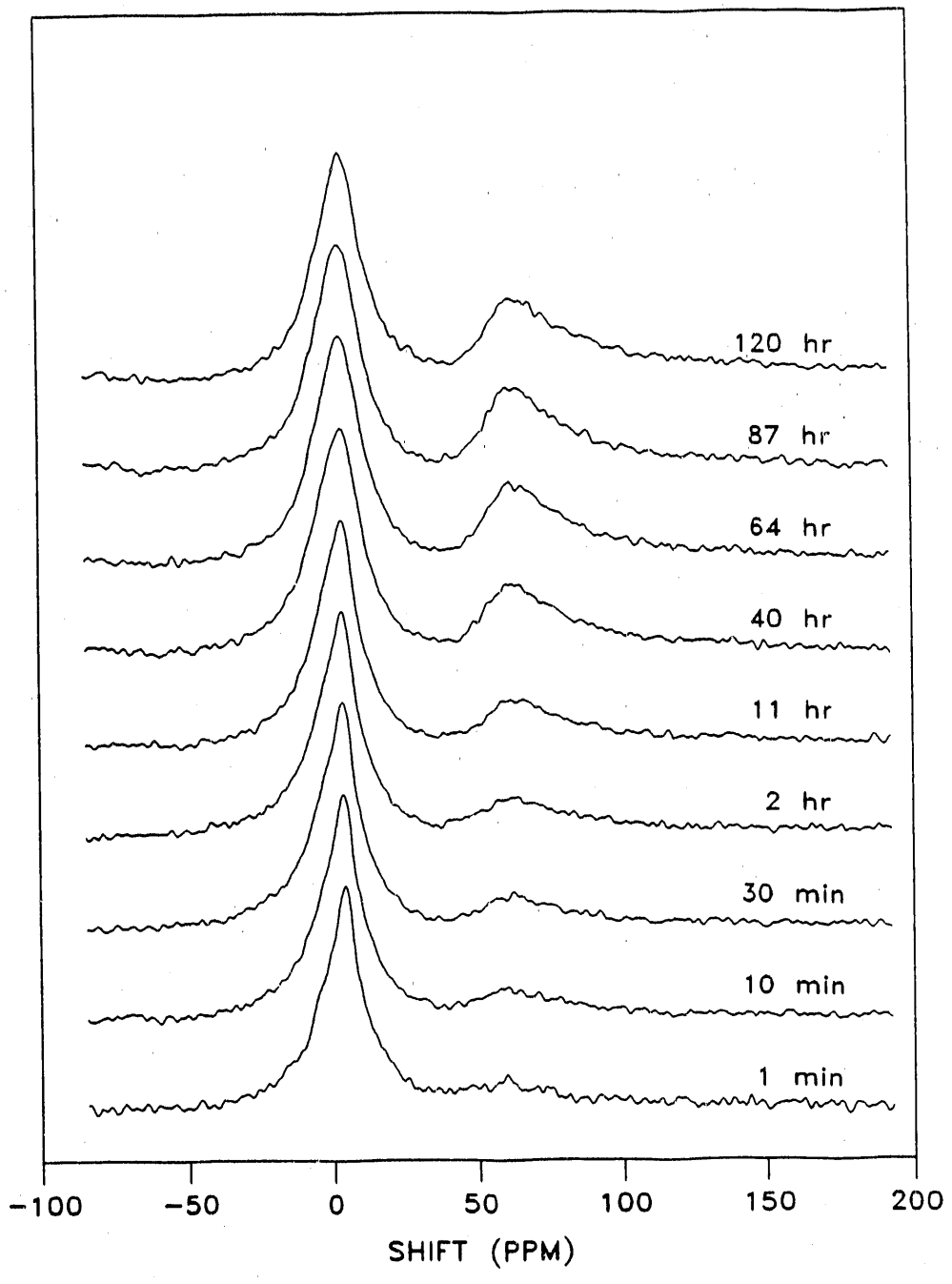

Figure 10. PMR spectra on a 4% Ru/SiO_2 catalyst showing the progress of hydrogen-deuterium exchange with time at 294 K. The catalyst was initially under 5 Torr deuterium. Each spectrum is a result of two hundred scans of data accumulation

inhibit adsorption of hydrogen on ruthenium, as mentioned earlier, it may slow the hydrogen-deuterium exchange as well.

As the upfield peak grows with time, the first moment of the upfield peak moves farther upfield. As shown earlier in Figure 9, the irreversible hydrogen on Ru has a smaller upfield shift than the reversible hydrogen. Therefore, this change of lineshift with time simply indicates that the exchanged hydrogen fills the ruthenium adsorption sites for the irreversible hydrogen first before covering sites for the reversible hydrogen.

Figure 11 shows the PMR spectra on a 4% Ru/SiO_2 catalyst which has been evacuated at 10^{-6} Torr for 10 min at room temperature after being dosed with 5 Torr deuterium at 77 K. In other words, only the irreversible deuterium is present on the surface of ruthenium; the reversible deuterium has been removed by evacuation. As shown in the figure, the initial intensity of the upfield peak is not observable and the peak does not grow with time, indicating the absence of hydrogen deuterium exchange.

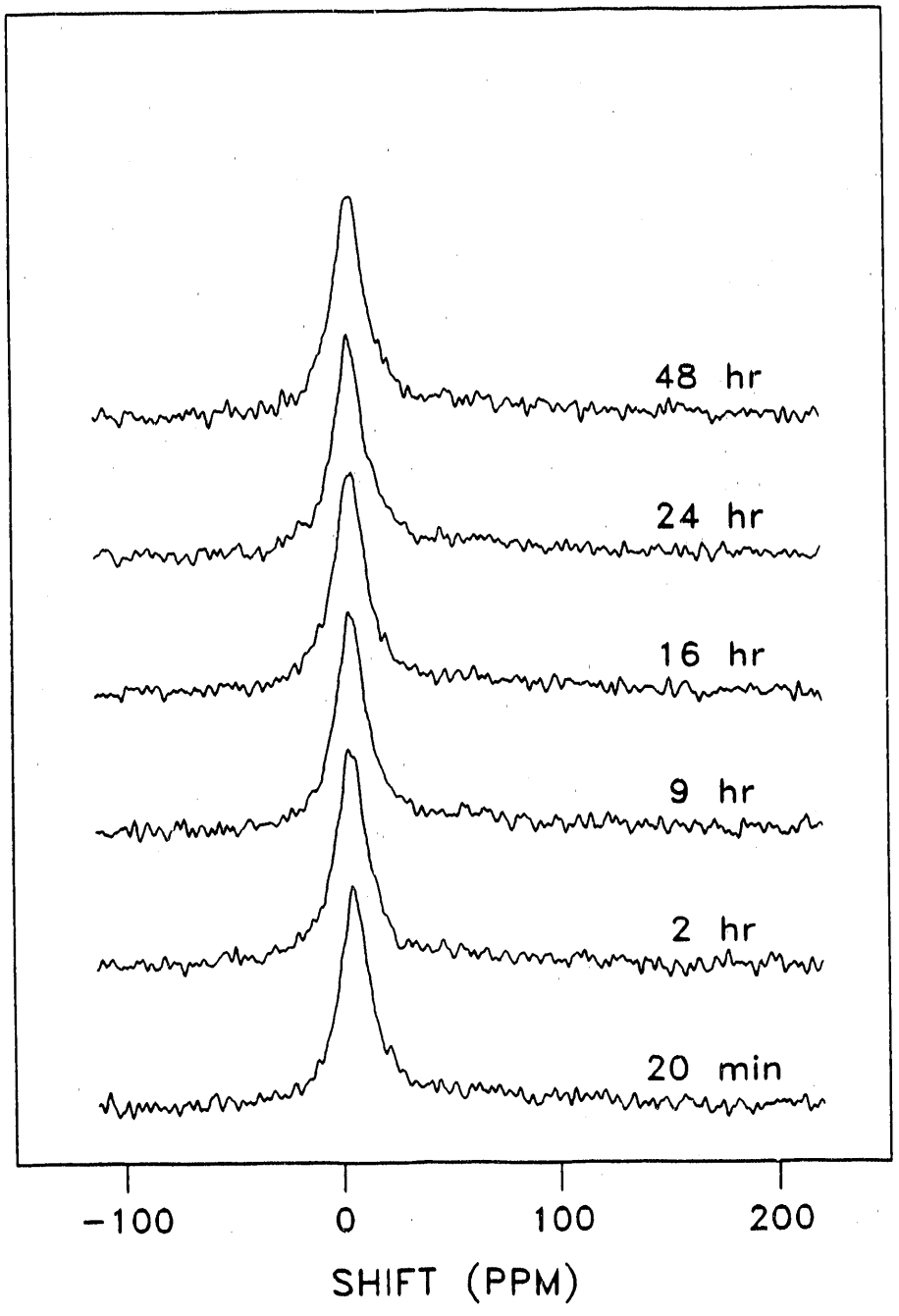

Figure 11. PMR spectra on a 4% Ru/SiO_2 catalyst showing the absence of hydrogen-deuterium exchange at 294 K. The catalyst sample was exposed initially under 5 Torr deuterium at 77 K and was then evacuated to 10^{-6} Torr for 10 min at 294 K. Each spectrum is a result of five hundred scans of accumulation

DISCUSSION

Hydrogen Spillover

The present study indicates that there are two states of weakly bound hydrogen in Ru/SiO_2 catalysts: (a) reversibly adsorbed hydrogen on ruthenium, and (b) spiltover hydrogen on the silica support. The amounts of these two adsorbed states of hydrogen increases with increase in hydrogen pressure in the pressure range 0-30 Torr, especially that of reversible hydrogen on ruthenium. The reversible hydrogen on ruthenium and most of the spiltover hydrogen can be readily removed at room temperature under vacuum. The reversibility of the weak adsorption for these two types of hydrogen and also their dependence upon the hydrogen pressure indicate the existence of a dynamic equilibrium among the gas-phase hydrogen and these two states of weakly adsorbed hydrogen.

Evidence of hydrogen spillover has been presented by the increased discrepancy in counting hydrogen between the method of total hydrogen chemisorption and the PMR technique as the ruthenium loading is increased. While there are only very moderate changes in the ruthenium particle size and the metal dispersion, the total ruthenium surface area has increased significantly with increase in the ruthenium loading. Thus, hydrogen spillover appears to be in some way related to the total available ruthenium surface area in the catalysts. As

shown earlier in Figure 7, the amount of spiltover hydrogen increases with an increase in the total ruthenium surface area.

The noticeable changes in the lineshift and linewidth of the downfield peak (silanol group) with ruthenium loading as shown earlier in Figure 3 may also be a subtle indication of hydrogen spillover. Since there are only two resonance lines observed, and the upfield resonance line is associated only with the Knight shift of adsorbed hydrogen on the surface of ruthenium, the line position of the spiltover hydrogen must be near that of the silanol group and its signal is buried under the large resonance line of the silanol proton.

The effect of dosed hydrogen in shortening the spin-lattice relaxation time of the silanol proton is obvious and convincing evidence of hydrogen spillover. Evacuation of the catalyst sample after dosing hydrogen does not return T_1 of the silanol proton fully back to T_1 of a sample under vacuum without dosing hydrogen. This indicates that some of the spiltover hydrogen is not readily removed by evacuation and remains in the silica support. The sharp decrease in T_1 of the silanol proton with increase in ruthenium loading under the same treatment by hydrogen also points to the conclusion of hydrogen spillover. This is consistent with the fact that more spiltover hydrogen is present in catalysts with higher ruthenium loadings.

Although the nature of the spiltover hydrogen sites cannot be clearly identified by PMR, it is reasonable to postulate that the bridge oxygen between silicon atoms in the support is responsible for holding the spiltover hydrogen. The spiltover hydrogen residing on the bridge oxygen is weakly bound and readily returns to the gas phase. Thus, a constant supply of atomic hydrogen is required to maintain a measurable amount of spiltover hydrogen. The atomic hydrogen supply can only come from the hydrogen adsorbed on ruthenium. The spiltover hydrogen diffuses from the source to the bridge oxygen sites in the vicinity of the source; i.e., spiltover hydrogen populates only those sites that are near the Ru particles. Further diffusion of the spiltover hydrogen across the silica support may result in a recombination of the spiltover hydrogen to molecular hydrogen. This argument is well supported by the fact that the amount of spiltover hydrogen increases as the total number of Ru particles or the total Ru surface area is increased. A very recent PMR spin-labeling experiment performed on a Rh/SiO_2 catalyst indicates the existence of an unidentified hydrogen species in the immediate neighborhood of the Rh particles (24). The species is likely to be the spiltover hydrogen.

Using the average ruthenium particle sizes listed in Table 2, we estimate the average distance between two Ru particles is to be about 1400 Å for the 1% Ru/SiO_2 catalyst

and 880 Å for the 12% Ru/SiO_2 catalyst. As noted by Sheng and Gay (18) in their study on some Pt/SiO_2 catalysts, the relaxation effect on silanol protons cannot be explained solely by spin diffusion due to dipolar T_2 processes that originates near the metal particles and propagating such long distances. Thus the relaxation effect of the silanol proton can only be caused by the spiltover hydrogen. It is conceivable that T_1 of the spiltover hydrogen is very short, probably on the same order of magnitude as T_1 of the adsorbed hydrogen on Ru (on the order of 10 ms) or even shorter. This short T_1 may be due to weak bonding of the spiltover hydrogen atom to the bridge oxygen atom, which may have a strong relaxation effect. If the distribution of spiltover hydrogen in the silica support is such that most of the spiltover hydrogen is in the vicinity of a Ru particle, then those silanol protons near the Ru particle are expected to relax much faster than those away from the Ru particle. As the total number of ruthenium particles and the total number of surface ruthenium atoms in the catalyst increase, the amount of spiltover hydrogen also increases. An increasing number of silanol protons would then experience the T_1 relaxation effect due to interaction with the spiltover hydrogen. One such possible mechanism of spin interaction is through spin diffusion via dipolar T_2 processes between the spiltover hydrogen and the silanol proton. Another possible form of

interaction may come from chemical exchange between the spiltover hydrogen and the silanol proton. But chemical exchange between the spiltover hydrogen and the silanol proton is much too slow compared to the observed T_1 of the silanol proton, as indicated by the result of the hydrogen-deuterium exchange experiment shown in Figure 10. Therefore, the effect of chemical exchange on the T_1 of the silanol proton is insignificant at room temperature.

As can be seen in Figure 7, the amount of reversible hydrogen on Ru and the amount of spiltover hydrogen increase as the total amount of surface Ru is increased, although they follow a different trend. It seems reasonable to suggest that the increase in the amount of spiltover hydrogen is caused by the increase in the amount of reversible hydrogen on ruthenium. Yet the different increasing trend has also suggested some variation in efficiency of hydrogen spillover. Figure 12 shows the direct correlation between the spiltover hydrogen and the reversible hydrogen on ruthenium on a basis of per surface ruthenium atom. Clearly, hydrogen spillover is more efficient for Ru particles with lower dispersion, even though the fraction of reversible hydrogen per surface Ru atom is less. In other words, spiltover hydrogen coming off a larger ruthenium particle can diffuse farther onto the silica support. This particular result is consistent with the observations of narrower linewidth and longer T_1 for the

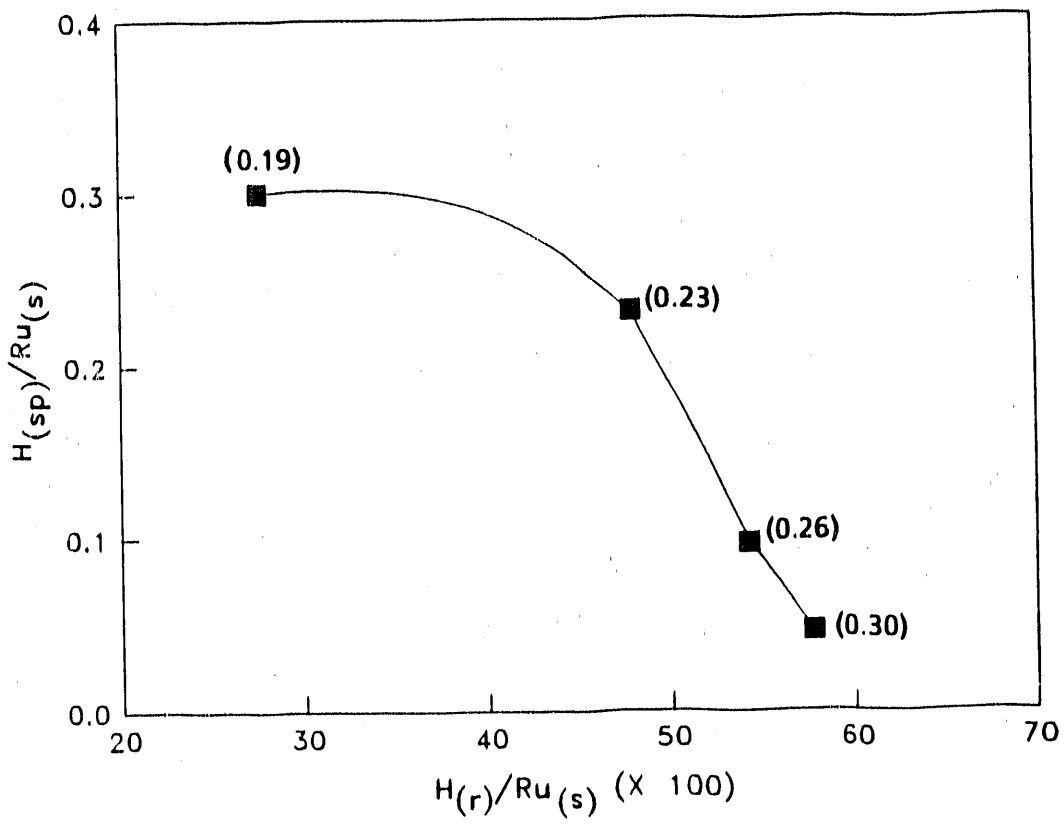

Figure 12. Plot of spiltover hydrogen per surface ruthenium atom versus reversible hydrogen on ruthenium per surface ruthenium atom. The enclosed numbers in parenthesis are values of ruthenium dispersion calculated from PMR measurements of the irreversible hydrogen

reversible hydrogen on larger ruthenium particles. Such observations indicate a higher degree of mobility and weaker interaction with the surface ruthenium atoms.

Thermodynamics indicates that it is unlikely that the irreversibly adsorbed hydrogen on ruthenium would spill over to the silica support at room temperature. This would be a highly endothermic process, with an energy barrier of at least 16 kcal/mol (25, 26). However, hydrogen spillover from the reversibly adsorbed hydrogen on ruthenium to the silica support would seem to be energetically possible at room temperature. The reversibility of this adsorbed state of hydrogen on ruthenium indicates that there is little or no energy barrier that may prevent removal of this state of hydrogen from the surface of ruthenium.

Note that there is an absence of chemical exchange between the deuterium adsorbed on Ru and the silanol proton when the reversible deuterium is removed by evacuation, as indicated by Figure 11. This observation confirms the notion that the irreversible hydrogen on ruthenium does not spill over onto the support. The present results indicate that chemical exchange between the reversibly adsorbed hydrogen on ruthenium and the silanol proton occurs via the spiltover hydrogen that acts as an intermediate for the exchange.

In the case of a hydrogen-deuterium exchange, some of the silanol protons are replaced by the incoming spiltover

deuterium and become spiltover hydrogen, which, in turn, migrates back to a Ru particle and appears as the reversibly adsorbed hydrogen. As indicated by the set of spectra in Figure 10, the reversibly adsorbed hydrogen will replace the irreversibly adsorbed deuterium and become irreversibly adsorbed. The process continues until the surface of Ru is saturated with both adsorbed states of hydrogen.

Hydrogen Adsorbed on Ruthenium

The mobility of the reversible hydrogen on ruthenium is evident from the linewidth of its resonance spectrum, as shown previously in Figure 8. Of all the ruthenium catalysts investigated in this study, the linewidth of the resonance corresponding to the irreversible hydrogen on ruthenium is always 4-6 kHz wider than that corresponding to the weakly bound hydrogen on ruthenium. In other words, the effect of motional averaging of internal interactions between atoms of the reversible hydrogen on Ru results in a reduction of the resonance linewidth by about 5 kHz relative to that of the strongly bound species. If the line broadening of the peak corresponding to hydrogen adsorbed on ruthenium arises from the combined effects of H-H dipolar interactions, chemical shift anisotropy, and magnetic susceptibility broadening, then fast motion should at least average some of the line broadening due to dipolar interactions and chemical shift

anisotropy.

The variation of the upfield resonance shift with the Ru loading (also the dispersion) shown in Figure 9 may be due both to the effect of different Ru adsorption sites and to magnetic susceptibility variations arising from change in the Ru particle size. The effect of different Ru adsorption sites can be clearly seen from the results of T_1 on the adsorbed hydrogen (Table 2). The trend to longer T_1 of the adsorbed hydrogen with increase in ruthenium particle size (or decrease in dispersion) indicates a weaker interaction between the adsorbed hydrogen and the ruthenium adsorption sites. The adsorption sites may be categorized into two types: (I) surface ruthenium atoms on low index planes of crystallites, much like those in ruthenium single crystals; and (II) surface ruthenium atoms on edges and corners or around defect structures, which are less fully coordinated atoms than the first type. As the ruthenium dispersion increases, the fraction of Type II ruthenium atoms increases. If T_1 of the adsorbed hydrogen on Type II ruthenium atoms is much shorter than that on Type I ruthenium atoms, then the observed trend in T_1 can be easily explained. In addition, if the lineshift of the adsorbed hydrogen on Type II Ru atoms is farther upfield than that on Type I Ru atoms, the observed shift variation may also be explained. However, to what extent the magnetic susceptibility of ruthenium particles may

influence the lineshift of the adsorbed hydrogen cannot be determined in the present study. But, since the change in ruthenium particle size with ruthenium loading is moderate, the effect of magnetic susceptibility may be of secondary importance.

The ratio of the reversible hydrogen to surface Ru, as a function of the Ru dispersion, is shown in Figure 13. This ratio is the difference between the total H/Ru ratio and the irreversible H/Ru one measured by PMR divided by the Ru dispersion as measured by PMR of the irreversibly adsorbed hydrogen. The trend to larger $H_{(r)}/Ru_{(s)}$ with increase in dispersion is an indication that the reversible hydrogen is at least in part associated with Type II ruthenium atoms. Some of the reversible hydrogen is also associated with Type I ruthenium atoms since $H_{(r)}/Ru_{(s)}$ for a clean ruthenium powder (about 0.3) is about the same as that for the 12% ruthenium catalyst as measured by the volumetric technique. It is reasonable to conceive that the irreversible hydrogen sits in threefold hollow sites among Type I ruthenium atoms and is relatively less mobile while the reversible hydrogen moves freely on top of surface ruthenium atoms. For the Type II ruthenium atoms, multiple hydrogen adsorption is possible because they are less fully coordinated. In this case, one irreversible hydrogen and one or more reversible hydrogen can be adsorbed on the same site.

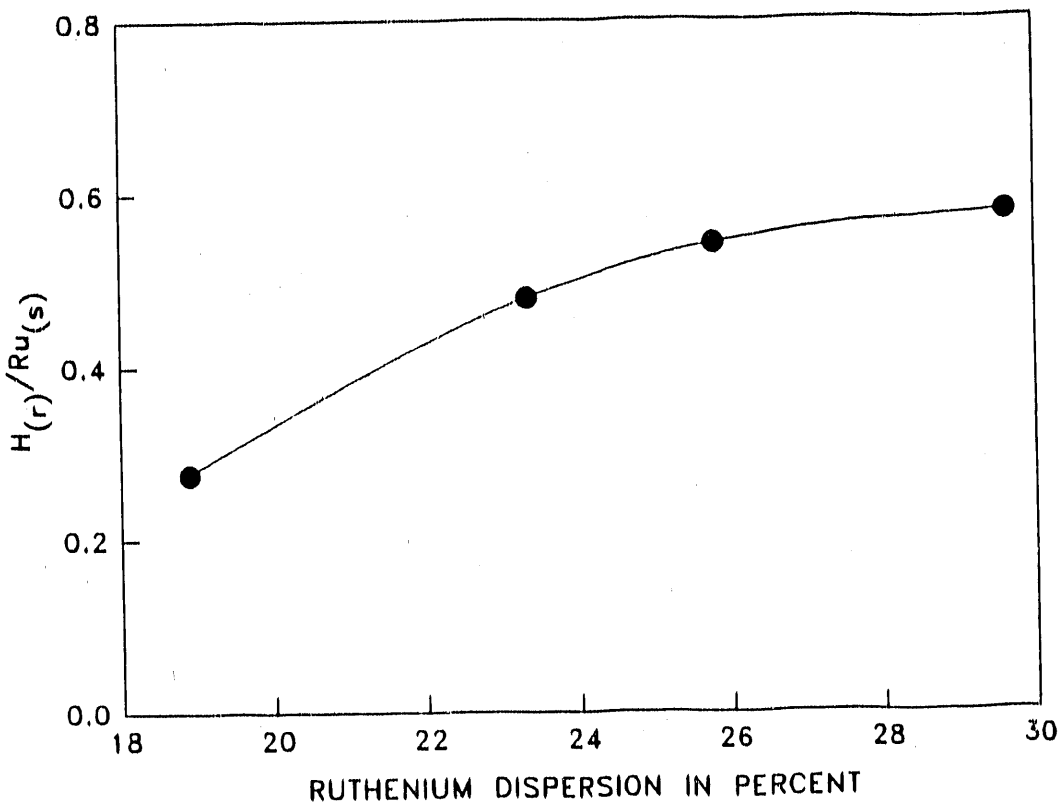

Figure 13. Plot of the ratio of reversible hydrogen on ruthenium to surface ruthenium versus ruthenium dispersion. The amount of reversible hydrogen is measured by PMR. The ruthenium dispersion is calculated from the amount of irreversible hydrogen measured by PMR

CONCLUSIONS

Hydrogen adsorption on Ru/SiO_2 catalysts at ambient temperature generates two adsorbed states of hydrogen on ruthenium, irreversible hydrogen and reversible hydrogen, and two states of hydrogen on silica, spiltover hydrogen and physisorbed hydrogen. The physisorbed hydrogen is of minor importance. The reversible hydrogen on ruthenium is the source of hydrogen spillover. The presence of spiltover hydrogen makes possible the exchange between the hydrogen adsorbed on ruthenium and the silanol proton in the silica support at room temperature. Both the reversible hydrogen and the spiltover hydrogen introduce errors in determining the ruthenium dispersion by the conventional volumetric method. Measurements of the irreversible hydrogen by both PMR and hydrogen chemisorption are in good agreement. The amount of the irreversible hydrogen would appear to be appropriate to use in determination of ruthenium dispersion.

From PMR it is inferred that the reversible hydrogen on ruthenium is much more mobile at room temperature than the irreversible hydrogen. Multiple hydrogen adsorption on ruthenium is suggested for catalysts with high dispersion. At least two different types of ruthenium adsorption sites exist on the surface of ruthenium particles: sites with low index planes and sites with defect-like structures. The relative distribution of these two types of adsorption sites

varies with the ruthenium dispersion. Sites with a lower Ru coordination interact more strongly with the adsorbed hydrogen, possibly due to subtle variations in local valence electron density.

ACKNOWLEDGMENT

This work was fully supported by the U.S. Department of Energy, Office of Basic Energy Sciences, Contract W-7405-ENG-82. The support of the Engineering Research Institute of Iowa State University is also acknowledged.

REFERENCES

1. Dalla Betta, R. A., J. Catal. 34, 57 (1974).

2. Kubicka, H., J. Catal. 12, 233 (1968).

3. Sinfelt, J. H., and Yates, D. J. C., J. Catal. 8, 82 (1967).

4. Gay, I. D., J. Catal. 80, 231 (1983).

5. Taylor, K. C., J. Catal. 38, 299 (1975).

6. Goodwin, J. G., Jr., J. Catal. 78, 182 (1982).

7. Yang, C. H., and Goodwin, J. G., Jr., J. Catal. 78, 182 (1982).

8. Chen, Y. W., Wang, H. T., and Goodwin, J. G., Jr., J. Catal. 83, 415 (1983).

9. Sinfelt, J. H., Lam, Y. L., Cusumano, J. A., and Barnett, A. E., J. Catal. 42, 227 (1976).

10. Rouco, A. J., Haller, G. L., Oliver, J. A., and Kemball, C., J. Catal. 84, 297 (1983).

11. Sermon, P. A., and Bond, G. C., Catal. Rev. 8, 211 (1973).

12. Conner, W. C., Jr., Pajonk, G. M., and Teichner, S. J., in Advances in Catalysis, edited by D. D. Eley, P. W. Selwood, and Paul B. Weisz. (Academic Press, New York, 1986), Vol. 34, pp. 1-79.

13. Narita, T., Miura, H., Sugiyama, K. Matsuda, T., and Gonzalez, R. D., J. Catal. 103, 492 (1987).

14. Narita, T., Miura, H., Sugiyama, K., Matsuda, T., and Gonzalez, R. D., Appl. Catal. 32, 185 (1987).

15. Lu, K., and Tatarchuk, B. J., J. Catal. 106, 166 (1987).

16. Lu, K., and Tatarchuk, B. J., J. Catal. 106, 176 (1987).

17. De Menorval, L. C., and Fraissard, J. P., Chem. Phys. Lett. 77, 309 (1981).

18. Sheng, T. C., and Gay, I. D., J. Catal. 71, 119 (1981).

19. Sheng, T. C., and Gay, I. D., J. Catal. 77, 53 (1982).

20. King, T. S., Wu, X., and Gerstein, B. C., J. Am. Chem. Soc. 108, 6056 (1986).

21. Wu, X., Gerstein, B. C., and King, T. S., J. Catal. 123, 43 (1990).

22. Cheung, T. T. P., Worthington, L. E., Murphy, P. D. B., and Gerstein, B. C., J. Magn. Reson. 41, 158 (1980).

23. Sanz, J., and Rojo, J. M., J. Phys. Chem. 89, 4974 (1985).

24. Root, T. W., and Duncan, T. M., Chem. Phys. Lett. 137, 57 (1987).

25. Shimizu, H., Christmann, K., and Ertl, G., J. Catal. 61, 412 (1980).

26. Feulner, P., and Menzel, D., Surf. Sci. 154, 465 (1985).

SECTION II

CHARACTERIZATION OF SILICA-SUPPORTED CU MONOMETALLIC AND RU-CU BIMETALLIC CATALYSTS BY HYDROGEN CHEMISORPTION AND NMR OF ADSORBED HYDROGEN

CHARACTERIZATION OF SILICA-SUPPORTED CU MONOMETALLIC AND RU-CU BIMETALLIC CATALYSTS BY HYDROGEN CHEMISORPTION AND NMR OF ADSORBED HYDROGEN

Xi Wu[1]

Bernard C. Gerstein[2]

Terry S. King[1]

[1]Department of Chemical Engineering and Ames Laboratory

231 Sweeney Hall

Iowa State University

Ames, Iowa 50011

[2]Department of Chemistry and Ames Laboratory

229 Spedding Hall

Iowa State University

Ames, Iowa 50011

ABSTRACT

Monometallic Ru/SiO_2 and Cu/SiO_2 catalysts and a series of $Ru\text{-}Cu/SiO_2$ bimetallic catalysts were studied in detail by hydrogen chemisorption and nuclear magnetic resonance (NMR) of adsorbed hydrogen. NMR indicates that adsorption of hydrogen on pure Cu/SiO_2 at room temperature results in formation of a mobile, atom-like adsorbed species. Spillover of hydrogen from Ru to Cu in the $Ru\text{-}Cu/SiO_2$ bimetallic catalysts was clearly shown by the two techniques. Two distinct adsorbed states of hydrogen were observed on surfaces of the Ru-Cu bimetallic particles. One state is reversibly adsorbed at room temperature while the other is irreversibly adsorbed. The reversible hydrogen exhibits rapid motion at the surface; the irreversible hydrogen is less mobile. Surface compositions for all the $Ru\text{-}Cu/SiO_2$ bimetallic catalysts were obtained from the NMR resonance lineshifts of the reversible hydrogen. The results show a preferential segregation of Cu to surfaces of Ru particles, and indicate formation of large Cu islands on ruthenium and separate pure Cu particles at very high copper loadings.

INTRODUCTION

Supported Ru-Cu bimetallic catalysts (1-14), Ru-Cu aggregates (15, 16), and single crystal Ru surfaces dosed with copper (17-29) have been the frequent subjects of fundamental investigations of catalytic phenomena. Most previous investigations searched for evidence of the ensemble (or geometric) effect and electronic (or ligand) effect, suggested to be the two most important factors in the right interpretation of the catalytic behavior of the supported Ru-Cu bimetallic catalysts (2).

Ruthenium and copper are known to be immiscible in the bulk (30). Therefore, if there is any direct interaction between the two metals on a microscopic level, it is likely to occur at the interface. On the silica-supported Ru-Cu bimetallic catalysts, Sinfelt et al. (15) have proposed a microscopic model of "bimetallic clusters" with copper atoms covering the surfaces of ruthenium particles in a manner analogous to chemisorption. This model was supported later by results from extended X-ray absorption fine structure (EXAFS) (31). To account for the observed drop in ethane hydrogenolysis activity with increasing copper content of these supported bimetallic catalysts, Sinfelt and coworkers (2, 4) have suggested the ensemble effect as one possible explanation.

The most studied Ru-Cu model system is the single

crystal Ru(001) surface with varying degrees of copper coverage. No convincing evidence of the ensemble effect was observed for this system catalyzing the ethane hydrogenolysis reaction (32). Two recent studies (28, 33) showed that copper forms large two-dimensional islands before completion of a monolayer. Kim et al. (33) have concluded that the model Cu/Ru(001) bimetallic system could not be applied directly to the Ru-Cu bimetallic aggregates and supported Ru-Cu bimetallic catalysts because of the highly defected nature of aggregates and small particles.

Electronic interaction between ruthenium and copper may also influence catalytic behavior. An XPS study on Ru-Cu aggregates (16) showed no evidence of core level electronic interactions between the two metals. A number of studies by UPS (24, 34) and thermal desorption of CO (21, 24-25, 27) on the Cu/Ru(001) model system indicated the existence of a small electronic perturbation around the Ru-Cu interface region, probably via the valence electrons of the metals. Thermal desorption of adsorbed hydrogen from the same model system (26) seemed not to be sensitive enough to observe variations in binding energies associated with an electronic effect. If this electronic perturbation is significant, then the activation energies for various reactions on Ru could be altered by incorporation of Cu.

Sinfelt reported seeing no variation in activation

energy for the ethane hydrogenolysis reaction when copper is added to silica-supported ruthenium (2). Similarly, Bond and Turnham (11), studying CO hydrogenation, found the activation energy to be invariant with copper content. On the other hand, Lai and Vickerman (13) did measure a variation in activation energy for the CO hydrogenation reaction. Recent work in our laboratories that used chlorine-free Ru-Cu/SiO_2 catalysts also indicated variations in activation energies for the ethane hydrogenolysis reaction (35).

To clearly distinguish between ensemble and electronic effects (if they exist) and to interpret catalytic results properly, one must know the amount of active metal (in this case Ru) available at the surface. Hydrogen chemisorption has been used to titrate the amount of Ru at the surface in the Ru-Cu bimetallic system. The method is based on the assumption that Cu does not dissociatively adsorb molecular hydrogen, and it seems to be true for single crystal copper surfaces where the adsorption of molecular hydrogen is an activated process with an activation energy of about 5 kcal /mol (36, 37). However, conflicting results on the observed influence of Cu in hydrogen chemisorption capacity of Ru have been reported on silica-supported Ru-Cu catalysts. Sinfelt et al. (2, 4, 15) reported a marked suppression of hydrogen chemisorption by Cu while Haller and co-workers (5, 6) found no significant influence of Cu on the hydrogen chemisorption

capacity of ruthenium. This latter finding was attributed to spillover of atomically adsorbed hydrogen from ruthenium sites to adjacent copper sites after dissociative adsorption of molecular hydrogen on ruthenium. Recent studies (38, 39) on the Cu/Ru(001) model system also revealed such a hydrogen spillover phenomenon at temperature above 230 K. This view was later supported by an NMR study on hydrogen chemisorbed on Ru-Cu/SiO_2 catalysts at room temperature (40). These results confirmed the spillover of hydrogen from ruthenium to copper on supported Ru-Cu bimetallic catalysts.

With only a few exceptions (5-7) the ruthenium salt $RuCl_3 \cdot nH_2O$ has been used as a precursor in preparing Ru-Cu/SiO_2 catalysts in previous investigations. The effect of chlorine contamination on the hydrogen chemisorption capacity of Ru has been overlooked until recently. A number of recent studies (41-43) have indicated that a substantial amount of chlorine remains on the surfaces of ruthenium particles after reduction at normal reduction temperatures (573 - 773 K), and the residual chlorine inhibits adsorption of hydrogen on ruthenium. Recent results in the authors' laboratory have supported this picture (44). If the incorporation of Cu further inhibits the reducibility of $RuCl_3$, then one may observe an apparent suppression of hydrogen chemisorption capacity upon addition of copper. The introduction of chlorine complicates the characterization of Ru/SiO_2 and Ru-

Cu /SiO_2 catalysts by hydrogen chemisorption. The inability to characterize these bimetallic catalysts cast doubt upon the interpretation of reaction data obtained from these catalysts in the previous investigations.

The objectives of the present study were to re-examine the phenomenon of hydrogen spillover from Ru to Cu and to determine the overall surface compositions of the Ru-Cu bimetallic particles on clean Ru-Cu/SiO_2 catalysts by means of hydrogen chemisorption and nuclear magnetic resonance of adsorbed hydrogen.

EXPERIMENTAL METHODS

Catalyst Preparation

The Ru/SiO_2 and Cu/SiO_2 catalysts were prepared by incipient wetness impregnation of a ruthenium or copper impregnating solution with a dried Cab-O-Sil HS5 (300 m^2/g BET surface area) silica support. The $Ru-Cu/SiO_2$ catalysts were prepared by co-impregnation of a mixed ruthenium-copper impregnating solution in the same manner. The impregnating solutions were prepared by dissolving either $Ru(NO)(NO_3)_3$ salt (AESAR) or $Cu(NO_3)_2 \cdot 6H_2O$ (AESAR, 99.999%) or both in distilled water. About 2.2 ml of impregnating solution per gram of SiO_2 was sufficient to bring about incipient wetness. The slurries obtained after impregnation and mixed were dried for 24 hours at room temperature and 4 hours in air at 383 K. The ruthenium loading for all ruthenium-containing catalysts was kept at 4% by total weight of the support and metals. The copper loading for the Cu/SiO_2 catalyst was 5%. A total of ten different $Ru-Cu/SiO_2$ catalysts were prepared to give a wide range of copper loading. The amount of copper in each $Ru-Cu/SiO_2$ catalyst and the Cu/SiO_2 catalyst was determined by atomic absorption spectroscopy.

Volumetric Adsorption Apparatus

The adsorption apparatus was a multiport Pyrex glass manifold with 127.3 cm^3 in volume connected to a high-vacuum system, which included a turbo-molecular pump (Balzers, Model TPH050), a fore-pump trap, and a two-stage mechanical pump. The apparatus was designed to have a flow-through capability for reduction of catalyst samples. High-vacuum greaseless, bakeable stopcocks (Ace Glass) with Teflon plugs and FETFE o-ring seals were employed to manipulate gas storage, dosage, or both and eliminate hydrocarbon contamination in the manifold. The manifold was capable of a vacuum better than 10^{-7} Torr (1 Torr = 133.3 Pa) after bakeout. Pressure below 10^{-2} Torr were monitored by a cold cathode vacuum gauge (Varian, Model 860A). Pressures from 0.01 Torr to 1000 Torr were measured by two absolute Baratron pressure gauges (MKS).

A flow-through Pyrex cell mounted with a coarse glass frit (35 μm in average pore diameter) was used to contain catalyst samples for the volumetric adsorption experiments. A small furnace was used to provide uniform heating to the cell. The temperature inside the furnace was controlled by a proportional temperature controller (Omega) to within ± 1 K.

Catalyst Reduction and Volumetric Adsorption

Approximately one gram of a catalyst sample was loaded into the flow-through cell, which was then attached to one of

the sample ports of the manifold. The temperature around the cell was raised to 423 K while helium gas flowed through the sample bed in the cell. Then helium was switched off and replaced by hydrogen gas at a flow rate of 50 cm^3/min. A pre-reduction period of 1 hour proceeded at that temperature. Temperature was then raised at a rate of 10 K/min to 723 K. Further reduction was carried out for two additional hours at 723 K. Helium (99.999%) and hydrogen (99.8%) gases (Liquid Air Co.) were used as received. After reduction, the sample was evacuated for two hours at 723 K to remove traces of water and surface hydrogen. The reduction temperature used for the 5% Cu/SiO_2 catalyst was 623 K.

Hydrogen for volumetric adsorption and dosage on NMR samples was purified by passing it through a catalytic hydrogen purifier (Engelhard Deoxo) in series with a gas purifier with Drierite and a 5Å molecular sieve (Alltech) to remove traces of oxygen and moisture. Hydrogen adsorption experiments were performed at ambient temperature (294 K). The total hydrogen adsorption isotherm was measured in the pressure range of 0-60 Torr. The isotherm for the reversible hydrogen adsorption was measured under the same conditions after a 10-minute evacuation to a pressure of 10^{-6} Torr following the total adsorption. The irreversible hydrogen uptake was obtained by taking the difference between the extrapolated values of the total and the reversible isotherms

at zero pressure. Equilibration times used were 4 hours for the first dose and 1 hour for subsequent doses.

NMR Sample Treatment

A specially designed stainless steel needle-bellows assembly was used for direct reduction of a catalyst sample in flowing hydrogen inside a 5-mm NMR tube. The syringe needle (18 gauge) was capable of moving vertically by more than 6 cm through adjustable compression and extension of the bellows. Vacuum-tight connections were made between the NMR tube and the needle-bellows assembly and also between the assembly and the manifold described above. In addition, a small cylindrical furnace provided uniform heating around the NMR tube, and the temperature of the furnace was controlled to within ± 1 K.

With helium gas flowing through the needle, the needle was lowered to the bottom of the NMR tube, which contained approximately 60 mg of catalyst sample. The reduction procedure was the same as previously described for the volumetric adsorption experiment, with a hydrogen flow rate of 15 cm^3/min. After reduction, the needle was elevated out of the sample, and evacuation proceeded for 2 hours at the reduction temperature before the sample was allowed to cool to ambient temperature. Up to four samples could be reduced simultaneously. Purified hydrogen was then dosed through the

needle to each sample separately, and the system was allowed to equilibrate for 4 hours. The NMR tube containing the sample was then immersed in a water bath and was sealed off with a micro-torch. The sample weight was measured after the NMR tube was sealed. For the deuterium exchange experiment, deuterium gas (Linde, 99.5%) instead of hydrogen was used as the adsorbate.

NMR Experiments

The home-built NMR spectrometer (46) used for the present study was operated at 220 MHz for proton resonance. A proton-free probe with a doubly wound coil (47) was used for all the NMR measurements. The probe quality factor Q was set at about 100 to obtain the optimal values of sensitivity and ringdown time for a fixed pulse power. A detailed description of the spectrometer's rapid-recovery receiving system has been published elsewhere (48).

All NMR spectra collected were under a repetitive 90° single pulse sequence. The recycle time between rf pulses was set at 0.2 sec to selectively suppress the intensity of the resonance corresponding to protons in the silanol group in the silica support, which has a relatively long spin-lattice relaxation time T_1 (on the order of seconds). This repetition rate avoids T_1 saturation on all resonances corresponding to hydrogen adsorbed on ruthenium and copper.

The total number of scans for data acquisition on each sample was 10,000. The inversion recovery pulse sequence (180°-τ-90°) was applied to measure the spin-lattice relaxation times of both the silanol protons (in the time domain) and the hydrogen adsorbed on metals (in the frequency domain). A pure water sample was used as the reference standard for the observed lineshifts.

For spin counting, the water reference was doped with $FeCl_3$ to yield a resonance of a comparable linewidth with the observed resonances. The doped water was sealed in a glass capillary tube that had the same length as the sample in the NMR tube to offset errors due to B_1 inhomogeneity in the coil. All NMR measurements were taken at ambient temperature (294 ± 1 K).

RESULTS

Copper Monometallics

The amount of hydrogen adsorbed on a pure SiO_2 sample treated in the same way as a silica-supported catalyst was measured. The results shown in Figure 1 indicate that there is a very small amount of adsorbed hydrogen on pure SiO_2 in the hydrogen pressure range of 5 to 30 Torr. However, a linear extrapolation of the adsorption isotherm to zero hydrogen pressure yields no hydrogen uptake. Consequently, hydrogen adsorption by the support has no contribution in similar measurements on silica-supported metal catalysts.

The volumetric technique applied to the 5% Cu/SiO_2 catalyst indicated that there was hydrogen adsorption by copper, as shown also in Figure 1. By linear extrapolation of either the total or the reversible isotherm to zero pressure, it is clear that a small amount of chemisorbed hydrogen exists on copper. On the same basis, this hydrogen uptake was less than 3% of that for a 4%Ru/SiO_2 catalyst (shown later). The dispersion of the 5%Cu/SiO_2 catalyst was about 0.06 as measured by nitrous oxide adsorption (49).

NMR of adsorbed hydrogen on the 5% Cu/SiO_2 catalyst yielded similar results. As shown in Figure 2, NMR spectra of hydrogen adsorbed on a 5% Cu/SiO_2 sample display two distinct resonance lines. The line near the reference shift

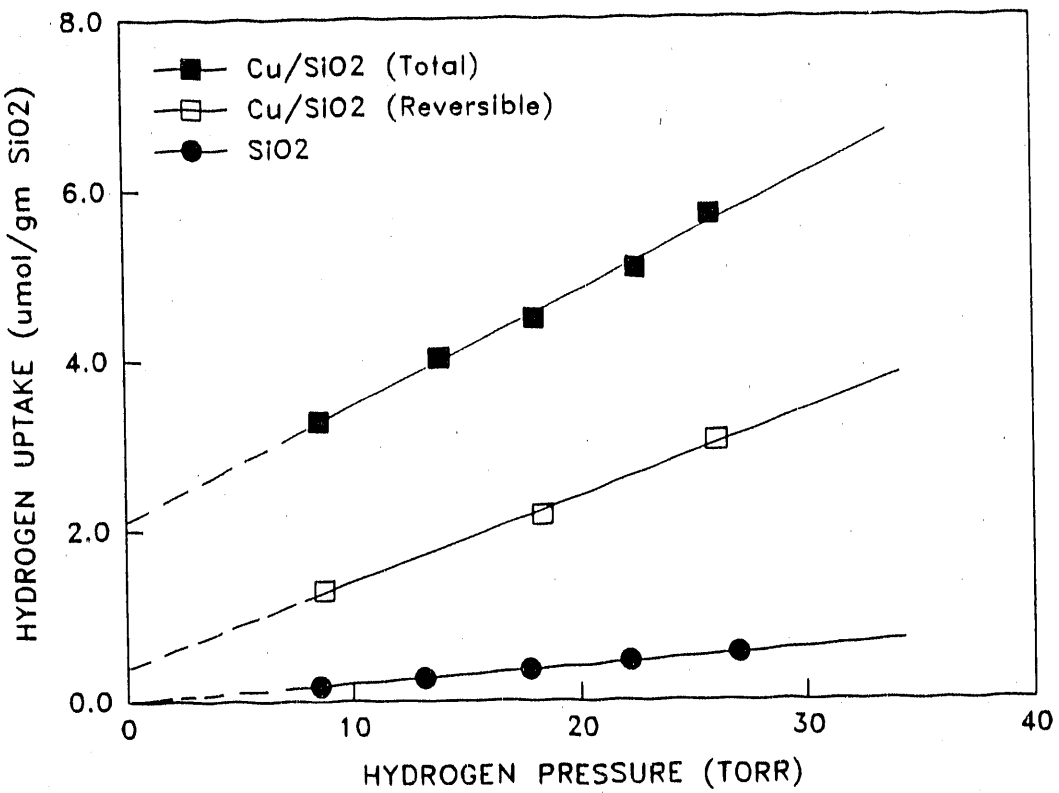

Figure 1. Hydrogen adsorption isotherms (294 K) measured by the volumetric technique on a pure SiO_2 sample and a 5% Cu/SiO_2 catalyst

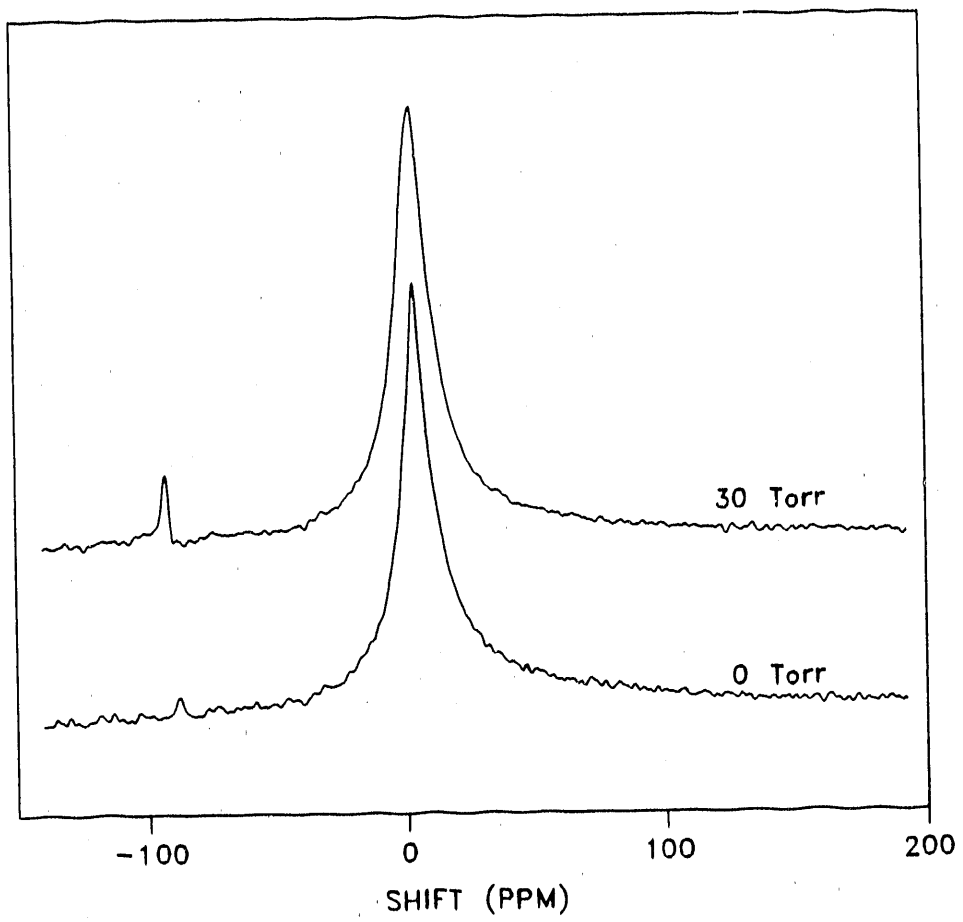

Figure 2. NMR spectra of adsorbed hydrogen on a 5% Cu/SiO_2 catalyst. Hydrogen pressures are as indicated. "0 Torr" denotes an evacuation condition of 10^{-6} Torr for 10 min at 294 K after adsorption under 30 Torr hydrogen. Water is used as a reference for the lineshift

position (4 ± 1 ppm) was identified as the proton in the silanol group (Si-OH) in the silica support. Only this resonance line appeared for samples of pure SiO_2 either in vacuum or under 30 Torr hydrogen gas. The resonance line downfield to that of the silanol proton was assigned to hydrogen adsorbed on pure copper surfaces. For the Cu/SiO_2 sample under 30 Torr hydrogen gas, the position of the downfield peak is at -93 ppm, and the peak displays a sharp feature with a linewidth (full width at half maximum) of about 730 Hz. A similar shift value for hydrogen adsorbed on a copper powder relative to an unknown reference has been reported (50). When the Cu/SiO_2 sample is evacuated to 10^{-6} Torr for 10 min after dosage of 30 Torr hydrogen gas, the downfield peak is diminished in intensity but observable. Its position has moved from -93 ppm to -88 ppm. The amount of adsorbed hydrogen determined by proton spin counting via NMR agrees roughly with volumetric adsorption measurements.

The H/Cu ratio is about 10% of what would be expected from a complete coverage of hydrogen at the measured copper dispersion. In other words, only 10% of the surface copper atoms are capable of adsorbing hydrogen. This result agrees with results from studies on bulk Cu surfaces (50-52) which also show low coverages by hydrogen.

Ruthenium-Copper Bimetallics

In Figure 3 is shown a single NMR spectrum of a mixture of Cu/SiO_2 and Ru/SiO_2 under 30 Torr hydrogen. The physical mixture was prepared by mechanically mixing an approximately equal amount of a reduced 4% Ru/SiO_2 and 5% Cu/SiO_2 catalyst. The mixture was then reduced again at 623 K for 1 hour. The sample prepared in this manner should contain only separate Ru and Cu metal particles. As shown in Figure 3, two well separated resonance lines other than the silanol proton resonance line were observed. The upfield peak relative to the silanol proton peak was located at + 62 ppm and had a relatively intense resonance signal. This upfield peak is identified as the resonance of hydrogen adsorbed on pure ruthenium surfaces (53). The intensity of the downfield peak (-93 ppm), associated with hydrogen adsorbed on copper, was relatively weak. The spectrum clearly demonstrates the coexistence of only separate pure Ru and Cu particles in the Ru/Cu physical mixture.

A set of NMR spectra for the 4% Ru/SiO_2 catalyst and the 4% $Ru-Cu/SiO_2$ catalysts with a wide range of copper loading are shown in Figure 4. The copper content is given as an atomic percent of the total number of metal atoms in a given catalyst. NMR of ^1H on all catalyst samples was obtained with the sample under 60 Torr hydrogen gas. As expected for the Ru/SiO_2 catalyst, a distinct resonance line corresponding

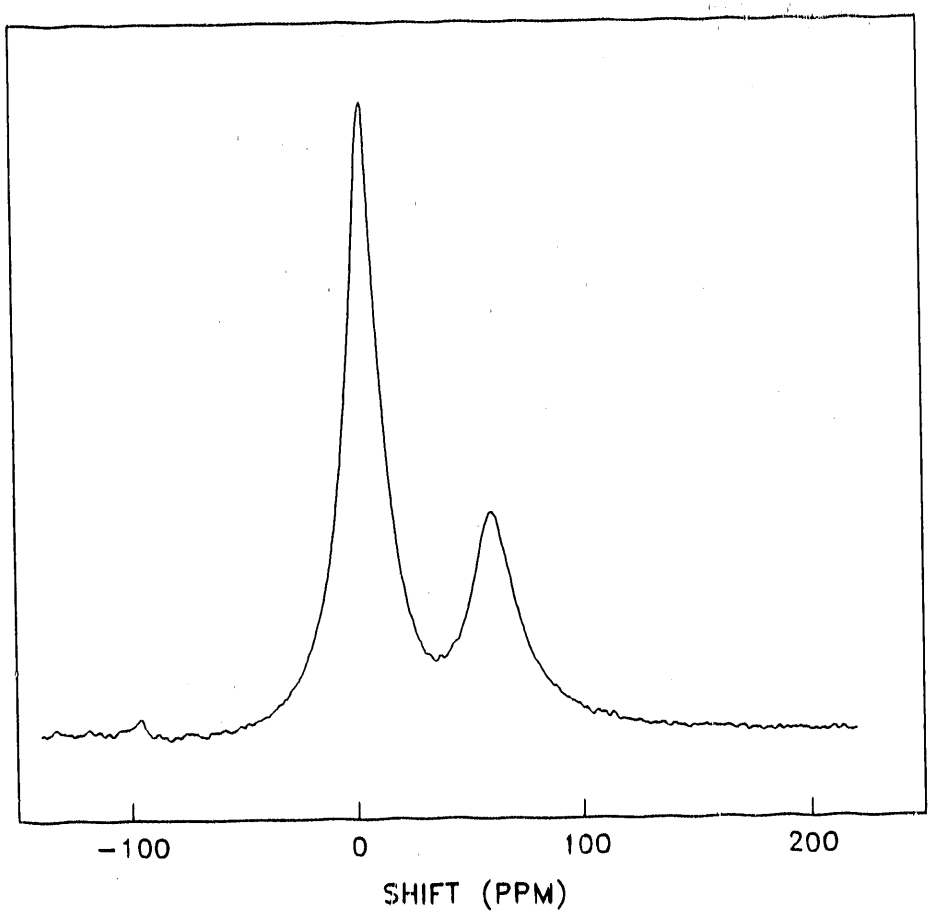

Figure 3. An NMR spectrum on a Ru/SiO_2 + Cu/SiO_2 physical mixture under 30 Torr hydrogen. The mixture contains approximately equal amounts of a 4% Ru/SiO_2 and a 5% Cu/SiO_2 catalyst

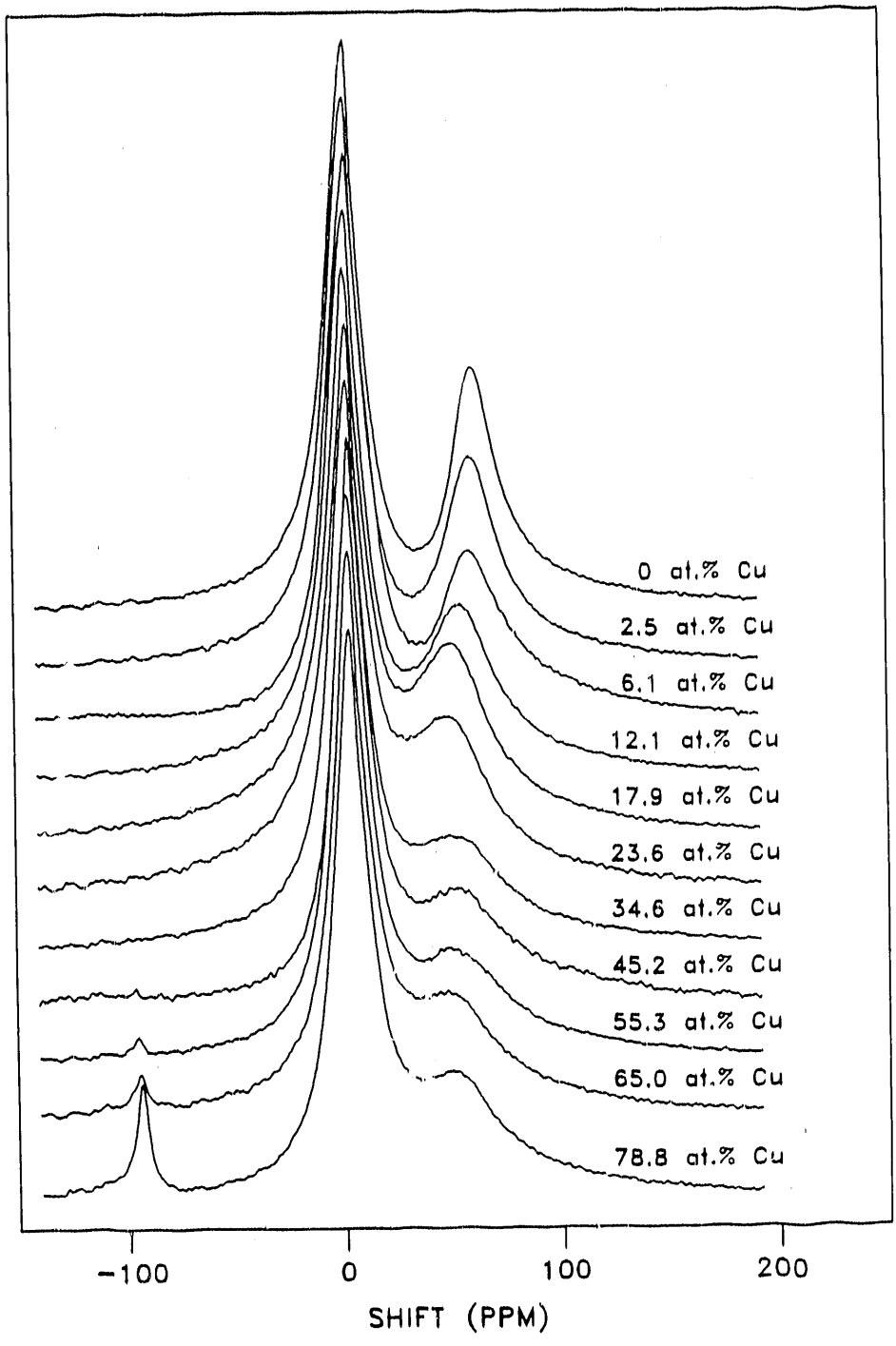

Figure 4. NMR spectra of adsorbed hydrogen on a series of Ru-Cu/SiO_2 bimetallic catalysts under 60 Torr hydrogen. The copper bulk compositions expressed as atomic percent are as indicated

to hydrogen adsorbed on ruthenium appeared at + 61 ppm upfield of the reference (53). Three interesting features developed as the copper loading was increased: (1) the position of the upfield peak moved downfield toward the silanol proton peak with an increase in the copper loading; (2) the linewidth of the upfield peak became broadened and its intensity lowered as the copper loading was increased, and the combined effect of these two trends resulted in a reduced spectral resolution due to increased overlap between the upfield peak and the silanol proton peak; and (3) a peak became visible downfield of the silanol proton peak, at copper bulk compositions of about 45 at.% and higher. The downfield peak intensity was increased with an increase in the copper loading. Also, there was a small upfield shift of the downfield peak with an increase in the copper loading.

The silanol proton peak has a symmetric lineshape. The upfield peak is asymmetric. The upfield resonance can be deconvoluted by subtracting the silanol proton peak from the spectrum. The intensity of the upfield peak can then be obtained by integrating the area under the deconvoluted upfield peak. The location of the upfield peak is taken to be the first moment of the deconvoluted resonance line.

The changes of the upfield peak position and resonance linewidth with variation in the copper loading are clearly an effect solely due to incorporation of copper because the Ru

loading and the hydrogen pressure are kept constant for all the catalyst samples. As shown earlier in Figure 3, the resonance position and linewidth of the upfield resonance corresponding to hydrogen adsorbed on pure Ru surfaces is not affected by physically mixing Cu/SiO_2 with Ru/SiO_2. This result indicates that copper and ruthenium do come together to form Ru-Cu bimetallic particles upon reduction of the coimpregnated $Ru/Cu/SiO_2$ materials.

The position of the downfield resonance for $Ru-Cu/SiO_2$ catalysts with a copper composition greater than 45 at.% were in the range of -93 ppm to -97 ppm. The assignment of this downfield peak to hydrogen adsorbed on pure copper surfaces was reasonable because we observed a similar lineshift on a pure Cu/SiO_2 catalyst sample (Figure 2). The emergence of this peak may indicate the formation of large Cu islands on the Ru-Cu bimetallic particles or buildup of separate copper particles.

Figure 5 shows a set of NMR spectra for the 4% Ru/SiO_2 catalyst and six 4% $Ru-Cu/SiO_2$ catalysts having various copper loadings. All catalyst samples were evacuated to 10^{-6} Torr for 10 min after adsorption with 60 Torr hydrogen. Obviously, the upfield peak corresponding to the irreversibly adsorbed hydrogen on surfaces of pure Ru or Ru-Cu bimetallic particles exhibits an asymmetric resonance line that is considerably broader than the upfield peak under 60 Torr

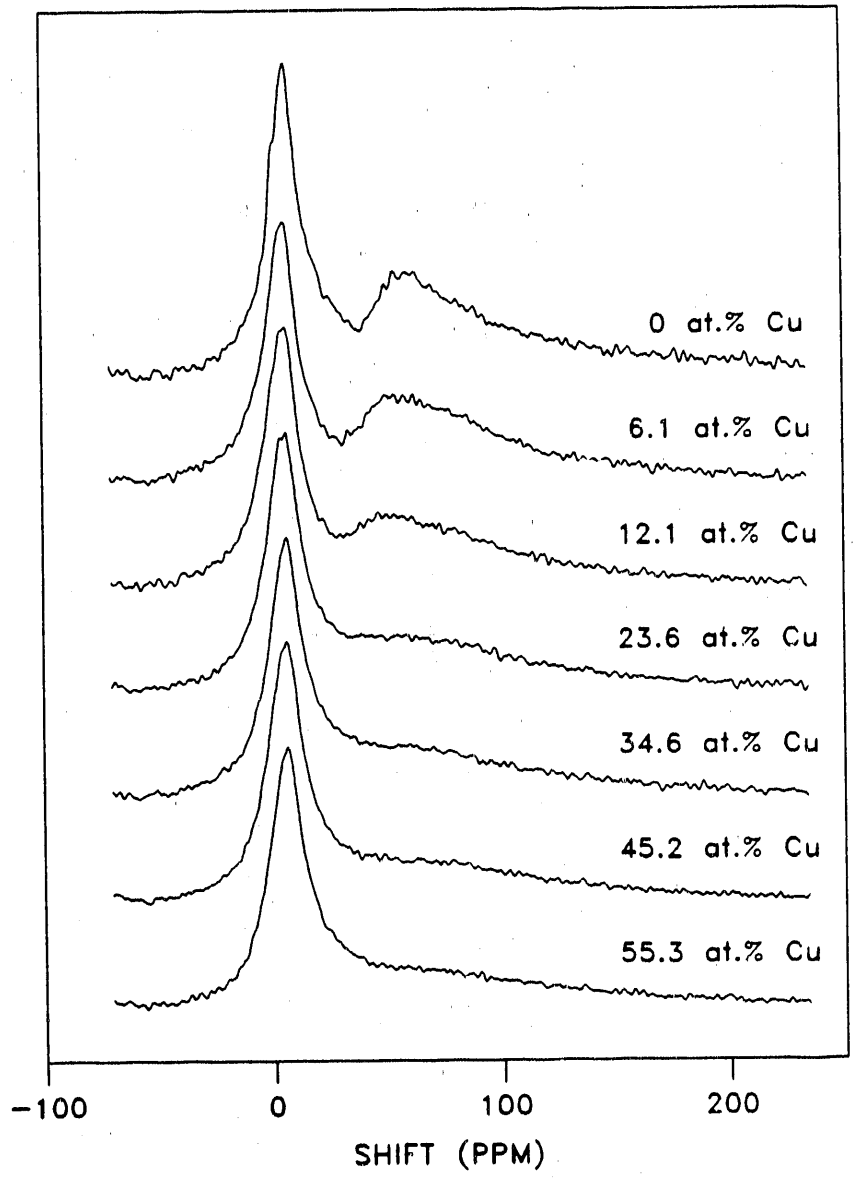

Figure 5. NMR spectra of the irreversibly adsorbed hydrogen on a series of Ru-Cu/SiO_2 bimetallic catalysts. The copper bulk compositions expressed as atomic percent are as indicated

hydrogen (see Figure 4). While the intensity of this peak decreases with an increase in the Cu loading, its linewidth increases from 10.9 kHz for the pure Ru/SiO_2 sample to 22.6 kHz for the Ru-Cu bimetallic sample having a bulk copper composition of 55.3 atom percent. No resonance signals downfield from the silanol proton peak were observed for all the catalysts shown in this figure. However, we did observe a very weak resonance signal downfield of the silanol proton peak for a $Ru-Cu/SiO_2$ bimetallic catalyst sample with a bulk copper composition of 78.8 at.% (not shown in Figure 5). This NMR spectrum will be shown later along with spectra for the same catalyst under various hydrogen pressures.

The asymmetry of the upfield peaks shown in Figure 4 was caused by the asymmetric feature of the upfield resonances corresponding to the irreversible hydrogen as shown in Figure 5. As indicated in previous investigations on a number of pure Ru/SiO_2 catalysts, the spectral asymmetry for samples under 5 Torr hydrogen may be removed simply by subtracting the corresponding resonance line for the strong hydrogen adsorption from the observed spectra (53). The result is a near-symmetric resonance resembling a Lorentzian line that corresponds to the reversibly adsorbed hydrogen on ruthenium. The same approach was applied here for all the $Ru-Cu/SiO_2$ bimetallic catalysts by subtracting the resonance line for the irreversibly adsorbed hydrogen from that corresponding to

the same catalyst under 60 Torr hydrogen. The resulting difference spectra were indeed nearly symmetric and were much narrower. The linewidth was in the range of 3.6 to 8.9 kHz compared to 10.9 to 24.0 kHz for the irreversible hydrogen, with the Ru/SiO_2 catalyst having the narrowest linewidth. This spectral narrowing is an indication of a higher degree of mobility for the reversibly adsorbed than the irreversibly adsorbed hydrogen.

In Figure 4 and Figure 5, the upfield peak-integrated intensity decreased with an increase in copper content. The apparent decrease in the upfield peak intensity in both cases was associated with line broadening of the irreversibly adsorbed hydrogen with addition of copper. The loss of intensity is caused by the increased loss of the initial intensity due to receiver ring-down in the time domain. The relative intensity of the upfield peak corresponding to the reversible hydrogen as measured from the difference spectrum remains roughly the same for all the Ru/SiO_2 and $Ru-Cu/SiO_2$ samples.

The intensity measurements for the upfield peak were performed on all the Ru/SiO_2 and $Ru-Cu/SiO_2$ catalysts under various hydrogen pressures in a range from 5 to 60 Torr. Similar to what was observed on numerous Ru/SiO_2 catalysts (53), adsorption isotherms obtained in this manner exhibit nearly straight lines over this hydrogen pressure range. The

slopes of these isotherms match closely those obtained by the volumetric method of hydrogen chemisorption. All isotherms were extrapolated to zero hydrogen pressure to obtain values of the H/Ru ratio. The dependence of the upfield resonance intensity with the hydrogen pressure indicates that more reversibly adsorbed hydrogen is present on surfaces of Ru and Ru-Cu particles under higher hydrogen pressure.

The values of the H/Ru ratio (extrapolated to zero pressure) for the total and the strong hydrogen adsorption as measured by both hydrogen chemisorption and NMR of adsorbed hydrogen are shown in Figure 6 as functions of atomic percent copper. Contrary to that reported by Sinfelt (2), perhaps due to different catalyst precursors used, addition of copper to ruthenium does not suppress the hydrogen chemisorption capacity in case of both the total and the strong hydrogen adsorption as measured by the volumetric technique. Rather, it slightly enhances the capacity for hydrogen chemisorption. This observation agrees with the results reported by Rouco et al. (5). The apparent hydrogen chemisorption capacity measured by the upfield resonance intensity from the proton NMR spectrum decreases with the addition of copper. This apparent loss of intensity is due to the increasingly broad spectral features as shown in Figures 4 and 5. However, the chemisorption capacity for the reversible hydrogen (taken as the difference between the total and the irreversible

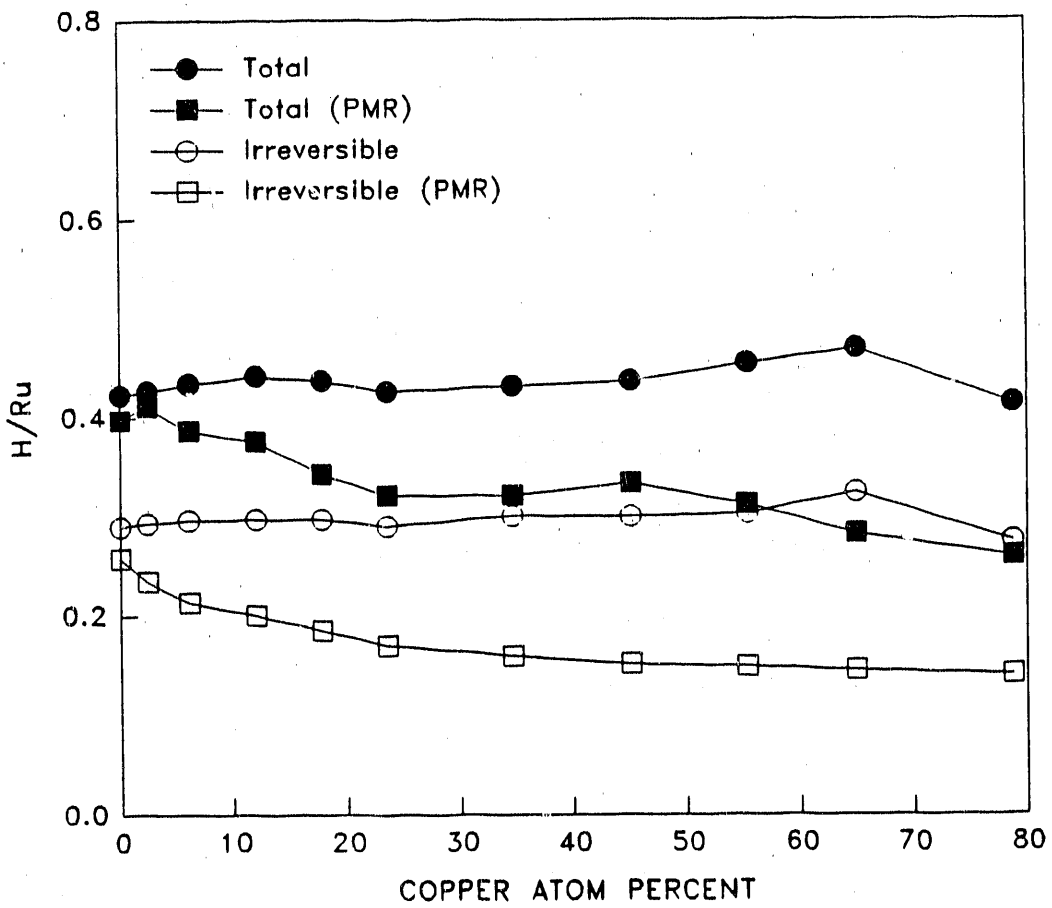

Figure 6. The H/Ru ratios for both the total and the irreversible adsorption of hydrogen on a series of Ru-Cu/SiO_2 bimetallic catalysts. Results from measurements by both the volumetric technique and proton NMR are shown for comparison

adsorption) remains almost unchanged for all the Ru/SiO_2 and $Ru-Cu/SiO_2$ catalysts as measured by both the volumetric technique and NMR of adsorbed hydrogen.

The effect of copper content on the location of the upfield resonance line has been illustrated in Figure 4. The numerical values of this lineshift as calculated by the first moment as a function of copper content are shown in Figure 7. Also shown in the figure are the shifts in first moment for the reversibly adsorbed hydrogen obtained from the difference spectra between the NMR spectra under 60 Torr hydrogen and the corresponding NMR spectra for the irreversible hydrogen. The results in Figure 7 indicate that the first moment of the resonance for the reversibly adsorbed hydrogen is slightly upfield relative to the resonance corresponding to all the hydrogen adsorbed at 60 Torr on the Ru/SiO_2 and $Ru-Cu/SiO_2$ catalysts. For both the reversible and total hydrogen, a similar trend for the lineshift as a function of copper content was observed. A relatively large change in the upfield peak lineshift occurred at copper bulk compositions between 0 and 20 atomic percent. Further increase in the copper content resulted in only a small decrease in the lineshift. Although the resonance shifts for the strong hydrogen are not shown, they are slightly further downfield than those under 60 Torr hydrogen and exhibit the same trend as a function of the copper content. The shift associated

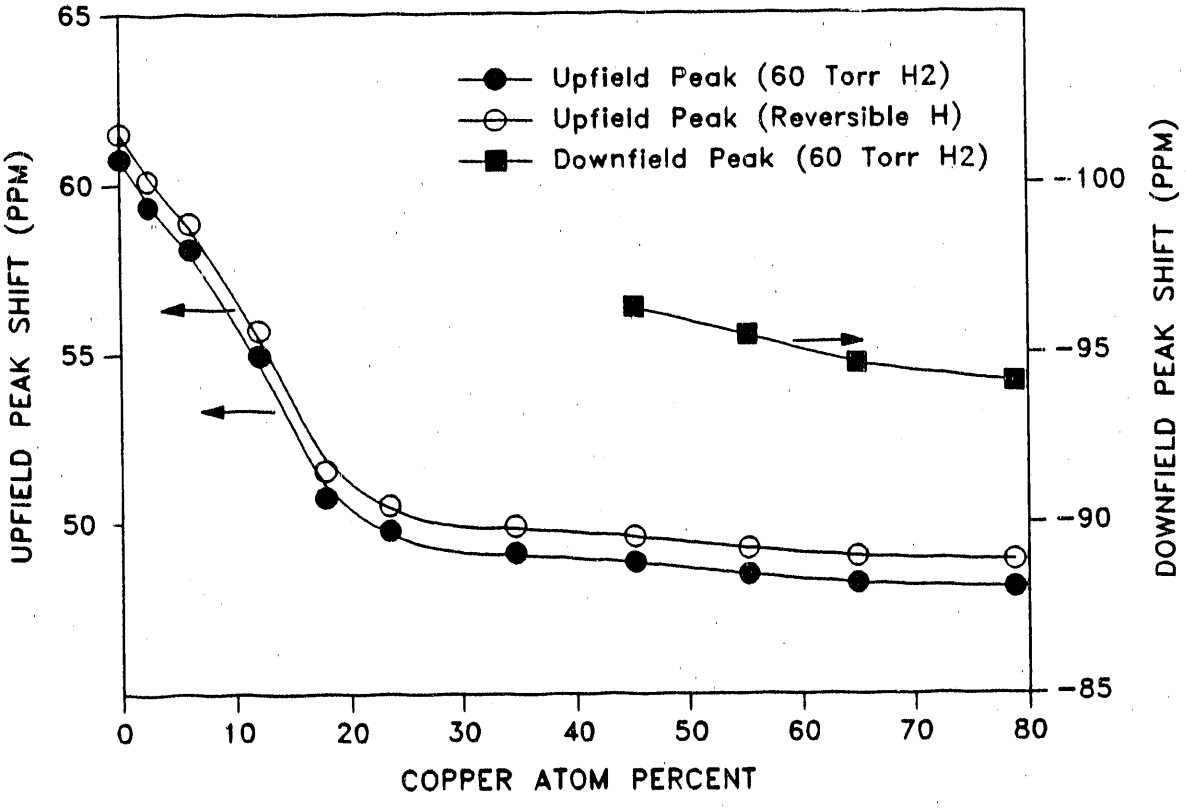

Figure 7. Variations of both upfield and downfield lineshifts under 60 Torr hydrogen with the copper composition for Ru-Cu/SiO_2 bimetallic catalysts. Upfield lineshifts for the reversible hydrogen are also shown

with the irreversibly adsorbed hydrogen is not shown because the line broadening due to addition of copper makes the exact location of the resonance line for the irreversible hydrogen difficult to determine, especially at high copper content.

The shifts of downfield peak (assigned to hydrogen adsorbed on Cu) are also plotted in Figure 7 as a function of the copper content. A small change in the shift was observed over the range of copper bulk compositions from 45 to 79 at.%. The trend of this peak's shift toward upfield with increase in the copper content may be an indication of subtle changes in adsorption properties of surface copper sites due to variations in copper particle size. Increase in copper particle number and size with increase in the copper content was indicated by the increase in the signal intensity of the hydrogen adsorbed on copper surfaces as shown earlier in Figure 4.

Over 95% of the total hydrogen population in all the catalyst samples investigated in the present study comes from protons in the silanol group. Therefore, measurements on the spin-lattice relaxation time T_1 of the silanol proton can be performed in the time domain with the inversion recovery pulse sequence, and the influence by the proton population on the metal(s) can be neglected. Exponential profiles were obtained in plots of the measured magnetization versus the delay time, τ, for samples of a pure SiO_2 and a reduced 4%

Ru/SiO_2 in the absence of dosed hydrogen. The measured T_1's for the two samples were 31.6 sec and 16.9 sec, respectively. Small deviations from the exponential were observed for all Ru/SiO_2 and $Ru-Cu/SiO_2$ catalyst samples in the presence of dosed hydrogen due to the relaxation effect from hydrogen spillover to the silica support, as discussed in the case of Ru/SiO_2 (53). Nevertheless, the same method was applied to obtain a single T_1 value for each of these samples.

Figure 8 shows variation with the copper content of the T_1 for the silanol protons. The results for samples under 60 Torr hydrogen and for samples evacuated to 10^{-6} Torr for 10 min after equilibrium with 60 Torr hydrogen are shown. For all catalyst samples under 60 Torr hydrogen, the spin-lattice relaxation time remains essentially unchanged at about 2.5 seconds. For the evacuated samples, there was a moderate decrease in T_1 as the copper content was increased.

The spin-lattice relaxation time for hydrogen adsorbed on the metals was measured in the frequency domain by using inversion recovery. The initial magnetizations were obtained indirectly by integrating the area of the resonance line corresponding to hydrogen adsorbed on Ru, Cu, or Ru-Cu. A linear regression of the log of this area versus delay time for each sample yielded the values of T_1.

The value of T_1 of hydrogen chemisorbed on Ru/SiO_2 and $Ru-Cu/SiO_2$ (the peak farthest upfield) was determined under

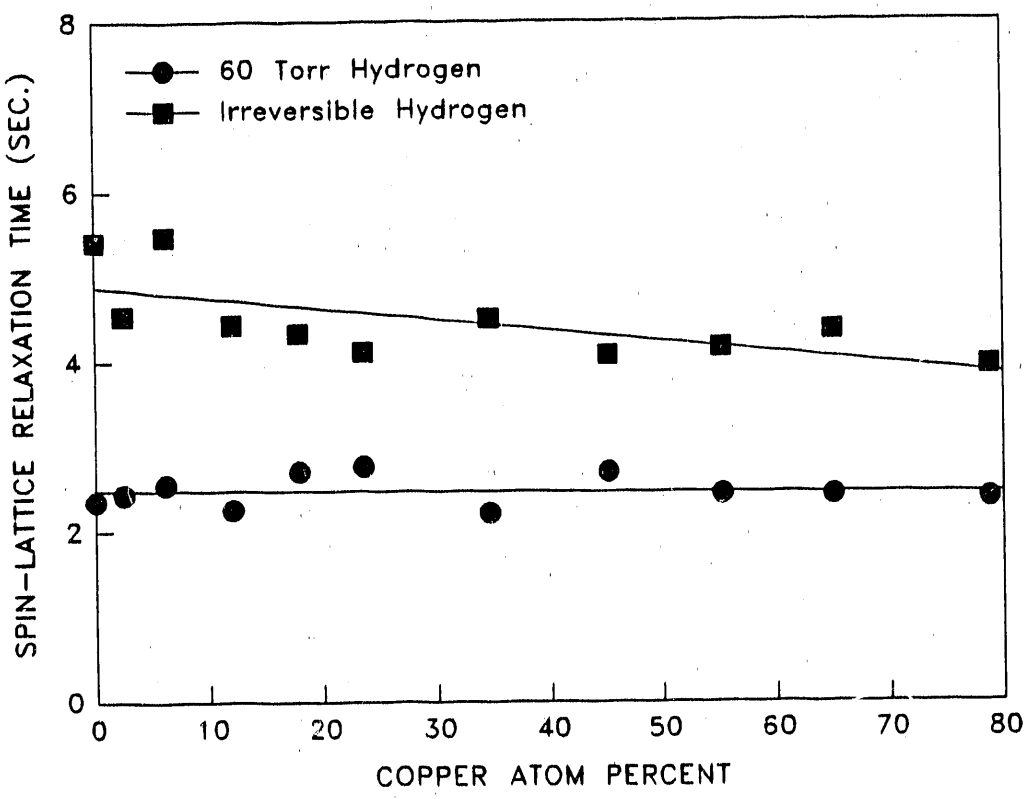

Figure 8. Variations of spin-lattice relaxation times of the silanol proton with the copper composition for Ru-Cu/SiO_2 bimetallic catalysts. Results for both 60 Torr hydrogen and the irreversible hydrogen are shown

two conditions: under 60 Torr hydrogen and after evacuation to 10^{-6} Torr for 10 min following exposure to 60 Torr gaseous hydrogen (irreversibly adsorbed hydrogen). The results are shown in Figure 9. Note that the irreversibly bound hydrogen has a longer T_1 than the hydrogen corresponding to the total (irreversible plus reversible) adsorption. The addition of copper tends to increase the T_1 value. Because of the above-mentioned line-broadening effect by copper, the exact values of T_1 for the weakly adsorbed hydrogen at bulk compositions greater than 35 at.% Cu were difficult to determine here. However, they seemed to follow the same trend as those under 60 Torr hydrogen.

The proton NMR spectra of hydrogen on Ru-Cu/SiO_2 with the highest copper loading (78.8 at.% Cu) under various hydrogen pressures are shown in Figure 10. The spectrum denoted as "0 Torr" represents a catalyst sample evacuated to 10^{-6} Torr for 10 min after exposure to 60 Torr hydrogen. Some obvious spectral features can be readily seen. First, the signal intensities of both the upfield peak and the downfield peak relative to the silanol proton peak increase with increasing hydrogen pressure. Secondly, both upfield and downfield peaks exhibit some degree of line narrowing as the hydrogen pressure is increased. The linewidths for the upfield peak are comparable to those reported earlier, namely about 9 kHz under 120 Torr hydrogen and about 24 kHz under

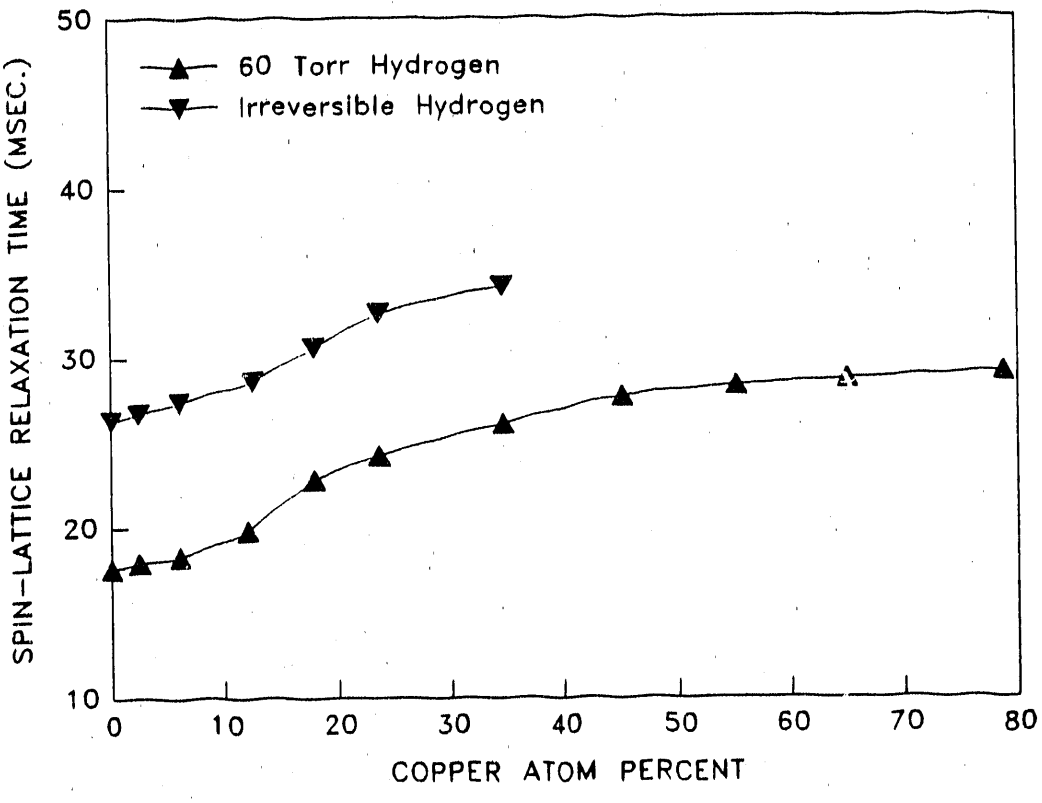

Figure 9. Variations of spin-lattice relaxation times of the upfield peak with the copper bulk composition for Ru-Cu/SiO_2 bimetallic catalysts. Results for both 60 Torr hydrogen and the irreversible hydrogen are shown

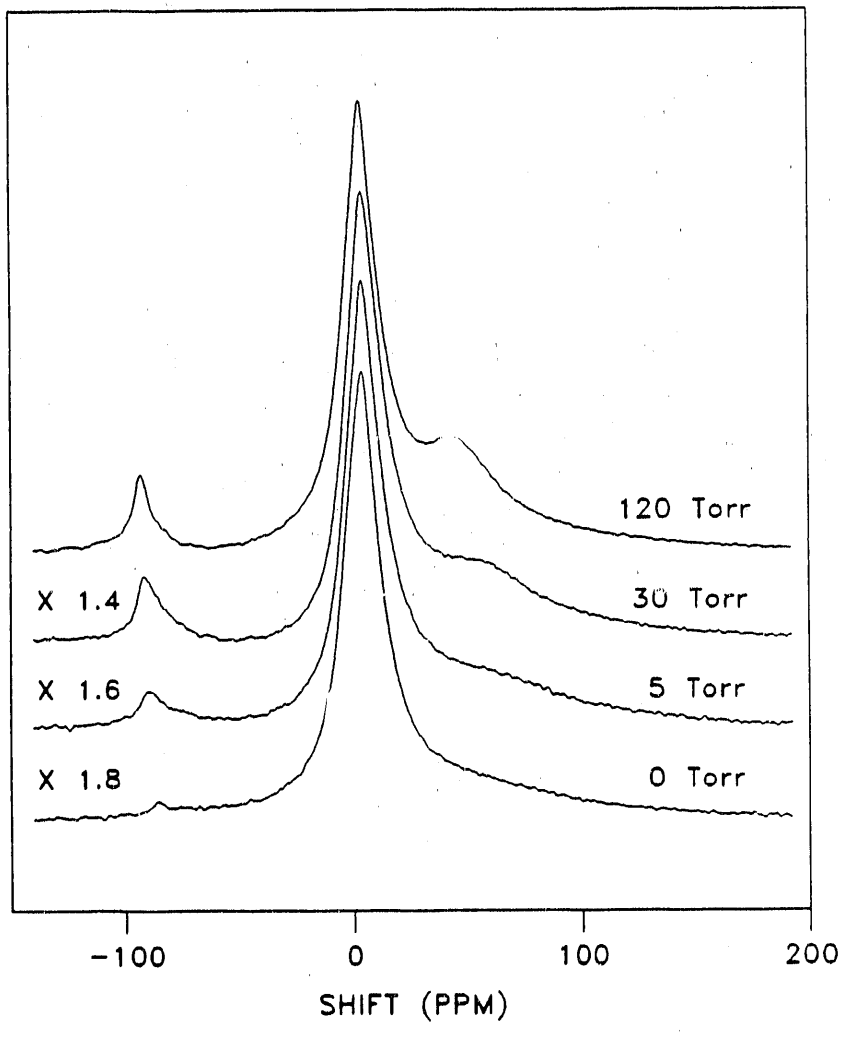

Figure 10. NMR spectra of adsorbed hydrogen on a Ru-Cu/SiO_2 bimetallic catalyst with 78.8 at.% Cu under various hydrogen pressures. The hydrogen pressures are as indicated. "0 Torr" denotes an evacuation condition of 10^{-6} Torr for 10 min at 294 K after adsorption under 60 Torr hydrogen

the evacuation condition. The linewidths for the downfield peak decrease from 3.9 kHz under 5 Torr hydrogen to 2.3 kHz under 120 Torr hydrogen. The third feature is a noticeable downfield shift of the downfield resonance as the hydrogen pressure is increased. These observations indicate a buildup of the highly mobile, reversibly adsorbed hydrogen on the surfaces of the metal particles as the hydrogen pressure is increased.

The relative signal intensities (normalized to those under 120 Torr hydrogen) for both the upfield peak and the downfield peak and also the lineshift for the downfield peak are plotted in Figure 11 versus the hydrogen pressure. The relative intensities for the two peaks follow roughly the same trend as the hydrogen pressure is increased. Note that there is a strong dependence of the amount of reversibly bound hydrogen on hydrogen pressure. Also, the measured intensities over the hydrogen pressure range of 5 to 60 Torr fall approximately on a straight line in both cases.

For the same Ru-Cu/SiO_2 catalyst (78.8 at.% Cu), the spin-lattice relaxation times on the silanol peak, the upfield peak, and the downfield peak were measured by the methods mentioned earlier. The results are shown in Figure 12 as functions of hydrogen pressure. As expected, the T_1 of the silanol proton exhibited a decrease from 4 sec to 1.8 sec over a hydrogen pressure range from 0 to 120 because of

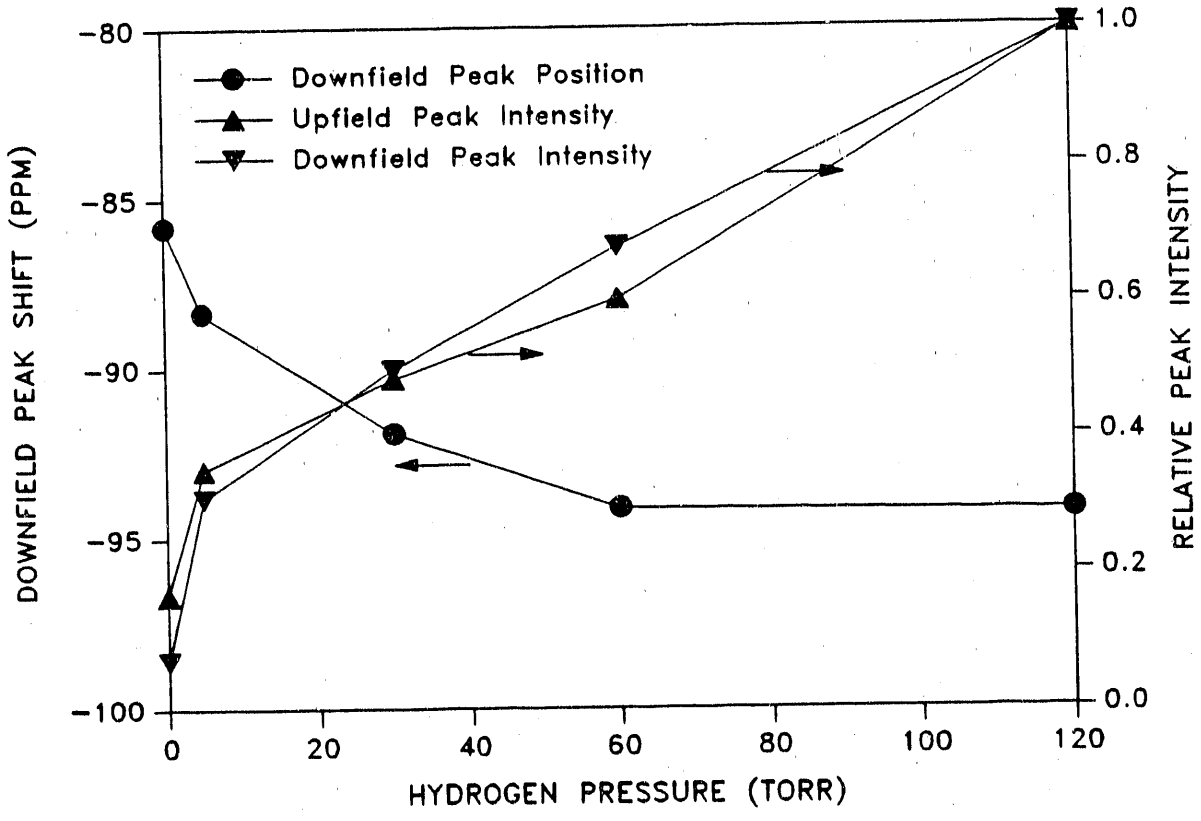

Figure 11. Variations of the downfield peak shift and relative peak intensities with the hydrogen pressure on a Ru-Cu/SiO_2 bimetallic catalyst with 78.8 at.% Cu. Both the upfield and downfield peak intensities are normalized to that under 120 Torr hydrogen

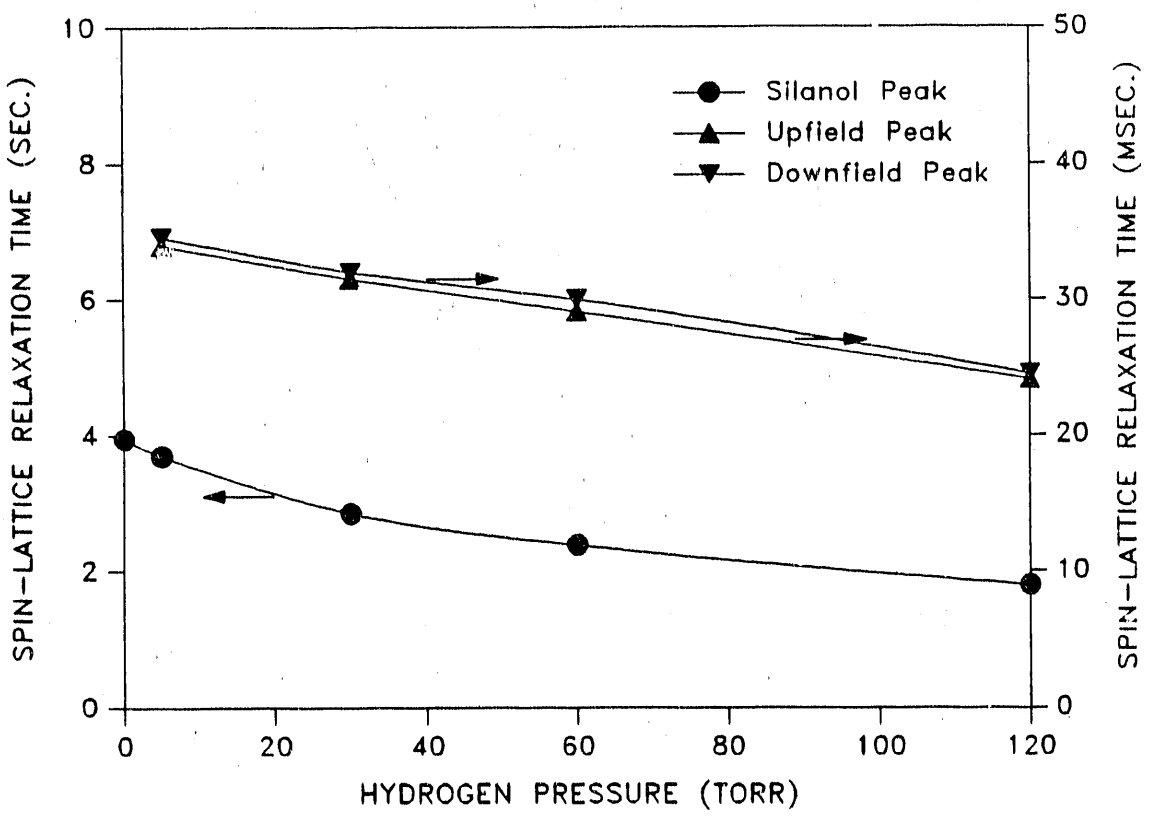

Figure 12. Variations of the spin-lattice relaxation times for all three observed peaks with the hydrogen pressure on a Ru-Cu/SiO_2 bimetallic catalyst with 78.8 at.% Cu

increased hydrogen spillover from the metals to silica. This higher degree of hydrogen spillover is a direct consequence of increased adsorption of the reversible hydrogen on the metals. The T_1's of hydrogen adsorbed on the metal surfaces exhibited nearly identical numerical values for both the upfield and the downfield peak and the same decreasing trend with increasing hydrogen pressure.

Hydrogen-deuterium exchange experiments were performed on the Ru-Cu/SiO_2 catalyst with the highest copper loading (78.8 at.% Cu) and the 5% Cu/SiO_2 catalyst. For the Ru-Cu/SiO_2 catalyst, the exchange was monitored under two conditions: under 60 Torr deuterium and after evacuation to 10^{-6} Torr for 10 min following exposure to 60 Torr deuterium. As clearly shown in Spectrum A in Figure 13, deuterium adsorbed on surfaces of the Ru-Cu bimetallic and Cu particles does exchange with the silanol protons in the silica support under 60 Torr deuterium. This is evident by the growth of the upfield and the downfield intensity with time. Although the progress of the exchange was not closely followed, the exchange rate was comparable to that for the 4% Ru/SiO_2 catalyst (53). On the other hand, the irreversibly adsorbed deuterium on surfaces of the Ru-Cu bimetallic particles does not exchange with the silanol protons, as indicated by the absence of the upfield or downfield peaks in Spectrum B in Figure 13. For a pure 5% Cu/SiO_2 catalyst sample under 60

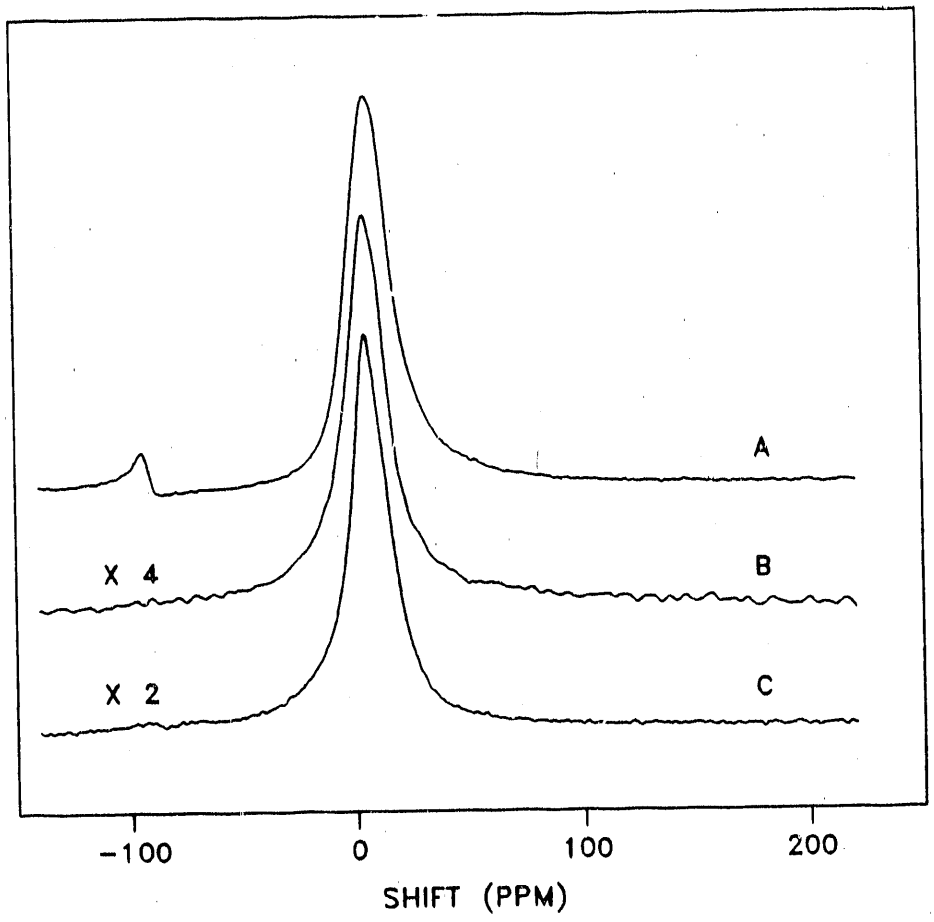

Figure 13. NMR spectra of adsorbed hydrogen on (A) Ru-Cu/SiO_2 with 78.8 at.% Cu under 60 Torr deuterium; (B) Ru-Cu/SiO_2 with 78.8 at.% Cu, evacuated to 10^{-6} Torr for 10 min after exposure to 60 Torr deuterium; (C) 5% Cu/SiO_2 under 60 Torr deuterium. All measurements were taken after an exchange period of 24 h at 294 K

Torr deuterium, the proton NMR spectrum (Spectrum C in Figure 13) seems to indicates a very weak downfield peak located at about where hydrogen adsorbed on copper should resonate. This means that deuterium adsorbed on pure Cu does exchange with the silanol proton in the silica. This observation was confirmed on a Cu/SiO_2 catalyst with higher Cu dispersion (see Section V).

DISCUSSION

Hydrogen Spillover

Hydrogen is capable of dissociative adsorption on Ru to produce reversibly and irreversibly adsorbed hydrogen. Once hydrogen is chemisorbed on the Ru surfaces it can freely migrate to adjacent Cu sites. This type of spillover (from one metal site to an adjacent metal site of a different type) allows the entire surface, Ru and closely associated Cu, to become populated with irreversibly and reversibly adsorbed hydrogen. In the present study, the Ru loading was kept constant at 4 wt.% and the sample preparation conditions were identical for all catalysts. Therefore, it seems to be reasonable to expect to have roughly the same Ru particle size for all samples. If copper exists exclusively on the surfaces of Ru particles, as is often suggested for the Ru-Cu binary system (15, 54), we would expect to observe a nearly constant amount of hydrogen uptake except for very high Cu loadings (Cu at.% > 50%) for which separate Cu particles are very likely to form. This effect was observed in the present work over the bulk composition range of 0 to 45 at.% Cu with a small enhancement for compositions greater than 45 at.% Cu (Figure 6). This means that there are approximately the same total number of available adsorption sites at surfaces of metallic and bimetallic particles to accommodate irreversibly

and reversibly bound hydrogen. The observation is consistent with the explanation of hydrogen spillover from ruthenium to copper. In addition, the NMR results (see Figure 4) clearly demonstrate the ability of copper to adsorb hydrogen.

It has been proposed from work on pure Ru/SiO_2 catalysts (53) that the reversibly adsorbed hydrogen on the surface of Ru particles is responsible for hydrogen spillover from Ru to the silica support. This concept applies directly to the Ru-Cu/SiO_2 system. Specifically, the reversibly bound hydrogen on both Ru and Cu can spill over onto the silica support. The discrepancy between the volumetric measurements and the NMR measurements in the case of the total adsorption (Figure 6) appears to be due partly to hydrogen spillover from the metals to the silica support. However, a major portion of this discrepancy was caused by an interaction between the adsorbed hydrogen and surface Cu atoms, which in turn caused excessive line broadening. This effect will be discussed later.

The presence of copper in the bimetallic catalysts does not appear to inhibit the spillover of hydrogen from the metal particles to the silica support. The amount of the reversible hydrogen and the T_1 of the silanol protons both remaining constant (Figs. 6 and 8, respectively) indicate that the amount of spiltover hydrogen on the support is not affected by copper content. However, the silanol spin-

lattice relaxation time as well as hydrogen-on-metal peak intensities are dependent on hydrogen pressure because of variation in the amount of reversible hydrogen on the metals. Also, the relatively longer silanol proton T_1 in the case of evacuation indicates partial removal of spiltover hydrogen from the silica support.

Similar to the case of pure Ru/SiO_2 (53), the hydrogen-deuterium exchange on $Ru-Cu/SiO_2$ occurs only in the presence of reversible deuterium (Figure 13, spectrum A); it does not occur in the presence of irreversible deuterium alone (Figure 13, spectrum B). This result indicates that reversible hydrogen is also responsible for hydrogen spillover from the metals to the silica support in the $Ru-Cu/SiO_2$ bimetallic system.

Hydrogen Adsorbed on Cu Monometallics

Atomic hydrogen adsorbs readily on single crystal copper surfaces while molecular hydrogen must overcome a small energy barrier of about 5 kcal/mol to achieve dissociative chemisorption (36, 37). Therefore, it would appear to be unlikely for molecular hydrogen to adsorb dissociatively on Cu at room temperature. The lineshift for hydrogen adsorbed on Cu/SiO_2 (-93 ppm) determined here agrees with that for hydrogen adsorbed on Cu powder (50). The state of hydrogen adsorbed on pure, silica-supported copper may be atomic or,

perhaps, molecular. If an immobile, molecularly adsorbed hydrogen existed on copper we would expect that dipolar broadening would result in a peak on the order of 200 kHz (900 ppm) in width. Two-dimensional, random motion would reduce the apparent width by about a factor of two. Complete narrowing of the peaks would require liquid-like, three-dimensional random motion. The observed linewidth of less than one kHz suggests either a liquid-like motion for a molecularly adsorbed species or a dissociatively adsorbed hydrogen unaffected by homonuclear dipole broadening.

By means of exchange of deuterium adsorbed on Cu with the silanol proton, atomic hydrogen may be introduced onto the Cu surfaces. It appears that atomic hydrogen adsorbed on Cu resonates at about the same frequency (Figure 13C) as that of hydrogen directly adsorbed on the copper surfaces. Thus the state of hydrogen adsorbed on pure Cu resembles atomic hydrogen.

The sharp line feature in the NMR spectrum for Cu/SiO_2 catalyst under 30 Torr hydrogen (Figure 2) is an indication of rapid motion for the adsorbed hydrogen. The very same downfield peak with much broader linewidths was observed when both Ru and Cu were present (see Figs. 3, 4, and 10). The adsorbed state of hydrogen on Cu is obviously different when Ru is present compared to when ruthenium is not present. In the case of pure Cu, the signal intensity for the adsorbed

hydrogen was very weak and most of it was readily removed by evacuation. In the case of Ru-Cu bimetallics, the hydrogen adsorbed on Cu is perhaps less mobile, as suggested by the broader lines. Also, the signal intensities are stronger on the basis of the same amount of copper, especially for the Ru-Cu bimetallics with the highest copper loadings. The adsorbed hydrogen on Cu in the Ru-Cu bimetallics is likely to be in the atomic state since atomic hydrogen could migrate from Ru or Ru-Cu bimetallic particles to adjacent copper particles. This same mechanism may be possible on the Ru/Cu physical mixture even though the migration path is quite long. A substantial portion of the adsorbed hydrogen on copper is reversible; a portion of the adsorbed hydrogen is irreversible and bound strongly on Cu surfaces.

The nature of strongly bound hydrogen species on pure Cu (Figs. 1 and 2) is perhaps due to dissociative adsorption of hydrogen on defect-like Cu sites. The hydrogen thus adsorbed may be unable to migrate to Cu sites on low index planes because of strong bonding. The nearly identical lineshift value for this hydrogen species (-88 ppm) to that for the irreversible hydrogen on pure Cu in the Ru-Cu bimetallics (-86 ppm) seems to support this postulation. Results on Cu/SiO_2 catalysts with higher copper dispersion also support this idea (44).

Hydrogen Adsorbed on Ru-Cu Bimetallics

Similar to what was observed on pure Ru/SiO_2 catalysts (53), there are two distinct adsorbed states of hydrogen on surfaces of Ru-Cu bimetallic catalysts as well, namely the irreversibly and the reversibly adsorbed hydrogen. On the basis of evidence from the NMR resonance linewidths, the reversibly adsorbed hydrogen on surfaces of the bimetallic particles has a higher degree of mobility than that of the irreversible hydrogen.

It was shown earlier in Figure 5 that the resonance line for the irreversible hydrogen tended to become broader as the copper content was increased. The increased linewidth is attributed to increasing heteronuclear dipolar interaction between hydrogen and copper atoms. Both ^{63}Cu and ^{65}Cu are quadruple nuclei having a gyromagnetic ratio of 1.128 kHz G^{-1} and 1.209 kHz G^{-1}, respectively, and a combined natural abundance of 100%. On the other hand, the NMR active Ru isotopes ^{99}Ru and ^{101}Ru have much smaller gyromagnetic ratios (0.144 kHz G^{-1} and 0.210 kHz G^{-1}, respectively) and are less abundant (12.7% and 17.1%, respectively). The heteronuclear dipole broadening is proportional to the gyromagnetic ratio of the two nuclei involved. Hence, the effective copper-proton dipole interaction is estimated to be about seven times the effective ruthenium-proton dipole interaction (for the same internuclear distance). As copper is added to the

surfaces of Ru particles, the concentration of copper nuclei at the surface is increased, and increasing heteronuclear dipole broadening is expected to occur. Assuming that the observed increase in linewidth (13.1 kHz) is a result of only this heteronuclear Cu-H dipole interaction (because the homogeneous H-H dipole interaction is expected to be the same on all Ru-Cu/SiO_2 samples), and assuming that this strongly adsorbed hydrogen on copper is relatively immobile, one can estimate the hydrogen-copper internuclear distance to be 1.4 Å. This H-Cu internuclear distance is in good agreement with the value 1.5 Å, the sum of the covalent radii for hydrogen and copper atoms.

We ascribe a major portion of the discrepancy in the amount of chemisorption between the volumetric measurements and the NMR measurements in the case of irreversible hydrogen (see Figure 6) to shortening of the spin-spin relaxation time T_2 (from 35 μs to 16 μs) due to increased H-Cu heteronuclear dipole interaction as the copper content is increased. The limitation from pulse ringdown (10 μs) of the NMR receiving system have prevented us from measuring the full NMR signal intensities. As mentioned before, the amount of reversible hydrogen measured by NMR remained roughly constant. Thus, a major portion of the discrepancy between the two techniques in the case of total adsorption was a direct consequence of the errors introduced in measurements on the irreversible

hydrogen.

For the Ru-Cu/SiO_2 catalyst with 78.8 at.% Cu, the longitudinal relaxation of the hydrogen adsorbed on sites corresponding to the upfield peak is similar to that of hydrogen adsorbed on pure copper surfaces (Figure 12). This indicates that the upfield peak represents an adsorbed hydrogen species in an environment resembling the pure Cu surfaces. It is likely to be a Cu adsorption site close to or on a Ru particle. In addition, the asymptotic behavior of the T_1 relaxation of hydrogen adsorbed on sites corresponding to the upfield peak with increasing copper content (Figure 9) indicates an increasing deposition of copper on surfaces of ruthenium particles, reaching a complete copper coverage at very high (78.8 at.%) copper content.

The downfield shift for the hydrogen reversibly adsorbed on bimetallic particles (from 62 ppm for Ru to 49 ppm; see Figure 7) was an effect solely due to addition of copper. Previous work has demonstrated that the variation of this peak is due to the fast exchange of adsorbed hydrogen to and from copper and ruthenium environments (40). The asymptotic behavior of this shift extrapolates to a value of 49 ppm at 78.8 at.% Cu corresponding to reversibly adsorbed hydrogen on copper very close to or on the ruthenium particles. From the difference in these lineshifts, it is estimated that the fast-exchange frequency for the reversible hydrogen between

Ru and Cu-on-Ru sites is at least 3 kHz at room temperature. Since no fast exchange between hydrogen adsorbed on pure Cu sites (downfield peak) and hydrogen adsorbed on Cu-on-Ru sites (upfield peaks) was observed here, the fast-exchange frequency should be less than the frequency difference between these two resonances, or 31 kHz.

It is interesting to note that resonance line for the hydrogen adsorbed on copper close to or on ruthenium appears upfield instead of downfield with respect to the reference shift. The downfield resonance for the hydrogen adsorbed on pure Cu sites may be attributed to Knight shift interaction by the 4s conduction electrons in copper (50). On the other hand, the upfield resonance line for the hydrogen adsorbed on pure Ru sites may be due to Knight shift interaction by the 4d conduction electrons via an opposite spin polarization. One possible explanation for the observed shift is that the sublayer Ru atoms have a stronger spin polarization effect on the adsorbed hydrogen than the overlayer Cu atoms. Another possible explanation invokes a minor electronic perturbation on the Cu 3d electrons by the Ru 4d conduction electrons, and the perturbed Cu 3d electrons would exert a stronger spin polarization on the adsorbed hydrogen than the Cu 4s valence electrons. The second explanation seems to agree with a theoretical calculation (55) and experimental UPS results (24, 34).

Surface Composition

The influence of Cu on the lineshift of the reversibly adsorbed hydrogen on the bimetallic surfaces may be used as a measure of surface composition for the Ru-Cu bimetallic catalysts. In the fast exchange limit, the observed NMR lineshift is the average lineshift of the reversible hydrogen on the two metal adsorption sites weighted by the relative population of these two adsorption sites. When all the adsorption sites are filled it is expressed as

$$\delta_{obs} = X_{Ru}\delta_{Ru} + X_{Cu}\delta_{Cu}$$

where δ_{obs} is the observed lineshift for the reversible hydrogen on the Ru-Cu bimetallics; δ_{Ru} and δ_{Cu} are lineshifts for the reversible hydrogen on Ru and Cu deposited on Ru, respectively; X_{Ru} and X_{Cu} are surface fractions of Ru and Cu, respectively. Since the sum of X_{Ru} and X_{Cu} is unity, the surface fraction of ruthenium may be expressed in terms of lineshifts as follows:

$$X_{Ru} = (\delta_{obs} - \delta_{Cu})/(\delta_{Ru} - \delta_{Cu})$$

Hence, the shift values shown in Figure 7 can then be readily used to compute surface compositions.

Figure 14 shows the trend for the surface fraction of Ru

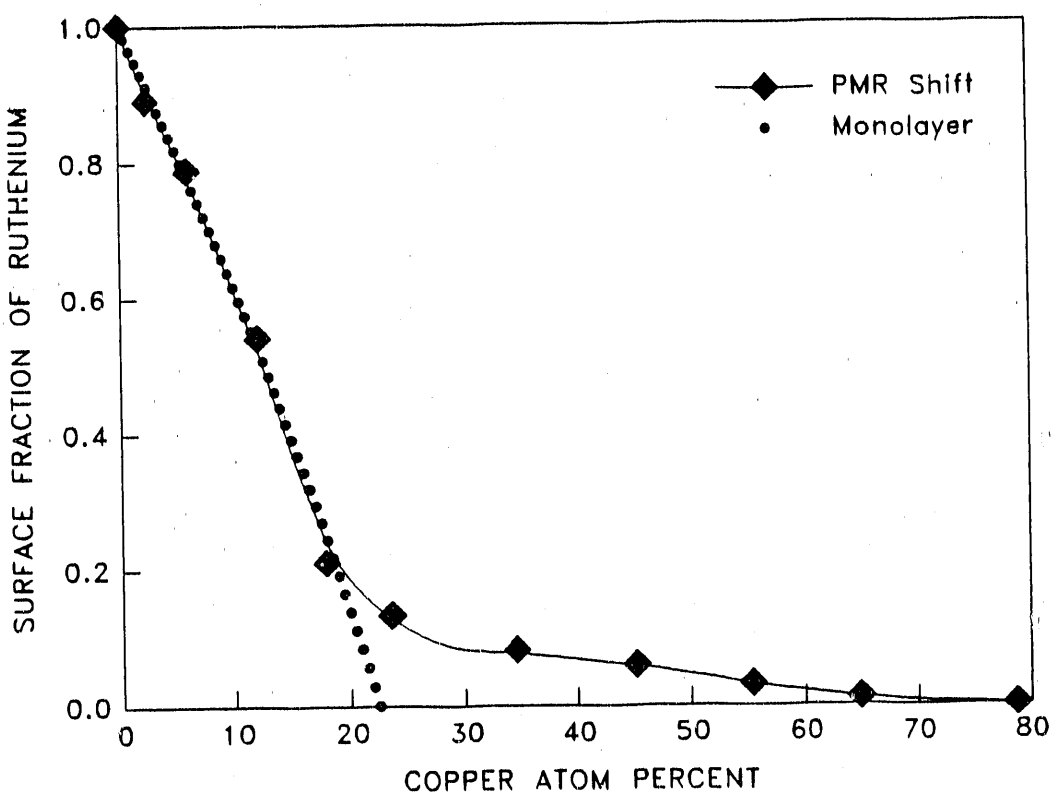

Figure 14. Plot of surface fraction of ruthenium as a function of the copper content for a series of Ru-Cu/SiO_2 bimetallic catalysts. The Ru surface fraction is calculated from the observed upfield NMR lineshift corresponding to the reversible hydrogen. The Ru surface fraction corresponding to a monolayer growth of Cu on Ru is also shown for comparison

as a function of the bulk copper composition expressed in atomic percent. As can be seen, X_{Ru} falls quickly as the overall composition is increased from 0 to 20 at.% Cu. It begins to level off at about 35 at.% Cu and approaches zero at 78.8 at.% Cu, where complete masking of the surfaces of Ru particles by Cu was assumed to occur.

Also shown in Figure 14 is the surface composition of ruthenium in the bimetallic particles under the assumption that all the copper resides at the surface in a single monolayer. For the particles, all with a dispersion of about 29% (as determined from the irreversible hydrogen uptake shown in Figure 6 assuming a stoichiometric ratio of one for both $H_{(irr)}/Ru_{(s)}$ and $H_{(irr)}/Cu_{(s)}$), a monolayer of copper will completely cover the surface at an overall copper composition of 22.5 at.%. The monolayer assumption and the surface composition determined from NMR agree very well up to a copper content of about 18 at.%; this agreement indicates that copper does tend to cover the ruthenium particles in a thin layer until a complete monolayer is nearly formed. At an overall copper content of 18.5 at.% (surface coverage of 78.3 at.% copper) copper islands, separate copper particles, or both begin to form. A complete coverage of the Ru surface by Cu can be obtained only at very high Cu loadings. This view was justified by the emergence of the downfield peak (see Figure 4), which represents hydrogen adsorbed on bulk

copper.

Surface composition is the most important parameter in characterization of Ru-Cu bimetallic catalysts. The ability to measure surface composition allows calculation of turnover frequencies for various catalytic reactions, which in turn provides valuable insight into the catalytic nature of these bimetallic catalysts.

CONCLUSIONS

Both hydrogen chemisorption and NMR of adsorbed hydrogen clearly indicate hydrogen spillover from Ru to Cu. From NMR measurements, it is indicated that pure copper is capable of adsorbing hydrogen. There are two adsorbed states of atomic hydrogen on the surfaces of bimetallic particles in the Ru-Cu/SiO_2 catalysts: irreversibly and reversibly adsorbed states. The reversible hydrogen is more mobile than the irreversible hydrogen. The surface compositions of the Ru-Cu bimetallic catalysts can be obtained from the NMR resonance lineshifts associated with rapid exchange of the reversibly bound hydrogen at the surface. Copper atoms preferentially segregate to the surface of the bimetallic particles and in so doing cover the ruthenium in nearly a monolayer fashion. The formation of three-dimensional Cu islands and pure Cu particles is possible at high Cu surface coverages.

ACKNOWLEDGMENT

This work was fully supported by the U.S. Department of Energy, Office of Basic Energy Sciences, Contract W-7405-ENG-82. The support of the Engineering Research Institute of Iowa State University is also acknowledged.

REFERENCES

1. Sinfelt, J. H., Barnett, A. E., and Carter, J. L., U. S. Patent 3,617,518, Nov. 2, 1971.

2. Sinfelt, J. H., J. Catal. 29, 308 (1973).

3. Prestridge, E. B., Via, G. H., and Sinfelt, J. H., J. Catal. 50, 115 (1977).

4. Sinfelt, J. H., Acc. Chem. Res. 10, 15 (1977).

5. Rouco, A. J., Haller, G. L., Oliver, J. A., and Kemball, C., J. Catal. 84, 297 (1983).

6. Haller, G. L., Resasco, D. E., and Wang, J., J. Catal. 84, 477 (1983).

7. Hong, A. J., Rouco, A. J., Resasco, D. E., and Haller, G. L., J. Phys. Chem. 91, 2665 (1987).

8. Hong, A. J., McHugh, B. J., Bonneviot, L., Resasco, D. E., Weber, R. S., and Haller, G. L., Proc. 9th Int. Congr. Catal., M. J. Phillips, and M. Terman, eds. (Chemical Institute of Canada, Ottawa, 1988), pp. 1198-1205.

9. Shastri, A. G., Schwank, J., and Galvagno, S., J. Catal. 100, 466 (1986).

10. Damiani, D. E., Derez Millan, E. D., and Rouco, A. J., J. Catal. 101, 162 (1986).

11. Bond, G. C., and Turnham, B. D., J. Catal. 45, 128 (1976).

12. Bond, G. C., and Yide, X., J. Mol. Catal. 25, 141 (1984).

13. Lai, S. Y., and Vickerman, J. C., J. Catal. 90, 337 (1984).

14. Schoenmaker-stolk, M. C., Verwijs, J. W., and Scholten, J. J. F., Appl. Catal. 30, 339 (1987).

15. Sinfelt, J. H., Lam, Y. L., Cusumano, J. A., and Barnett, A. E., J. Catal. 42, 227 (1976).

16. Helms, C. R., and Sinfelt, J. H., Surf. Sci. 72, 229 (1978).

17. Christmann, K., Ertl, G., and Shimizu, H., J. Catal. 61, 397 (1980).

18. Shimizu, H., Christmann, K., and Ertl, G., J. Catal. 61, 412 (1980).

19. Vickerman, J. C., Christmann, K., and Ertl, G., J. Catal. 71, 175 (1981).

20. Vickerman, J. C., and Christmann, K., Surf. Sci. 120, 1 (1982).

21. Vickerman, J. C., Christmann, K., Ertl, G., Heiman, P., Himpsel, F. J., and Eastman, D. E., Surf. Sci. 134, 367 (1983).

22. Christmann, K., and Ertl, G., J. Mol. Catal. 25, 30 (1984).

23. Brown, A., and Vickerman, J. C., Surf. Sci. 140, 261 (1984).

24. Richter, L., Bader, S. D., and Brodsky, M. B., J. Vac. Sci. Technol. 18, 578 (1981).

25. Bader, S. D., and Richter, L., J. Vac. Sci. Technol. A1, 1185 (1983).

26. Yates, J. T., Jr., Peden, C. H. F., and Goodman, D. W., J. Catal. 94, 576 (1985).

27. Paul, J., and Hoffman, F. M., Surf. Sci. 172, 151 (1986).

28. Houston, J. E., Peden, C. H. F., Blair, D. S., and Goodman, D. W., Surf. Sci. 167, 427 (1986).

29. Park, C., Bauer, E., and Poppa, H., Surf. Sci. 187, 86 (1987).

30. Hansen, M., Constitution of Binary Alloys, 2nd ed. (McGraw-Hill, New York, 1958).

31. Sinfelt, J. H., Via, G. H., and Lytle, F. W., J. Chem. Phys. 72, 4832 (1980).

32. Peden, C. H. F., and Goodman, D. W., in Catalyst Characterization Science: Surface and Solid State Chemistry, ACS Symp. Ser. No. 288. (American Chemical Society, Washington, DC, 1985), pp. 185-198.

33. Kim, K. S., Sinfelt, J. H., Eder, S., Markert, K., and Wandelt, K., J. Phys. Chem. 91, 2337 (1987).

34. Houston, J. E., Peden, C. H. F., Feibelman, P. J., and Hamann, D. R., Phys. Rev. Lett. 56, 375 (1986).

35. Smale, M. W., and King, T. S., J. Catal. 119, 441 (1989).

36. Balooch, M., Cardillo, M. J., Miller, D. R., and Stickney, R. E., Surf. Sci. 46, 358 (1974).

37. Greuter, F., and Plummer, E. W., Solid State Commun. 48, 37 (1983).

38. Goodman, D. W., Yates, J. T., Jr., and Peden, C. H. F., Surf. Sci. 164, 417 (1985).

39. Goodman, D. W., and Peden, C. H. F., J. Catal. 95, 321 (1985).

40. King, T. S., Wu, X., and Gerstein, B. C., J. Am. Chem. Soc. 108, 6056 (1986).

41. Narita, T., Miura, H., Sugiyama, K., Matsuda, T., and Gonzalez, R. D., J. Catal. 103, 492 (1987).

42. Lu, K., and Tatarchuk, B. J., J. Catal. 106, 166 (1987).

43. Lu, K., and Tatarchuk, B. J., J. Catal. 106, 176 (1987).

44. Wu, X., Gerstein, B. C., and King, T. S., J. Catal. 123, 43, (1990).

45. Chueng, T. T. P., Worthington, L. E., Murphy, P. D. B., and Gerstein, B. C., J. Magn. Reson. 41, 158 (1980).

46. Fry, C. G., Iwamiya, J. H., Apple, T. M., and Gerstein, B. C., J. Magn. Res. 63, 214 (1985).

47. Gerstein, B. C., "Alternating Circuit Theory and Pulsed NMR," IS-49244C-13, Available from NTIS, U. S. Dept. of Commerce, 5265 Port Royal Road, Springfield, VA.

48. Stoll, M. E., "A Fast Recovery, Low Noise Receiver-Amplifier for Pulsed NMR Experiments," SAND80-8797 (Sandia National Laboratory, Livermore, Ca., 1980).

49. King, T. S., Goretzke, W. J., and Gerstein, B. C., J. Catal. 107, 583 (1987).

50. Ito, T., and Kadowaki, T., Japan. J. Appl. Phys. 14, 1673 (1975).

51. Shield, L. S., and Russell, W. W., J. Phys. Chem. 64, 1592 (1960).

52. Rossington, D. R., and Holden, S. J., Nature (London) 199, 589 (1963).

53. Wu, X., Gerstein, B. C., and King, T. S., J. Catal. 118, 238 (1989).

54. Wu, X., Smale, M. W., Gerstein, B. C., and King, T. S., AIChE Annual Meeting, New York, November 1987. Paper No. 15a.

55. Ma, C. Q., Ramana, M. V., and Copper, B. R., J. Vac. Sci. Technol. A1, 1095 (1983).

SECTION III

CHARACTERIZATION OF SILICA-SUPPORTED RU-AG AND RU-AU BIMETALLIC CATALYSTS BY HYDROGEN CHEMISORPTION AND NMR OF ADSORBED HYDROGEN

CHARACTERIZATION OF SILICA-SUPPORTED RU-AG AND RU-AU BIMETALLIC CATALYSTS BY HYDROGEN CHEMISORPTION AND NMR OF ADSORBED HYDROGEN

Xi Wu[1]

Bernard C. Gerstein[2]

Terry S. King[1]

[1]Department of Chemical Engineering and Ames Laboratory

231 Sweeney Hall

Iowa State University

Ames, Iowa 50011

[2]Department of Chemistry and Ames Laboratory

229 Spedding Hall

Iowa State University

Ames, Iowa 50011

ABSTRACT

Silica-supported Ru-Ag and Ru-Au bimetallic catalysts were studied by both hydrogen chemisorption and by nuclear magnetic resonance (NMR) of adsorbed hydrogen. The two techniques yielded nearly the same capacity for hydrogen chemisorption on both series of bimetallic catalysts. A small difference measured by the two methods was attributed to hydrogen spillover from ruthenium onto the silica support. This effect of hydrogen spillover was less pronounced in Ru-Ag/SiO_2 than in Ru-Au/SiO_2 as indicated by the longer spin-lattice relaxation times of the silanol proton. The results of these studies are used to infer that a much stronger interaction exists between silver and ruthenium than between gold and ruthenium in the supported bimetallics. Both NMR results and volumetric chemisorption results show that the residual chlorine on Ru inhibits the hydrogen chemisorption capacity of the Ru/SiO_2 catalyst and Ru-Au/SiO_2 bimetallic catalysts. The variation of the adsorbed hydrogen chemical shift with chlorine coverage clearly indicates an electronic interaction that is due to chlorine adsorption. A direct comparison between clean Ru-Cu/SiO_2 (from a previous study), Ru-Ag/SiO_2, and Ru-Au/SiO_2 bimetallic catalysts was made in this study to illustrate the varying degrees of interaction between ruthenium and copper, silver, or gold.

INTRODUCTION

Among Ru-Group IB bimetallic catalysts there have been relatively few studies of supported Ru-Ag (1-3) and Ru-Au (4-9) catalysts, while the Ru-Cu system has been extensively investigated. The lack of interest in the Ru-Ag and Ru-Au bimetallic systems is attributable to the absence of unusual chemisorptive and catalytic behaviors in comparison with the Ru-Cu bimetallic system when silica is used as the support. Except for the Ru-Au/MgO (6) bimetallic catalysts, the trends of catalytic activities of Ru-Ag/SiO_2 (2) and Ru-Au/SiO_2 (6) bimetallic catalysts nearly match those of measurements from hydrogen chemisorption.

Similar to the Ru-Cu alloy, large miscibility gaps exist in both the Ru-Ag and Ru-Au binary alloys (10). However, these two bimetallic systems may behave differently in a highly dispersed state. Previous investigations seem to indicate that when supported on silica, Ru-Ag and Ru-Au do form bimetallic particles for high contents of silver or gold, respectively (2, 7). Monte Carlo simulations on silica-supported Ru-Group IB bimetallic particles (11, 12) have indicated that Ag and Au are more strongly segregated at Ru surfaces than Cu, and they tend to form Ag and Au islands at high Ag and Au concentrations.

It is well known that Ag and Au do not dissociatively adsorb molecular hydrogen; they adsorb only atomized hydrogen

at temperatures below about 195 K (13). Therefore, unlike the Ru-Cu/SiO_2 catalysts where hydrogen can spill over from Ru to Cu (14, 15), selective hydrogen chemisorption can be applied directly at room temperature to titrate the amount of Ru exposed at the surface of the bimetallic particles in Ru-Ag/SiO_2 and Ru-Au/SiO_2 catalysts. The absence of this metal-to-metal hydrogen spillover simplifies characterization of these supported bimetallic catalysts.

The readily available metal salt $RuCl_3$ nH_2O has been used most frequently as a precursor in the preparation of supported Ru catalysts and ruthenium-containing bimetallic catalysts except for the Ru-Ag system, where $Ru(NO)(NO_3)_3$ has been used to avoid AgCl precipitation. A number of recent studies (16-19) have indicated that chlorine contamination exists on the surfaces of Ru particles in Ru/SiO_2 catalysts prepared from the chloride salt. This chlorine effect not only inhibits adsorption of hydrogen but also influences the catalytic activity of Ru/SiO_2 catalysts. It is likely that Ru-Au/SiO_2 catalysts used in the previous investigations were also contaminated by chlorine.

The objective of the present study was to determine the fractions of ruthenium exposed at the surfaces of Ru-Ag and Ru-Au bimetallic particles on clean Ru-Ag/SiO_2 and Ru-Au/SiO_2 bimetallic catalysts by means of hydrogen chemisorption and nuclear magnetic resonance (NMR) of adsorbed hydrogen. These

results are compared with those on Ru-Cu/SiO_2 bimetallic catalysts from a previous study (15). The effect of chlorine on the Ru-Au bimetallic catalysts was also examined in the present study.

EXPERIMENTAL

Catalyst Preparation

The Ru-Ag/SiO_2 catalysts were prepared by incipient wetness impregnation of a mixed solution of $Ru(NO)(NO_3)_3$ (AESAR) and $AgNO_3$ (AESAR, 99.999%) with a dried Cab-O-Sil MS5 (300 m^2/g BET surface area) silica support. The Ru-Au/SiO_2 catalysts were prepared by coimpregnation of a solution of $RuCl_3 \cdot 3H_2O$ (AESAR) and $HAuCl_4 \cdot H_2O$ (AESAR, 99.999%) with the same support. Two Ru/SiO_2 catalysts were prepared from $Ru(NO)(NO_3)_3$ and $RuCl_3$ $3H_2O$, respectively, with the same preparation method. About 2.2 ml of impregnating solution per gram of SiO_2 was used to achieve incipient wetness. The slurries obtained after impregnation were dried for 24 hours at ambient temperature and 4 hours in air at 383 K. The ruthenium loading for all catalysts was kept at 4% by total weight of the support and metals. A total of five different Ru-Ag/SiO_2 and five different Ru-Au/SiO_2 catalysts were prepared to give a wide range of silver and gold loading, respectively.

Volumetric Adsorption Apparatus

The volumetric adsorption apparatus has been described previously (15, 20). It consists of a multiport Pyrex glass manifold (127.3 cm^3) in connection with a high-vacuum system,

which includes a small turbo-molecular pump (Balzers, model TPH050), a fore-pump trap, and a mechanical pump. This apparatus is capable of flow-through reduction of catalyst samples. High-vacuum greaseless, bakeable stopcocks with Teflon plugs (Ace Glass) and FETFE o-ring seals were used on the manifold to manipulate either storage or dosage of gas, or both, and eliminate hydrocarbon contamination. Pressures inside the manifold were monitored over a wide range from 10^{-7} Torr to 10^{3} Torr by a cold cathode vacuum gauge (Varian, model 860A) and two absolute Baratron pressure gauges (MKS).

A flow-through Pyrex cell mounted with a coarse glass frit (35 μm in average pore diameter) was used to contain catalyst samples for the volumetric adsorption experiments. A small matching furnace was used to provide uniform heating around the cell. The temperature inside the furnace was controlled by a proportional temperature controller (Omega) to within ± 1 K.

Catalyst Reduction and Volumetric Adsorption

For the Ru/SiO_2 catalyst prepared from $Ru(NO)(NO_3)_3$ and the $Ru\text{-}Ag/SiO_2$ bimetallic catalysts, reduction by flowing hydrogen was carried out directly inside the Pyrex cell that is connected to the adsorption apparatus. Approximately one gram of a catalyst sample was loaded into the flow-through cell, which was then attached to one of the sample ports of

the manifold. While helium gas was allowed to flow through the sample bed in the cell, the temperature of the cell was raised to 423 K. Then helium was switched off and replaced by hydrogen at a flow rate of 50 cm^3/min. A pre-reduction period of one hour proceeded at that temperature. The temperature was then raised at 10 K/min to 723 K. Further reduction was carried out for two additional hours at 723 K. Helium (99.999%) and hydrogen (99.8%) gases (Liquid Air Co.) were used as received. The sample was then evacuated for two hours at 723 K to an ultimate pressure of 10^{-6} Torr to remove traces of water and surface hydrogen.

Hydrogen for volumetric adsorption was purified by passing it through a catalytic hydrogen purifier (Engelhard Deoxo) in series with a gas purifier with Drierite and 5 Å molecular sieve (Alltech) to remove traces of oxygen and moisture. Hydrogen adsorption experiments were performed at room temperature (294 K). The total hydrogen adsorption isotherm was measured in the pressure range of 0-30 Torr. The reversible hydrogen adsorption isotherm was collected under the same conditions after a 10 min evacuation period to 10^{-6} Torr following the total adsorption. The irreversible hydrogen uptake was obtained simply by taking the difference between the values of the total and the reversible adsorption isotherms extrapolated to zero pressure. An equilibration time of 4 hours was used for the initial dose and 1 hour for

subsequent doses.

For the Ru/SiO_2 catalyst prepared from $RuCl_3\ 3H_2O$ and the $Ru-Au/SiO_2$ catalysts, two different sample treatment procedures were carried out. First, the catalyst samples were reduced for 4 hours and adsorption isotherms measured following the same procedure as described above. Secondly, the reduced catalyst samples were washed repeatedly in hot distilled water (90-95°C) to eliminate residual chlorine in the catalysts. Successive cycles of wash (one wash consisted of about 20 ml of water per gram sample) and reduction were performed for each sample. The washed samples were dried and reduced again in the flow-through cell at 673 K for 2 hours followed by a two-hour evacuation period before hydrogen chemisorption measurements were taken. The procedure for hydrogen chemisorption was identical with that for the Ru/SiO_2 catalyst made via a chlorine-free precursor and $Ru-Ag/SiO_2$ catalysts and was carried out on the washed samples after every wash. The water after wash was analyzed by atomic absorption spectroscopy for Ru and Au contents.

NMR Sample Treatment

A needle-bellows assembly made of stainless steel was used for direct reduction of a catalyst sample in flowing hydrogen inside a 5-mm NMR tube (15). The syringe needle (18 gauge) was capable of moving vertically by more than 6 cm

through adjustable compression and extension of the bellows. Vacuum-tight connections were made between the NMR tube and the needle-bellows assembly and also between the assembly and the manifold described above. In addition, a cylindrical furnace provided uniform heating around the NMR tube and the temperature of the furnace was monitored and controlled to better than ± 1 K.

With helium gas flowing through the needle, the needle was lowered to the bottom of the NMR tube, which contained approximately 60 mg of catalyst sample. The procedure for hydrogen reduction was the same as previously described for the volumetric adsorption experiment, with a hydrogen flow rate of 15 cm^3/min. After reduction, the needle was lifted out of the sample, and evacuation proceeded for 2 hours at the reduction temperature before the sample was allowed to cool to ambient temperature. Up to four samples could be reduced simultaneously. Purified hydrogen was then dosed through the needle separately to each sample and the system was allowed to equilibrate for 4 hours. The NMR tube that contains the sample was then immersed in a water bath and sealed off with a micro-torch. The exact sample weight was measured after the NMR tube was sealed by subtracting the tare weight of the tube, which was measured prior to loading the sample.

NMR Experiment

The home-built NMR spectrometer (21) used for the present study was operated at 220 MHz for proton resonance. A proton-free probe with a doubly wound coil (22) was used for all the NMR measurements. The probe quality factor Q was set at about 100 to obtain the optimal values of sensitivity and ring down time for a fixed pulse power (23). A detailed description of the spectrometer's rapid-recovery receiving system has been published elsewhere (24).

All NMR spectra were collected under a repetitive 90° single-pulse sequence. The recycle time between rf pulses was set at 0.2s to selectively suppress the intense signal associated with protons in the silanol group in catalyst samples, which has a relatively long spin-lattice relaxation time T_1 (on the order of seconds). The above repetition rate avoids T_1 saturation of the peak corresponding to hydrogen adsorbed on ruthenium. The total number of scans for the data acquisition on each sample was 10,000. The inversion recovery pulse sequence (180°-τ-90°) was applied to measure the spin-lattice relaxation times of the silanol protons (in the time domain) and of the hydrogen adsorbed on ruthenium (in the frequency domain). A pure water sample was used as the reference standard for the observed lineshifts.

For accuracy in spin counting, the water sample was doped with sufficient $FeCl_3$ such that the linewidths of the

standard and unknown were comparable. The doped water was sealed in a capillary tube having the same length as the catalyst sample in the NMR tube to offset errors due to B_1 inhomogeneity of the coil. All NMR measurements were taken at ambient temperature.

RESULTS

A set of NMR spectra measured on a 4% Ru/SiO_2 catalyst (prepared from $Ru(NO)(NO_3)_3$ and 4% $Ru-Ag/SiO_2$ catalysts having various silver loadings are shown in Figure 1. All catalyst samples were under 5 Torr hydrogen gas. As can be seen, two distinct resonance lines were observed: (1) the downfield peak at 4 ± 1 ppm corresponding to the silanol proton from the silica support, and (2) the upfield peak in the range of 64 to 69 ppm corresponding to hydrogen adsorbed on ruthenium surfaces. As the silver content was increased from 0 to 50 at.%, a significant decrease in the upfield peak intensity was observed. Also, there is a moderate increase in linewidth for the upfield peak from 6.3 kHz to 11.2 kHz over the range of silver mentioned above. An asymmetric feature on the upfield peak for both the Ru/SiO_2 catalyst and $Ru-Ag/SiO_2$ catalyst with 13.4 at.% Ag can be seen in this figure. In the case of Ru/SiO_2 catalyst, this asymmetric feature becomes obvious when compared with a Lorentzian line as shown in the same figure. This asymmetry appeared to have vanished for $Ru-Ag/SiO_2$ catalysts with a silver content of 20 at.% or higher. For these catalysts with higher silver content, the upfield peak was well fitted by a Lorentzian lineshape, as illustrated by the catalyst with 30 at.% Ag in the same figure. In addition, the lineshift for the upfield peak as calculated by the first moment is farther upfield by

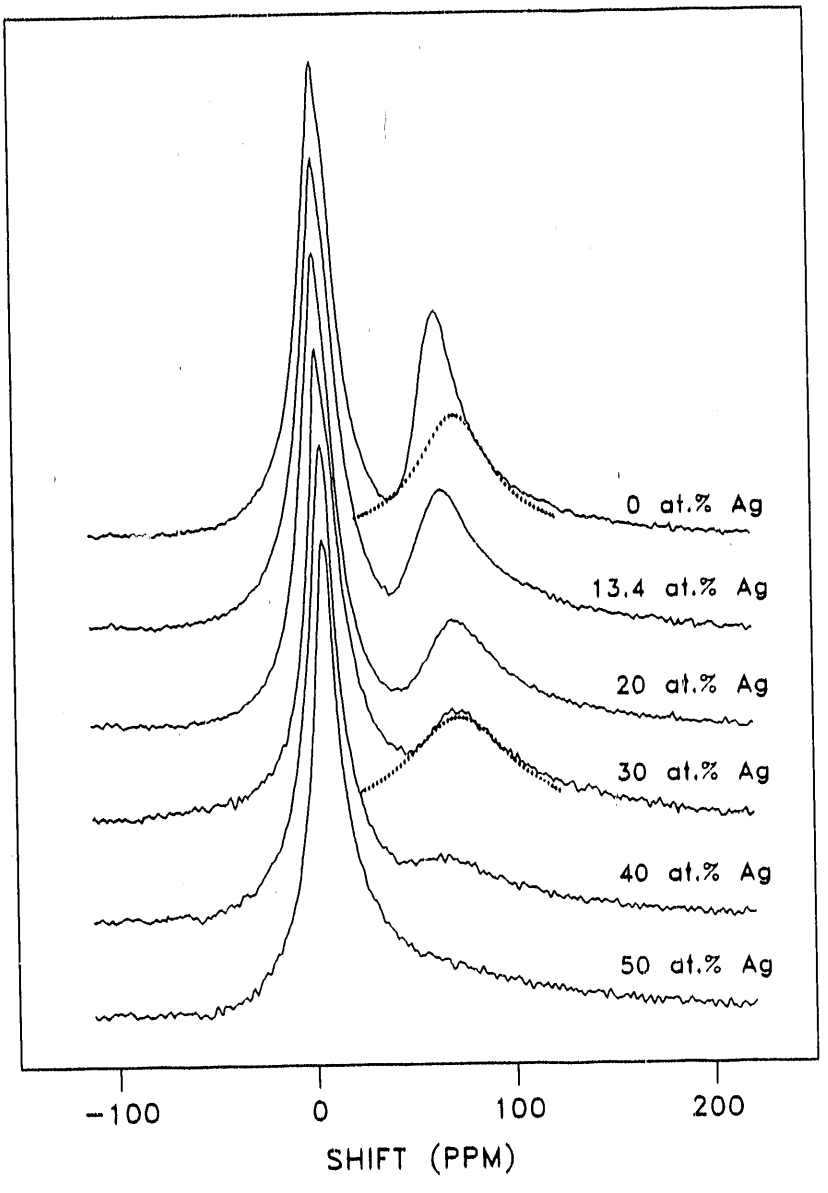

Figure 1. NMR spectra of adsorbed hydrogen on a series of $Ru-Ag/SiO_2$ bimetallic catalysts under 5 Torr hydrogen. The silver bulk compositions expressed in atomic percent are as indicated. A dotted Lorentzian line is drawn under the upfield peak for the catalyst with 0 at.% Ag to show the asymmetry of this peak. Also, the symmetry of the upfield peak for the catalyst with 30 at.% Ag is illustrated by comparison with a dotted Lorentzian line drawn underneath this peak. Water is used as reference for the lineshift

about 5 ppm for the two Ru-Ag/SiO_2 bimetallic catalysts with 20 at.% Ag and 30 at.% Ag than that for the pure Ru/SiO_2 catalyst.

Figure 2 shows four different NMR spectra for Ru/SiO_2 and Ru-Au/SiO_2 catalysts prepared by the two different sample treatment methods noted earlier. Note that all catalyst samples were under 5 Torr hydrogen gas. Spectra A and B as indicated in the figure represent NMR resonances on a 4% Ru /SiO_2 catalyst and a 4%Ru-Au/SiO_2 catalyst with 20 at.% gold content, respectively. These two catalysts were prepared by using $RuCl_3$ $3H_2O$ salt as a precursor. The sample treatment procedure of repetitive hot water wash as described above was used to eliminate all residual chlorine from these catalysts. Both spectra showed two well-resolved resonances with a similar lineshape, lineshift, and intensity for the upfield and the downfield peak, respectively. The upfield peaks were asymmetric as were the peaks for Ru-Ag/SiO_2 catalyst with 0 at.% and 13.4 at.% silver content (Figure 1). The lineshift for the upfield peak in both spectrum A and spectrum B was nearly identical at about 67 ppm. And unlike Ru-Ag/SiO_2 catalysts, an increase in the gold content did not result in a significant decrease in the upfield peak intensity for Ru-Au/SiO_2 catalysts. Although not shown in the figure, the NMR spectrum for a Ru-Au/SiO_2 catalyst with 50 at.% gold content (treated with hot water wash) exhibits a spectral feature

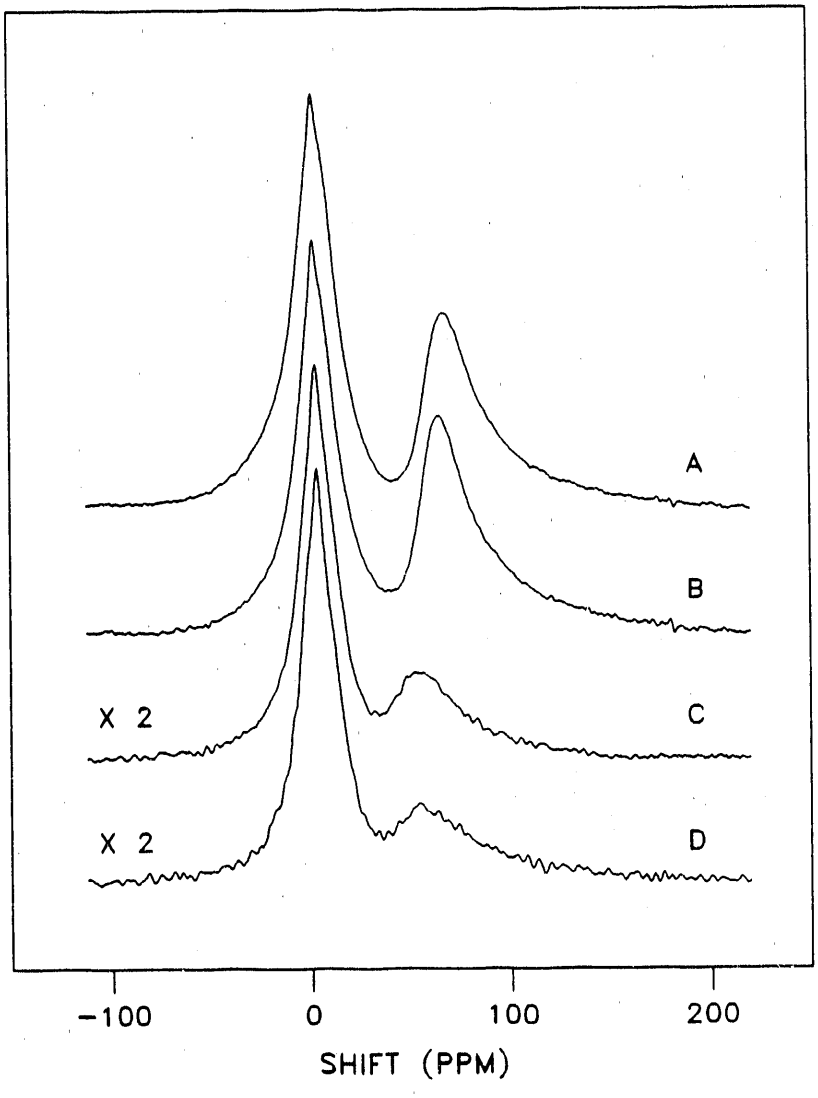

Figure 2. NMR spectra of adsorbed hydrogen on (A) 4% Ru/SiO_2 (five washes); (B) 4% $Ru-Au/SiO_2$ with 20 at.% Au (five washes); (C) 4% Ru/SiO_2 (not washed); (D) 4% $Ru-Au/SiO_2$ with 20 at.% Au (not washed). All catalyst samples were under 5 Torr hydrogen. Water is used as reference for the lineshift

similar to that of spectrum A or spectrum B.

Also shown in Figure 2 are spectrum C and spectrum D representing NMR resonances on the same 4% Ru/SiO_2 catalyst and the 4% $Ru-Au/SiO_2$ catalyst with 20 at.% gold content, respectively. However, these two catalysts were treated only by direct hydrogen reduction and were not washed with hot water; thus, they contained a considerable amount of residual chlorine. Clearly, the upfield peak intensities of these two spectra were greatly reduced as compared to spectrum A and spectrum B (by a factor of about 5). More interestingly, the upfield peaks appear farther downfield at about 52 ppm as compared to 67 ppm for the peak in spectrum A and spectrum B. Similar spectral features were also observed for unwashed $Ru-Au/SiO_2$ catalysts with higher gold contents.

The effectiveness of the hot water washing procedure in eliminating residual chlorine on Ru from a Ru/SiO_2 catalyst prepared from $RuCl_3\ 3H_2O$ was first reported by Miura et al. (19). This procedure effectively eliminates chlorine from the reduced Ru/SiO_2 catalyst without loss of ruthenium. This finding was verified in the present study by atomic absorption spectroscopy of the water after wash showing only trace amounts of ruthenium (<0.5 ppm). Also, no gold was detected in the water from washing $Ru-Au/SiO_2$ catalysts by this technique, indicating no loss of gold from these catalysts due to the washing procedure.

Figure 3 shows NMR spectra for four different catalysts that were evacuated to 10^{-6} Torr for 10 min after adsorption under 5 Torr hydrogen. Spectrum A and Spectrum B represent NMR resonances on a 4% Ru/SiO_2 catalyst and a 4% $Ru-Au/SiO_2$ catalyst with 20 at.% gold content, respectively. Both catalysts were prepared using the chloride metal salts and the reduced catalysts were washed repeatedly by hot water. As shown in the figure, these two spectra display nearly identical resonance features in terms of NMR lineshift, lineshape, and intensity. The upfield peaks of these two spectra are more asymmetric and shift slightly farther downfield than those of the corresponding Spectra A and B in Figure 2. Spectrum C and spectrum D in Figure 3 represent NMR resonances on a 4% Ru/SiO_2 catalyst (prepared from the nitrate salt) and a 4% $Ru-Ag/SiO_2$ catalyst with 20 at. % silver content, respectively. These two spectra also show a small downfield shift of the upfield peaks in comparison with the corresponding spectra in Figure 1. Clearly, the upfield peak intensity was suppressed to a greater extent by silver than by gold for the same Ag or Au atomic percent.

While the upfield peak is asymmetric, the downfield peak corresponding to the silanol proton is symmetric in lineshape and can be fitted well with a simple Lorentzian line. By subtracting the downfield peak from the spectrum, the true intensity of the upfield peak can be obtained by integrating

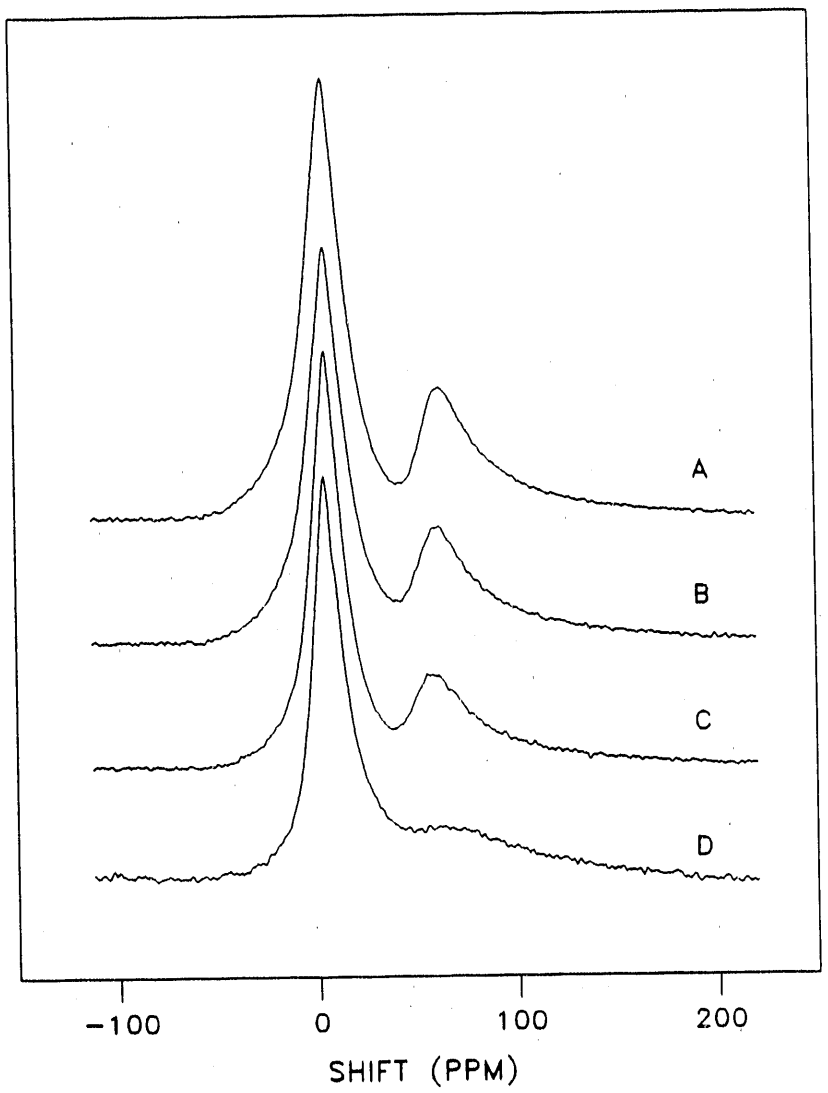

Figure 3. NMR spectra of the irreversibly adsorbed hydrogen on (A) 4% Ru/SiO_2 (five washes); (B) 4% $Ru-Au/SiO_2$ with 20 at.% Au (five washes); (C) 4% Ru/SiO_2 (prepared from nitrate salt); (D) 4% $Ru-Ag/SiO_2$ with 20 at.% Ag. All catalyst samples were evacuated to 10^{-6} Torr for 10 min after exposure to 5 Torr hydrogen. Water is used as reference for the lineshift

the area under the peak. The intensity measurements for the upfield peak were performed on all the Ru/SiO_2, $Ru-Ag/SiO_2$, and $Ru-Au/SiO_2$ catalysts under various hydrogen pressures ranging from 5 to 30 Torr. As already observed on numerous pure Ru/SiO_2 catalysts (20), isotherms obtained in this manner also exhibit nearly straight lines over this hydrogen pressure range for $Ru-Ag/SiO_2$ and $Ru-Au/SiO_2$ bimetallic catalysts. The slope of these isotherms match closely with those obtained by volumetric hydrogen chemisorption. All isotherms were extrapolated to zero hydrogen pressure to obtain values of the H/Ru ratio.

The values of the H/Ru ratio for the total and the irreversible hydrogen adsorption on the $Ru-Ag/SiO_2$ catalysts as measured by both the hydrogen chemisorption and NMR of adsorbed hydrogen are shown in Figure 4 as functions of the silver content expressed in silver atomic percent. Good agreement between the two techniques was found for both the total and the irreversible hydrogen adsorption although the NMR measurements consistently gave slightly lower H/Ru values. Suppression of the hydrogen chemisorption capacity of the pure Ru/SiO_2 catalyst by incorporation of silver was evident from the results in this figure as well as those in Figure 1. This result is in agreement with that obtained by Rouco et al. (2).

Figure 5 shows the values of the H/Ru ratio for the

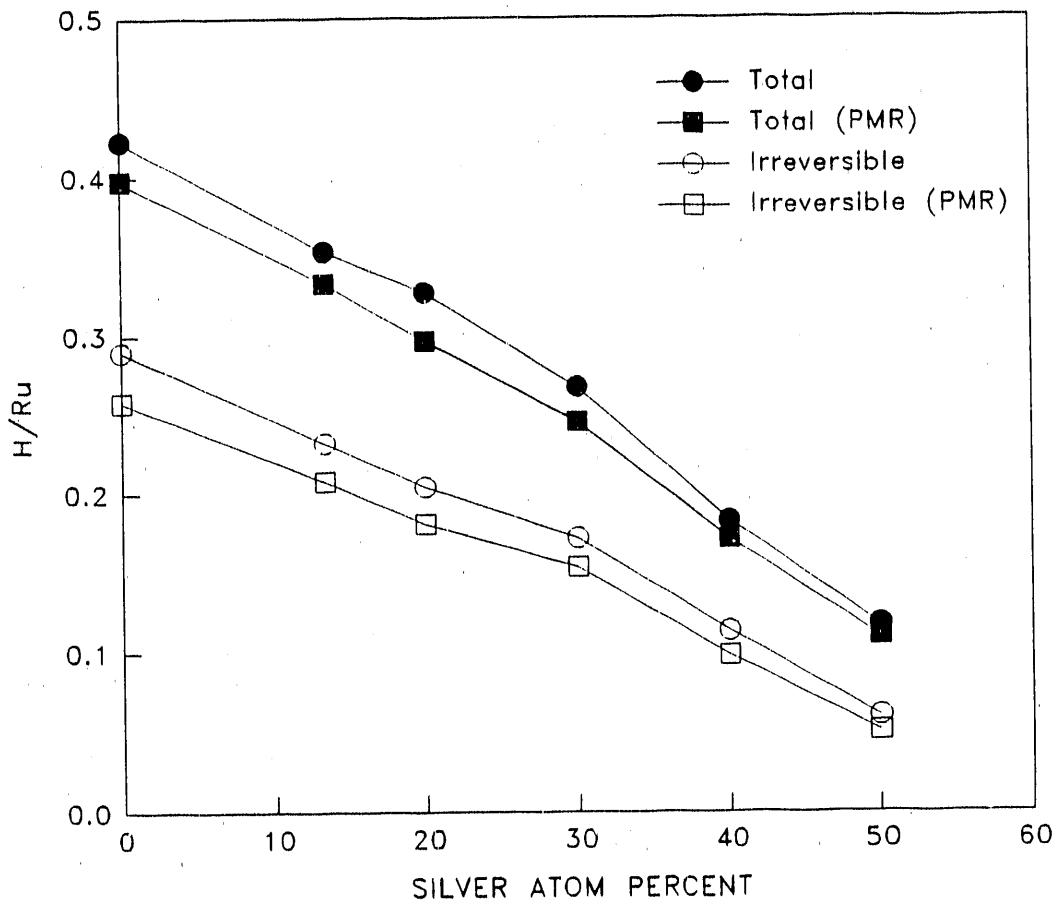

Figure 4. The H/Ru ratios for both the total and the irreversible adsorption of hydrogen on a series of Ru-Ag/SiO_2 bimetallic catalysts. Results from measurements by both hydrogen chemisorption and proton NMR are shown for comparison

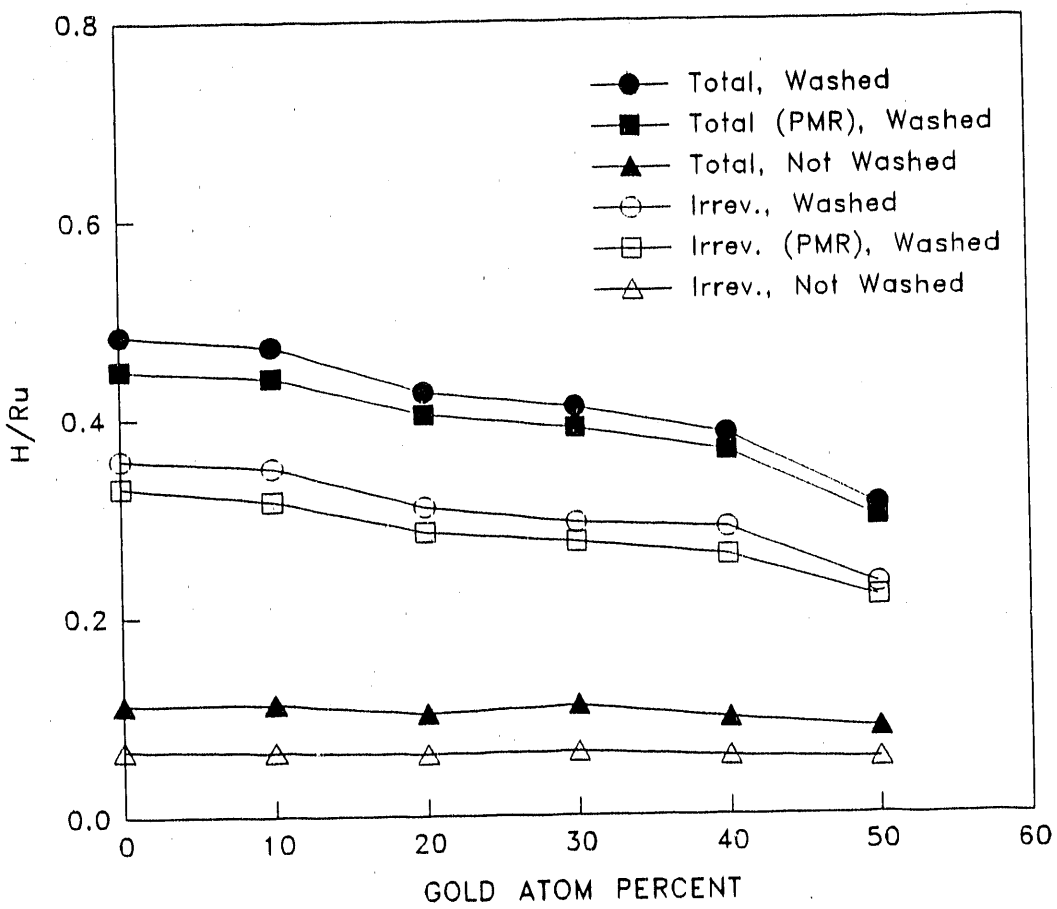

Figure 5. The H/Ru ratios for both the total and the irreversible adsorption of hydrogen on a series of Ru-Au/SiO_2 bimetallic catalysts. Results from measurements by both volumetric technique and proton NMR on the washed catalysts (five washes) are shown for comparison. Also shown are the H/Ru ratios measured by the volumetric technique on the unwashed catalysts

total and the irreversible hydrogen adsorption as measured by both hydrogen chemisorption and NMR of adsorbed hydrogen on Ru/SiO_2 and $Ru-Au/SiO_2$ catalysts that were treated by hot water wash. Also shown in the same figure are the results from hydrogen chemisorption on the unwashed Ru/SiO_2 and $Ru-Au/SiO_2$ catalysts. Again, good agreement between the two techniques on the washed Ru/SiO_2 and $Ru-Au/SiO_2$ catalysts was obtained for both the total and the irreversible hydrogen adsorption, with only small discrepancies.

Washing by hot water on the Ru/SiO_2 and $Ru-Au/SiO_2$ catalysts was carried out in steps. Hydrogen chemisorption and NMR measurements were taken on these catalysts after every wash. It was found that the hydrogen chemisorption capacity increased as the number of washes was increased and that this increase leveled off after five washes. This finding agrees with that reported by Miura et al. (19). It was concluded that after five washes chlorine was completely removed from the Ru/SiO_2 and $Ru-Au/SiO_2$ catalysts.

On the clean catalysts, addition of gold resulted in only a small decrease in the hydrogen chemisorption capacity, as shown by the gradual decreasing trends of H/Ru ratio with increasing gold content in Figure 5. The almost invariant trends of H/Ru ratio with increasing gold content for the chlorine-contaminated catalysts could be misleading because the effect of chlorine contamination rather than the effect

of gold incorporation is dominating in this case. Clearly, chlorine suppresses the hydrogen chemisorption capacity by as much as 70% to 80% on Ru/SiO_2 and $Ru-Au/SiO_2$ catalysts. Shastri and Schwank (7) have reported a decrease in the hydrogen chemisorption capacity with increasing gold content on $Ru-Au/SiO_2$ catalysts, but in their study the ruthenium loading in the catalyst was not kept constant and chlorine-contaminated catalysts were used.

The lineshift values for the upfield peak on both the $Ru-Ag/SiO_2$ and $Ru-Au/SiO_2$ (five washes) catalysts are shown in Figure 6 under two conditions of hydrogen adsorption: (1) 5 Torr hydrogen; and (2) evacuated to 10^{-6} Torr for 10 min after adsorption under 5 Torr hydrogen. Lineshifts farther upfield were observed for the $Ru-Ag/SiO_2$ bimetallic catalysts as compared with those of the Ru/SiO_2 catalysts, especially for the ones with 20 at.% Ag and 30 at.% Ag in the case of adsorption under 5 Torr hydrogen. Because of the diminishing intensity of the upfield peak at high silver contents (40 at.% and 50 at.%), lineshift values in these cases become increasingly uncertain and are not reported here. On the other hand, sufficiently strong intensities of the upfield peaks for the $Ru-Au/SiO_2$ catalysts at high gold contents were present to determine the lineshift values. As shown in the figure, lineshifts remain essentially constant with only a small decrease with an increase in gold content under both

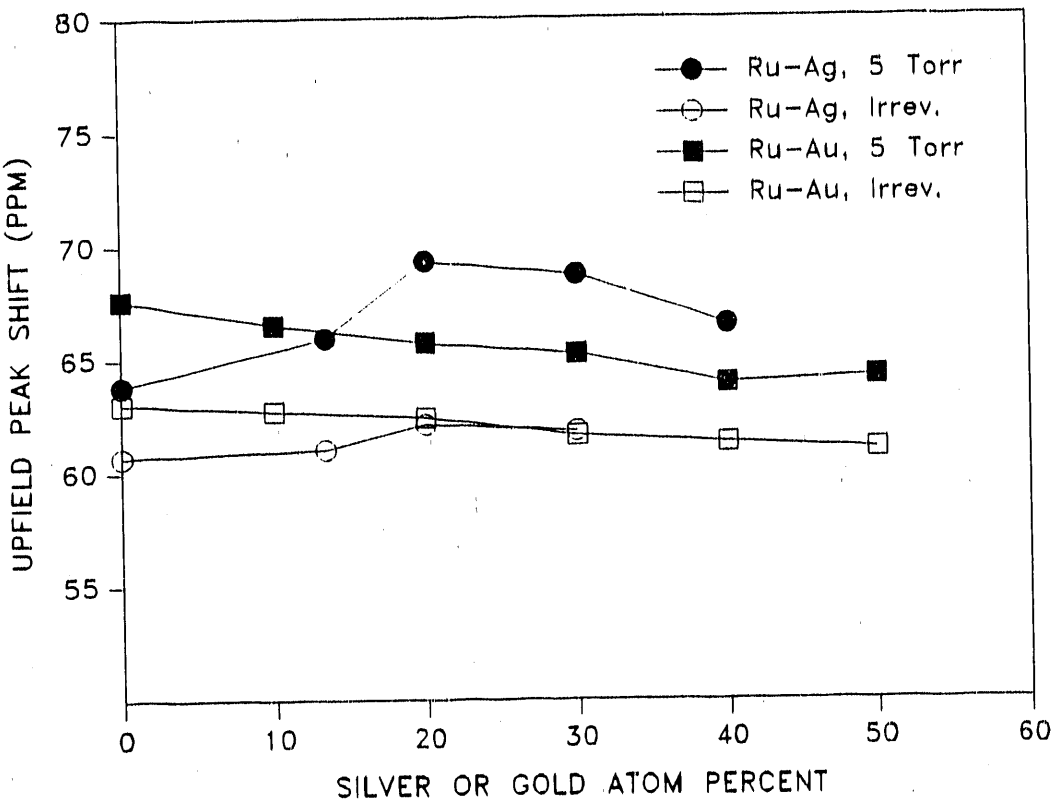

Figure 6. Variations of the upfield lineshift with bulk compositions for both Ru-Ag/SiO_2 and Ru-Au/SiO_2 (five washes) bimetallic catalysts. Lineshift values for both 5 Torr hydrogen and the irreversible hydrogen are shown

conditions of hydrogen adsorption. The discrepancy in the lineshift values between the two Ru/SiO_2 catalysts was due to variations in the metal dispersion and particle sizes (20) resulted from different procedures in catalyst preparation.

The spin-lattice relaxation times for hydrogen adsorbed on ruthenium surfaces (upfield peak) in Ru/SiO_2, $Ru-Ag/SiO_2$, and $Ru-Au/SiO_2$ catalysts were measured by the inversion recovery technique in the frequency domain. The results are shown in Figure 7 for both adsorption under 5 Torr hydrogen and evacuation to 10^{-6} Torr for 10 min after adsorption under 5 Torr hydrogen. As indicated in the figure, there exist a small increase of T_1 with increasing silver content and a small decrease of T_1 with increasing gold content. However, because the changes were comparable to the experimental uncertainty (± 1 msec), the observed trends may be regarded as essentially constant over the range of Ag or Au content. Again, the discrepancy in T_1's between the two pure Ru/SiO_2 catalysts was due to variations in the ruthenium particle size.

Figure 8 shows results of the spin-lattice relaxation times of the silanol proton on all Ru/SiO_2, $Ru-Ag/SiO_2$, and chlorine-free $Ru-Au/SiO_2$ catalysts under the two conditions of hydrogen adsorption mentioned above. The measurements were taken in the time domain by using inversion recovery. Since over 95% of the total proton population in these

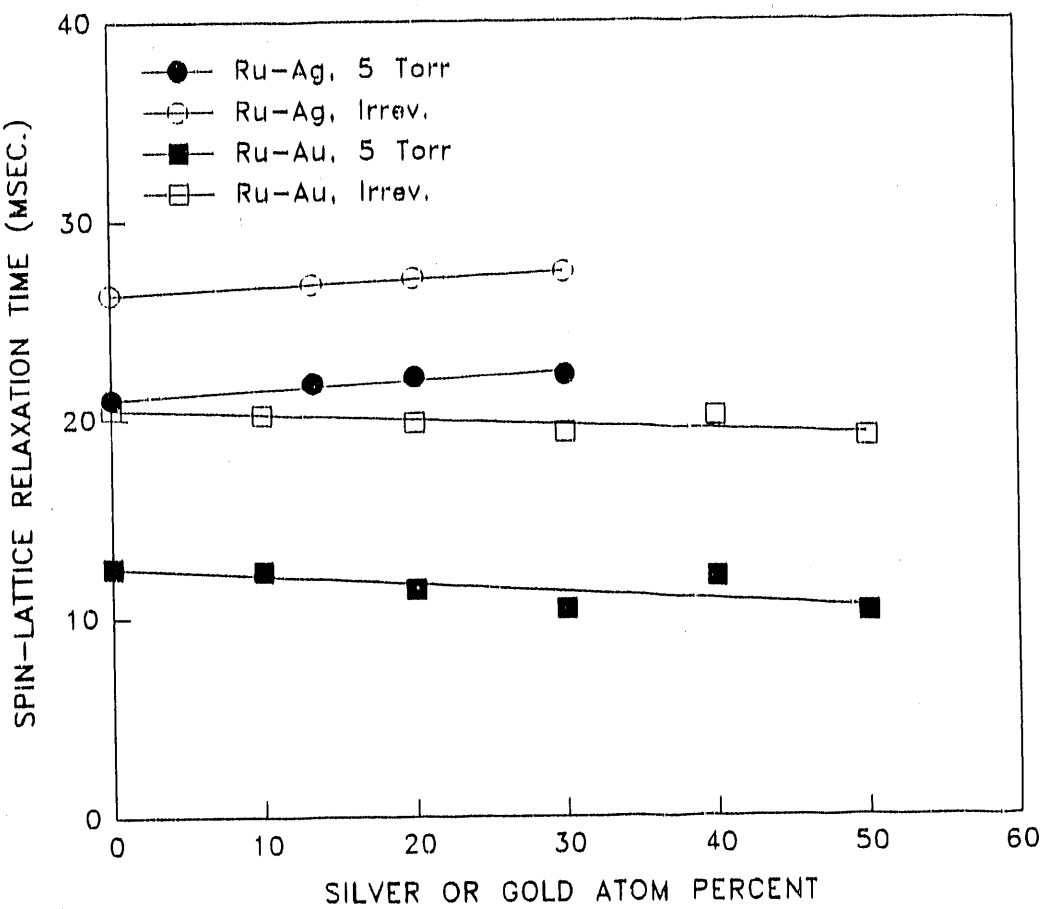

Figure 7. Variations of spin-lattice relaxation times of hydrogen adsorbed on ruthenium with bulk metal compositions for both Ru-Ag/SiO_2 and Ru-Au/SiO_2 (five washes) bimetallic catalysts. Results for both 5 Torr hydrogen and the irreversible hydrogen are shown

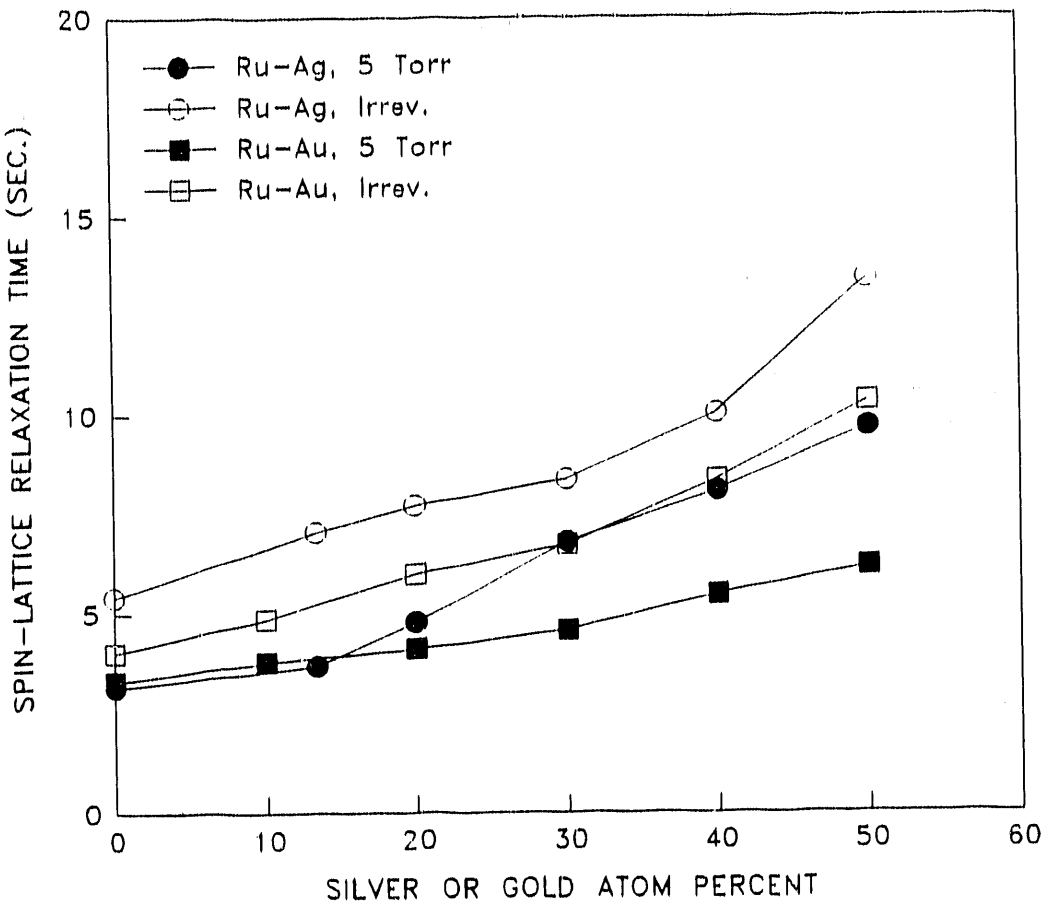

Figure 8. Variations of spin-lattice relaxation times of the silanol proton with bulk metal compositions for both Ru-Ag/SiO_2 and Ru-Au/SiO_2 (five washes) bimetallic catalysts. Results for both 5 Torr hydrogen and the evacuation condition (10^{-6} Torr for 10 min after exposure to 5 Torr hydrogen) are shown

catalysts was in the form of the silanol group, influence on the T_1 measurements from the hydrogen adsorbed on ruthenium was neglected. In all cases, there was an increase of T_1 as the Ag or Au content was increased. However, a significant difference in the T_1 trends between the Ag and Au series was observed, especially under the adsorption condition of 5 Torr hydrogen. A larger increase in T_1's of the silanol proton for Ru-Ag/SiO_2 catalysts was clearly shown in the figure in the case of 5 Torr hydrogen. Note that the spin-lattice relaxation times of the silanol proton on 4% Ru/SiO_2 and 4%Ru-Ag/SiO_2 catalysts were about 17 sec as measured on samples without hydrogen dosage. The longest T_1's were observed for the Ru-Ag/SiO_2 series under the evacuation conditions after hydrogen dosage. As the silver content reached 50 at.%, a T_1 of about 14 sec was measured under the evacuation condition, approaching the value measured under the condition of no hydrogen dosage.

DISCUSSION

Hydrogen Spillover

In a previous study on pure Ru/SiO_2 catalysts (20), the reversibly bound hydrogen on ruthenium surfaces has been determined to be the source of hydrogen spillover from the metal onto the silica support. In the same study, it has been proposed that the exchange of hydrogen atoms between the reversible hydrogen adsorbed on ruthenium and the silanol group occurs via the weakly adsorbed spiltover hydrogen, which acts as the intermediate for the exchange. A hydrogen-deuterium exchange experiment monitored by ^1H NMR clearly shows that the exchange process is much too slow at room temperature compared with T_1's of the silanol group. For this reason, the observed shortening of T_1's of the silanol group upon introduction of hydrogen gas is attributed to spin-diffusion via a T_2 process among the spiltover hydrogen, and the silanol proton rather than chemical exchange or spin-diffusion between the silanol protons. Thus, the value of the silanol proton T_1 is a monitor of the extent of hydrogen spillover (i.e., a higher degree of hydrogen spillover is indicated by a relatively shorter T_1 of the silanol proton). When this concept is applied to the $Ru-Ag/SiO_2$ and $Ru-Au/SiO_2$ systems, a suppression of hydrogen spillover from hydrogen adsorbed on Ru to the support is evident by the increase of

silanol proton T_1 with increasing Ag or Au content (see Figure 8). This suppressive effect on hydrogen spillover is stronger for Ag than for Au. The observation is consistent with the fact that silver suppresses the amount of the weakly adsorbed hydrogen on ruthenium to a greater extent than does gold (Figures 4 and 5).

On the Ru-Ag/SiO_2 and Ru-Au/SiO_2 catalysts investigated in the present study, there is no indication from the NMR measurements of any resonance arising from hydrogen adsorbed on silver or gold. Only resonances associated with the silanol proton and the hydrogen adsorbed on ruthenium are observed. Therefore, the amount of hydrogen adsorbed on Ru in these bimetallic catalysts can be measured directly by NMR without any complication of hydrogen spillover from ruthenium to silver or gold, unlike the case of Ru-Cu bimetallic system (14, 15).

For these two bimetallic systems, hydrogen spillover from Ru to the silica support presents the only intrinsic error in measuring the amount of hydrogen adsorbed on Ru exposed at surface by the volumetric technique. In the case of total hydrogen adsorption, where reversibly adsorbed hydrogen is present on ruthenium, the small discrepancy in the H/Ru ratio observed by the volumetric technique and that determined by NMR may be due to this hydrogen spillover effect. However, since the amount of spiltover hydrogen is

less than 10% of the total hydrogen adsorption at ambient temperature, experimental errors from measurements in spin counting, volumetric measurements, or both may contribute to the discrepancy as well.

Hydrogen Adsorbed on Ru-Ag and Ru-Au Bimetallics

Since there is no hydrogen spillover from ruthenium to silver or gold, one may expect to observe the same spectral features in the proton NMR on the Ru-Ag/SiO_2 or Ru-Au/SiO_2 catalysts as are observed with the Ru/SiO_2 catalysts. This result is found for the Ru-Au/SiO_2 catalysts (washed), which show essentially no changes in NMR linewidth, lineshift, and the spin-lattice relaxation time of the hydrogen adsorbed on ruthenium with increasing gold content. This means that incorporation of gold has little or no influence on the local electronic environment of the surface Ru atoms. However, different NMR spectral features have been observed on the Ru-Ag/SiO_2 bimetallic catalysts, most noticeably the lineshape and lineshift of the upfield peak corresponding to hydrogen adsorbed on ruthenium. The asymmetric lineshape of the upfield peak on Ru/SiO_2 under 5 Torr hydrogen (Figure 1) may be due to many factors such as orientational chemical shift anisotropy, varied shifts on different adsorption sites, or varied distribution of the irreversible and the reversible hydrogen on these adsorption sites. Since the same ruthenium

loading was used, the metal particle size is expected to remain roughly constant between Ru/SiO_2 and $Ru-Au/SiO_2$ catalysts. Thus the chemical shift anisotropy and the effect of magnetic susceptibility of Ru are not expected to change significantly between these catalysts, and are not inferred to be the cause of the changes in lineshape and lineshift (Figures 1 and 6).

For the $Ru-Au/SiO_2$ series the dispersion of pure Ru/SiO_2 catalyst as measured by the amount of strongly bound hydrogen was 0.29. At this dispersion, a substantial fraction (about 20%) of the Ru atoms exposed at the surface are located at the defect-like edge and corner positions of the Ru metal particles. If the hydrogen adsorbed on these sites exhibits a shift that is somewhat farther downfield relative than that adsorbed on basal plane ruthenium atoms, then the asymmetric lineshape for the pure Ru/SiO_2 catalyst may be accounted for. As silver atoms are introduced into the system, they deposit preferentially at the low coordination sites before covering the basal planes of Ru particles, as is the case with most strongly surface-segregating systems (25). As a consequence, the resonance lineshape become symmetrical and the apparent lineshift moves farther upfield with increasing content of silver. Conceivably, a similar effect could occur on $Ru-Au/SiO_2$ catalysts. However, since gold has the tendency to form three-dimensional particles rather than to spread out on

surfaces of ruthenium particles (see discussion below), its influence on the NMR spectral features is far less pronounced than that of silver.

Suppression of the hydrogen chemisorption capacity by chlorine contamination on Ru/SiO_2 and $Ru-Au/SiO_2$ catalysts is striking (Figures 2 and 5). The effect of chlorine is more than just preferential blocking of certain sites, as noted for silver. With chlorine present, a downfield shift of the upfield peak was observed (Figure 2). The magnitude of the shift indicates a change of the local electronic environment of the adsorption sites associated with the residual chlorine contamination at surfaces of Ru and Ru-Au particles. This electronic interaction may be a direct chemical shift or an indirect one via the Knight shift due to varied Ru conduction electron density. The latter explanation would seem to be more reasonable since the observed shift was larger than the usual values for chemical shift. Bonding between chlorine and surface Ru atoms may result in increased localization of the Ru 4d electrons and less spin polarization influencing the adsorbed hydrogen atoms.

Comparison among Ru-Group IB Bimetallics

Figure 9 presents variations of the relative fractional Ru dispersion as functions of Cu, Ag, or Au content expressed in metal atomic percent. For the $Ru-Ag/SiO_2$ and $Ru-Au/SiO_2$

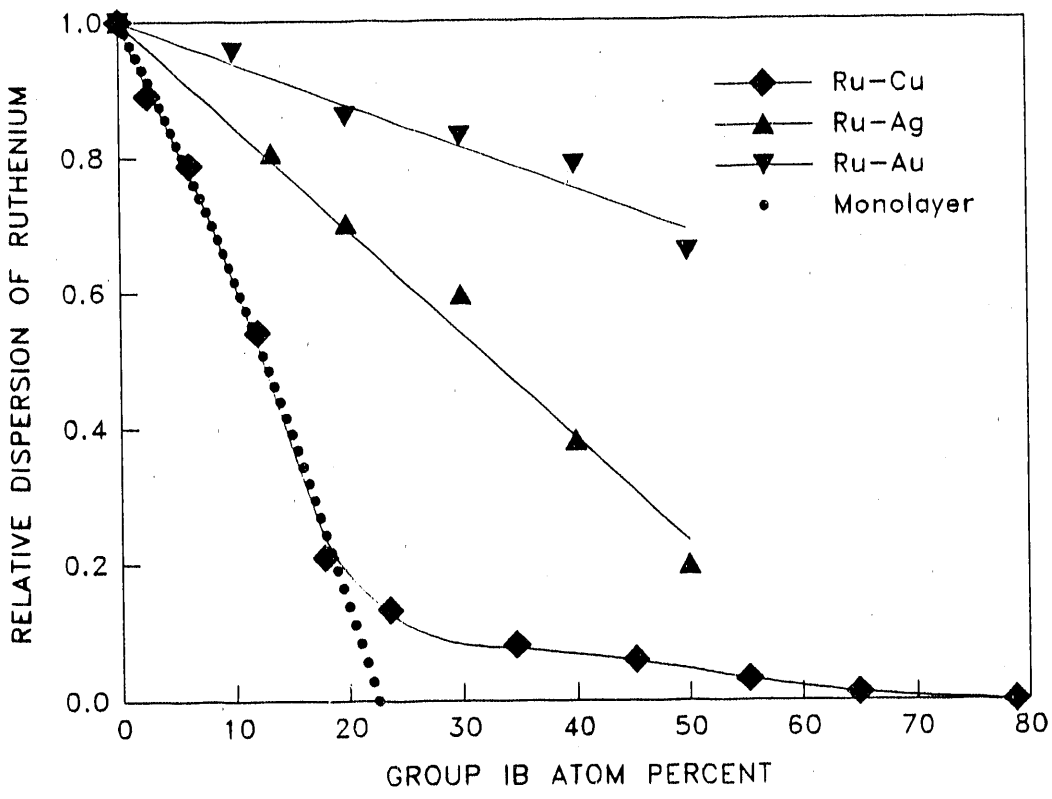

Figure 9. Plot of relative fractional Ru dispersion as functions of the copper, silver, and gold content for a series of Ru-Cu/SiO_2, Ru-Ag/SiO_2, and Ru-Au /SiO_2 (washed) bimetallic catalysts, respectively. The fractional Ru dispersion for the bimetallics is normalized to the dispersion for the respective pure Ru/SiO_2 catalyst in the series. The normalized fractional Ru dispersion corresponding to a monolayer growth of a second metal on Ru is also shown for comparison

(washed) catalysts, the Ru dispersion was obtained from the H/Ru ratio of the irreversibly adsorbed hydrogen measured by NMR. All values of the fractional Ru dispersion for Ru-Ag/SiO_2 and Ru-Au/SiO_2 bimetallic catalysts were normalized to the respective Ru dispersion of the pure Ru/SiO_2 catalyst in the series (0.29 and 0.36, respectively). The values of the normalized fractional Ru dispersion for the Ru-Cu/SiO_2 series were obtained from the surface composition determined by NMR in a previous study (15). The surface composition was converted to the fractional Ru dispersion by multiplying it by the corresponding H/Ru values as measured by chemisorption of the irreversibly adsorbed hydrogen. Therefore, a direct comparison can be made on a common basis among these three classes of bimetallic catalysts. Also shown in the same figure are a set of calculated values of the normalized fractional Ru dispersion by assuming a one-to-one monolayer growth of the second metallic element (Cu, Ag, or Au) on Ru surfaces.

The above results clearly show that different trends in fractional ruthenium dispersion are present for these three ruthenium-containing bimetallic catalysts. The results are taken to indicate the differences in interaction at the interface between ruthenium and copper, silver, or gold. Copper covers the ruthenium surfaces in a monolayer fashion until a high copper coverage (78%) is reached. Then, growth

of three-dimensional copper islands on ruthenium surfaces begins as more copper is added to the system (15). Silver interacts with the ruthenium surfaces to a lesser extent, covering the same fraction of the ruthenium surfaces at much higher bulk composition (atomic percent) than copper. Gold has little interaction with ruthenium surfaces and tends to form three-dimensional islands on the Ru surfaces or separate gold particles in the support.

The fractional dispersion results for the ruthenium-copper catalysts shown in Figure 9 are in good agreement with Monte Carlo simulations (11) which indicate that copper will segregate almost completely to the surface. At low copper concentrations the defect-like edge and corner sites exhibit the strongest driving force for segregation. Experimental evidence for the preferential population of Ru defect sites by Cu has been presented by Kim et al. (26). Once nearly all the edge and corner lattice positions are populated by copper the basal planes are covered by pseudomorphic two-dimensional islands of copper. This monolayer growth of Cu overlayers on Ru surfaces has been noted in various studies employing Ru single crystals (26-29). In addition, results from studies of small Ru-Cu bimetallic particles indicate that a core of ruthenium is surrounded by a thin layer of copper (26-34).

The results given in Figure 9 indicate that neither the Ru-Ag nor Ru-Au systems display such strong interaction

Table 1. Thermodynamic data for Ru and Group Ib metals

Metal	Heat of sublimation[a] (kJ/mol)
Ru	651.8
Cu	337.0
Ag	284.2
Au	368.4

Binary system	Heat of mixing[b] (kJ/mol)
Ru-Cu	17
Ru-Ag	34
Ru-Au	23

[a]Data from Reference (35).

[b]Estimate from Reference (36).

between the constituent metals as does Ru-Cu. This behavior may be understood by noting the values of the bulk cohesive energy (as indicated by the heat of sublimation) for the group Ib metals compared to ruthenium and by noting the estimated heats of mixing for the three bimetallic systems (see Table 1). As shown in the table, all three bimetallic systems have an estimated heat of mixing that is large and

endothermic. For this reason, bulk alloys are not formed. The differences in the cohesive energies, however, indicate that forming a ruthenium surface relative to any of the group Ib metals is energetically unfavorable. A comparison of the values given in Table 1 shows that covering Ru particles with Cu results in a considerable lowering of the energy of the system. Less energy is saved when silver covers ruthenium. Because of the higher cohesive energy of gold relative to copper, the tendency for gold to form a thin layer on the surface of ruthenium is significantly less than that for copper. As shown in Figure 9, gold and ruthenium display little tendency to form true bimetallic systems. This view is consistent with the microdiffraction study of Cowley and Plano (9) who observed no direct association of gold and ruthenium for particles in the 1 to 3 nm range.

CONCLUSIONS

NMR of adsorbed hydrogen indicates no spillover of hydrogen from ruthenium to either silver or gold in Ru-Au/SiO_2 and Ru-Au/SiO_2 catalysts. Hydrogen spillover from the reversibly adsorbed hydrogen on Ru onto the silica support is suppressed by addition of silver or gold. This effect is more pronounced in Ru-Ag/SiO_2 bimetallic catalysts as indicated by the much longer spin-lattice relaxation times of the silanol proton in the support. The preferential location of silver atoms on defect-like ruthenium sites assists in the differentiation of hydrogen adsorbed on the various ruthenium sites. Gold does not form bimetallics with ruthenium as efficiently as silver. This is indicated by the smaller variation in hydrogen chemisorption capacity measured by the NMR and the volumetric technique. Both techniques clearly show the poisoning effect of residual chlorine on the hydrogen chemisorption capacity of the Ru/SiO_2 catalyst and Ru-Au/SiO_2 bimetallic catalysts. A direct comparison between clean Ru-Cu/SiO_2, Ru-Ag/SiO_2, and Ru-Au/SiO_2 bimetallic catalysts indicates that copper has the strongest tendency to cover surfaces of ruthenium particles among Group IB metals.

ACKNOWLEDGMENT

This work was fully supported by the U. S. Department of Energy, Office of Basic Energy Science, Contract No. W-7405-ENG-82. The support of the Engineering Research Institute of Iowa State University is also acknowledged.

REFERENCES

1. Sinfelt, J. H., Barnett, A. E., and Carter, J. L., U. S. Patent 3,617,518, Nov. 2, 1971.

2. Rouco, A. J., Haller, G. L., Oliver, J. A., and Kemball, C., J. Catal. 84, 297 (1983).

3. Damiani, D. E., Perez Millan, E. D., and Rouco, A. J., React. Kinet. Catal. Lett. 36, 15 (1988).

4. Bassi, I. W., Garbassi, F., and Vlaic, G., J. Catal. 64, 405 (1980).

5. Galvagno, S., Schwank, J., and Parravano, G., J. Catal. 69, 283 (1981).

6. Datye, A. K., and Schwank, J., J. Catal. 93, 256 (1985).

7. Shastri, A. G., and Schwank, J., J. Catal. 95, 271 (1985).

8. Shastri, A. G., and Schwank, J., J. Catal. 95, 284 (1985).

9. Cowley, J. M., and Plano, R. J., J. Catal. 108, 199 (1987).

10. Hansen, M., Constitution of Binary Alloys, 2nd eds. (McGraw-Hill, New York, 1958).

11. Smale, M. W., and King, T. S., J. Catal. 119, 441 (1989).

12. Wu, X., Smale, M. W., Gerstein, B. C., and King, T. S., AIChE Annual Meeting, New York, November 1987. Paper No. 15a.

13. Hayward, D. O., and Trapnell, B. M., Chemisorption, 2nd ed. (Butterworths, Washington, 1964).

14. King, T. S., Wu, X., and Gerstein, B. C., J. Am. Chem. Soc. 108, 6056 (1986).

15. Wu, X., Gerstein, B. C., and King, T. S., J. Catal. 121, 271 (1990).

16. Marita, T., Miura, H., Sugiyama, K., Matsuda, T., and Gonzalez, R. D., J. Catal. 103, 492 (1987).

17. Lu, K., and Tatarchuk, B. J., J. Catal. 106, 166 (1987).

18. Lu, K., and Tatarchuk, B. J., J. Catal. 106, 176 (1987).

19. Miura, H., Hondou, H., Sygiyama, K., Matsuda, T., and Gonzalez, R. D., Proc. 9th Int. Congr. Catal., M. J. Phillips, and M. Terman, eds. (Chemical Institute of Canada, Ottawa, 1988), pp. 1307-1313.

20. Wu, X., Gerstein, B. C., and King, T. S., J. Catal. 118, 238 (1989).

21. Chueng, T. T. P., Worthington, L. E., Murphy, P. D. B., and Gerstein, B. C., J. Magn. Reson. 41, 158 (1980).

22. Fry, C. G., Iwamiya, J. H., Apple, T. M., and Gerstein, B. C., J. Magn. Reson. 63, 214 (1985).

23. Gerstein, B. C., "Alternating Circuit Theory and Pulsed NMR," IS-49244C-13, Available from NTIS, U. S. Dept. of Commerce, 5265 Port Royal Road, Springfield, VA.

24. Stoll, M. E., "A Fast Recovery, Low Noise Receiver-Amplifier for Pulsed NMR Experiments," SAND80-8797 (Sandia National Laboratory, Livermore, Ca., 1980).

25. Strohl, J. K., and King, T. S., J. Catal. 116, 540 (1989).

26. Kim, K. S., Sinfelt, J. H., Eder, S., Markert, K., and Wandelt, K., J. Phys. Chem. 91, 2337 (1987).

27. Goodman, D. W., and Peden, C. H. F., J. Catal. 95, 321 (1985).

28. Yates, J. T., Peden, C. H. F., and Goodman, D. W., J. Catal. 94, 576 (1985).

29. Peden, C. H. F., and Goodman, D. W., Ind. Eng. Chem. Fundam. 25, 58 (1986).

30. Houston, J. E., Peden, C. H. F., Feibelman, P. J., and Hamann, D. R., Phys. Rev. Lett. 56, 375 (1986).

31. Sinfelt, J. H., Acc. Chem. Res. 10, 15 (1977).

32. Sinfelt, J. H., Lam, Y. L., Cusumano, J. A., and Barnett, A. E., J. Catal. 42, 227 (1976).

33. Sinfelt, J. H., Science 195, 641 (1977).

34. Sinfelt, J. H., Via, G. H., and Lytle, F. W., J. Chem. Phys. 72, 4832 (1980).

35. Hultgren, R., Desai, P. D., Hawkins, D. T., Gleiser, M., Kelley, K. K., and Wagman, D. D., Selected Values of the Thermodynamic Properties of the Elements, (American Society for Metals, Metals Park, Ohio, 1973).

36. Miedema A. R., Philips Technical Rev. 36(8), 217 (1976).

SECTION IV

A PROTON NMR STUDY ON THE EFFECT OF CHLORINE ON HYDROGEN CHEMISORPTION BY SILICA-SUPPORTED RU MONOMETALLIC AND RU-CU BIMETALLIC CATALYSTS

A PROTON NMR STUDY ON THE EFFECT OF CHLORINE ON HYDROGEN CHEMISORPTION BY SILICA-SUPPORTED RU MONOMETALLIC AND RU-CU BIMETALLIC CATALYSTS

Xi Wu[1]

Bernard C. Gerstein[2]

Terry S. King[1]

[1]Department of Chemical Engineering and Ames Laboratory

231 Sweeney Hall

Iowa State University

Ames, Iowa 50011

[2]Department of Chemistry and Ames Laboratory

229 Spedding Hall

Iowa State University

Ames, Iowa 50011

ABSTRACT

Silica-supported Ru catalysts prepared from the $RuCl_3 \cdot 3H_2O$ precursor were found to contain a considerable amount of residual chlorine after reduction. The amount of chlorine determined by x-ray fluorescence spectroscopy was less than one monolayer on the ruthenium surfaces. Both the volumetric hydrogen chemisorption and ^1H NMR techniques show suppression of hydrogen adsorption capacity on the chlorine-contaminated catalysts. The effect of residual chlorine on the NMR shift and the spin-lattice relaxation time for the chemisorbed hydrogen indicates a strong electronic interaction between Cl and surface Ru, which results in the weakening of the H-Ru bonding at the Ru surfaces. The variations of the hydrogen coverage with chlorine coverage suggests that the mechanism for suppression of hydrogen adsorption involves both physical site blocking and short range electronic effects. Similar suppressive effects of Cl on hydrogen chemisorption capacity were also observed on the $Ru\text{-}Cu/SiO_2$ bimetallic catalysts. The presence of chlorine does not inhibit hydrogen spillover from Ru to Cu and exchange of the adsorbed hydrogen between adsorption states on the two metals. The residual chlorine in both the Ru/SiO_2 and the $Ru\text{-}Cu/SiO_2$ bimetallic catalysts can be removed effectively by washing with water.

INTRODUCTION

Selective hydrogen chemisorption is the most commonly used technique to measure the fraction of Ru atoms exposed at the surface (dispersion) in supported Ru catalysts. However, the method may not be accurate when the ruthenium surfaces are contaminated with various adatoms. Chlorine is the most likely contaminant in supported Ru catalysts since these catalysts are usually prepared using ruthenium trichloride.

The effect of residual chlorine on the chemisorptive properties of Ru/SiO_2 catalysts has been studied by Gonzalez and co-workers (1). They found that catalysts prepared from the precursor $RuCl_3 \cdot 3H_2O$ contained residual chlorine after reduction at normal reduction temperatures (573 - 773 K) and the residual chlorine significantly suppressed the hydrogen chemisorption capacity. This effect of chlorine on hydrogen chemisorption was confirmed by Lu and Tatarchuk (2, 3) using the method of adding Cl onto clean Ru/SiO_2 catalysts. They attributed the attenuated hydrogen chemisorption at ambient temperatures to a short-ranged electronic modification of the surface Ru atoms by the pre-adsorbed chlorine. They also observed that hydrogen adsorption on chlorine-contaminated Ru catalysts is an activated process with activation energies in the range of 4 to 16 kcal/mole. Based on their observations of increased activation energy for hydrogen adsorption with decrease in ruthenium particle size, they proposed that the

electronegative Cl atoms preferentially adsorb on defect-like Ru sites and inhibit electron donation from the basal plane Ru sites to hydrogen molecules.

The reducibility of ruthenium trichloride precursors incorporated on an alumina support has been studied by a number of researchers (4-6). It has been shown by Bossi et al. (6) that Cl^- ions have a much stronger tendency to remain in the Ru/Al_2O_3 than in the Ru/SiO_2 catalysts after hydrogen reduction under the same conditions. The presence of Cl^- ions indicate an incomplete reduction of Ru^{3+} to Ru^0.

Chen et al. (7) have studied the effect of chlorine on the chemisorption of carbon monoxide on Ru/SiO_2 catalysts using infrared spectroscopy. Their results indicate a significant change of the bonding of CO to surface Ru in the presence of coadsorbed chlorine. The Ru-CO bonding strength is likely altered by withdrawal of d electron density from Ru to the coadsorbed electronegative element. This effect may enhance CO dissociation and consequently increase methanation activity on Ru/Al_2O_3 catalysts (8). For the same reaction, Iyagba et al. (9) also found an initial increase in methane selectivity with increasing chlorine content on Ru/SiO_2 catalysts. However, the presence of chlorine on the Ru/SiO_2 catalysts strongly inhibits the hydrogenolysis of propane, as observed by Miura et al. (10). This opposite effect is possibly caused by chlorine site blocking and poisoning of a

group of ruthenium atoms necessary for the reaction.

Direct observations of the effect of residual chlorine on hydrogen chemisorption by Ru catalysts are possible via proton NMR. A comparison of two separate studies on the chlorine-contaminated Ru/SiO_2 (11) and the clean Ru/SiO_2 (12) catalysts indicates a significant difference in the NMR resonance lineshift for the hydrogen adsorbed on ruthenium surfaces. A downfield shift of the this resonance line in the presence of Cl was confirmed in a carefully conducted study (13).

The effect of chlorine on the hydrogen chemisorptive properties on the $Ru-Cu/SiO_2$ bimetallic catalysts has been overlooked since the very first publication on this type of bimetallic catalysts by Sinfelt (14). Recent studies on chlorine-contaminated (15) and chlorine-free (16) $Ru-Cu/SiO_2$ catalysts by NMR of adsorbed hydrogen have also indicated significant differences in the NMR resonance lineshifts for hydrogen chemisorbed on the bimetallic surfaces. While incorporation of Cu to Ru maintains or even slightly enhances the hydrogen chemisorption capacity via a Ru-to-Cu hydrogen spillover mechanism (16), the presence of Cl may adversely effect hydrogen adsorption on the Ru-Cu bimetallic system, and thus further complicate characterization of the $Ru-Cu/SiO_2$ catalysts.

To better understand the effect of chlorine on Ru/SiO_2

and Ru-Cu/SiO_2 catalysts, a detailed study was conducted. ^1H NMR was used as a direct probe to observe the influence of residual chlorine on the hydrogen adsorbed on ruthenium. Other techniques such as volumetric adsorption and x-ray fluorescence were also employed to provide supplementary information to assist the interpretations of the NMR results.

EXPERIMENTAL

Catalyst Preparation

The pure Ru/SiO_2 catalysts were prepared by incipient wetness impregnation of a solution of $RuCl_3 \cdot 3H_2O$ (AESAR) with a dried Cab-O-Sil HS5 silica support (300 m^2/g BET surface area). The $Ru-Cu/SiO_2$ bimetallic catalysts were prepared by coimpregnation of a solution of $RuCl_3 \cdot 3H_2O$ (AESAR) and $Cu(NO_3)_2 \cdot 6H_2O$ (AESAR, 99.999%) with the same support. About 2.2 ml of impregnating solution per gram of SiO_2 was needed to achieve incipient wetness. The slurries obtained after impregnation were dried for 24 hours at room temperature and 4 hours in air at 383 K. Three pure Ru/SiO_2 catalysts were prepared with a Ru loading of 4%, 5%, and 10%, respectively. The Ru loading for all but two Ru-Cu bimetallic catalysts was kept at 5% by total weight of the support and metals. A total of ten different $Ru-Cu/SiO_2$ catalysts were prepared to give a wide range of copper loading. Two Ru-Cu bimetallic catalysts with the highest Cu contents were prepared with a Ru loading of about 3% to avoid excessive overall metal loadings.

Catalyst Reduction

Catalyst reduction was carried out using a volumetric adsorption apparatus with a high-vacuum system described

previously (12, 13, 16). Reduction by hydrogen was performed directly inside a Pyrex cell of the adsorption apparatus. Approximately one gram of a catalyst sample was loaded into the flow-through cell, which was then attached to one of the sample ports of the manifold. While helium gas was allowed to flow through the sample bed in the cell, the temperature of the cell was raised to 423 K. Then helium was switched off and replaced by hydrogen at a flow rate of 50 cm^3/min. A pre-reduction period of 1 hour proceeded at that temperature. The temperature was then raised at a rate of 10 K/min to 723 K. Further reduction was carried out for two additional hours at 723 K. Helium (99.999%) and hydrogen (99.8%) gases (Liquid Air Co.) were used as received.

Water Elution Treatment

The technique of hot water washing was first used by Muira et al. (10) to eliminate residual chlorine from a Ru/SiO_2 catalyst, although no experimental details were given. In the present study, the reduced Ru/SiO_2 catalyst samples were washed repeatedly in hot distilled water (90-95°C). Successive cycles of wash (one wash consisted of about 20 ml of water per gram sample) and reduction were performed for each sample. The washed samples were dried and reduced again in the flow-through cell at 673 K for 2 hours followed by a two-hour evacuation period to an ultimate

pressure of 10^{-6} Torr to remove traces of water and surface hydrogen before hydrogen chemisorption measurements were taken. Hydrogen chemisorption was carried out at room temperature on the washed samples after every wash. The water after wash was measured for acidity by a digital ATC pH meter (Cole-Parmer) and also analyzed by atomic absorption spectroscopy for Ru content.

For the Ru-Cu bimetallic catalysts, both cold (20°C) and hot water washing were used for removal of chlorine. First, the reduced catalyst samples were washed repeatedly by cold water. They were then dried and reduced again in flowing hydrogen before being washed repeatedly by hot water. The water after wash was also measured for pH value and analyzed by atomic absorption spectroscopy for both ruthenium and copper contents.

Volumetric Adsorption

The volumetric adsorption was also carried out in the above-mentioned adsorption apparatus. Hydrogen gas for volumetric adsorption was purified by simply passing it through a catalytic hydrogen purifier (Engelhard Deoxo) in series with a gas purifier with Drierite and 5 Å molecular sieve (Alltech) to remove traces of oxygen and moisture. Hydrogen adsorption experiments were performed at ambient temperature (294 K). The total hydrogen adsorption isotherm

was measured in a pressure range of 0-30 Torr. The isotherm for reversible hydrogen adsorption was collected under the same conditions after a 10 min evacuation period to 10^{-6} Torr following the total adsorption. The irreversible hydrogen uptake was obtained by taking the difference between the values of the total and the reversible isotherms extrapolated to zero pressure. An equilibration time of 4 hours was used for the initial dose and 1 hour for subsequent doses.

X-ray Fluorescence Analysis

A selected number of Ru/SiO_2 and $Ru-Cu/SiO_2$ catalyst samples were analyzed quantitatively by the method of x-ray fluorescence (XRF) to determine the chlorine contents in these catalysts. The catalysts were reduced at least once prior to x-ray fluorescence analysis. Initially, a reduced catalyst sample (about 0.1 g) was prepared for quantitative analysis by combining with silica (0.3 g Alfa) in a Spex grinding mill and the mixture was homogenized for 3 minutes. Then, the resulting sample was poured into a Spex cup for XRF analysis. Polypropolene film with a thickness of 6.3 μm was used to seal the sample in the Spex cup.

Two different techniques were employed to quantify the amount of Cl present in the catalyst samples. The first method consisted of spiking the catalyst samples with the analyte (chlorine in this case) and then extrapolating to

obtain the initial concentration of Cl in the samples. The second method simply compared the intensity of a standard (NaCl) containing 1000 ppm Cl with those from the catalyst samples. The two methods yielded very close results on all the samples with experimental errors of 1.5% or less. The average result between the two measurements was reported.

The analyses were carried out using a Siemens SRS-200 sequential x-ray fluorescence spectrometer. A chromium x-ray tube operated at 50 kV and 50 mA was used as the excitation source.

NMR Sample Treatment

A needle-bellows assembly made of stainless steel was used for direct reduction of a catalyst sample in flowing hydrogen inside a 5-mm NMR tube (12). The syringe needle (18 gauge) was capable of moving vertically by more than 6 cm through adjustable compression and extension of the bellows. Vacuum-tight connections were made between the NMR tube and the needle-bellows assembly and also between the assembly and the manifold described above. In addition, a cylindrical furnace provided uniform heating around the NMR tube and the temperature of the furnace was monitored and controlled to better than ± 1 K.

With helium gas flowing through the needle, the needle was lowered to the bottom of the NMR tube, which contained

approximately 60 mg of catalyst sample. The procedure for reduction in flowing hydrogen was the same as previously described for the volumetric adsorption experiment, with a hydrogen flow rate of 15 cm^3/min. After reduction, the needle was lifted out of the sample, and evacuation proceeded for 2 hours at the reduction temperature before the sample was allowed to cool to ambient temperature. Up to four samples could be reduced simultaneously. Purified hydrogen was then dosed through the needle separately to each sample and the system was allowed to equilibrate for 4 hours. The NMR tube containing the sample was then immersed in a water bath and sealed off with a micro-torch. The exact sample weight was measured after the NMR tube was heat-sealed by subtracting the tare weight of the tube, which was measured prior to loading the sample.

NMR Experiment

The home-built NMR spectrometer (17) used for the present study was operated at 220 MHz for proton resonance. A proton-free probe with a doubly wound coil (18) was used for all the NMR measurements. The probe quality factor Q was set at about 100 to obtain the optimal values of sensitivity and ring down time for a fixed pulse power. A detailed description of the spectrometer's rapid-recovery receiving system has been published elsewhere (19).

All NMR spectra were collected under a repetitive 90° single-pulse sequence. The recycle time between rf pulses was set at 0.2s to selectively suppress the intense signal associated with protons in the silanol group in the catalyst support, which has a relatively long spin-lattice relaxation time T_1 (on the order of seconds). The above repetition rate avoids T_1 saturation of the peak corresponding to hydrogen adsorbed on ruthenium. The total number of scans for data acquisition on each catalyst sample was 10,000 for adequate signal-to-noise ratio. The inversion recovery pulse sequence (180°-τ-90°) was applied here to measure the spin-lattice relaxation times of the silanol protons (in the time domain) and of the hydrogen adsorbed on ruthenium (in the frequency domain). A pure water sample was used as the reference standard for the observed lineshifts.

For accuracy in spin counting, the water sample was doped with sufficient $FeCl_3$ such that the linewidths of the standard and unknown were comparable. The doped water was sealed in a capillary tube having the same length as the catalyst sample in the NMR tube to offset errors due to B_1 inhomogeneity of the coil. All NMR measurements were taken at ambient temperature (294 ± 1 K).

A pulse spin labeling experiment was performed on a Ru Cu/SiO_2 catalyst to test the exchange for hydrogen adsorbed on different metal adsorption sites. In this experiment, a

soft prepulse was used to selectively invert spins which would be at the frequency associated with protons on Ru. The pulse was 40 μs wide, corresponding to a 3-dB bandwidth of ± 6.25 kHz (± 28 ppm) and was centered at 50 ppm upfield. After a delay period τ (varying between 50 μs and 60 ms) following the soft prepulse, the magnetization of all protons was placed in the x-y plane of the rotating frame with a hard (2 μs pulse width) $90°_x$ pulse, and the magnetization was monitored along the y direction of the rotating frame.

RESULTS

Ru Monometallics

Two ^1H NMR spectra for the reduced and unwashed 10% Ru/SiO_2 catalyst samples under different hydrogen adsorption conditions are shown in Figure 1. Spectrum A corresponds to adsorption under 30 Torr hydrogen; Spectrum B corresponds to the condition of evacuation to 10^{-6} Torr for 10 min after adsorption under 30 Torr hydrogen. The spectra indicate an intense resonance at about 4 ppm corresponding to the silanol proton in the silica support and a broad shoulder resonance upfield at about 50 ppm corresponding to hydrogen adsorbed on ruthenium. The results reported here are in agreement with the previous observations on chlorine-contaminated Ru/SiO_2 catalysts (11, 13, 15). The spectra can be deconvoluted by fitting a Lorentzian line for the silanol peak and a Gaussian line for the hydrogen-on-ruthenium peak. Thus the intensity of the hydrogen-on-metal peak can be obtained by integrating the area of the deconvoluted peak.

Figure 2 shows two ^1H NMR spectra for the washed (six washes) 10% Ru/SiO_2 catalyst under two different hydrogen adsorption conditions. Spectrum A corresponds to adsorption under 30 Torr hydrogen and Spectrum B corresponds to the condition of high vacuum to 10^{-6} Torr for 10 min after adsorption under 30 Torr hydrogen. Similarly, two resonance

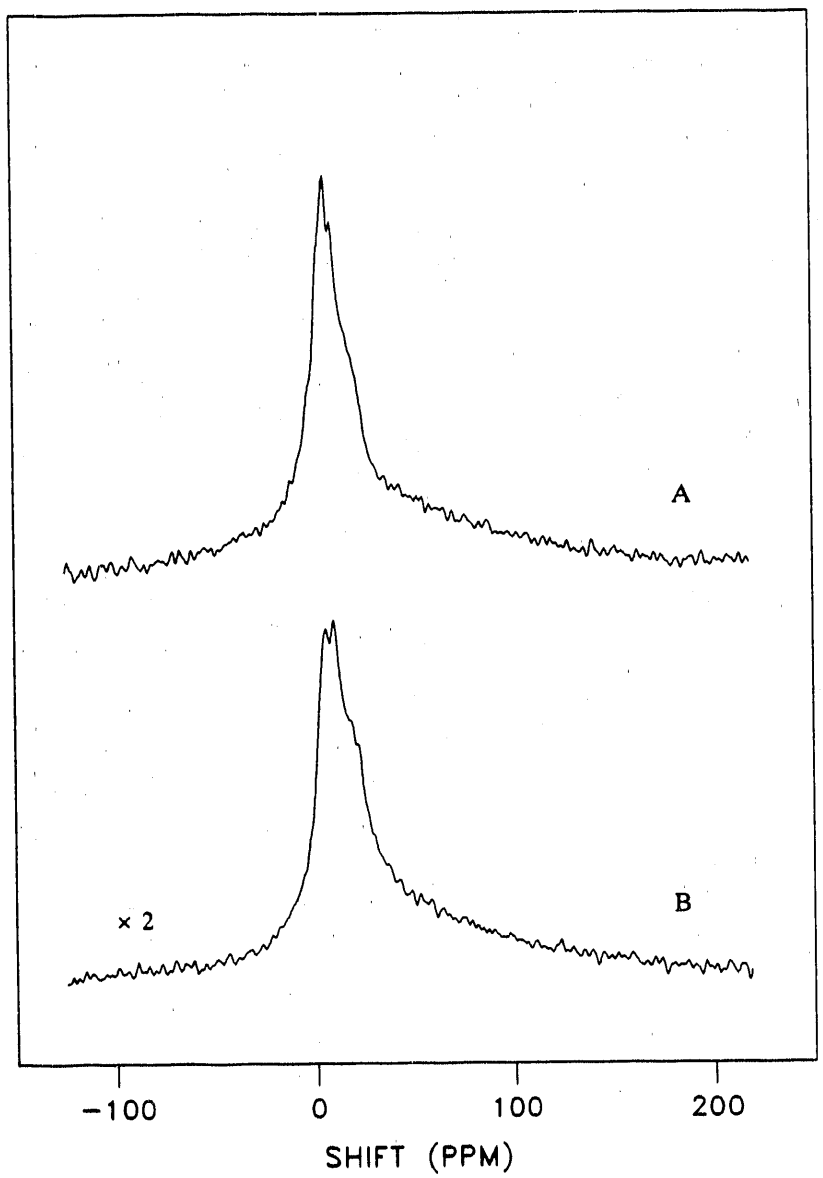

Figure 1. NMR spectra of adsorbed hydrogen on an unwashed 10% Ru/SiO_2 catalyst under the condition of A) 30 Torr hydrogen gas, and B) evacuation to 10^{-6} Torr for 10 min after adsorption under 30 Torr gaseous hydrogen. Pure water was used as the reference for the lineshift

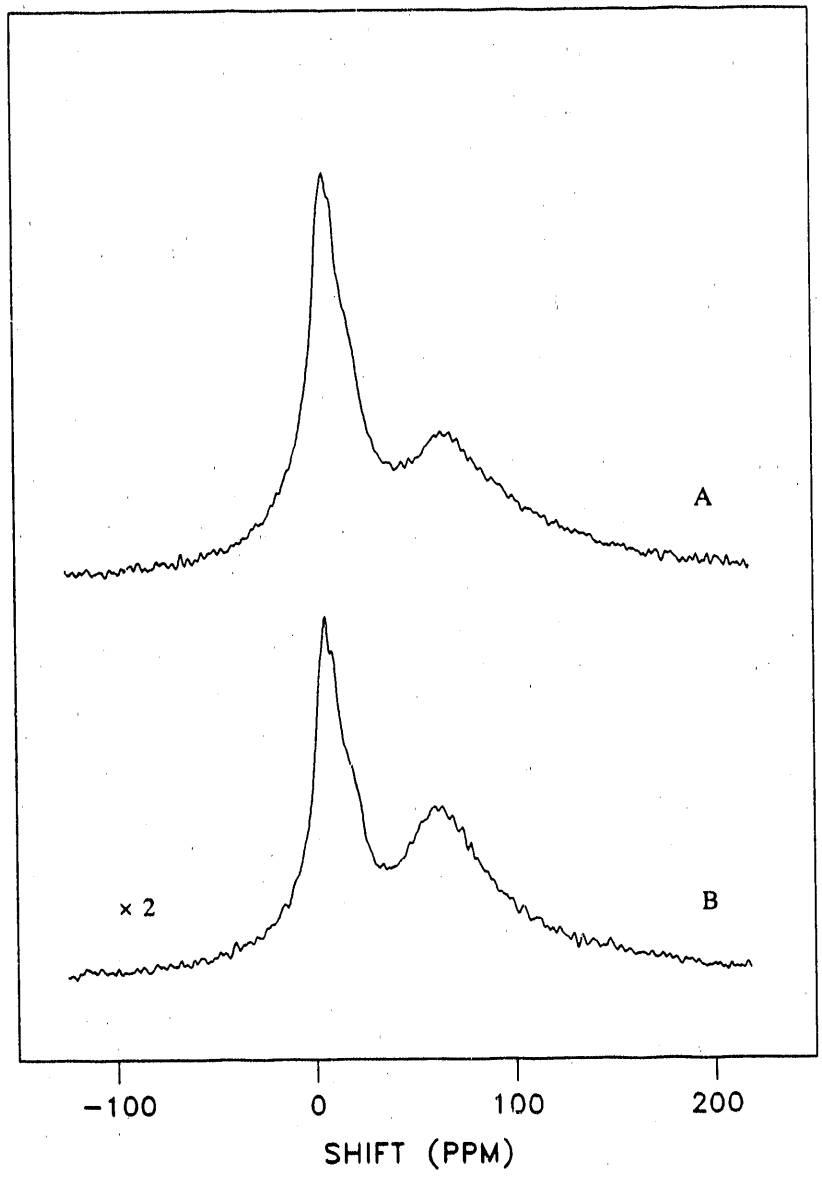

Figure 2. NMR spectra of adsorbed hydrogen on an washed (six washes) 10% Ru/SiO_2 catalyst under the condition of A) 30 Torr hydrogen gas, and B) evacuation to 10^{-6} Torr for 10 min after adsorption under 30 Torr hydrogen. Water was used as the reference for the lineshift

peaks are observed in each spectrum. The downfield peak at about 4 ppm represents the silanol proton in the silica support and the upfield peak represents hydrogen adsorbed on ruthenium. The first moment of the upfield peak in Spectrum A corresponding to both the reversible and the irreversible hydrogen adsorbed on Ru resonates at 63 ppm. Spectrum B, corresponding to only the irreversible hydrogen adsorbed on ruthenium has a first moment of 61 ppm. The two overlapped resonances can be deconvoluted by fitting two Lorentzian lines, and then the intensity for the hydrogen-on-ruthenium peak can be obtained by integrating the peak. The measured intensities of the hydrogen-on-metal peaks for the washed catalysts are about 4 to 5 times the intensities for the unwashed catalysts.

The effect of hot water washing on hydrogen adsorption capacity for the 10% Ru/SiO_2 catalyst is illustrated in Figure 3. Measurements form both the total and the weak hydrogen adsorption are shown in the figure. The results indicate a significant enhancement in hydrogen chemisorption after the first two washes and only small improvements for further washes. Note that the amounts of both the reversible and the irreversible hydrogen adsorption increase after washing. The results from the NMR measurements for the unwashed and the washed (six times) catalysts are also shown in the figure. The values measured by NMR are consistently

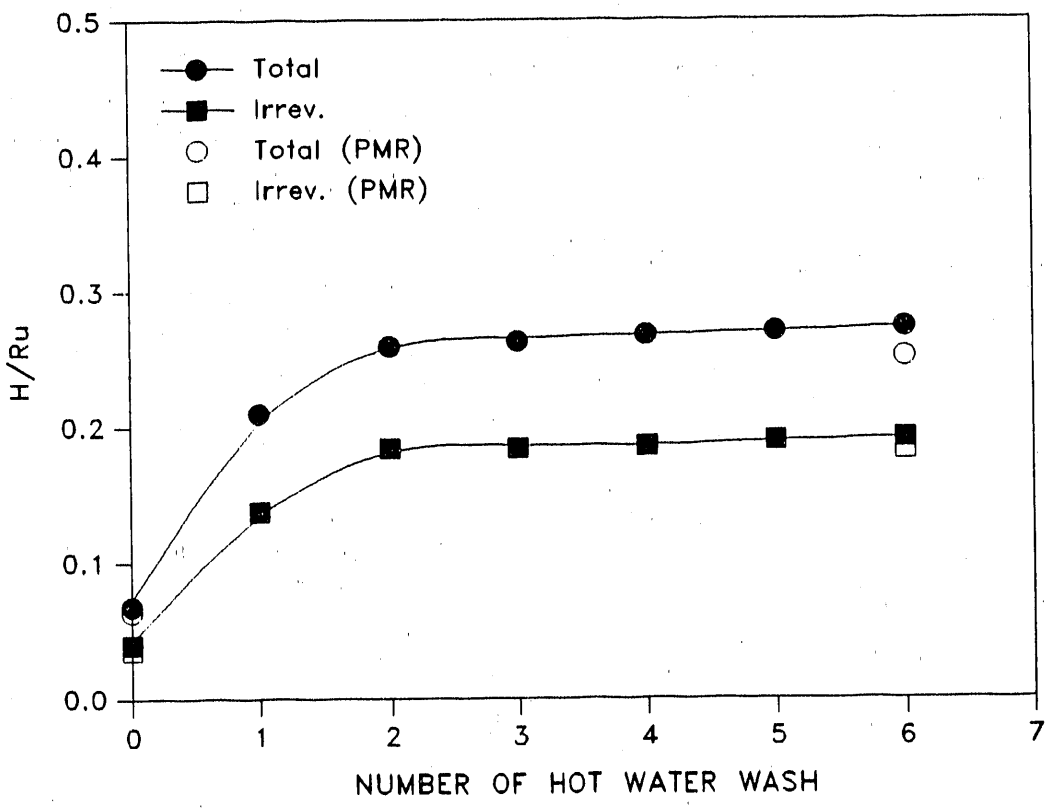

Figure 3. Variations of the H/Ru ratios for both the total and the reversible adsorption measured by the volumetric technique as functions of the number of hot water wash on a 10% Ru/SiO_2 catalyst. Values from the NMR measurements are also shown

lower than but very close to the values obtained by the volumetric hydrogen chemisorption.

The volumetric hydrogen chemisorption and the ^{1}H NMR techniques were also applied to measure the chemisorptive properties of the 4% Ru/SiO_2 catalysts. Three NMR spectra collected under 30 Torr hydrogen pressure for A) 4% Ru/SiO_2 with five washes; B) 4% Ru/SiO_2 with only one wash; and C) unwashed 4% Ru/SiO_2 samples are shown in Figure 4. Again, two resonances representing the silanol proton (downfield peak) and the hydrogen adsorbed on ruthenium (upfield peak) are observed. The first moment of the upfield peak in Spectra A, B, and C is located at about 65 ppm, 57 ppm, and 47 ppm, respectively. Hot water washing not only moves the upfield peak further toward upfield but also increase the upfield peak intensities by a factor of about 6.

Similar trends in the upfield lineshifts and intensities were observed for the same set of 4% Ru/SiO_2 catalysts under the condition of evacuation to 10^{-6} Torr for 10 min after adsorption in 30 Torr hydrogen, as shown in Figure 5. The maxima in the upfield peaks in Spectra A, B, and C are centered at about 62 ppm, 56 ppm, and 46 ppm, respectively. The upfield resonance line for the unwashed 4% Ru/SiO_2 catalyst (Figure 5) has a rather weak intensity and appears as a shoulder on the right hand side of the intense silanol peak.

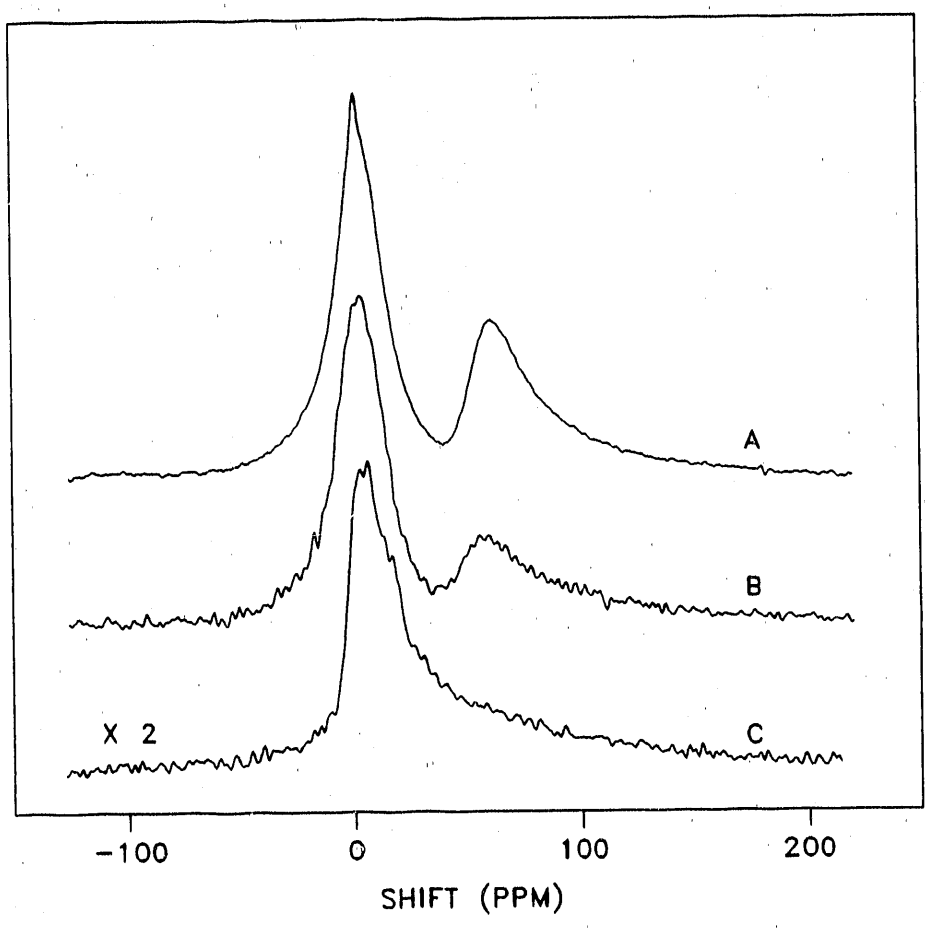

Figure 5. NMR spectra of adsorbed hydrogen on a 4% Ru/SiO_2 catalyst under evacuation condition (10^{-6} for 10 min) after adsorption under 30 Torr hydrogen for a catalyst sample with A) five washes, B) one wash, and C) no wash by hot water. Pure water was used as the reference for the lineshift

Hot water washing on a chlorine-contaminated 4% Ru/SiO_2 catalyst has a similar effect on the hydrogen chemisorption capacity as on a 10% Ru/SiO_2 catalyst. As shown in Figure 6, the amount of adsorbed hydrogen on ruthenium increases with increasing number of hot water washings. It is noticed that the increasing trend is more gradual for the 4% Ru/SiO_2 than for the 10% Ru/SiO_2 catalyst and it levels off after about five washes. The intensity measurements on the upfield peaks of the NMR spectra shown earlier in Figures 4 and 5 were also plotted in Figure 6 for direct comparison with the volumetric hydrogen chemisorption. The results obtained from the two methods are in good agreement although the NMR measurements consistently give lower values (8% lower at 6 washes) than those from volumetric measurements. Hot water washing increases the total hydrogen chemisorption capacity by a factor of about 6 for the 4% Ru/SiO_2 catalyst.

The solution after hot water washing was found to be acidic, especially for the first few washes. The acidity of the washed solution decreased as the number of water washes increased and eventually became nearly neutral. For example, the solution after one wash for the 4% Ru/SiO_2 catalyst indicated a pH value of 2.9, and that after five washes indicated a pH value of 7.1, approaching the pH value of 7.5 for the distilled water. Also, the solution after one wash was found to contain Cl^- ions as indicated qualitatively by

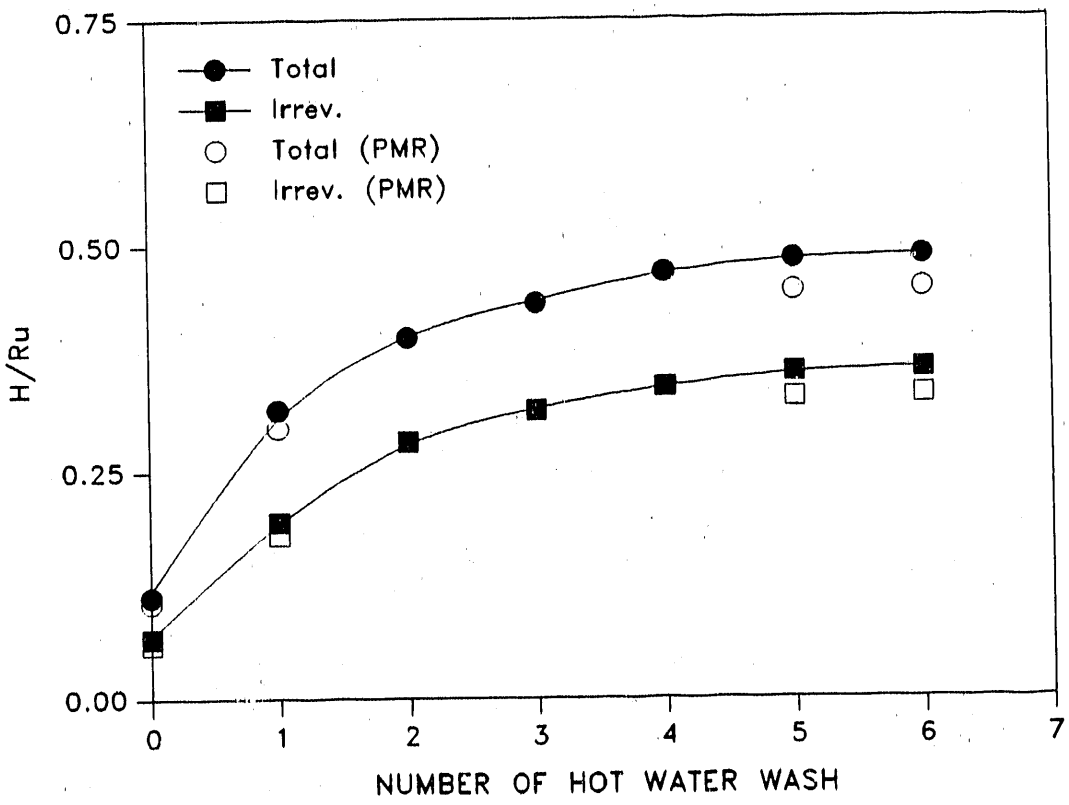

Figure 6. Variations of the H/Ru ratios for both the total and the reversible adsorption measured by the volumetric technique as functions of the number of hot water wash on a 4% Ru/SiO_2 catalyst. Values from the NMR measurements are also shown

observing the formation of a white precipitation when silver nitrate was added. In a separate experiment, the $RuCl_3 \cdot 3H_2O$ precursor was first dissolved in distilled water and then heated to about 90°C. The resulting solution became a black suspension with the formation of $Ru(OH)_3$ precipitation in an acidic solution with a pH value as low as 1.5 (measured at room temperature).

The hot water washing procedure was first reported by Miura et al. (10) as an effective means of removing residual chlorine from a Ru/SiO_2 catalyst prepared from the $RuCl_3 \cdot 3H_2O$ precursor. This procedure has the advantage over the ammonia washing procedure in that it does not wash out Ru from the catalyst. This finding was verified in the present study by atomic absorption spectroscopy on the solution after wash showing only trace quantities of ruthenium (< 0.5 ppm).

Numerical values for results from hydrogen adsorption and ^1H NMR measurements on the 4% Ru/SiO_2 catalyst are listed in Table 1 for a selected number of hot water washing. As indicated, the results obtained by the two techniques are in good agreement. Since the amount of irreversibly adsorbed hydrogen on ruthenium is independent of the hydrogen pressure (12), the H/Ru ratio for this adsorbed state of hydrogen is used to measure the fraction of ruthenium exposed at the metal surfaces.

The effect of residual chlorine on the bonding and the

Table 1. Hydrogen chemisorption and ^1H NMR results on a 4% Ru/SiO_2 catalyst

Number of hot water wash[a]	Total H/Ru		Irreversible H/Ru	
	Adsorption	^1H NMR	Adsorption	^1H NMR
0	0.112	0.105	0.066	0.062
1	0.318	0.296	0.194	0.180
5	0.484	0.449	0.359	0.331
6	0.488	0.452	0.363	0.334

[a]Approximately 20 ml of distilled water per gram of catalyst was counted as one wash.

electronic state of the adsorbed hydrogen on ruthenium can be revealed by measuring the variations of the peak location and the spin-lattice relaxation time as a function of chlorine coverage. Table 2 lists the ^1H NMR results on the lineshift for the hydrogen-on-ruthenium peak and the spin-lattice relaxation times for both the upfield and the downfield peaks obtained from the 4% Ru/SiO_2 catalyst under 30 Torr hydrogen pressure. As shown earlier in Figure 4, the upfield peak location moved upfield as the number of washes increased. This is also indicated by an increasing lineshift value as

Table 2. Proton NMR results showing the effects of hot water washing on a 4% Ru/SiO_2 catalyst.

Number of hot water wash[a]	Upfield peak shift (ppm)[b]	Spin-lattice relaxation time(sec.) Upfield peak[b]	Downfield peak[b]
0	47	0.025	7.4
1	57	0.015	5.1
5	65	0.011	2.4
6	66	0.011	2.2

[a]Approximately 20 ml of distilled water per gram of catalyst was counted as one wash.

[b]All catalyst samples were under 30 Torr hydrogen at equilibrium at room temperature.

shown in Table 2. The difference in the lineshift value between the thoroughly washed (six washes) and the unwashed catalysts was as large as 19 ppm. It is interesting to note that the spin-lattice relaxation times for both the hydrogen-on-ruthenium (upfield) peak and the silanol (downfield) peak decreased as the number of wash increased. The magnitude of changes for these measured parameters are also significant.

The correlation between the number of washes and the

chlorine content in the 4% Ru/SiO_2 catalyst was established by experimental data obtained from the x-ray fluorescence spectroscopy. Table 3 illustrates these data and values derived from these data. The weight percentage of chlorine in the catalyst was measured from the x-ray fluorescence spectroscopy, and the molar ratio Cl/Ru and the chlorine coverage $Cl/Ru_{(s)}$ were computed based on these results.

The calculations are based on the assumptions that no chlorine was retained in the silica support after reduction in hydrogen and that chlorine was only associated with the surface ruthenium. The first assumption seems to be valid since no chlorine was detected by XRF on a pure SiO_2 sample treated with 6N HCl solution and reduced under the same conditions as the catalyst samples. Also, the results of the calculated chlorine coverage are reasonable since chlorine is not expected to remain inside the bulk Ru particles at the reduction temperature (723 K) because of its volatility.

The results shown in Table 3 indicate a considerable amount of Cl was in the unwashed catalyst but no Cl was found after six washes. Note that all the Cl/Ru molar ratios are less than the dispersion for the clean (washed six times) Ru/SiO_2 catalyst (also see Table 1). The $Cl/Ru_{(s)}$ ratios indicate submonolayer coverage of chlorine in all catalyst samples, and about 65% of the Ru surfaces was covered by Cl in the unwashed catalyst.

Table 3. Chlorine contents in 4% Ru/SiO_2 catalysts as measured from x-ray fluorescence spectroscopy

Number of hot water wash[a]	Cl wt%[b]	Cl/Ru[c]	$Cl/Ru_{(s)}$[d]
0	0.330	0.2352	0.649
1	0.120	0.0855	0.236
5	0.012	0.0086	0.024
6	0.000	0.0000	0.000

[a]Approximately 20 ml of distilled water per gram of catalyst was counted as one wash.

[b]The XRF results are in weight percentage of chlorine on the basis of total catalyst weight.

[c]The values are molar ratios.

[d]The values are the chlorine coverage calculated on the basis of the dispersion for the chorine-free catalyst.

Direct correlations between the NMR lineshifts for the hydrogen-on-ruthenium peak and the chlorine coverage are plotted in Figure 7. A similar decreasing trend for the lineshift variations with the chlorine coverage was found both under 30 Torr hydrogen and evacuation after exposure to 30 Torr hydrogen. In both cases, the decreasing trend was

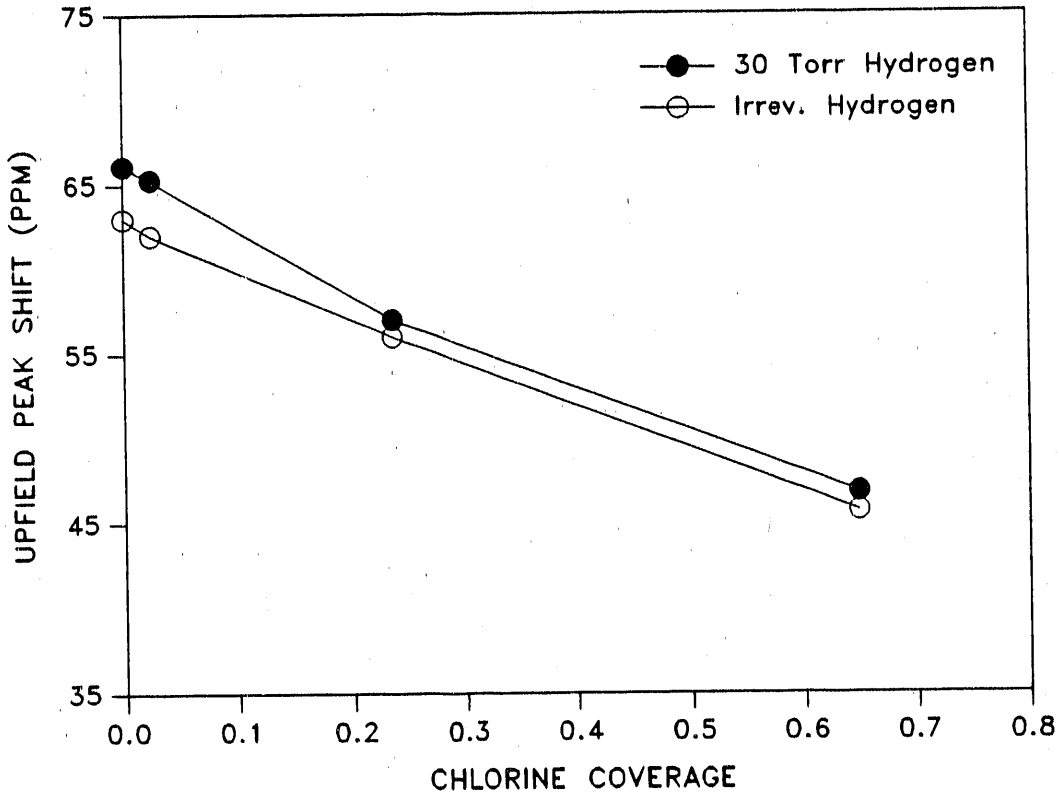

Figure 7. Variations of the upfield peak shift on a 4% Ru/SiO_2 catalyst under 30 Torr hydrogen and evacuation after adsorption in 30 Torr hydrogen as functions of chlorine coverage

Table 4. Chlorine contents on a series of unwashed Ru-Cu/SiO_2 bimetallic catalysts as measured by x-ray fluorescence spectroscopy

Catalyst	Cl wt%[a]	Cl/M[b]
5% Ru	0.35	0.20
5% Ru-0.16% Cu	0.46	0.25
5% Ru-0.24% Cu	0.36	0.19
5% Ru-0.39% Cu	0.36	0.18

[a]Values are in weight percentage as measured from XRF.

[b]Values represent the Cl to (Ru + Cu) molar ratios.

somewhat more gradual at high than at low chlorine coverage.

Ru-Cu Bimetallics

The x-ray fluorescence method revealed a considerable amount of chlorine in reduced 5% Ru/SiO_2 and 5% $Ru-Cu/SiO_2$ catalysts, as shown in Table 4. A comparable amount of residual chlorine was found in all catalysts, with somewhat higher values for the bimetallic catalysts.

The effect of chlorine on hydrogen adsorbed on the Ru-Cu bimetallic catalysts is even more complex than that on the monometallic Ru catalysts. Figure 8 shows a set of ^1H

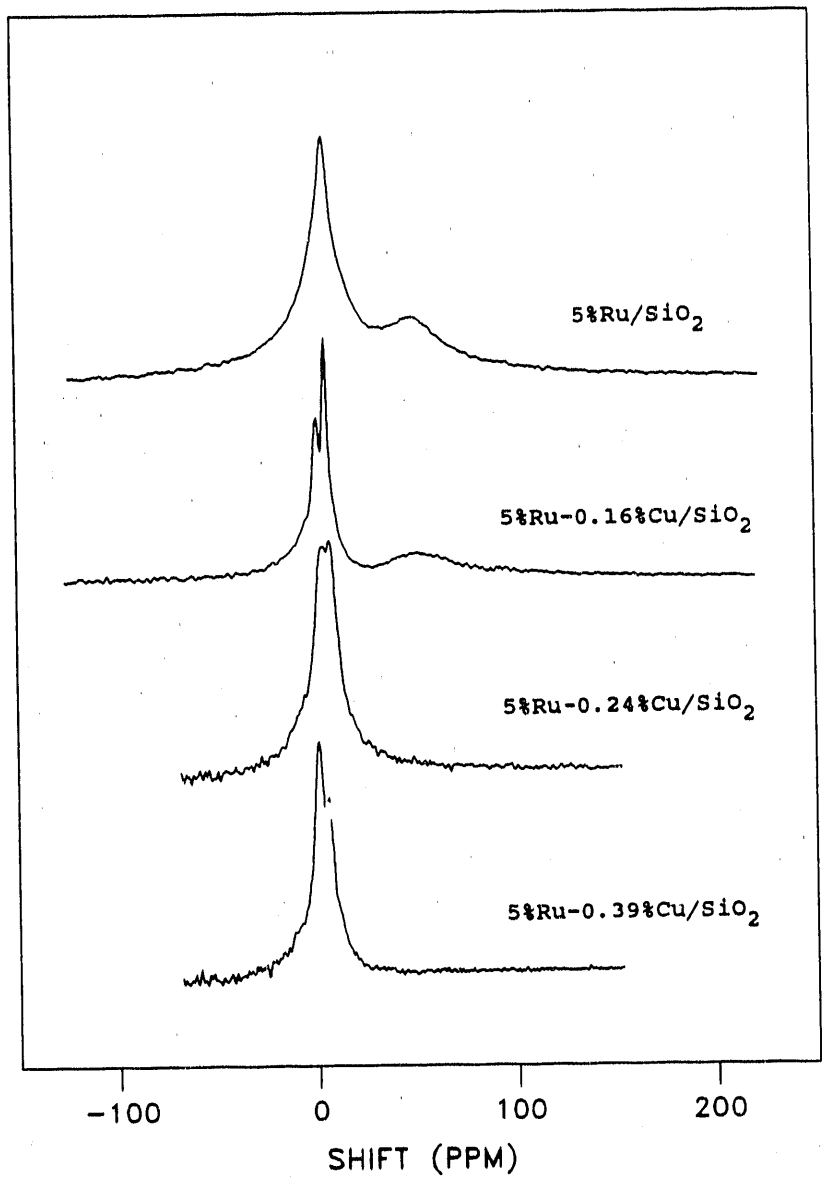

Figure 8. A set of NMR spectra on a 5% Ru/SiO_2 catalyst and three 5% $Ru-Cu/SiO_2$ with various copper loadings under 30 Torr hydrogen gas. All catalyst samples were not washed after reduction. Pure water is used as the reference for the lineshift

NMR spectra on chlorine-contaminated 5% Ru/SiO_2 and 5% Ru-Cu/SiO_2 catalysts with various copper loadings under the adsorption condition of 30 Torr hydrogen. Two resonance peaks were observed on the 5% Ru/SiO_2 catalyst at about 5 ppm and 47 ppm, corresponding to the silanol proton (downfield peak) and the hydrogen adsorbed on ruthenium (upfield peak), respectively, as noted earlier on the 4% and 10% Ru/SiO_2 catalysts. When copper is added to the catalyst, a third peak emerges downfield of the silanol peak and appears at 3 to 1 ppm. This peak moves somewhat further downfield as the copper content increases. The spectra also shows that the hydrogen-on-ruthenium peak diminishes in intensity and that the third peak is stronger in intensity as the copper loading increases.

This peak observed downfield of the silanol peak was originally assigned to adsorbed hydrogen exchanging between surface ruthenium and copper atoms (15). However, in the absence of Cl these third resonance is located considerably more upfield and appears on the right side of the silanol peak (16). Therefore, the peak observed here is assigned to hydrogen exchanging on both Ru and Cu surface atoms which are influenced by chlorine.

To test the identification of this peak associated with exchanging hydrogen, a pulse spin labeling experiment was performed on the 5% Ru-0.39% Cu/SiO_2 bimetallic catalyst

under 30 Torr hydrogen. The delay time between a soft 180° prepulse and a hard 90° sampling pulse was varied to observe its effect on the resulting spectrum. The variation of the ^1H NMR spectral features with the delay time under the soft-delay-hard pulse sequence is shown in Figure 9. As can be seen, the soft pulse applied at the location of 50 ppm, where the hydrogen chemisorbed on ruthenium resonates, decreased the intensity of the third peak, associated with exchanging hydrogen, for relatively short delay times. The effect of the soft pulse on the exchange peak diminished as the delay time increased. At delay periods of 40 ms and longer, the soft pulse had no effect upon the exchange peak. These results are interpreted as indicating that the third peak is associated with hydrogen exchanging between chlorine-contaminated Cu and Ru in the intermediate exchange regime.

The water elution technique used for the chlorine-contaminated Ru/SiO_2 catalysts was extended to the $Ru-Cu/SiO_2$ bimetallic catalysts. To minimize the loss of copper from the catalysts, the reduced catalyst samples were first washed repeatedly in cold distilled water, then reduced again and washed in hot water. The XRF method indicated that about 50% to 60% of the residual chlorine was washed out after repeated cold water washing and virtually all chlorine was eliminated from the catalysts after repeated hot water washing.

Figure 10 shows the results of volumetric hydrogen

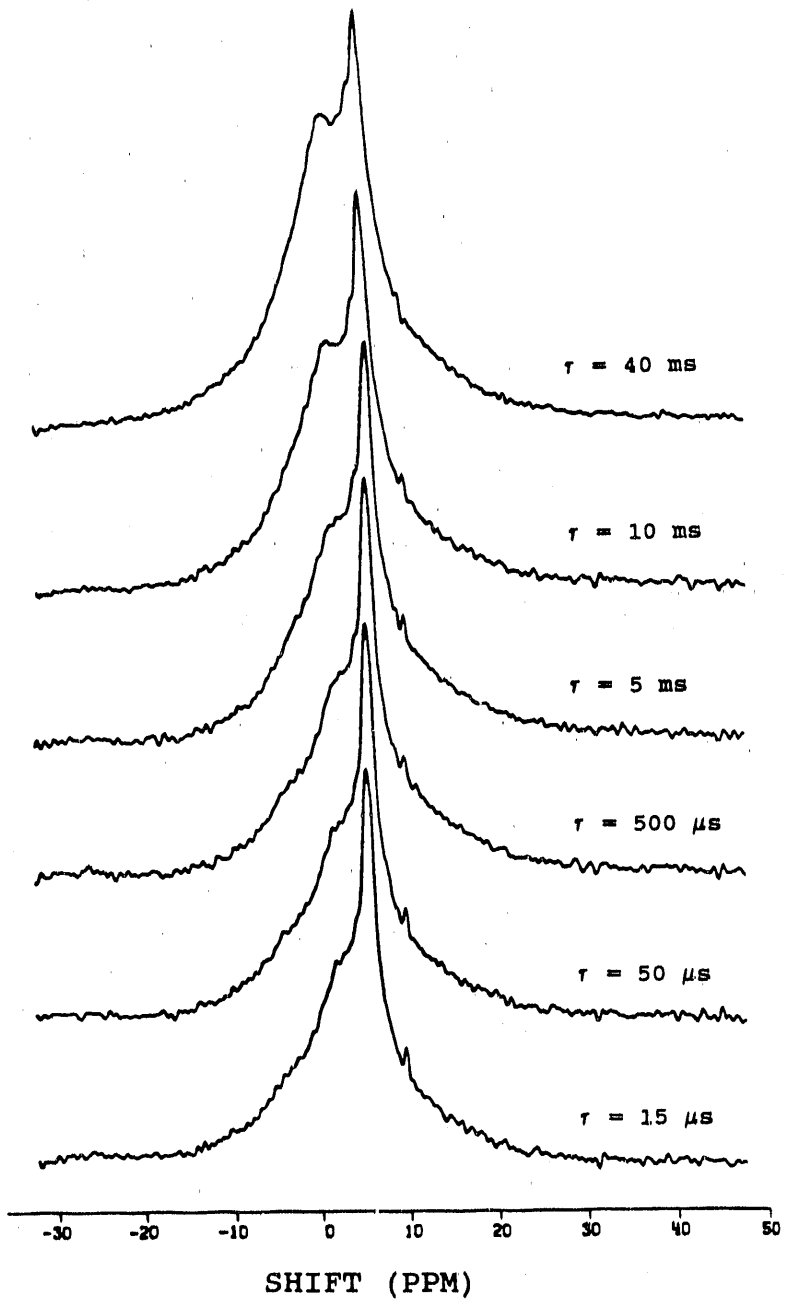

Figure 9. A set of NMR spectra on a 5% Ru-0.39% Cu/SiO_2 catalyst under 30 Torr hydrogen. The spectra were collected from a spin labeling experiment with a soft-and-hard pulse sequence. The delay time between the soft and the hard pulse is as indicated in the figure. Pure water was used as the reference for the lineshift

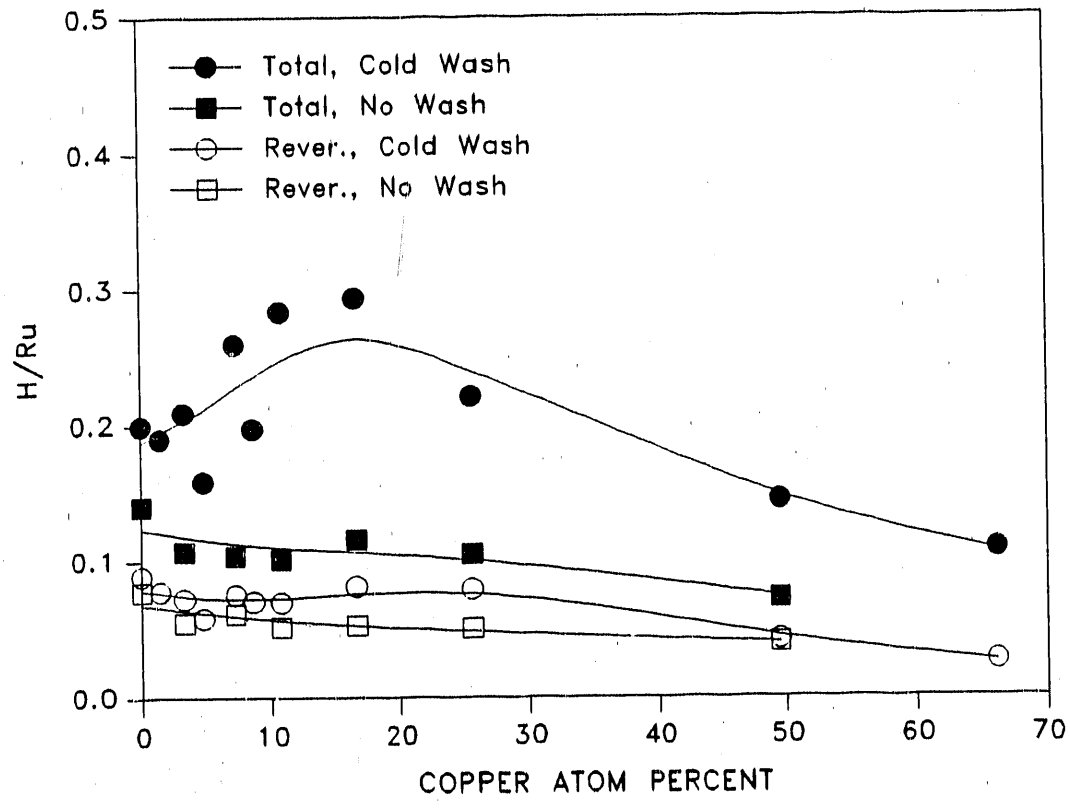

Figure 10. The H/Ru ratios for both the total and the reversible adsorption of hydrogen on a series of 5% Ru-Cu/SiO_2 bimetallic catalysts. Results from measurements on the unwashed catalysts and the cold-water-washed catalysts are shown for comparison

chemisorption for the unwashed and the cold-water-washed 5% Ru/SiO_2 and 5% $Ru-Cu/SiO_2$ catalysts. The total hydrogen chemisorption capacity increased by a factor of two or even more in some cases for the cold-water-washed catalysts. The trend of total hydrogen adsorption for the unwashed catalysts shows only a very moderate decrease with increasing copper content, while that for the cold-water-washed catalysts exhibits a maximum value at about 17 at.% copper, although the data are scattered. The trends for the weak hydrogen adsorption are quite similar for catalysts under the two different treatment conditions and the amounts for the cold-water-washed catalysts are only slightly larger than those for the unwashed catalysts.

Hot water washing further increases the total hydrogen chemisorption capacity of the same set of catalysts by nearly a factor of two, as shown in Figure 11. Similar trends in the total hydrogen chemisorption capacity were observed for both the cold-water-washed and hot-water-washed catalysts. A maximum in total hydrogen chemisorption was found at about 17 at.% Cu for the two treatment conditions. The reversible hydrogen chemisorption also displays similar trends for catalysts under the two treatment conditions, with only a gradual decrease with increasing copper content.

The irreversible hydrogen chemisorption capacity is used to count the total number of metal atoms exposed at the

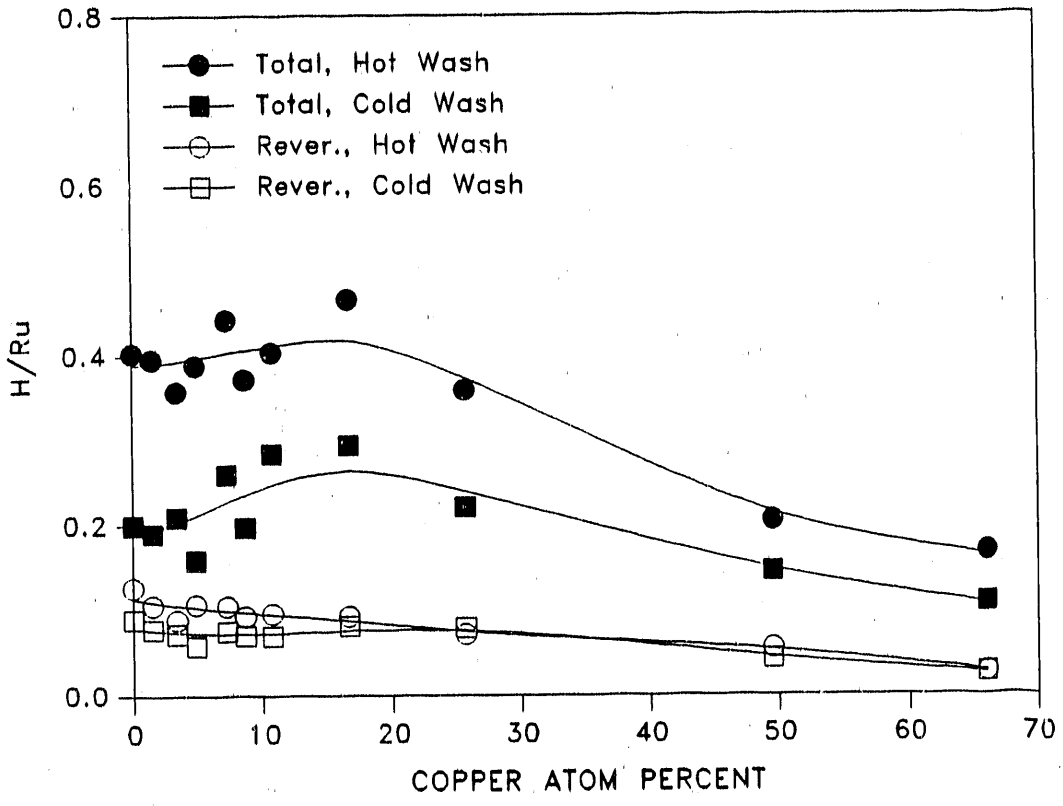

Figure 11. The H/Ru ratios for both the total and the reversible adsorption of hydrogen on a series of 5% Ru-Cu/SiO_2 bimetallic catalysts. Results from measurements on the cold-water-washed catalysts and the hot-water-washed catalysts are shown for comparison

Table 5. Results of irreversible hydrogen chemisorption on a series of Ru-Cu/SiO_2 catalysts under different water washing conditions

Catalyst in wt.%	Cu content in at.%	H/Ru No wash	H/Ru Cold wash	H/Ru Hot wash
5% Ru	0.0	0.063	0.110	0.276
5%Ru-0.048%Cu	1.5	-----	0.112	0.290
5%Ru-0.11%Cu	3.4	0.052	0.137	0.269
5%Ru-0.16%Cu	4.8	-----	0.100	0.281
5%Ru-0.24%Cu	7.1	0.042	0.184	0.337
5%Ru-0.30%Cu	8.7	-----	0.127	0.279
5%Ru-0.39%Cu	11.0	0.050	0.214	0.308
5%Ru-0.63%Cu	16.6	0.063	0.212	0.373
5%Ru-1.09%Cu	25.6	0.054	0.142	0.287
3.6%Ru-2.19%Cu	49.5	0.032	0.102	0.150
2.5%Ru-3.12%Cu	66.1	-----	0.082	0.142

metallic (12) and the bimetallic surfaces (16), since the quantity is independent of hydrogen pressure (for P > 3 Torr) and is not affected by hydrogen spillover from the metal(s) to the support (12). The quantity is taken as the difference between the total and the reversible hydrogen chemisorption

capacity. The values of the irreversible adsorption for catalysts that are unwashed, washed with cold water, and washed with hot water are listed in Table 5. The results show that the irreversible adsorption capacity increases by a factor of 2 to 3 with cold water washing and by a factor of 5 to 6 with hot water washing.

Striking differences between the hot-water-washed and the unwashed catalysts are also observed by the proton NMR spectroscopy. Figure 12 shows the NMR spectra for the hot-water-washed 5% Ru/SiO_2 and three 5% $Ru-Cu/SiO_2$ catalysts under 30 Torr hydrogen. Only two resonances were observed, corresponding to the silanol proton and the hydrogen adsorbed on Ru or Ru-Cu surfaces. The upfield resonance exhibits a considerable shift toward upfield after hot water washing compared with the unwashed catalysts, as shown in Figure 8. The intensities of the upfield peak is much stronger for the hot-water-washed catalysts than the unwashed catalysts.

The lineshift of the upfield peak moves downfield with increasing copper content, as reported for the clean $Ru-Cu/SiO_2$ bimetallic catalysts (16). The values of lineshift for the corresponding catalysts shown in Figure 12 are listed in Table 6. The change in the upfield peak lineshift is as much as 7 ppm for an increase in copper content from 0 to 11 at.% Cu. The magnitude of change is comparable with that reported on the clean $Ru-Cu/SiO_2$ bimetallic catalysts (16).

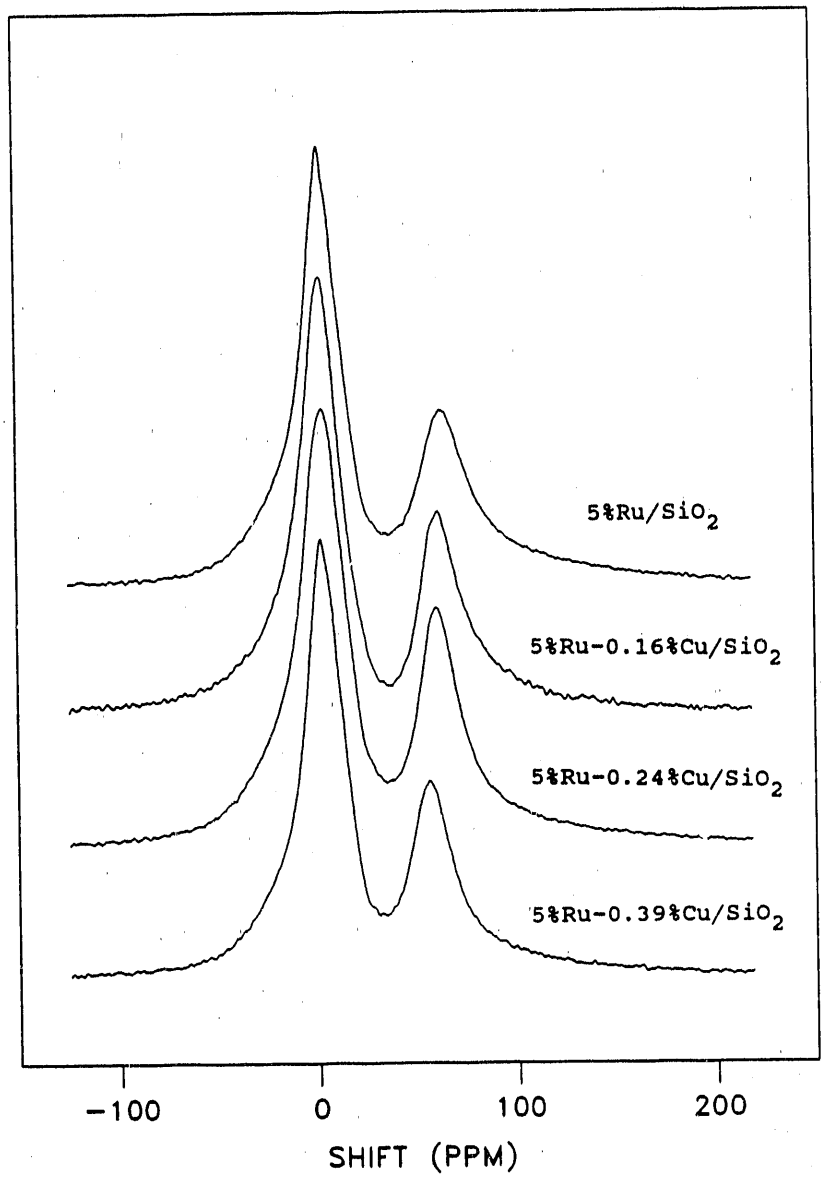

Figure 12. A set of NMR spectra on a 5% Ru/SiO_2 catalyst and three 5% $Ru-Cu/SiO_2$ with various copper loadings under 30 Torr hydrogen gas. All catalyst samples were washed thoroughly in cold then hot water. Water is used as the reference for the lineshift

Table 6. NMR lineshift values for hydrogen adsorbed on the metal(s) on a series of hot-water-washed Ru-Cu/SiO_2 catalysts

Catalyst	Copper at.%	Upfield peak shift[a] (ppm)
5% Ru	0.0	63.3
5% Ru-0.16% Cu	4.8	61.2
5% Ru-0.24% Cu	7.1	60.3
5% Ru-0.39% Cu	11.0	56.4

[a]All catalyst samples were under 30 Torr hydrogen.

DISCUSSION

Nature of Water Washing

The effectiveness of hot water washing in eliminating residual chlorine from Ru/SiO_2 catalysts has been observed by Miura et al. (10) and in the present study. However, the nature of the water washing process is poorly understood and has never been discussed in the literature. Sufficient experimental evidence has been gathered from the present study to enable us to propose a simple mechanism for this water washing process.

The experimental results have shown that chlorine does not remain in the silica support after reduction in flowing hydrogen at 450°C, as indicated by the XRF result on a silica support treated with hydrochloric acid. Since the ruthenium particles are likely to remain intact under the very mild condition of hot water washing and since all the residual chlorine in the catalysts can be washed out as indicated by XRF, the residual chlorine must be covering the Ru surfaces rather than staying inside the bulk Ru particles.

The fact that the washed solution is acidic and contains Cl^- ions indicates that the process is analogous to complete hydrolysis of $RuCl_3$ compound with formation of $Ru(OH)_3$ and HCl. Therefore, the water washing process on the Ru/SiO_2 catalysts is essentially a surface hydrolysis process, i.e.,

$$Ru_{(s)}Cl_x + xH_2O \quad <=====> \quad Ru_{(s)}(OH)_x + xHCl$$

with Cl being replaced by the OH group and entering the solution as HCl. The stoichiometric coefficient in the above equation should be less than one since only submonolayer Cl coverages were found in the Ru/SiO_2 catalysts (see Table 3). Since the hydroxyl group stays on the Ru surfaces after water washing, virtually no Ru is washed out by water, as verified by atomic absorption spectroscopy on the washed solution.

Furthermore, since the hydrolysis of $RuCl_3$ is in fact an endothermic process, increased temperature should favor the removal of Cl from the Ru surfaces. This is indeed observed on the 5% Ru/SiO_2 catalyst (see Figure 11 and also Table 5) showing a much enhanced hydrogen chemisorption capacity after hot water washing than after cold water washing.

The water washing process in the $Ru\text{-}Cu/SiO_2$ bimetallic catalysts may be similar to that in the Ru/SiO_2 catalysts since most copper compounds are expected to be completely reduced under the conditions used in this study. The fact that all Cl can be removed by hot water washing with only minimal loss of Cu indicates that the washing process is also a surface hydrolysis process.

Interaction between Ru and Cl

Kiskinova and Goodman (20) have studied the effect of Cl, S, and P on the saturation coverage and initial sticking coefficient of CO and H_2 on Ni(100). They find that the poisoning effect of Cl is slightly stronger than that of S, which is significantly more poisonous than P. They ascribe this effect to the differences in the electronegativities of the three poisons. The higher the electronegativity of the poison, the greater would be the assumed charge transfer between surface Ni atoms and the electronegative atoms. This charge transfer alters the surface electron density of Ni, resulting in suppressed adsorption of CO and H_2. Norskov et al. (21) and Lang et al. (22) have also proposed a model of short range (repulsive) electrostatic blocking of an adsorbed electronegative atom on the surface of a metal, which affects a certain area surrounding it.

In the case of chlorine adsorbed on small ruthenium particles, one may envision the surface Ru and Cl are being partially charged, i.e.,

$$Ru_{(s)}{}^{\sigma+}Cl_x{}^{\sigma-} \qquad (0 < \sigma < 1)$$

This seems to be reasonable because the surface ruthenium also interacts with and is stabilized electronically by the bulk Ru atoms. Alternatively, one may think of the Ru-Cl

interaction resulting in a redistribution of the electron density at the Ru surfaces. The electronegative Cl atoms tend to draw electrons from surface Ru atoms, which may further alter the electronic state of the bulk Ru atoms.

This postulate implies that the strength of the Ru-Cl interaction varies with the total number of bulk Ru atoms in a Ru particle. The Ru core serves as an "electron reservoir" to compensate for loss of valence electron density of surface Ru atoms due to charge transfer to chlorine. A stronger Ru-Cl interaction is expected for a smaller Ru particle (poorer charge compensation from the ruthenium core), while a weaker interaction is expected for a larger Ru particle. This will provide an alternate interpretation for the results obtained by Lu and Tatarchuk (3), who reported an increase in the activation energy for hydrogen adsorption with a decrease in Ru particle size. The results of the present study have also suggested such a variation of Ru-Cl interaction with the Ru particle size. The different trends shown in Figures 3 and 6 indicate that under identical conditions surface Cl adsorbed on a large Ru particle undergoes surface hydrolysis more easily than that adsorbed on a small Ru particle.

It has been suggested that adsorbed chlorine draws the 4d electrons from the surface Ru atoms (13), decreasing the density of 4d electrons of surface Ru which is essential for hydrogen chemisorption. This interpretation is consistent

with the observations from the present study which shows a striking change in lineshift for the hydrogen-on-ruthenium peak in the presence of chlorine (see Figures 4 and 7 and also Table 2). Since the valence d electrons are responsible for the upfield Knight shift of the hydrogen adsorbed on all noble transition metals (11), the downfield movement of this peak with increasing Cl coverage correlates with a decrease in the 4d electron density at the Ru surfaces. The entire ruthenium surface could be affected at sufficiently high Cl coverage.

The surface environments become more complicated when copper is also introduced into the system. On the clean Ru-Cu/SiO_2 bimetallic catalysts, the presence of copper is known to result in a downfield shift of the hydrogen-on-metals peak (16), as shown in Figure 12 and Table 6. However, when both chlorine and copper are present in the catalysts, the effect on the NMR lineshift of the hydrogen-on-metals resonance is much more drastic. The state of adsorbed chlorine in this case is not yet understood. It is possible that chlorine will bond to both ruthenium and copper at the bimetallic surfaces.

Effect of Cl on Adsorbed Hydrogen

Both the volumetric hydrogen adsorption and the ^1H NMR clearly indicate the suppressive effect of residual chlorine on hydrogen chemisorption by the Ru/SiO_2 catalysts. The chemisorption capacities of both the irreversible and the reversible hydrogen are markedly suppressed in the presence of chlorine (see Figures 3 and 6 and also Table 3). However, the trends for these two states of adsorbed hydrogen are quite different.

Figure 13 shows the relationship between the adsorption capacities for these two adsorbed states of hydrogen and the chlorine coverage on the 4% Ru/SiO_2 catalysts. The hydrogen adsorption capacities are normalized to the H/Ru ratio for the irreversible hydrogen measured on the thoroughly washed (six washes) catalyst. By assuming a stoichiometry of one irreversible hydrogen atom per surface Ru atom, the values correspond to the hydrogen coverage on Ru.

As can be seen in Figure 13, surface Cl atoms suppress the surface concentration of strongly adsorbed hydrogen to a greater extent than that of weakly adsorbed hydrogen. The surface concentration of the irreversibly adsorbed hydrogen exhibits a nearly linear decreasing trend with increasing Cl coverage while that of the reversibly adsorbed hydrogen shows only a gradual decreasing trend. Both trends are under the diagonal dashed line which would represent simple one-to-one

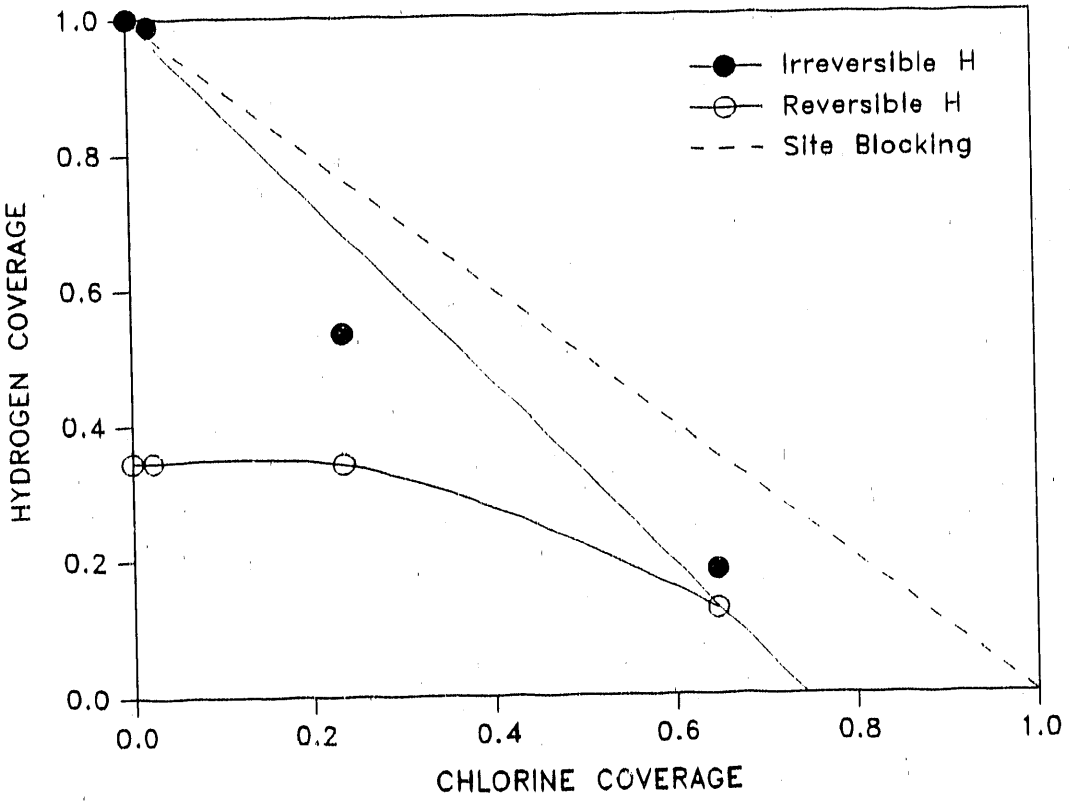

Figure 13. A plot of the hydrogen coverage for both the irreversible and the reversible hydrogen as functions of the chlorine coverage on a 4% Ru/SiO_2 catalyst. The diagonal dashed line represents simple site blocking on Ru by the chlorine

site blocking of surface Ru by the adsorbed chlorine. At a Cl coverage of about 0.76, the hydrogen coverage for the two adsorbed states extrapolates to zero. This implies that the adsorbed Cl not only simply blocks the Ru sites for hydrogen chemisorption but also poisons or deactivates adjacent Ru adsorption sites. On the average, about three adsorbed Cl atoms will block and deactivate four surface Ru atoms for hydrogen chemisorption.

The increasing trend of the spin-lattice relaxation time for the hydrogen adsorbed on Ru with increasing Cl coverage (see Tables 2 and 3) is an indication of weakening of the H-Ru interaction. This observation is consistent with the view of Ru 4d electron withdrawal by chlorine as discussed above and with the experimental observation of activated hydrogen adsorption by Lu and Tatarchuk (2, 3).

The effect of chlorine on the Ru-Cu bimetallic surfaces is similar to that on the Ru surfaces in terms of capacity for hydrogen chemisorption. The extent of the suppression by chlorine of hydrogen adsorption on the Ru-Cu bimetallics is comparable with that on the ruthenium catalysts (Figures 10 and 11 and Table 5). It has been shown in previous studies (15, 16) that hydrogen adsorbed on Ru can spill over to Cu in both contaminated and clean Ru-Cu bimetallic catalysts. This spillover phenomenon seems to prevail even in the presence of chlorine, as indicated by the trends of hydrogen adsorption

with copper content shown in Figures 10 and 11. These trends display either a near constant or even an enhanced hydrogen chemisorption capacity at low copper contents.

The mobility of adsorbed hydrogen on Ru and Ru-Cu has been indicated in the previous studies (12, 15, 16). An exchange rate for the adsorbed hydrogen (especially for the reversible hydrogen) which is of the order of the difference in chemical shift between the silanol proton and the protons adsorbed on the metal particles is believed to exist on the Ru and Ru-Cu surfaces. This hydrogen intermediate exchange on metal surfaces is indicated by the result from the spin-labeling experiment described earlier on a 5% Ru-0.39% Cu/SiO_2 catalyst with residual chlorine. The presence of chlorine only causes a large downfield shift for the hydrogen adsorbed on the Ru-Cu bimetallic surfaces but does not inhibit exchange of the adsorbed hydrogen.

If the downfield shift of the proton on this bimetallic catalyst (see Figure 9) is due to some effects other than intermediate exchange, then the 180° spin labeling prepulse would have no effect on the resultant spectrum because the prepulse excites a region excluding any observed resonances. If, on the other hand, the downfield shift of the proton on the bimetallic catalyst is due to an intermediate exchange of the adsorbed hydrogen on Ru and Cu, the prepulse should burn a relaxation hole in the homogeneously broadened spectrum of

the species associated with the exchange process in the intermediate exchange regime.

Furthermore, when there is an exchange of the adsorbed hydrogen on copper and ruthenium, there are two possible results of the spin labeling experiment. First, if chemical exchange exists on a time scale which is relatively slow compared to the time of the soft pulse, one would expect inverted spins initially at the center frequency of the soft pulse to exchange with spins out of this frequency range. Also, as τ increases, the intensity of the peak identified as that resulting from fast exchange would initially decrease with τ, and then increase as τ approaches 5 T_1. A second possibility is that the exchange rate is comparable to that of the time of the soft pulse. In this case, there is a continual exchange between H-Cu and H-Ru during the soft pulse. The effect of the soft pulse in this situation is to disturb the protons associated with the bimetallic surface from equilibrium, such that the initial intensity observed for such protons is reduced after a hard $90°_x$ pulse. The result would be an initial decrease in intensity of the observed fast exchange peak and an increase in intensity as τ is increased due to longitudinal relaxation of the hydrogen adsorbed on the bimetallic catalyst. It is the latter case that is observed, as shown in Figure 9. The exact frequency value for the fast-exchanging proton cannot be determined by

this experiment but is estimated to be on the order of 10 kHz or higher (about 50 ppm at a resonance frequency of 220 MHz).

It is interesting to note that both the "exchange peak" and the peak associated with hydrogen adsorbed on Ru are observed on the chlorine-contaminated 5% Ru-0.16% Cu/SiO_2 catalyst (see Spectrum B in Figure 8). This observation indicates that at low copper loadings separate Ru particles with little or no Cu exist in the Ru-Cu bimetallic catalyst. Hydrogen exchange between metal particles across the silica support is possible but is a much slower process with a time constant of order of hours (12).

Effect of Cl on Hydrogen Spillover to the Support

It has been observed in a study on a number of clean Ru/SiO_2 catalysts (12) that the reversibly adsorbed hydrogen on Ru is responsible for spillover of hydrogen from Ru onto the silica support. The extent of this spillover can be monitored by measuring the spin-lattice relaxation time of the silanol protons. A longer spin-lattice relaxation time is associated with less hydrogen spillover.

The results of the spin-lattice relaxation time (T_1) for the silanol proton on the 4% Ru/SiO_2 catalysts under 30 Torr hydrogen (Table 2) clearly indicate an increasing trend in T_1 as the chlorine coverage increases. This means that there is less hydrogen spillover to the silica support when the Ru

particles are contaminated with more chlorine. This view is in agreement with the fact that chlorine suppresses the adsorption of the reversible hydrogen (Figures 6 and 13), which is essential for the spillover.

The mobility of the reversibly adsorbed hydrogen on Ru may be limited to the vicinity of the Ru particles if the surface Ru atoms are partially charged or have an unbalanced distribution of electron density due to the presence of Cl, as discussed earlier. Then, the reduced hydrogen spillover may well be an indirect consequence of the Ru-Cl interaction.

CONCLUSIONS

Silica-supported ruthenium catalysts prepared from the ruthenium trichloride precursor contain a considerable amount of residual chlorine after reduction in flowing hydrogen at normal reduction temperatures. The residual chlorine remains in the Ru catalysts in the form of partially charged atoms adsorbed on surfaces of Ru particles. The surface chlorine suppresses effectively the chemisorption capacities of both the irreversible and the reversible hydrogen on Ru surfaces through simple site blocking and short range electronic effect on the surface Ru atoms. The suppressed adsorption of the reversible hydrogen on Ru due to the presence of surface Cl results in reduced hydrogen spillover from Ru to the silica support. The residual chlorine on Ru can be removed effectively via a simple hydrolysis process during water washing.

The Ru-Cu/SiO_2 bimetallic catalysts prepared from the ruthenium trichloride compound also contain residual chlorine after reduction. The presence of chlorine suppresses the hydrogen chemisorption capacity of the bimetallic catalysts but does not seem to prevent spillover of hydrogen from Ru to Cu at room temperature, as indicated by a spin labeling experiment. Fast exchange of hydrogen adsorbed on the Ru-Cu bimetallic surfaces occurs even in the presence of chlorine.

ACKNOWLEDGMENT

This work was fully supported by the U. S. Department of Energy, Office of Basic Energy Science, Contract No. W-7405-ENG-82. The support from the Analytical Services Laboratory of Engineering Research Institute of Iowa State University in performing all the x-ray fluorescence experiments is also acknowledged.

REFERENCES

1. Narita, T., Miura, H., Sugiyama, K., Matsuda, T., and Gonzalez, R. D., J. Catal. 103, 492 (1987).

2. Lu, K., and Tatarchuk, B. J., J. Catal. 106, 166 (1987).

3. Lu, K., and Tatarchuk, B. J., J. Catal. 106, 176 (1987).

4. Narita, T., Miura, H., Sugiyama, K., Matsuda, T., and Gonzalez, R. D., Appl. Catal. 32, 185 (1987).

5. Vlaic, G., Bart, J. C. J., Cavigiolo, W., Furesi, A., Ragaini, V., Cattania Sabbadini, M. G., and Burattini, E., J. Catal. 107, 263 (1987).

6. Bossi, A., Garbassi, F., Petrini, G., and Zanderighi, L., J. Chem. Soc. Faraday Trans. I 78, 1029 (1982).

7. Chen, H. W., Zhong Z., and White, J. M., J. Catal. 90, 119 (1984).

8. Mieth, J. A., and Schwarz, J. A., J. Catal. 118, 218 (1989).

9. Iyagba, E. T., Nwalor, J. U., Hoost, T. E., and Goodwin, J. G., Jr., J. Catal. 123, 1 (1990).

10. Miura, H., Hondou, H., Sygiyama, K., Matsuda, T., and Gonzalez, R. D., Proc. 9th Int. Congr. Catal., M. J. Phillips, and M. Terman, eds. (Chemical Institute of Canada, Ottawa, 1988), pp. 1307-1313.

11. Sheng, T. C., and Gay, I. D., J. Catal. 77, 53 (1982).

12. Wu, X., Gerstein, B. C., and King, T. S., J. Catal. 118, 238 (1989).

13. Wu, X., Gerstein, B. C., and King, T. S., J. Catal. 123, 43 (1990).

14. Sinfelt, J. H., J. Catal. 29, 308 (1973).

15. King, T. S., Wu, X., and Gerstein, B. C., J. Am. Chem. Soc. 108, 6056 (1986).

16. Wu, X., Gerstein, B. C., and King, T. S., J. Catal. 121, 271 (1990).

17. Cheung, T. T. P., Worthington, L. E., Murphy, P. D. B., and Gerstein, B. C., J. Magn. Reson. 41, 158 (1980).

18. Fry, C. G., Iwamiya, J. H., Apple, T. M., and Gerstein, B. C., J. Magn. Reson. 63, 214 (1985).

19. Stoll, M. E., "A Fast Recovery, Low Noise Receiver-Amplifier for Pulsed NMR Experiments," SAND80-8797 (Sandia National Laboratory, Livermore, Ca., 1980).

20. Kiskinova, M., and Goodman, D. W., Surf. Sci. 108, 64 (1981).

21. Norskov, J. K., Holloway, S., and Lang, N. D., Surf. Sci. 137, 65 (1984).

22. Lang, N. D., Holloway, S., and Norskov, J. K., Surf. Sci. 150, 24 (1985).

SECTION V

INVESTIGATIONS OF SILICA-SUPPORTED PT AND CU MONOMETALLIC AND PT-CU AND PT-AG BIMETALLIC CATALYSTS BY HYDROGEN CHEMISORPTION AND PROTON NMR

INVESTIGATIONS OF SILICA-SUPPORTED PT AND CU MONOMETALLIC AND PT-CU AND PT-AG BIMETALLIC CATALYSTS BY HYDROGEN CHEMISORPTION AND PROTON NMR

Xi Wu[1]

Bernard C. Gerstein[2]

Terry S. King[1]

[1]Department of Chemical Engineering and Ames Laboratory

231 Sweeney Hall

Iowa State University

Ames, Iowa 50011

[2]Department of Chemistry and Ames Laboratory

229 Spedding Hall

Iowa State University

Ames, Iowa 50011

ABSTRACT

Both hydrogen chemisorption and proton NMR have been applied to the study of Pt and Cu monometallic and Pt-Cu and Pt-Ag bimetallic catalysts supported on silica. NMR can investigate both strongly and weakly chemisorbed hydrogen on Pt surfaces. Platinum particle size has a large effect on the NMR lineshift as does the adsorbed state of hydrogen. Both hydrogen chemisorption and NMR indicate that copper is capable of adsorbing hydrogen at ambient temperature with a saturation hydrogen coverage of 20%. Hydrogen-deuterium exchange experiments indicate that hydrogen is adsorbed atomically on copper.

Hydrogen chemisorption on the Pt-Cu/SiO_2 bimetallic catalysts reveal spillover of hydrogen from Pt onto Cu. Deuteration of the silanol proton in silica allows much improved detection of the adsorbed hydrogen on Pt and Pt-Cu. The variation of NMR shift with Cu content can be used to estimate surface composition. Hydrogen chemisorption on Pt-Ag/SiO_2 bimetallic catalysts indicates different decreasing trends of hydrogen uptake with increasing silver content depending on the method of catalyst preparation. The Pt-Cu bimetallic catalysts exhibit a less pronounced surface segregation effect than Pt-Ag catalysts, i.e., silver tends to segregate more strongly to the surface than copper.

INTRODUCTION

Supported platinum catalysts have been a favorite subject of investigation because of their importance in various industrial applications, especially in catalytic reforming. Characterization of supported platinum catalysts has been performed by conventional methods such as hydrogen chemisorption, hydrogen-oxygen titration, x-ray diffraction, and transmission electron microscopy (1-3). Selective hydrogen chemisorption is frequently used to measure the dispersion of supported platinum catalysts. However, the phenomenon of hydrogen spillover from Pt onto the support presents an inherent experimental error for this type of measurement, as indicated by anomalously large H/Pt ratios (4, 5). Thus direct observation of the hydrogen adsorbed on the Pt surfaces is of great interest in characterization.

Direct observation of the adsorbed hydrogen on single crystal Pt (111) have been reported in a number of studies (6-8) employing electron energy loss spectroscopy (EELS). The results show that strongly bound hydrogen atoms sit in a three-fold hollow or a bridge site on the platinum surface. Temperature program desorption (TPD) has been applied for indirect observation of the hydrogen adsorbed on various single crystal Pt(111), Pt(332), Pt(553), Pt(997) surfaces by many investigators (6, 9-12). Results from TPD and hydrogen-deuterium exchange suggested dissociative adsorption of

hydrogen and existence of two adsorbed states of hydrogen on these Pt surfaces. These studies have also shown that adsorbed hydrogen is more strongly bound to low-coordination (defect-like) sites than to high-coordination sites (low-index planes) at low hydrogen overpressures.

Hydrogen is known to adsorb dissociatively in at least two different forms on Pt surfaces (13). First, a complete monolayer of strongly bound hydrogen is formed at pressures below 10^{-6} Torr. Secondly, a weakly bound form of adsorbed hydrogen appears at pressures above 10^{-4} Torr (14). This latter form of adsorbed hydrogen cannot be studied by EELS because the pressure is beyond the range where the method is applicable. However, infrared (IR) spectroscopy has been used for the study of the reversibly adsorbed hydrogen on supported Pt catalysts (15-20). Although the Pt-H bond stretching can be detected directly by IR, the observed band is often obscured by interference from CO impurity, and the method is not easily made quantitative.

In recent years, NMR of hydrogen chemisorbed on Pt catalysts has become a useful and promising method for the characterization of small Pt particles and elucidation of Pt surface environments. Hydrogen adsorbed on Pt powder (21) and on silica-supported Pt catalysts (22-24) has been studied by ^{1}H NMR to yield information on its lineshift, linewidth, relaxation times, and mobility on the Pt surfaces.

Spillover of the adsorbed hydrogen onto the silica support and subsequent exchange with the silanol proton can also be monitored by ^{1}H NMR (23, 25). However, the weak resonance from the adsorbed hydrogen as well as the limited shift and broad features of the resonance due to the adsorbed hydrogen are often overwhelmed by the relatively intense resonance from the silanol proton.

Hydrogen adsorption on Cu single crystal surfaces has been reported by Balooch et al. (26) to be an activated process with an activation energy of about 5 kcal/mole for dissociative adsorption of molecular hydrogen. Greuter and Plummer (27) have found that molecular hydrogen does not dissociate on a Cu(111) surface at room temperature whereas atomic hydrogen chemisorbs even above room temperature. This confirms the existence of an energy barrier for dissociation of hydrogen on Cu.

Low coverages for hydrogen adsorbed on Cu powders (28, 29) and films (30) has been reported consistently in the literature. Typical values for the hydrogen coverage on Cu range from 0.1 to 0.2. Hydrogen coverages higher than 0.2 on Cu surfaces at room temperature were never reported. However, whether the process of molecular hydrogen adsorption on Cu is dissociative or non-dissociative is still subject to debate. Alexander and Pritchard (30, 31) have shown that the process is a spontaneous dissociative adsorption on Cu films

in the temperature range of 242-337 K.

^1H NMR has been applied for the first time by Ito and Kadowaki (32) on hydrogen adsorbed on fine copper powders. They observed a weak proton resonance intensity at about -93 ppm downfield relative to an unidentified resonance used as the reference for the shift. They attributed the large shift to Knight shift interaction between the proton and the 4s conduction electrons of the copper atoms. They also reported a low hydrogen coverage (0.1) for their copper samples.

In the bulk state, different mixing behaviors exist between Pt and the various Group Ib metals (Cu, Ag, or Au) (33). Pt and Cu form ordered alloys; Pt and Ag mix randomly; Pt and Au show a large miscibility gap in the phase diagram. Monte Carlo simulations (34) of supported Pt-Ib bimetallic catalysts have shown that the Group Ib element segregates to the surface of the bimetallic particle and tends to occupy low-coordination sites first. At high concentrations of a Group Ib metal, Cu is shown to have the least tendency and Au shows the strongest tendency to segregate to the surface among the three Ib elements.

Platinum-copper bimetallic catalysts supported on silica (35-37) and alumina (38-40) have been studied by various techniques including the volumetric hydrogen chemisorption, X-ray diffraction, X-ray photoelectron spectroscopy (XPS), transmission electron microscopy (TEM), and also extended X-

ray absorption fine structure (EXAFS). All of these studies indicate a surface enrichment of copper. However, the surface composition of the bimetallic catalysts cannot be determined by these methods. In this case, the method of hydrogen chemisorption may give misleading results because of hydrogen spillover from Pt to Cu, as found in the case of Ru-Cu bimetallic catalysts (41).

Platinum-silver bimetallic catalysts have received little attention while most of the work on the other Pt-Ib bimetallics has been done on the platinum-gold bimetallic system. Adsorption of CO, N_2, and NO on the Pt-Ag/SiO_2 bimetallic catalysts has been investigated by infrared spectroscopy (42, 43). The results showed that increasing the Ag content would reduce the amount of molecules adsorbed by the catalysts possibly due to increased alloying of Pt with Ag. Sachtler and Somorjai (44) have investigated CO chemisorption and n-hexane conversion on Au-Pt(111) surface. They reported that the alloy surface was more active and selective for isomerization than the pure Pt(111). Most of the work on supported Pt-Au bimetallic catalysts involved reaction studies of certain alkanes and cycloalkanes (45-49). Analytical techniques such as X-ray diffraction (46, 48), electron microscopy (48, 50), infrared spectroscopy (51), and EXAFS (52) were also applied to the Pt-Au bimetallic system. The results indicated the coexistence of a separate bulk Pt

phase, a separate bulk Au phase, and a phase containing both Pt and Au.

In the present study, ^{1}H NMR was used to investigate Pt/SiO_2 and Cu/SiO_2 catalysts. Also, the technique was applied here for the first time to explore the possibility of characterizing silica-supported Pt-Cu and Pt-Ag bimetallic catalysts. Supplementary techniques such as volumetric hydrogen chemisorption and thermogravimetric analysis were also employed to assist interpretation of the NMR data.

EXPERIMENTAL

Catalyst Preparation

The Pt/SiO_2 catalysts were prepared by both incipient wetness impregnation and an ion exchange method to produce catalysts with different Pt dispersions. The silica support used, Cab-O-Sil HS5 with a BET surface area of 300 m^2/g, was dried in an oven before use. The two metal precursors, H_2PtCl_6 (AESAR) and $Pt(NH_3)_4(NO_3)_2$ (ALFA), were used for the impregnation and the ion exchange methods, respectively.

The Cu/SiO_2 catalysts were also prepared by the two methods with the same support to generate different copper dispersions. In the impregnation method, Puratronic Grade $Cu(NO_3)_2 \cdot 6H_2O$ (AESAR) was used as the metal salt precursor. In the ion exchange method, either the copper nitrate salt or $Cu(OH)_2$ dissolved in 26% aqueous ammonium hydroxide (in a pH of 9 to 10) was used as the metal precursor. Copper (II) hydroxide was generated from a solution of $Cu(NO_3)_2 \cdot 6H_2O$ via precipitation at a pH of 5 to 7 by adding an appropriate amount of aqueous ammonium hydroxide to the solution. The precipitated $Cu(OH)_2$ was filtered, washed, and dried before use.

The $Pt\text{-}Cu/SiO_2$ bimetallic catalysts were prepared by only the ion exchange method with $Pt(NH_3)_4(NO_3)_2$ and $Cu(NO_3)_2 \cdot 6H_2O$ (AESAR) as the precursors. The $Pt\text{-}Ag/SiO_2$ bimetallic

catalysts were prepared by both the ion exchange method and a sequential impregnation method. In the ion exchange method, $Pt(NH_3)_4(NO_3)_2$ and $AgNO_3$ (AESAR) metal salts were used as the precursors. In the sequential impregnation method, a reduced Pt/SiO_2 catalyst made by the impregnation method was re-impregnated in a $AgNO_3$ solution.

About 2.5 ml of solution containing the metal salt(s) per gram of SiO_2 was used for the impregnation method. About 6 ml per gram SiO_2 were employed for the ion exchange method. Ammonia was added to the solution to adjust the pH to between 9 and 10 in the ion exchange method, allowing the formation of ammine complexes of copper and silver. The higher pH values can result in more adsorption of the platinum ammine complex by silica (1-2). The catalyst slurries obtained were dried in air for 24 hours at room temperature and 8 hours at 383 K. The Pt/SiO_2 catalysts were made with Pt loadings of 4%, 5%, and 10%. The platinum loading for a series of Pt-Cu/SiO_2 bimetallic catalysts was kept at 5% by total weight of the support and metals. A total of eight different Pt-Cu/SiO_2 bimetallic catalysts were prepared to give a wide range of copper loading. Two series of Pt-Ag/SiO_2 bimetallic catalysts were prepared with a constant Pt loading of 4% (no NH_4OH added) and 5% (NH_4OH added), respectively, and also a wide range of silver loading. In addition, three Cu/SiO_2 catalysts with loadings of 2%, 5%, and 10% were made via the

impregnation method, and two Cu/SiO_2 catalysts with loadings of 5% and 10% were prepared by the ion exchange method.

Thermogravimetric Analysis

The reducibility of all the catalysts was examined by thermogravimetric analysis using a commercial Perkin-Elmer TGA 7 thermogravimetric analyzer with a high temperature furnace. About 40 mg of a catalyst sample was loaded into a platinum pan, which was placed inside the high temperature furnace. Before heating the sample, argon was used to flush the analyzer to remove oxygen from the system. Then, 5 vol.% hydrogen gas diluted in argon with a total flow rate of 45 cm^3/min was allowed to enter the analyzer and pass over the sample pan. The temperature of the furnace was programmed to be raised from 313 K to 573 K at a rate of 2 K/min. The data were recorded as weight percentage versus temperature.

Catalyst Reduction

Catalyst reduction was carried out with a multiport volumetric adsorption apparatus equipped with a high-vacuum system described previously (41). Reduction in flowing hydrogen was performed directly inside a Pyrex cell of the adsorption apparatus. Approximately one gram of a catalyst sample was loaded into the flow-through cell, which was then connected to one of the sample ports of the manifold. While

helium gas (99.999%) was allowed to flow through the sample bed in the cell at a rate of 100 cm^3/min, the temperature of the cell was raised to 423 K. The cell was maintained at that temperature and He was allowed to flow through it for 30 min to drive away excessive moisture in the sample. Then the helium was switched off, replaced by hydrogen (99.8%) at a flow rate of 50 cm^3/min and the temperature was raised at 5 K/min to either 673 K (for platinum-containing catalysts) or 573 K (for the copper catalysts). Reduction proceeded for two hours at this final temperature before the cell was evacuated for another two hours to 10^{-6} Torr and then allowed to be cooled to the ambient temperature for the adsorption experiments.

Volumetric Adsorption

Hydrogen for the volumetric adsorption was purified by passing it through a catalytic hydrogen purifier (Engelhard Deoxo) in series with a gas purifier with Drierite and 5 Å molecular sieve (Alltech) to remove traces of oxygen and moisture. Hydrogen adsorption experiments were performed at room temperature (294 ± 1 K). The total hydrogen adsorption isotherm was measured in the pressure range of 0 - 30 Torr. The reversible hydrogen adsorption isotherm was collected under the same conditions after a 10 min evacuation period to 10^{-6} Torr following the total adsorption. The irreversible

hydrogen uptake was obtained by taking the difference between values of the total and the reversible adsorption isotherms extrapolated to zero pressure. An equilibration time of 1 hour was used for the initial dose and 20 min for subsequent doses.

Silica Support Deuteration

Deuteration can effectively reduce the intense NMR signal associated with the silanol proton and hence improve spectral resolution for other resonances of interest, e.g., the peak corresponding to hydrogen adsorbed on platinum. Before deuteration, the catalyst was reduced in flowing hydrogen as described earlier. Then the catalyst was soaked in a 26 wt% ND_4OD solution in D_2O for at least two hours and dried at 383 K. This process was repeated three times using a fresh solution. Finally, the catalyst was reduced in flowing deuterium gas for one hour inside an NMR tube before being dosed with hydrogen gas at liquid nitrogen temperature. To prevent exchange of the adsorbed hydrogen with the OD group in the silica support, the catalyst sample was always evacuated for 10 min to a pressure of 10^{-6} Torr at ambient temperature after dosing with hydrogen (55).

Sample Treatment and NMR Experiment

Sample treatment before the NMR experiment was carried

out inside a 5-mm NMR tube by either the flow reduction or the static reduction method. In the flow reduction, fresh, unreduced catalysts were used, while only previously reduced catalysts were used in the static reduction method. Both methods yield virtually the same results.

Reduction by flowing hydrogen was carried out using a needle-bellows assembly (41) with the needle being inserting into the catalyst sample in the NMR tube. Approximately 60 mg of catalyst sample was loaded inside the NMR tube and helium then hydrogen was allowed to flow through the needle and the catalyst sample. The reduction procedure was the same as previously described for the volumetric adsorption experiment, but with a hydrogen flow rate of 15 cm^3/min. After reduction, the needle was lifted out of the catalyst sample, and evacuation proceeded for about two hours at the reduction temperature before the sample was allowed to cool to ambient temperature.

Reduction by static hydrogen was performed by a repeated cycle of reduction and evacuation. First, the sample loaded inside the NMR tube was heated to the reduction temperature and dosed with about 100 Torr hydrogen. Then, when the hydrogen consumption or the pressure change ceased, the sample was evacuated for 5 min. The sample was dosed again with hydrogen up to 760 Torr and allowed further reduction to proceed for 30 min before another five-minute evacuation. At

least three such cycles were performed on each catalyst for complete reduction. Finally, the catalyst was evacuated for two hours at the reduction temperature before being cooled down to ambient temperature.

Purified hydrogen was dosed to the catalyst sample and the system was allowed to equilibrate for one hour. The NMR tube containing the sample was then immersed in a water bath and sealed off with a micro-torch.

The home-built NMR spectrometer (53) used for the NMR experiments was operated at 220 MHz for proton resonance. A proton-free probe with a doubly wound coil (54) was used for all the NMR measurements. The probe quality factor Q was set at about 100 to obtain the optimal values of sensitivity and ring down time for a fixed pulse power. Detailed description of the spectrometer's rapid-recovery receiving system has been published elsewhere (55).

All NMR spectra were collected under a repetitive 90° single-pulse sequence. The recycle time between rf pulses was set at 0.2s to selectively suppress the intense signal associated with protons in the silanol group in catalyst samples, which has a relatively long spin-lattice relaxation time T_1 (on the order of seconds). The above repetition rate avoids T_1 saturation of the peak corresponding to hydrogen adsorbed on platinum. A pure water sample was used as the reference standard for the NMR lineshifts.

RESULTS

Thermogravimetric Analysis

The reducibility of metal salt precursors and supported catalyst materials was examined using thermogravimetric analysis (TGA) by observing the weight loss of the samples with increasing temperature in flowing hydrogen. Figure 1 shows the TGA data in a composite fashion for $Pt(NH_3)_4(NO_3)_2$ and $Cu(NO_3)_2 \cdot xH_2O$ metal salt, respectively. For the platinum salt, a rapid weight drop occurred in the temperature range of 65-80°C. However, at temperatures higher than 90°C, the sample weight remained constant at 50.3% of the original weight. For the copper salt, weight loss occurred in four stages over a temperature range from 70°C to 195°C. The final weight of the sample stayed constant at 24.7% of the original weight after 195°C.

TGA data for pure SiO_2 and three Cu/SiO_2 catalysts (prepared via the impregnation method) with copper loadings of 2%, 5%, and 10% are shown in Figure 2. For pure silica, the weight loss was less than 1.5% of the starting weight over the temperature range from 45°C to 300°C. For the copper catalysts, significant weight loss was observed over the same temperature range with greater weight loss for a catalyst with higher copper loading. The general features were a three-stage weight loss over the temperature range

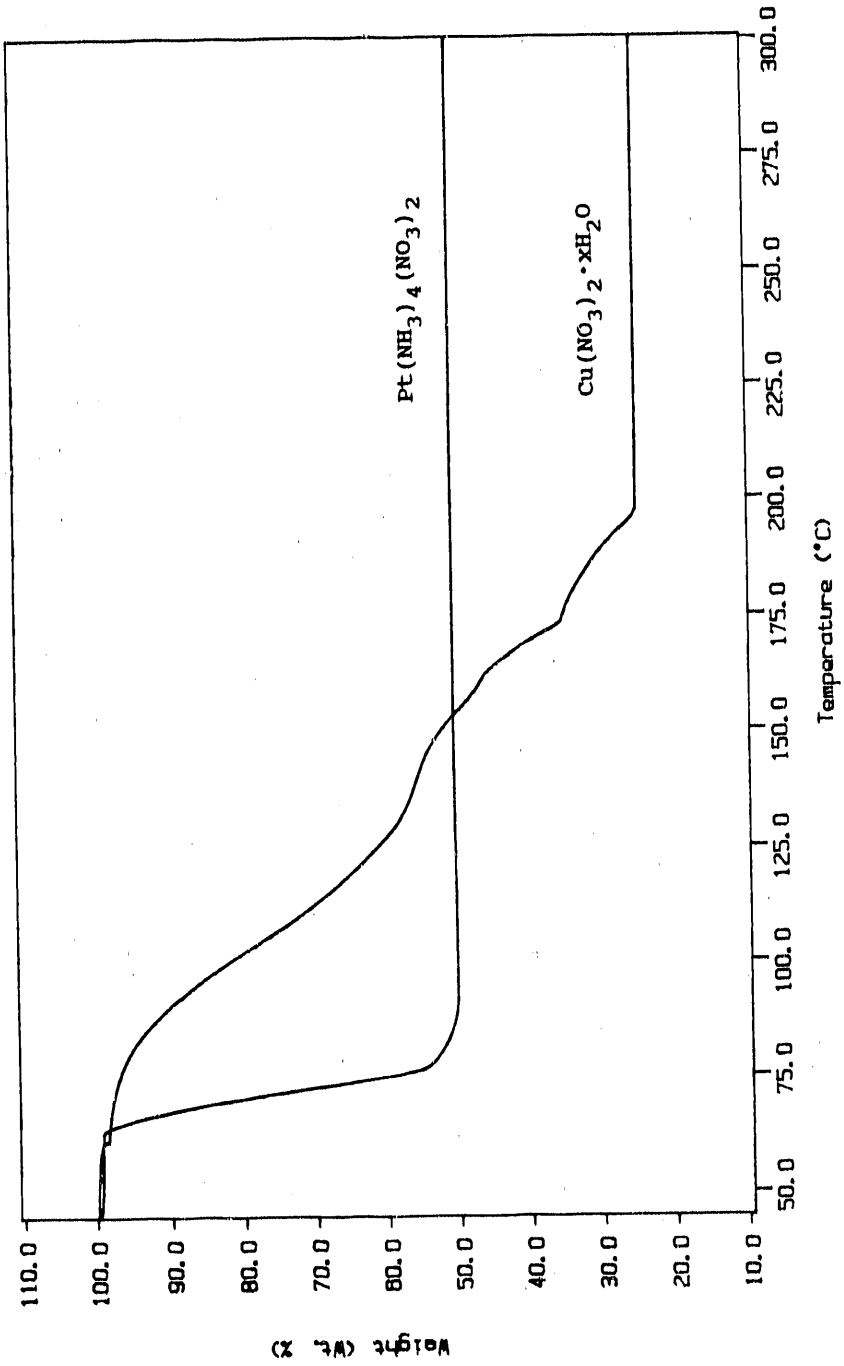

Figure 1. TGA data showing weight percent versus temperature for catalyst precursor compounds $Pt(NH_3)_4(NO_3)_2$ and $Cu(NO_3)_2 \cdot xH_2O$. The weight percentage is based on the initial weight of the sample

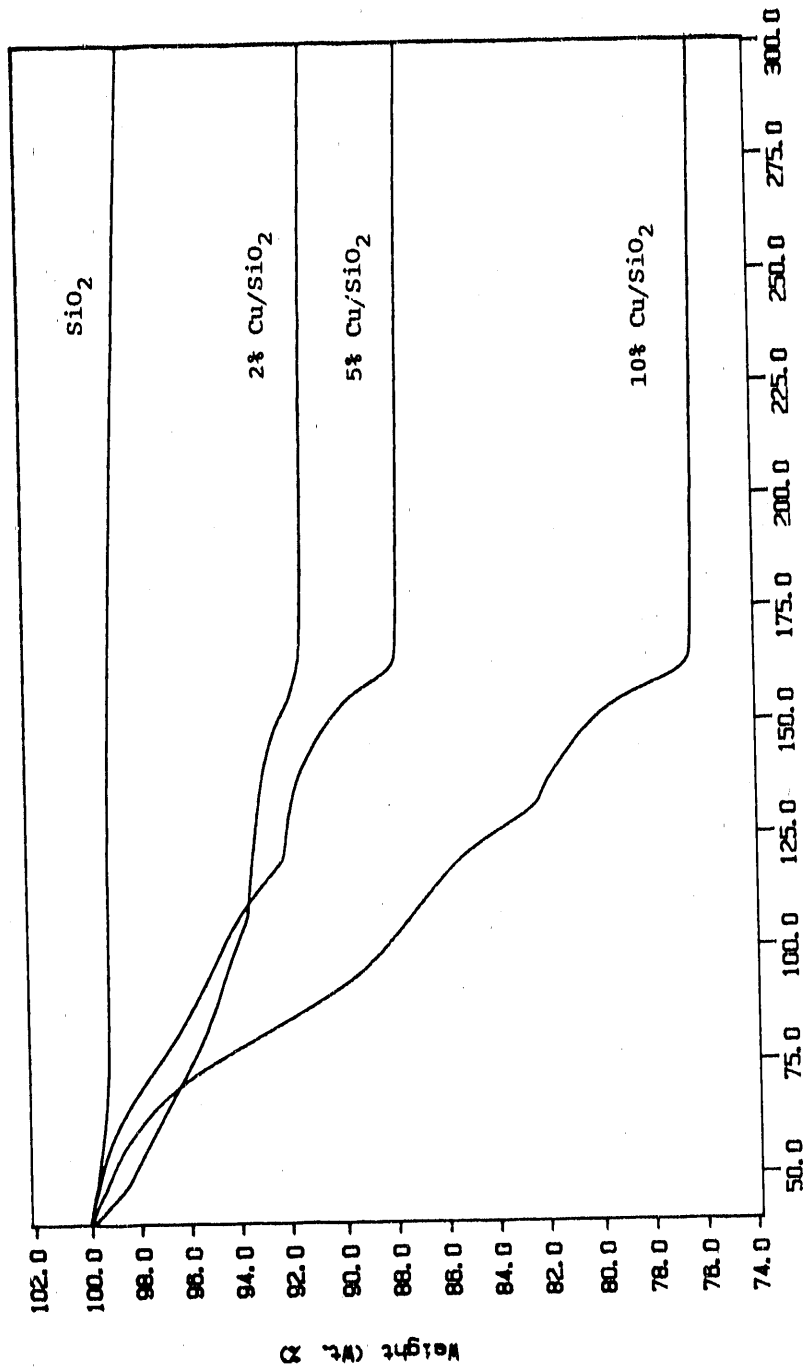

Figure 2. TGA data showing weight percent versus temperature for pure SiO_2 and three Cu/SiO_2 catalysts with Cu loadings of 2%, 5%, and 10%. The identification for the samples are as indicated in the figure

from 50°C to 160°C (similar to that of the pure Cu nitrate salt) and a gradual weight loss after 160°C (characteristic of a pure silica sample).

TGA data for a 5% Pt/SiO_2, a 5% Pt-2.44% Cu/SiO_2, a 5% Cu/SiO_2 catalyst (prepared via ion exchange method) are shown together in Figure 3. All three samples showed different percentages of weight loss with rapid weight drop at the low temperature end and only gradual weight loss at the high temperature end. For the Pt sample, two noticeable stages of weight loss were observed over the temperature range from 70°C to 160°C with a break point at about 142°C. For the bimetallic sample, the weight loss was also in two stages over the same temperature range with a break point at about 147°C. For the Cu sample, the TGA curve was rather smooth over the same temperature range with a break point at about 156°C.

TGA data for a 5% Pt/SiO_2, a 5% Pt-4.15% Ag/SiO_2, and a 5% Ag/SiO_2 catalyst (prepared via ion exchange method) are shown together in Figure 4. The TGA curve for the Pt sample is identical with the one already shown in Figure 3. For the bimetallic sample, a two-stage weight loss was observed over the temperature range from 70°C to 160°C with an obscured break point around 120°C. For the silver sample, a definite two-stage weight drop was detected over the same temperature range with a distinct break point at 102°C.

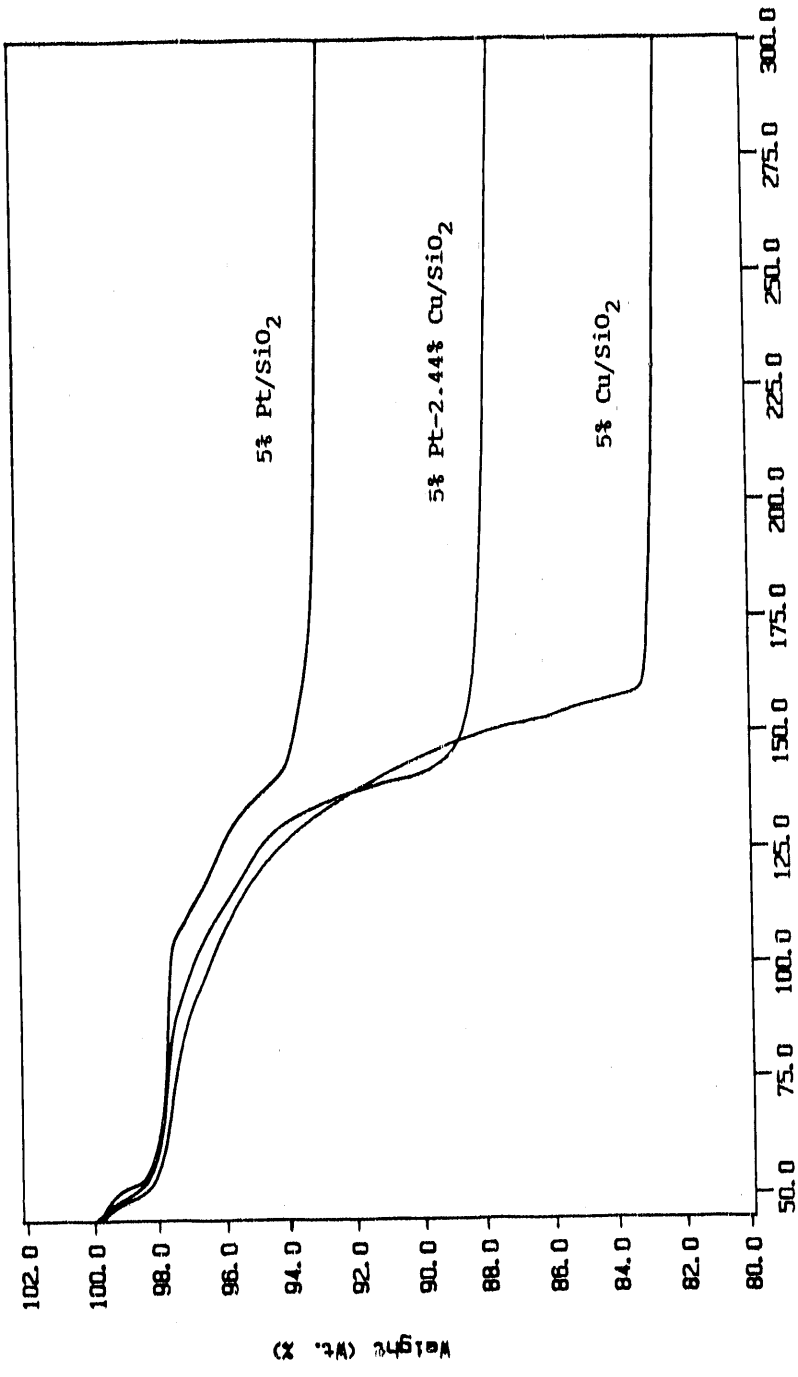

Figure 3. TGA data showing weight percent versus temperature for a 5% Pt/SiO_2, a 5% Pt-2.44% Cu/SiO_2, and a 5% Cu/SiO_2 catalyst. The identification for the samples are as indicated in the figure

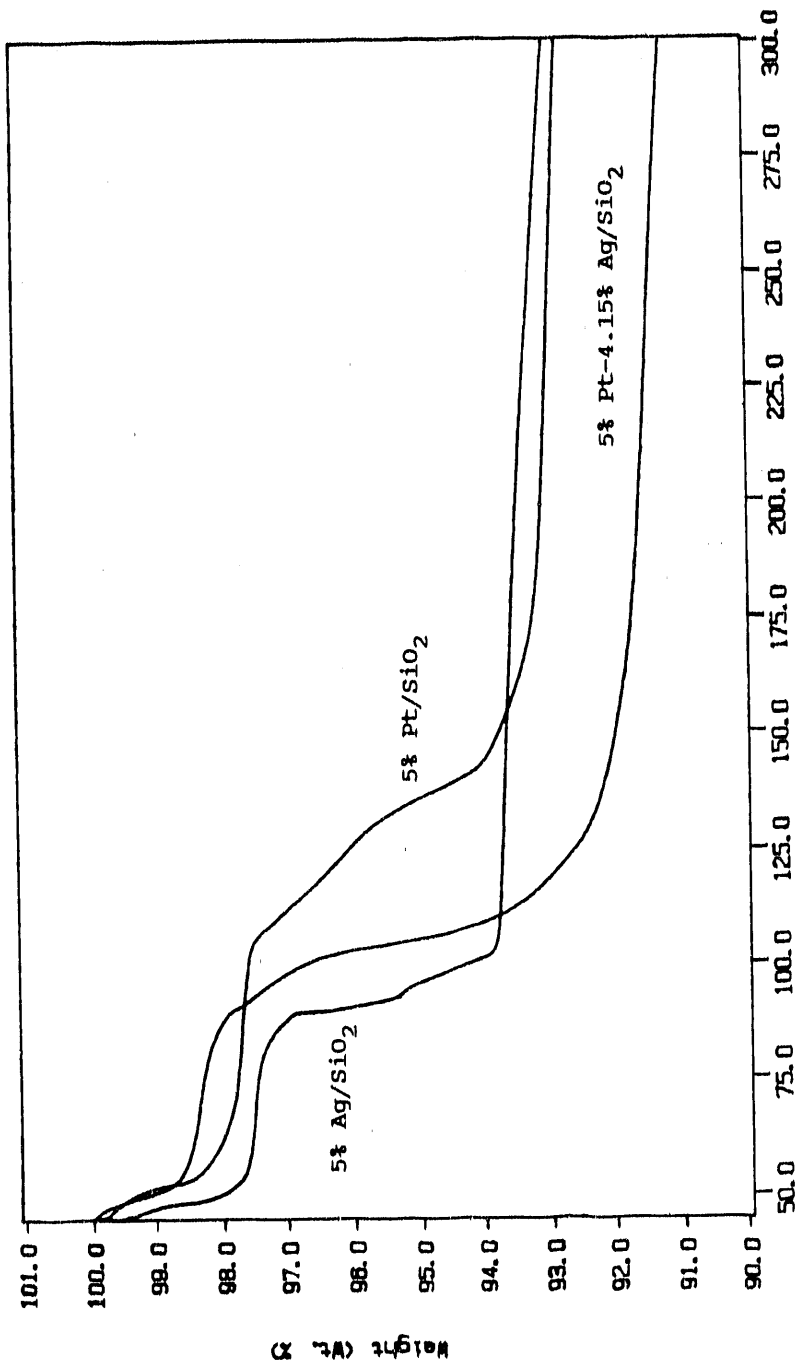

Figure 4. TGA data showing weight percent versus temperature for a 5% Pt/SiO_2, a 5% Pt-4.15% Ag/SiO_2, and a 5% Ag/SiO_2 catalyst. The identification for the samples are as indicated in the figure

Hydrogen Chemisorption

Adsorption isotherms at 294 K over an equilibrium pressure range of 0 to 40 Torr for a 2% Cu/SiO_2 (prepared by impregnation) and a 10% Cu/SiO_2 (prepared by ion exchange) catalyst are shown in Figure 5 . The adsorbates used here are hydrogen and carbon monoxide and only the total isotherms were plotted in the figure. All isotherms in this pressure range are nearly linear. For the 2% Cu/SiO_2 catalyst, the amount of hydrogen adsorption was higher and more pressure dependent than that of carbon monoxide. However, for the 10% Cu/SiO_2 catalyst, the difference between the two isotherms generated by the two adsorbates was much smaller. In the latter case, the amount of adsorbed hydrogen was roughly equal to the amount of adsorbed carbon monoxide. All the isotherms were extrapolated to zero pressure to obtain the H/Cu or CO/Cu ratios.

Table 1 illustrates values of copper dispersion and H/Cu and CO/Cu ratios for five Cu/SiO_2 catalysts measured by both the total and the reversible isotherms. The dispersion of Cu was measured by nitrous oxide adsorption as described by King et al. (56). In general, the dispersion values of 5% and 10% Cu/SiO_2 catalysts were low. However, lower Cu loading (2%) resulted in a much higher copper dispersion. The fact that the total H/Cu ratios are much higher than the weak H/Cu ratios for all the copper catalysts indicates a considerable

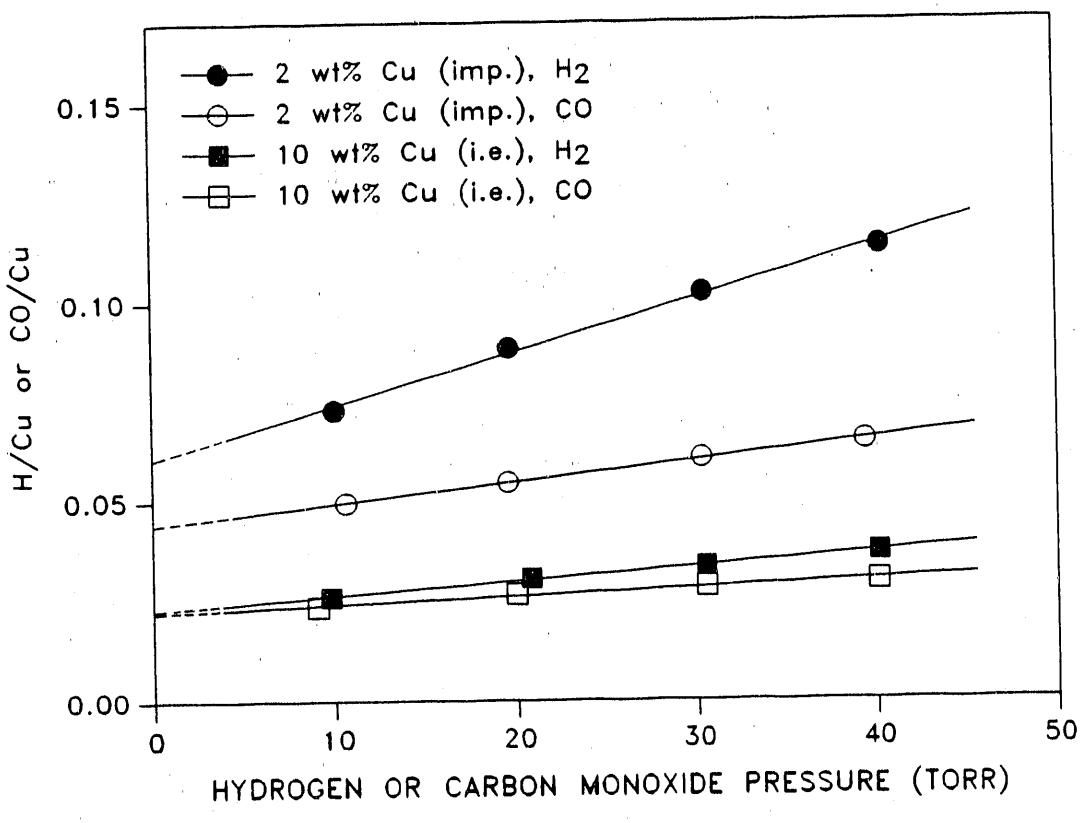

Figure 5. Hydrogen and carbon monoxide adsorption isotherms for a 2% Cu/SiO_2 (impregnation) and a 10% Cu/SiO_2 (ion exchange) catalyst. The total adsorption isotherms are shown for the two adsorbates

Table 1 Results of adsorption by nitrous oxide, hydrogen, and carbon monoxide on Cu/SiO_2 catalysts

Catalyst	Dispersion[a]	Total H/Cu	Weak H/Cu	Total CO/Cu	Weak CO/Cu
2% Cu[b]	0.302	0.061	0.016	0.044	0.039
5% Cu[b]	0.099	0.020	0.007	0.017	0.015
10% Cu[b]	0.049	0.009	0.003	0.007	0.006
5% Cu[c]	0.143	0.027	0.011	0.026	0.024
10% Cu[c]	0.118	0.023	0.012	0.022	0.019

[a]Dispersion was measured by nitrous oxide adsorption.

[b]The catalyst was prepared by impregnation method.

[c]The catalyst was prepared by ion exchange method.

amount of strongly bound hydrogen on these Cu catalysts. For the carbon monoxide adsorption, the total CO/Cu ratios were almost identical to the weak CO/Cu ratios, indicating that virtually no carbon monoxide was strongly bound on the copper catalysts.

The surface coverage of hydrogen or carbon monoxide was calculated by taking the ratio between the H/Cu or CO/Cu value and the value for Cu dispersion. Table 2 lists the values of hydrogen coverage on Cu for both the total and the

Table 2 Results of hydrogen and carbon monoxide surface coverage on Cu/SiO_2 catalysts

Catalyst	Total $H/Cu_{(s)}$	Strong $H/Cu_{(s)}$	Total $CO/Cu_{(s)}$	H/CO
2% Cu[a]	0.20	0.15	0.15	1.39
5% Cu[a]	0.20	0.13	0.17	1.18
10% Cu[a]	0.18	0.12	0.14	1.29
5% Cu[b]	0.19	0.11	0.18	1.04
10% Cu[b]	0.19	0.09	0.19	1.05

[a]The catalyst was prepared by impregnation method.

[b]The catalyst was prepared by ion exchange method.

strong hydrogen adsorption, the values of carbon monoxide coverage from the total adsorption, and the H/CO ratios on Cu for the total adsorption. Surprisingly constant values of the total hydrogen coverage were observed. The values of the strong hydrogen coverage also remained fairly constant in the range from 0.09 to 0.15. Also, the values of the carbon monoxide coverage were in the range of 0.14 to 0.19; they were slightly less than those of total hydrogen coverage. The H/CO ratios were between 1.0 and 1.4 on all the copper catalysts.

The amounts of adsorbed hydrogen on two different 10% Pt/SiO_2 catalysts expressed as the H/Pt ratio versus the equilibrium hydrogen pressure are shown in Figure 6. The two catalysts were prepared by the impregnation and the ion exchange method, respectively. Both the total and the reversible isotherms are shown in the figure. The results indicate straight lines for all the isotherms in the hydrogen pressure range from 10 to 30 Torr with the total and the reversible isotherm parallel to each other. All isotherms exhibit a very gradual increase of the measured H/Pt ratio with increasing hydrogen pressure. For the catalyst made by impregnation, the extrapolated isotherms gave H/Pt ratios of 0.299 and 0.093 at zero hydrogen pressure. For the catalyst prepared by ion exchange, H/Pt ratios of 0.467 and 0.105 were obtained.

Figure 7 shows the total and the reversible isotherms over the same hydrogen pressure range for a 5% Pt/SiO_2 and a 5% Pt-1.086% Cu/SiO_2 catalyst. An extrapolation to zero hydrogen pressure resulted in similar H/Pt ratios from the total (0.657 and 0.586) and the reversible (0.113 and 0.099) isotherm for the two catalysts.

The total and reversible isotherms for two Pt-Ag/SiO_2 bimetallic catalysts with the identical metal loadings but different preparation methods (sequential impregnation and ion exchange, respectively) are shown in Figure 8 over a

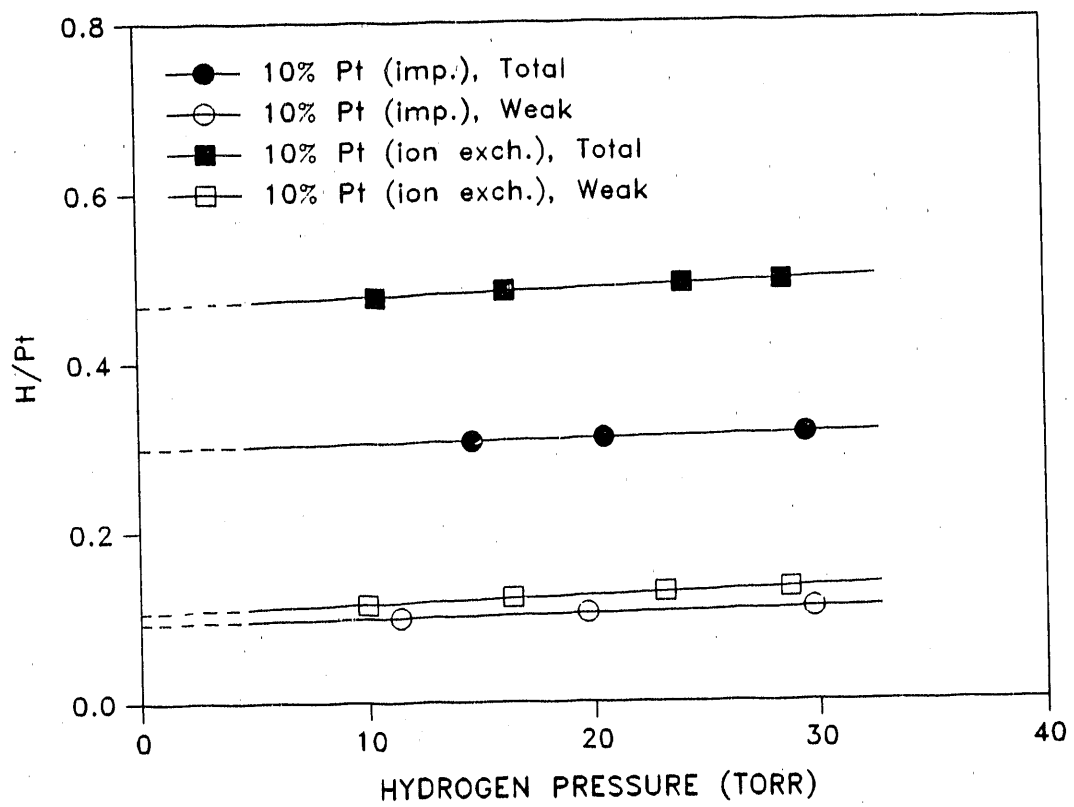

Figure 6. Hydrogen adsorption isotherms for a 10% Pt/SiO_2 (impregnation) and a 10% Pt/SiO_2 (ion exchange) catalyst. Both the total and the reversible isotherms are shown in the figure

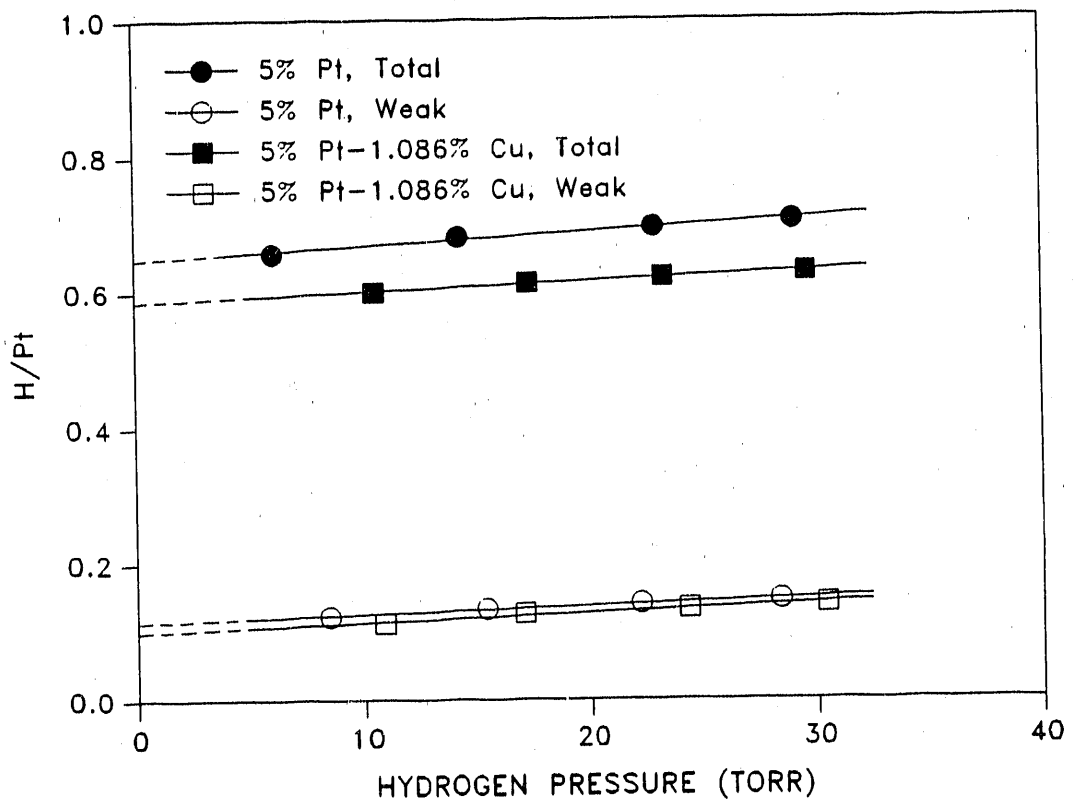

Figure 7. Hydrogen adsorption isotherms for a 5% Pt/SiO_2 and a 5% Pt-1.086% Cu/SiO_2 catalyst prepared by the ion exchange method. Both the total and the reversible isotherms are shown in the figure

hydrogen pressure range from 0 to 30 Torr. As can be seen, the amount of hydrogen adsorption for the catalyst made by the ion exchange method was more than twice that for the sequential impregnation catalyst.

The amount of hydrogen adsorption for a series of 5% Pt-Cu/SiO_2 catalysts is plotted against the Cu content expressed as Cu atomic percent as shown in Figure 9. For the total hydrogen adsorption, the H/Pt ratio remained roughly constant from 0 to 40 at.% Cu but decreased steadily from 40 to 80 at.% Cu with increasing copper content. At 80 at.% Cu, the amount of hydrogen adsorption is only 34% of the amount for the pure 5% Pt/SiO_2 catalyst. For the reversible hydrogen adsorption, the H/Pt ratio is much less than that of the total adsorption and decreased moderately with increasing copper content.

Figure 10 shows the H/Pt ratio versus silver content for both the total and reversible hydrogen adsorption on two series of Pt-Ag/SiO_2 catalysts. The 4% Pt-Ag/SiO_2 series was prepared by ion exchange for the Pt and impregnation for the Ag metal (no ammonia was added to allow formation of silver ammine complex). The 5% Pt-Ag/SiO_2 series was made by the ion exchange method on both metallic elements (ammonia was added to raise pH above 9). For the 4% Pt-Ag/SiO_2 series, both the total and the reversible hydrogen chemisorption remained nearly constant with increasing silver content up to

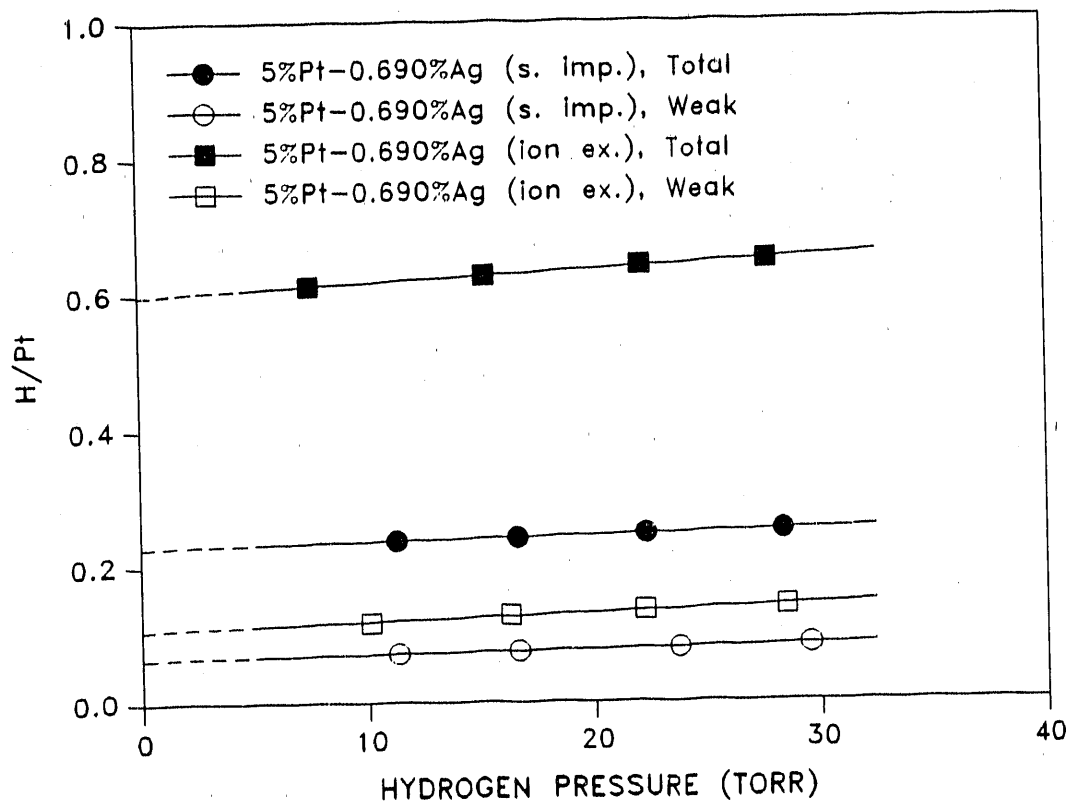

Figure 8. Hydrogen adsorption isotherms for a 5% Pt-0.69% Ag/SiO_2 (sequential impregnation) and a 5% Pt-0.69% Ag/SiO_2 (ion exchange) catalyst. Both the total and the reversible isotherms are shown

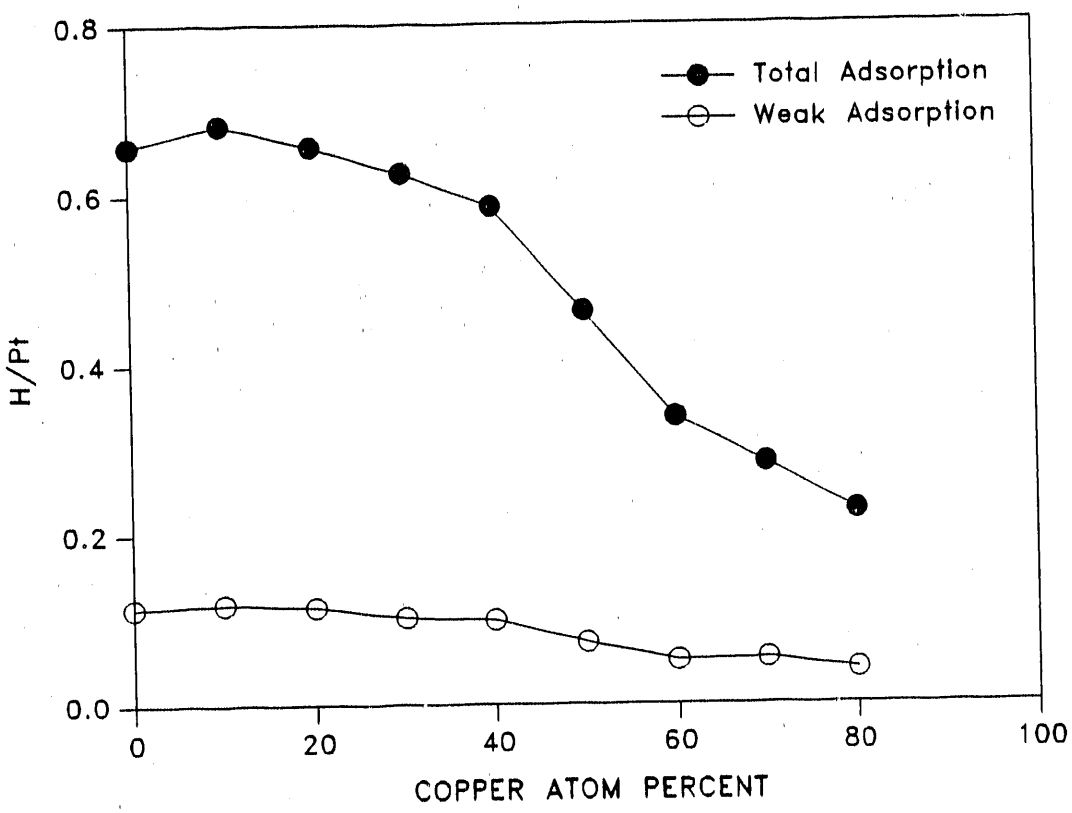

Figure 9. Plot of H/Pt ratio versus copper content for a series of 5% Pt-Cu/SiO_2 catalysts (ion exchange). Both the total and the reversible adsorption data are shown in the figure

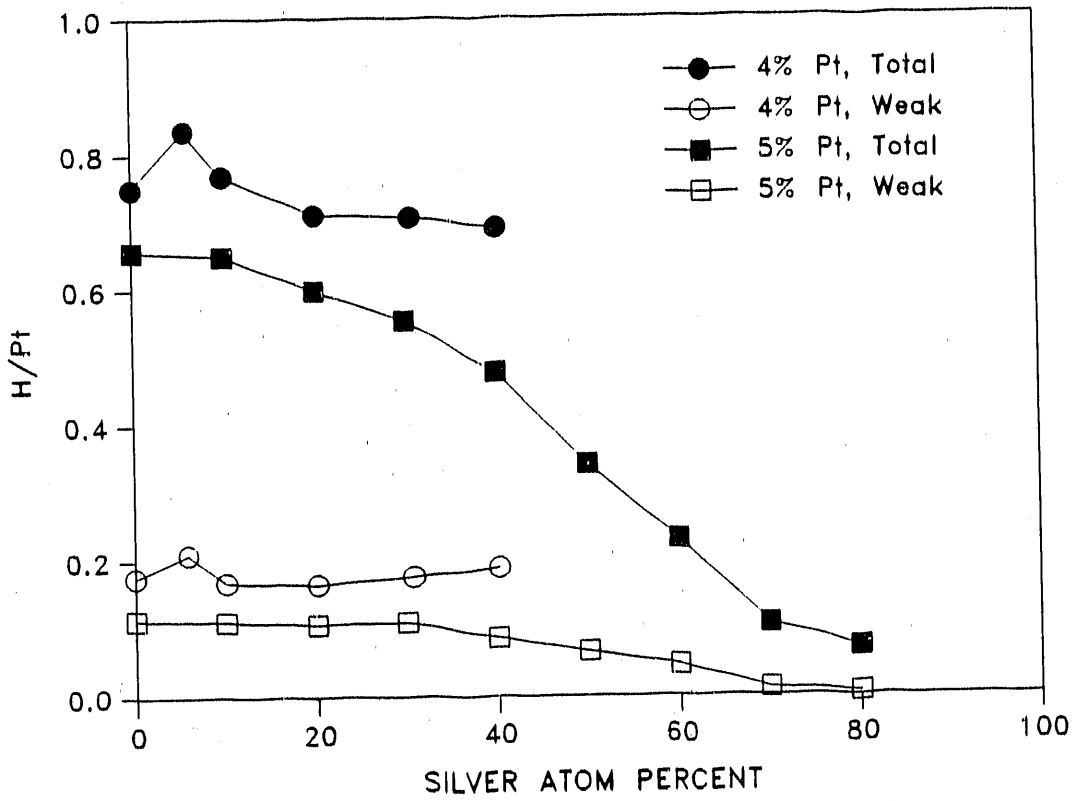

Figure 10. Plot of H/Pt ratio versus silver content for a series of 4% Pt-Ag/SiO_2 (mixed ion exchange and impregnation) and a series of 5% Pt-Ag/SiO_2 (ion exchange) catalysts. Both the total and the reversible adsorption data are shown

40 at.% Ag. For the 5% Pt-Ag/SiO_2 series, however, notable decrease in total adsorption was observed with increasing silver content. At 80 at.% Ag, the amount of total hydrogen chemisorption was only 11% of that by the pure 5% Pt/SiO_2 catalyst. Considerable decrease in the reversible hydrogen adsorption was also observed with increasing silver content. At 80 at.% Ag, the amount of reversible adsorption was almost zero.

Data for both the total and the reversible hydrogen adsorption on a series of 5% Pt-Ag/SiO_2 prepared by the sequential impregnation method are shown in Figure 11. In both cases, the amount of adsorption decreased considerably with increasing silver content. At 50 at.% Ag, the amount of the total chemisorption was only 14% and the amount of the reversible chemisorption was only 7% of that by the pure 5% Pt/SiO_2 catalyst.

The irreversible hydrogen adsorption is taken as the difference between the total and the reversible adsorption. Chemisorption data for the irreversible hydrogen on a series of 5% Pt-Cu/SiO_2 and a series of 5% Pt-Ag/SiO_2 catalysts (prepared by ion exchange method) are illustrated in Table 3. For the Pt-Cu bimetallic catalysts, the uptake of strongly adsorbed hydrogen remained roughly constant for Cu contents from 0 to 40 at.% Cu and then decreased as more Cu was added. For the Pt-Ag bimetallic catalysts, the amount of strongly

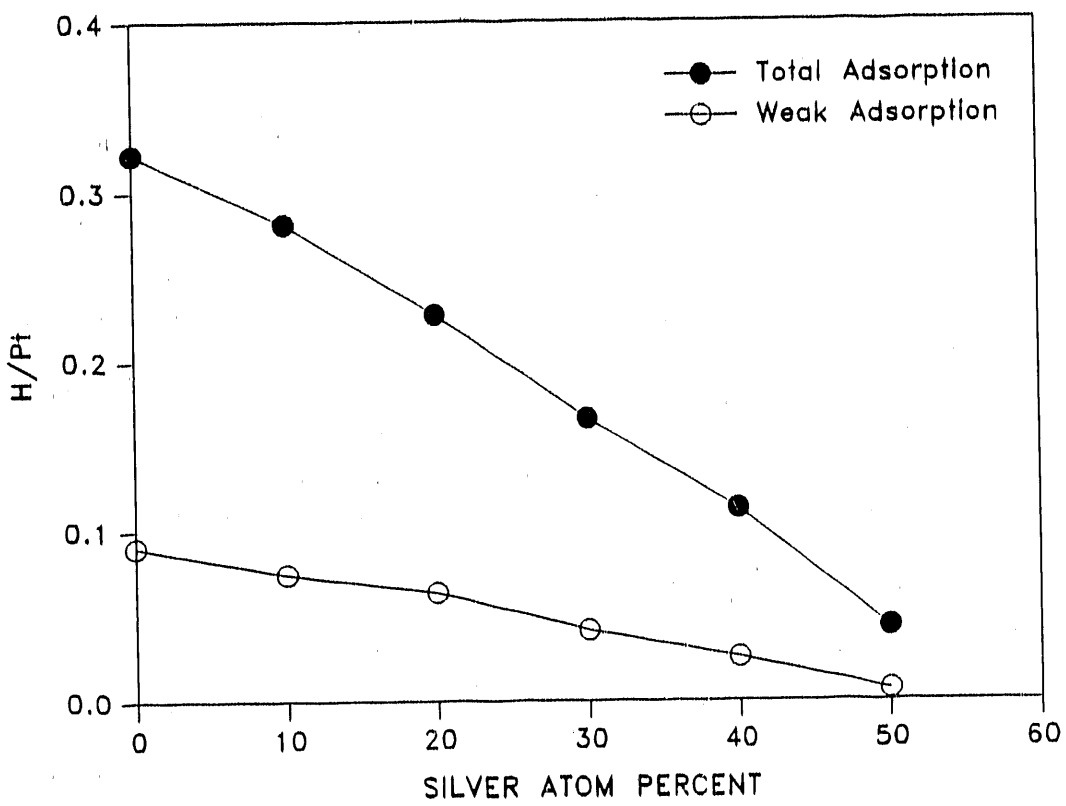

Figure 11. Plot of H/Pt ratio versus silver content for a series of 5% Pt-Ag/SiO_2 catalysts (sequential impregnation). Both the total and the reversible adsorption data are shown in the figure

Table 3. Irreversible hydrogen adsorption on a series of 5% Pt-Cu/SiO_2 and a series of 5% Pt-Ag/SiO_2 bimetallic catalysts

Ib at.%	H/Pt (Pt-Cu)	H/Pt (Pt-Ag)
0	0.544	0.544
10	0.565	0.540
20	0.543	0.493
30	0.524	0.445
40	0.487	0.392
50	0.390	0.276
60	0.286	0.185
70	0.230	0.095
80	0.186	0.066

adsorbed hydrogen decreased gradually for silver contents from 0 to 40 at.% Ag and then dropped more rapidly with further increase of silver. The amount of irreversible hydrogen adsorption was always more on a Pt-Cu catalyst than on a Pt-Ag catalyst at the same atomic percent for Group Ib metal.

Irreversible adsorption data for a series of 4% Pt-Ag/SiO_2 (ion exchange for Pt and impregnation for Ag) and a

Table 4. Irreversible hydrogen adsorption on a series of 4% Pt-Ag/SiO_2 and a series of 5% Pt-Ag/SiO_2 bimetallic catalysts

Catalyst	Ag at.%	H/Pt
4% Pt-Ag series[a]	0.0	0.574
	5.9	0.627
	10.1	0.601
	20.1	0.546
	30.7	0.531
	40.2	0.503
5% Pt-Ag series[b]	0.0	0.232
	10.0	0.207
	20.0	0.164
	30.0	0.125
	40.0	0.088
	50.0	0.037

[a]The catalysts were prepared by a mixed ion exchange and impregnation method.

[b]The catalysts were prepared by sequential impregnation.

series of 5% Pt-Ag/SiO_2 (sequential impregnation) catalysts are tabulated in Table 4. For the 4% Pt-Ag/SiO_2 series, the strong hydrogen uptake was nearly independent of the silver content and remained in the range of 0.5-0.63 for silver cont nts up to 40 at.% Ag. However, for the 5% Pt-Ag/SiO_2 series, the amount of irreversible hydrogen was a strong function of the silver content and it decreased considerably as the silver loading increased.

The adsorption data for the irreversible hydrogen from all four series of platinum-containing bimetallic catalysts are summarized in Figure 12. Clearly, both the 4% Pt-Ag series and the 5% Pt-Cu series with copper content up to 40 at.% Cu show a similar moderate decrease in capacity for hydrogen chemisorption as a function of increasing copper or silver content. The adsorption trend for the 5% Pt-Ag/SiO_2 series (ion exchange) leads to a more steady decrease than for the 5% Pt-Cu/SiO_2 series. By comparison, the 5% Pt-Ag series made by the sequential impregnation method exhibits the most pronoun ed decreasing trend among the three Pt-Ag bimetallic series.

NMR of Adsorbed Hydrogen

NMR spectra of chemisorbed hydrogen shown in Figure 13 are for a 10% Pt/SiO_2 catalyst prepared by impregnation (20.6% dispersion as was measured by the strong hydrogen

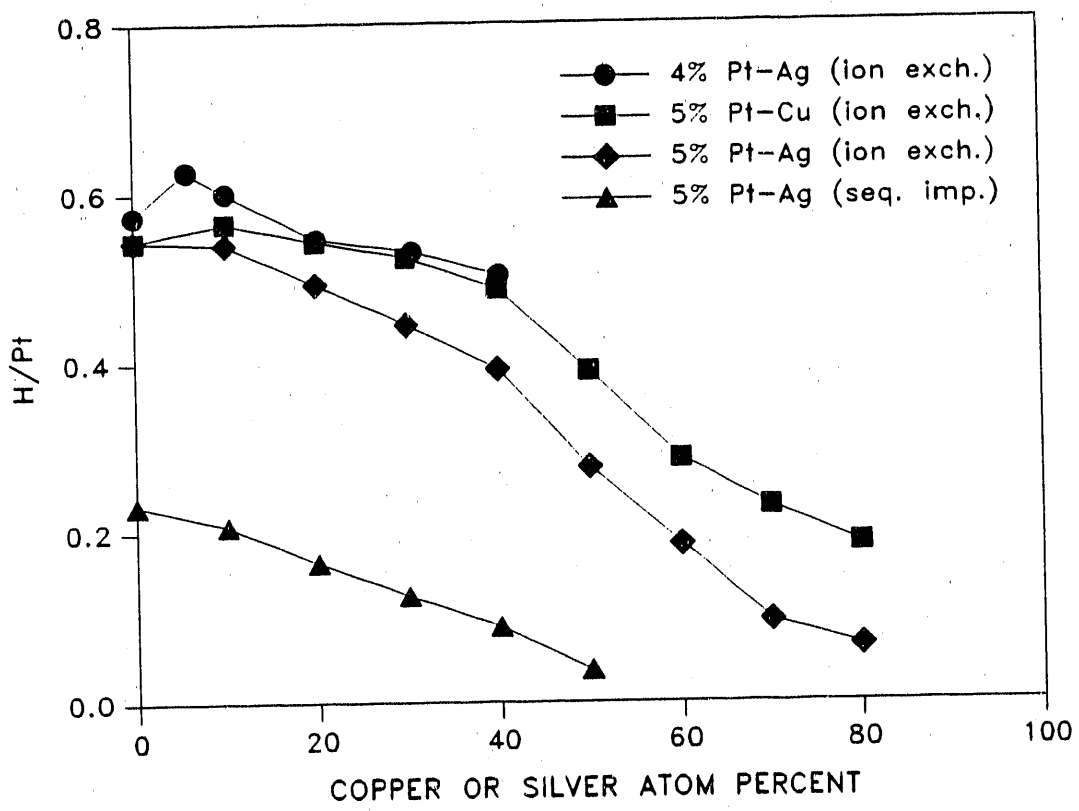

Figure 12. Plot of H/Pt ratio from the irreversible hydrogen adsorption versus copper or silver content for a series of Pt-Cu/SiO_2 and three series of Pt-Ag/SiO_2 bimetallic catalysts. The copper or silver content is expressed in atomic percent

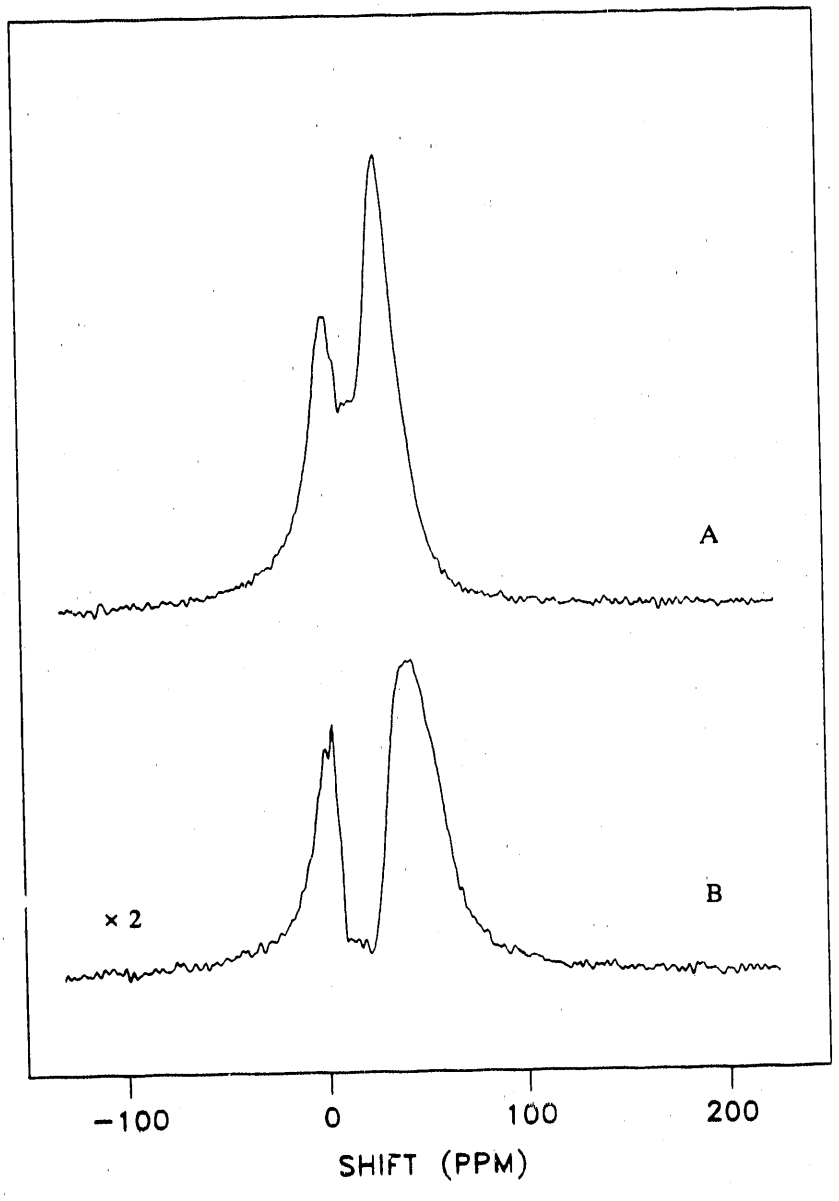

Figure 13. NMR spectra on a 10% Pt/SiO_2 catalyst prepared by the impregnation method after adsorption under A) 5 Torr hydrogen; B) 5 Torr hydrogen followed by evacuation to 10^{-6} Torr for 10 min

adsorption, see Figure 6) under the following two different adsorption conditions: 1) 5 Torr hydrogen gas; 2) evacuation to a pressure of 10^{-6} Torr for a ten-minute period after adsorption under 5 Torr hydrogen. Two well resolved peaks in both NMR spectra were observed. The downfield peak at about 4 ppm is assigned to the silanol proton from the silica support. The upfield resonance corresponds to hydrogen adsorbed on platinum surfaces, as already observed by other investigators (21-23). In Spectrum A, the upfield resonance indicated a shift at 29 ppm and a linewidth (full width at half maximum) of 4.85 kHz. A shift of 44 ppm and a linewidth of 6.78 kHz were observed for the upfield peak in Spectrum B.

Figure 14 shows two NMR spectra for a pure 10% Pt/SiO_2 catalyst (ion exchange) with a dispersion of 36.2% after hydrogen adsorption under 5 Torr overpressure (A); and 5 Torr hydrogen followed by evacuation (B). As can be seen, the two resonances are much closer to each other with considerable overlap than those observed in the catalyst prepared by impregnation. While the downfield resonance position remained at about 4 ppm, the upfield resonances have shifted downfield under both hydrogen adsorption conditions, as compared with those shown earlier in Figure 13. With a pressure of 5 Torr hydrogen, the upfield peak shift was about 25 ppm. A value of 31 ppm for the upfield peak shift was obtained for the sample evacuated after adsorption under 5

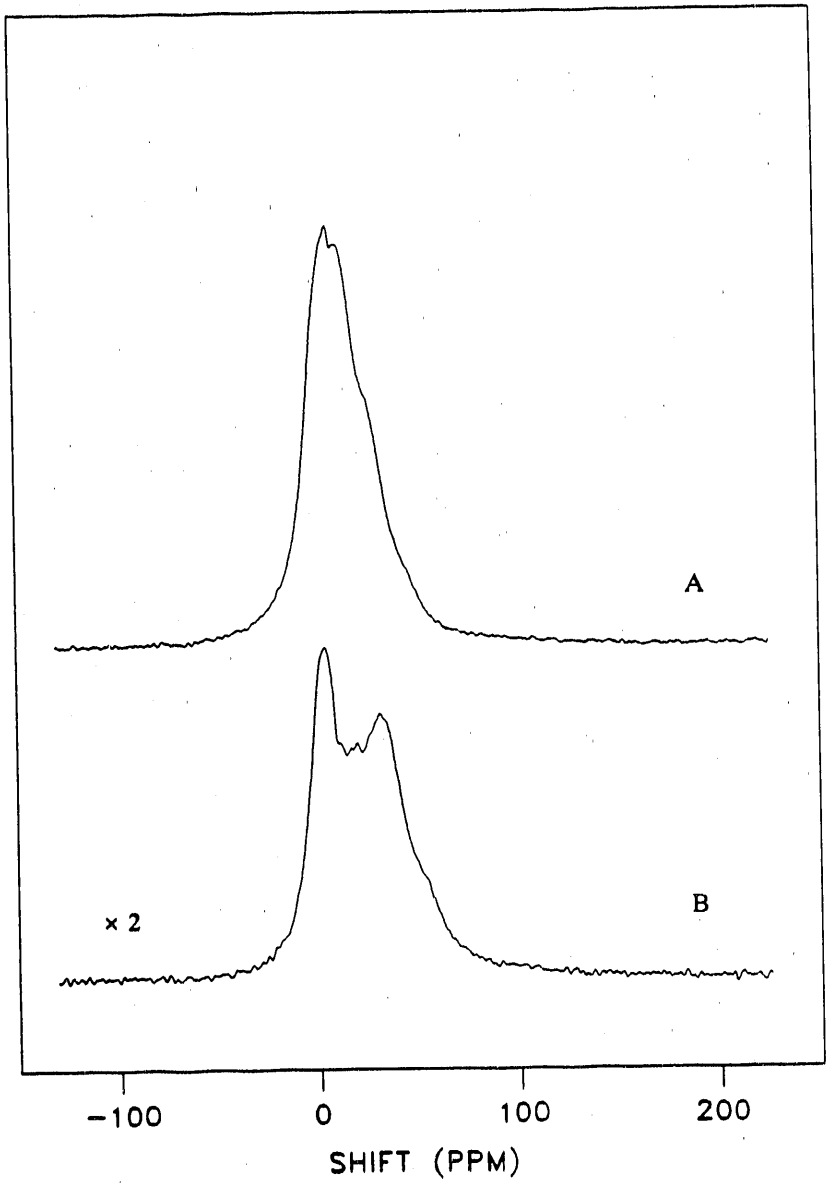

Figure 14. ^{1}H NMR spectra on a 10% Pt/SiO_2 catalyst prepared by the ion exchange method after adsorption under A) 5 Torr hydrogen; B) 5 Torr hydrogen followed by evacuation to 10^{-6} Torr for 10 min

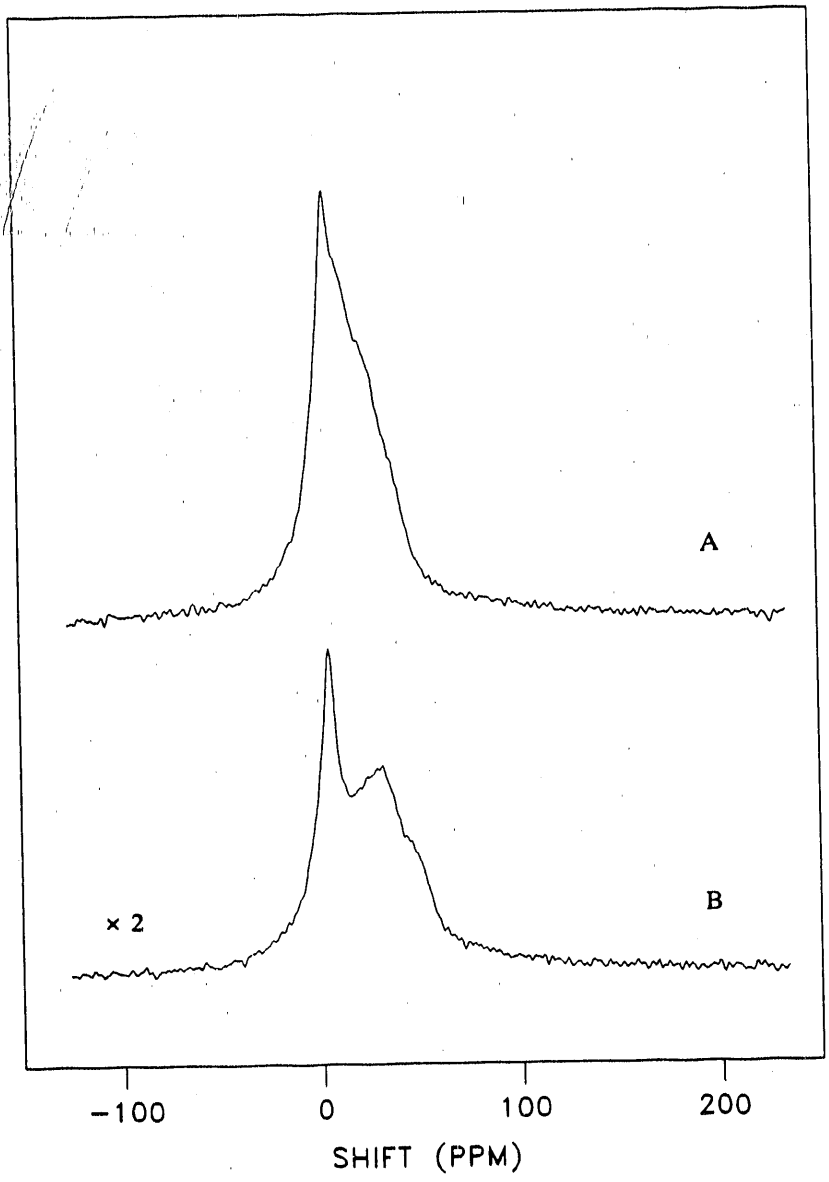

Figure 15. ^{1}H NMR spectra on a 4% Pt/SiO_2 catalyst prepared by the ion exchange method after adsorption under A) 5 Torr hydrogen; B) 5 Torr hydrogen followed by evacuation to 10^{-6} Torr for 10 min

Torr hydrogen.

^1H NMR spectra for a 4% Pt/SiO_2 catalyst (ion exchange) with a dispersion of 57.4% are shown in Figure 15 under the same hydrogen adsorption conditions mentioned above. The position of the downfield peak corresponding to the silanol proton remained at about 4 ppm. However, the upfield peak has moved even further downfield toward the silanol peak. The increased overlap between the two peaks resulted in an unresolved extended shoulder of the silanol peak in Spectrum A. By assuming a Lorentzian lineshape for the silanol peak and subtracting it from the spectrum, one can then find the first moment for the upfield resonance from the resulting difference spectrum. A lineshift value of 22 ppm was found under 5 Torr hydrogen and that of 30 ppm for the chemisorbed hydrogen after evacuation. It is interesting to notice that there is an observable shoulder peak upfield to the upfield resonance in Spectrum B.

The values for the upfield peak shift on four Pt/SiO_2 catalysts are summarized in Table 5. Obviously, the general trend indicates a downfield movement of the upfield peak with increasing platinum dispersion under both hydrogen adsorption conditions. In addition, the values of the upfield peak shift under 5 Torr hydrogen are smaller (shifted downfield) than those under the adsorption-evacuation condition in all cases. This observation is opposite to what was observed on

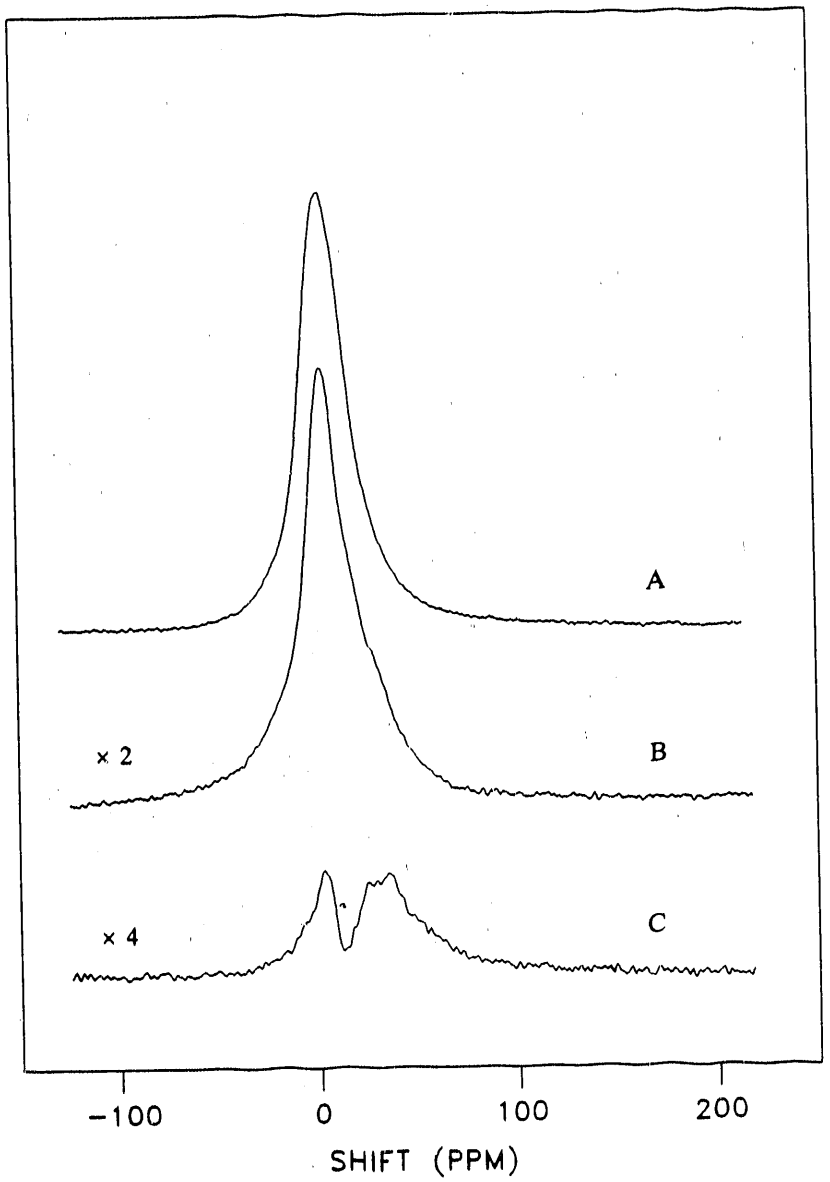

Figure 16. ^{1}H NMR spectra on a 5% Pt/SiO_2 catalyst prepared by the ion exchange method after adsorption under A) 5 Torr hydrogen; B) 5 Torr hydrogen followed by evacuation to 10^{-6} Torr for 10 min. Spectrum C represents the irreversibly adsorbed hydrogen on the same catalyst after deuteration

Table 5. NMR lineshift values for hydrogen adsorbed on Pt/SiO_2 catalysts

Catalyst	Dispersion	Upfield peak shift (ppm)	
		5 Torr H_2	Irreversible H
10% Pt[a]	0.206	29.4	43.9
10% Pt[b]	0.362	24.5	31.3
4% Pt[b]	0.430	28.4	32.3
4% Pt[b]	0.574	22.3	30.4

[a]The catalyst was prepared by impregnation method.

[b]The catalyst was prepared by ion exchange method.

pure Ru/SiO_2 catalysts (57).

NMR spectra for the hydrogen adsorbed on a 5% Pt/SiO_2 catalyst (prepared by the ion exchange method with a metal dispersion of 54.4%) are shown in Figure 16 under various hydrogen adsorption conditions. As can be seen in Spectra A and B, the silanol peak was much too intense for the upfield hydrogen-on-platinum peak to be observed. Also, the upfield peak tended to resonate close to the silanol peak because of the high Pt dispersion. In Spectrum A, the upfield peak for the catalyst under 5 Torr hydrogen was practically buried under the intense silanol peak. The upfield resonance was

observed only as a small shoulder under the silanol peak in Spectrum B when the catalyst sample was evacuated after hydrogen adsorption. However, deuteration of the silica support significantly reduce the intensity of the silanol resonance as shown in Spectrum C, allowing clear observation of the hydrogen-on-platinum peak. In this case, the catalyst sample was evacuated after hydrogen adsorption. Thus the observed upfield peak corresponds to the strongly bound hydrogen on highly dispersed platinum surfaces. This peak has an asymmetric lineshape with an extended shoulder on the right side of the peak. The lineshift and the linewidth for this peak were 33.3 ppm and 7.49 kHz, respectively.

Figure 17 shows two NMR spectra for a pure 5% Cu/SiO_2 catalyst (ion exchange) under different gas-dosing treatment. Spectrum A represents adsorption under 30 Torr hydrogen. As clearly shown, a downfield peak to the left of the silanol peak was observed, corresponding to hydrogen adsorbed on pure copper. This peak was located at -84 ppm with a linewidth of 2.93 kHz. To obtain Spectrum B, the catalyst sample was dosed with 30 Torr deuterium instead of hydrogen and allowed equilibration at room temperature for 24 hours. A downfield peak with a left shoulder peak was observed to the left of the silanol peak. The lineshift values for the downfield resonance and the shoulder peak were -77 ppm and -92 ppm, respectively.

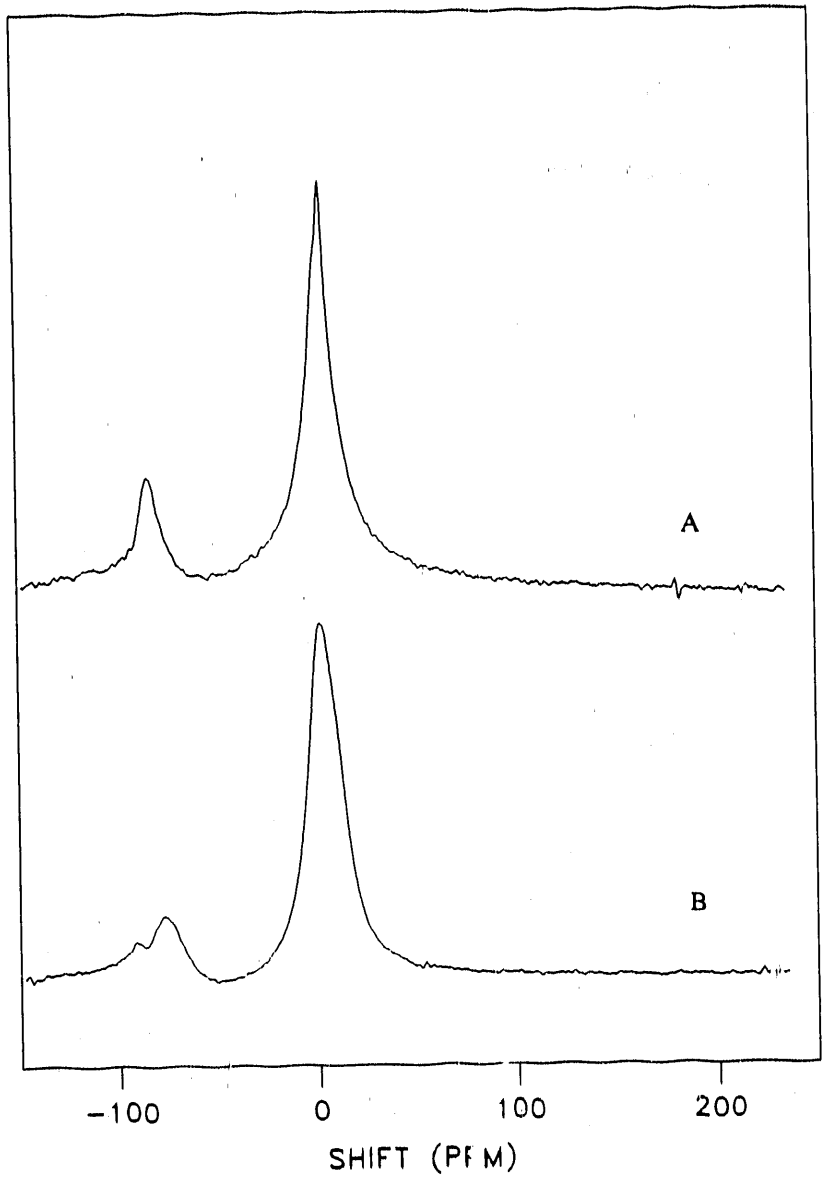

Figure 17. ^{1}H NMR spectra on a 5% Cu/SiO_2 catalyst prepared by ion exchange method. Spectrum A corresponds to adsorption under 30 Torr hydrogen. Spectrum B was obtained after 24 hours following adsorption under 30 Torr deuterium

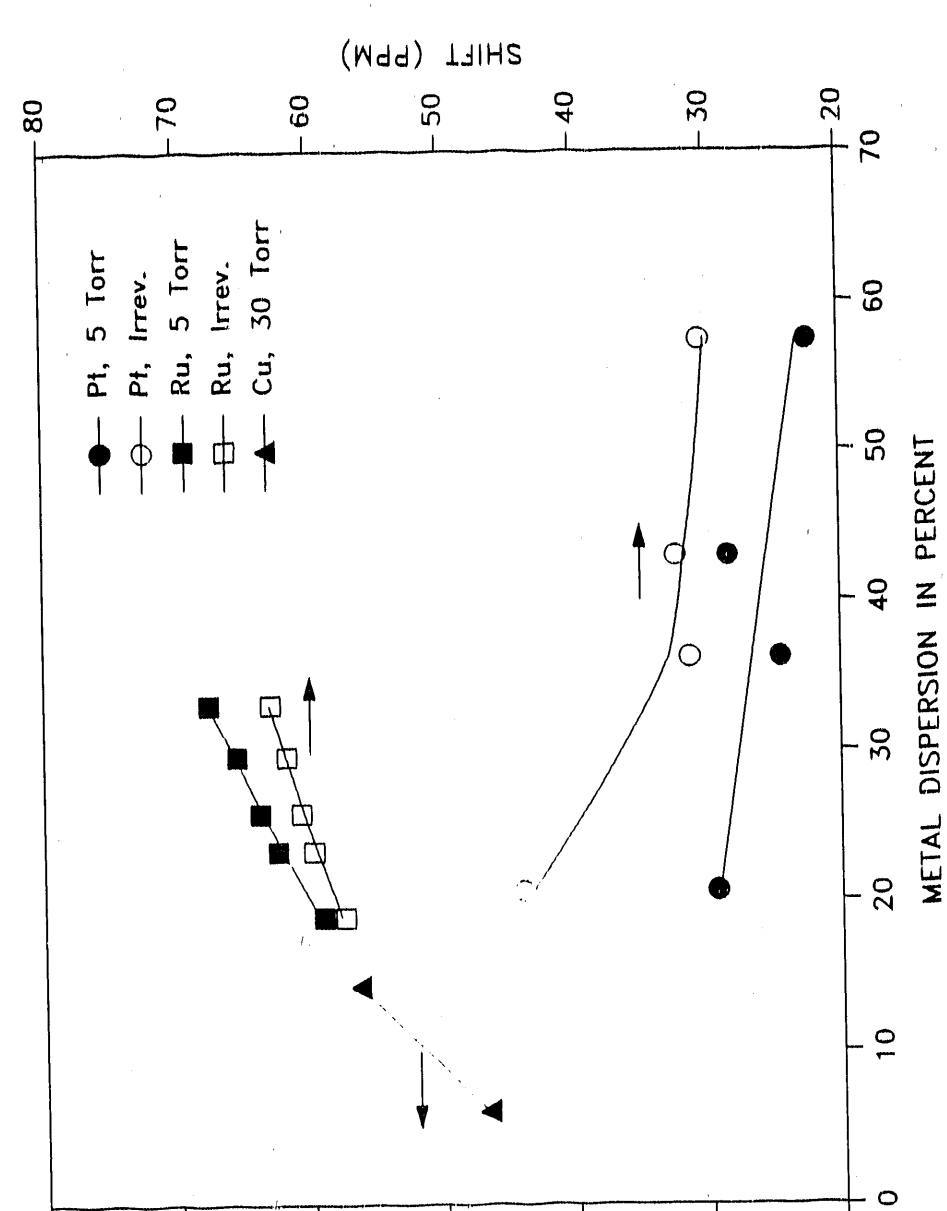

Figure 18. The lineshifts for the hydrogen-on-metal peak versus metal dispersion for ruthenium, platinum, and copper. The lineshift values for both the 5 Torr hydrogen and the irreversible hydrogen are shown for ruthenium and platinum

The trends for the shift of hydrogen-on-metal peak with metal dispersion are plotted in Figure 18 for the Pt/SiO_2, Ru/SiO_2, and Cu/SiO_2 monometallic catalysts. Clearly, an upfield trend of the shift of the hydrogen-on-metal peak with increasing dispersion was observed for both ruthenium and copper. On the other hand, a downfield trend of the shift of the hydrogen-on-platinum peak was measured with increasing platinum dispersion. It is also interesting to note that the shift of strongly bound hydrogen on platinum is slightly upfield to that of total hydrogen adsorption, while it is just the opposite on ruthenium (57, 58).

NMR spectra of adsorbed hydrogen for a series of 5% Pt-Cu/SiO_2 bimetallic catalysts are shown in Figure 19 with all the catalyst samples under 5 Torr hydrogen. Similar to what was observed in Figure 16, the intense silanol peak almost completely obscured the hydrogen-on-metal peak, which was expected to resonate on the upfield side under the silanol peak. However, a broad downfield resonance to the left of the silanol peak emerged for catalysts with a copper content of 70 at.% Cu or higher. For a series of 5% Pt-Ag/SiO_2 bimetallic catalysts under 5 Torr hydrogen, as shown in Figure 20, a similar problem occurred with the hydrogen-on-metal peak being overshadowed by the intense silanol peak. Under these circumstances, very little information can be extracted from these NMR spectra.

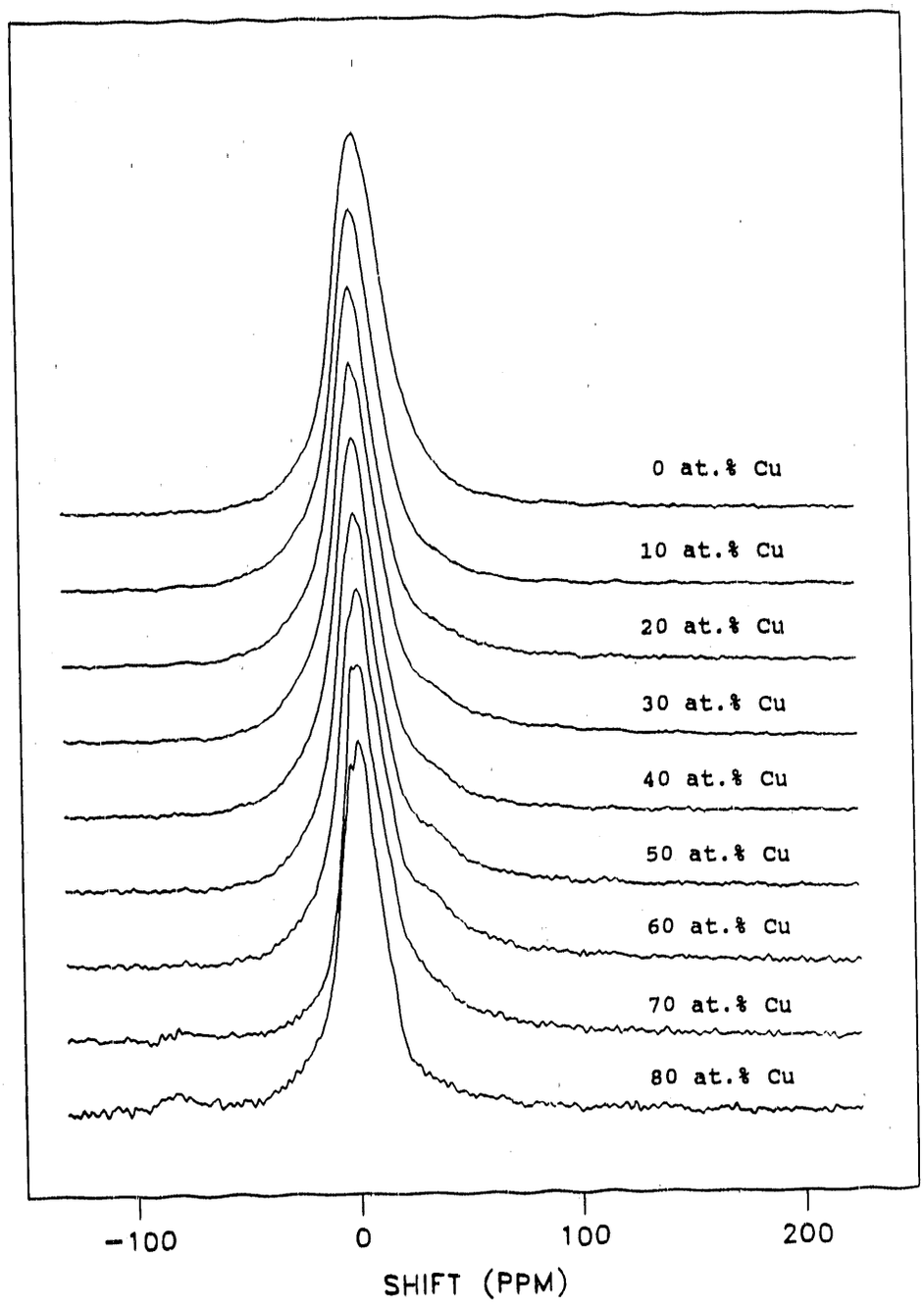

Figure 19. ^{1}H NMR spectra for a series of 5% Pt-Cu/SiO_2 bimetallic catalysts with different loadings for copper. All catalyst samples were under 5 Torr hydrogen

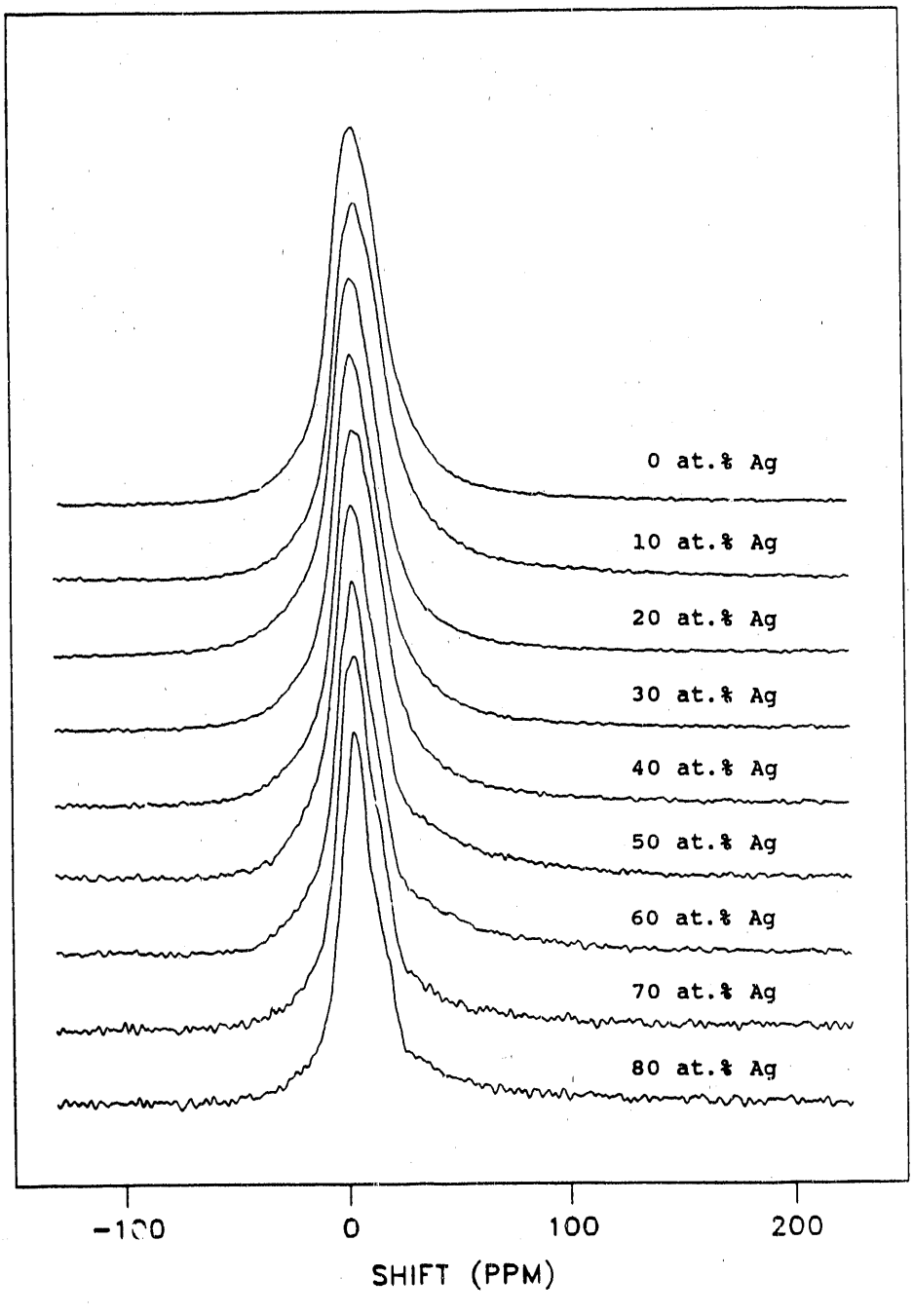

Figure 20. ^{1}H NMR spectra for a series of 5% Pt-Ag/SiO_2 bimetallic catalysts with different loadings for silver. All catalyst samples were under 5 Torr hydrogen

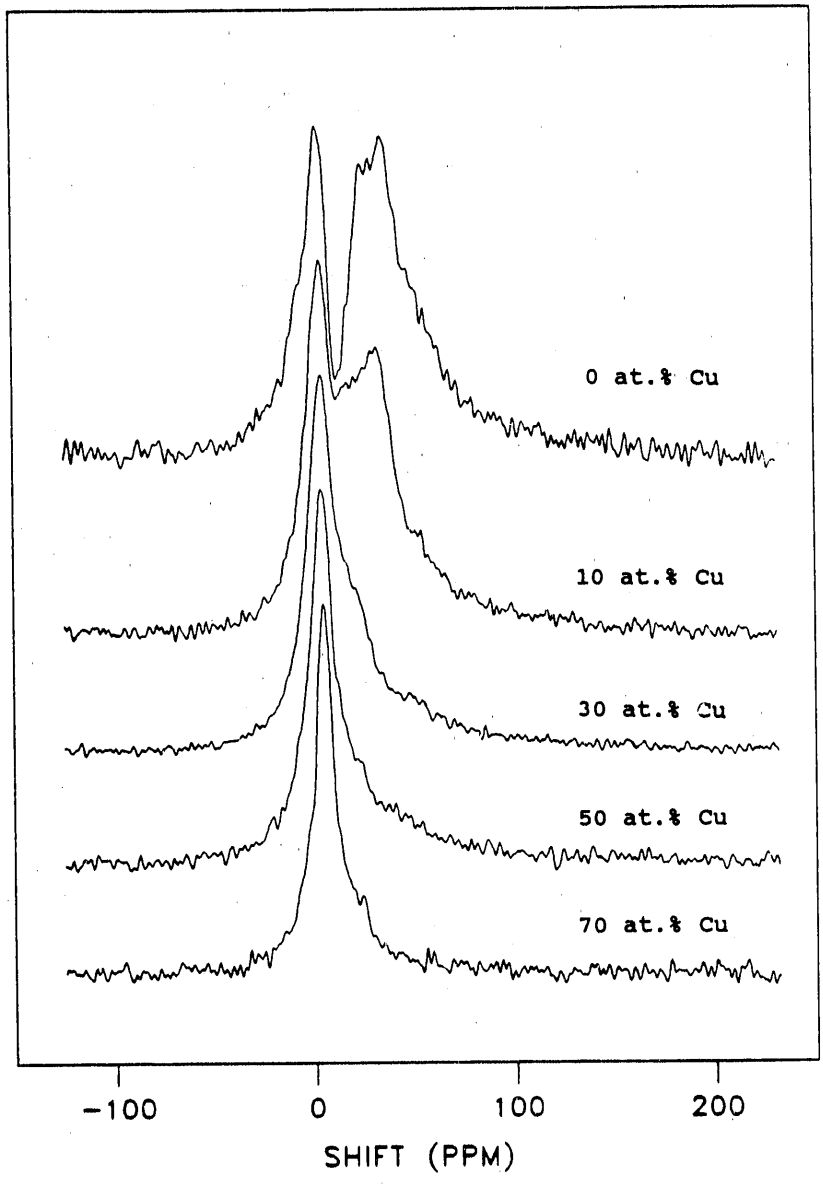

Figure 21. ^{1}H NMR spectra for a series of 5% Pt-Cu/SiO_2 bimetallic catalysts dosed with only the strongly adsorbed hydrogen. All catalyst samples were deuterated to reduce the silanol peak intensity

However, by deuterating the catalyst samples, the NMR spectra were much improved in resolution. Figure 21 shows a set of NMR spectra for a number of Pt/SiO_2 and $Pt-Cu/SiO_2$ catalysts with irreversible hydrogen chemisorption after deuteration of the silica support. The hydrogen-on-metal peak was well separated from the silanol peak for the 5% Pt/SiO_2 catalyst and the 5% $Pt-Cu/SiO_2$ catalyst with 10 at.% Cu content. Although the peak separation was quite poor for catalysts with higher copper content, a shoulder peak on the right side of the silanol peak could still be observed, corresponding to strongly bound hydrogen on Pt-Cu bimetallic particles. The intensity of this shoulder peak decreases with increasing copper content, in agreement with hydrogen chemisorption data (Table 3 and Figure 12). As expected, the silanol peak after deuteration was considerably narrower in linewidth (2.0-2.7 kHz) than before deuteration (4.2-4.9 kHz).

The estimated values of lineshift for the deconvoluted upfield peak after deuteration are tabulated in Table 6. Increasing copper content shifts this upfield peak downfield, as indicated by the smaller lineshift values at higher copper loadings. This effect of downfield movement by copper on platinum was analogous to that in the $Ru-Cu/SiO_2$ bimetallic catalysts (41), where copper also caused a downfield shift of the upfield peak.

Table 6 NMR lineshift values for strongly adsorbed hydrogen on Pt/SiO_2 and $Pt-Cu/SiO_2$ catalysts

Catalyst	Cu at.%	H/Pt[a]	Shift (ppm)
5% Pt	0	0.544	33.3
5%Pt-0.182%Cu	10	0.565	30.8
5%Pt-0.697%Cu	30	0.524	23.4
5%Pt-1.629%Cu	50	0.390	21.2
5%Pt-3.800%Cu	70	0.230	20.4

[a]The H/Pt ratio was measured from the irreversible hydrogen chemisorption.

DISCUSSION

Catalyst Reducibility

The TGA results shown in Figure 1 clearly indicates a complete reduction of the precursor compound $Pt(NH_3)_4(NO_3)_2$ at temperatures higher than 90°C and the compound $Cu(NO_3)_2 \cdot xH_2O$ at temperatures beyond 195°C. The decomposition and reduction of the tetraammineplatinum (II) nitrate occurred simultaneously in flowing hydrogen diluted in argon, as indicated by the monotonic weight drop of the TGA curve. The observed constant value of 50.3 wt% after reduction is in very good agreement with the value of 50.4 wt% calculated from the compound formula. For the Cu compound, dehydration and decomposition precedes reduction, as indicated by the multiple stages in the TGA curve. Based on the percentage of weight loss, one can calculate the number of water molecules in the copper compound to be about three.

The reduction of supported Cu/SiO_2 catalysts occurs at lower temperatures than the copper nitrate (see Figure 2). This is likely due to less mass transfer resistance during reduction for the highly dispersed copper nitrate in the support. The minute weight loss of the pure silica sample is due to dehydration and perhaps partial dehydroxylation of the silica. The Pt/SiO_2 catalyst precursor reduces at a somewhat lower temperature than the Cu/SiO_2 catalyst precursor while

the Ag/SiO_2 precursor reduces at an even lower temperature (see Figures 3 and 4). Interestingly, the reduction of Pt-Cu/SiO_2 and Pt-Ag/SiO_2 precursors occur at temperatures between those for their respective monometallic precursors. This indicates that there is intimate interaction between the two precursor compounds in the bimetallic catalysts, allowing formation of bimetallic particles after hydrogen reduction.

Deuteration Process

Deuteration of the OH group in a support is necessary when the background signal from the support is intense and tends to obscure resonances of interest. Tirendi et al. (59) have reported successful deuteration of an alumina support with liquid D_2O in flowing N_2 at room temperature. In comparison, silica is more difficult to deuterate because it is less acidic than alumina. This is the reason why deuterated ammonia, ND_3, dissolved in D_2O was used. The ionization effect of ammonia on the silanol group in the silica support facilitates the hydrogen-deuterium exchange and subsequent deuteration process.

This novel technique was successful in deuterating the support on the Pt/SiO_2 and the Pt-Cu/SiO_2 catalysts (see Figures 16 and 21). Partial deuteration of the silica support greatly improved the detectability of the hydrogen adsorbed on Pt and Pt-Cu surfaces. Complete deuteration of

the silanol proton in the silica support is possible through prolonged and repetitive treatment with a ND_4OD/D_2O solution. This process makes possible the study not only of the hydrogen adsorbed on highly dispersed monometallics and bimetallics by proton NMR, but also of hydrocarbons adsorbed on these catalysts since most protons in hydrocarbons resonate at frequencies very close to that of the silanol proton. The only limitation of this technique is that the weakly adsorbed hydrogen or the hydrogen in hydrocarbons may slowly exchange with the deuterated silanol group over time. Therefore, for Pt/SiO_2 and $Pt-Cu/SiO_2$ catalysts, only the strongly bound hydrogen was dosed in order to prevent the exchange, since the strongly adsorbed hydrogen does not exchange with the silanol deuterium at room temperature as shown by our results on the Ru/SiO_2 catalysts (55).

Besides marked reduction of the silanol peak intensity, deuteration also resulted in a much narrower silanol peak. This line narrowing (by as much as 2 kHz) was due to dilution of the silanol proton in the silica, increasing the average distance between the proton spins. This interesting result indicates that much of the original line broadening on the silanol resonance was caused by the homogeneous H-H dipole interaction since this interaction is proportional to the inverse cube of the internuclear distance.

Pt and Cu Monometallics

The platinum dispersion is obtained from the measured H/Pt ratio for the irreversible hydrogen assuming a complete monolayer hydrogen coverage with a stoichiometric ratio of one hydrogen atom to one surface platinum atom. The total H/Pt ratio is not used to measure Pt dispersion because of hydrogen spillover from Pt onto the silica support (4, 5). Sheng and Gay (23) also show that there is hydrogen spillover to SiO_2 by measuring the spin-lattice relaxation time of the silanol proton (on the order of a few seconds). This type of spillover is possibly due to the weakly bound hydrogen on platinum since the weakly bound hydrogen on ruthenium has been found to cause spillover onto the silica support (55).

As expected, high Pt dispersion has been obtained from catalysts prepared by the ion exchange method, while low Pt dispersions are measured on those catalysts prepared by the impregnation method. In addition, low Pt loadings have resulted in much higher dispersion possibly through formation of finer Pt particles.

In the present study, NMR of chemisorbed hydrogen has indicated a larger upfield shift on Pt catalysts with lower Pt dispersion. Sheng and Gay (23) have also observed such a trend with Pt dispersion. In addition, they have reported a decreasing upfield shift with increasing hydrogen coverage. However, the hydrogen coverage in their work was derived from

the adsorption isotherm and was poorly defined in view of hydrogen spillover and weakly bound hydrogen in the Pt/SiO_2 catalysts. This variation of shift with Pt dispersion may be due to either the effect of a change in the local magnetic susceptibility resulting from the change in the Pt particle size or the effect of Knight shift variation caused by a change in the local electron density of conduction electrons. The present study cannot distinguish these two effects.

The observed upfield peak along with a shoulder peak further upfield for a 4% Pt/SiO_2 catalyst (see Figure 15) may be due to a Pt particle size distribution. Since larger Pt particles cause a further upfield shift, the observation may simply mean that there is a small fraction of large platinum particles in coexistence with a large fraction of small Pt particles in the catalyst. Based on the upfield resonance linewidth measurements on a 10% Pt/SiO_2 catalyst with low dispersion (see Figure 13), it is inferred that the strongly bound hydrogen is much less mobile on the platinum surfaces than the reversibly bound hydrogen because of the measured broader resonance line. The line broadening for the upfield peak is associated with homogeneous H-H dipole interactions, chemical shift anisotropy, adsorption and heterogeneity sites, and local variations in magnetic susceptibility. All of these can be partially removed by motion of hydrogen adsorbed on the platinum surfaces on a time scale fast

compared to the inverse of the linewidth of the internal interaction causing the broadening.

The chemisorption data on Cu/SiO_2 catalysts (see Figure 5 and Table 1) clearly indicates the capability for copper to adsorb both hydrogen and carbon monoxide at room temperature. Both the strongly and weakly bound hydrogen exist on the Cu surfaces, as observed here and in a previous study (39) by NMR of adsorbed hydrogen as well as by volumetric adsorption. However, carbon monoxide can only weakly adsorb on the copper surfaces since it is nearly completely removed by evacuation. Note that the amount of hydrogen adsorption is about an order of magnitude less on copper than on platinum.

It is likely that the mode of bonding between hydrogen and surface copper is quite different from that between carbon monoxide and surface copper. In the case of hydrogen, the 1s orbital of hydrogen and the 4s orbital of copper would be expected to be the main states involved in the bonding, causing a large downfield Knight shift in the NMR spectra (32, 39). In the case of carbon monoxide, π bonds may be involved in the weak bonding. The event may be a weak chemisorption.

It is still uncertain whether the hydrogen adsorbed on copper is in an atomic or a molecular state. It is clear from many single crystal studies (26, 27) that dissociative adsorption of molecular hydrogen on copper is an activated

process with a small energy barrier of 5 kcal/mole. However, this energy barrier may be lowered on small polycrystalline Cu surfaces since the electronic environment of the copper surfaces may change significantly with copper particle size (see discussion below). When this happens, the process of spontaneous dissociative adsorption of hydrogen molecules may be possible at room temperature. Hydrogen-deuterium exchange on a dispersed 5% Cu/SiO_2 catalyst (see Figure 17) seems to indicate that the adsorbed hydrogen is in the atomic state since the source of hydrogen in this case comes from exchange with only the silanol proton in the silica support.

An interesting comparison of the hydrogen-on-metal shift versus metal dispersion for Pt, Ru, and Cu, as shown in Figure 18 revealed different trends for the three elements. The observed differences in trends are rather puzzling. Copper shows the same trend as Ru but a different shift direction for the total and the irreversible hydrogen adsorption (39). Also, the disparity in lineshift between the total and the irreversible hydrogen is larger for Pt (and Cu) than for Ru. The variation in Knight shift is caused by either a change in the valence conduction electron density at the metal surfaces or a variation in the local magnetic susceptibility resulting from a change in the metal particle size. Since the value of magnetic susceptibility of copper is more than an order of magnitude smaller than the other two

elements, its change with particle size is expected to be small. Thus, the considerable change in shift on copper is likely due to a change of electronic environment at the copper surfaces with changing Cu particle size. One cannot distinguish the two effects on shift for Ru and Pt since the cause of Knight shift for these two elements (primarily d states in the conduction band) is different from that for copper (primarily s states in the conduction band). However, the magnetic susceptibility remains the same for any particular catalyst with or without adsorbed hydrogen. Thus, the observed difference in shift between total adsorption and strong adsorption is likely due to variation of electronic state of the metal particles caused by varying degree of interaction with the adsorbed hydrogen. This variation of shift with the amount of adsorbed hydrogen has been observed on all the noble transition metal catalysts (22-24). The larger disparity in shift between the two hydrogen adsorption conditions on Pt shown in Figure 18 may indicate that the electronic environment of Pt surfaces is more susceptible to change by the adsorbed hydrogen than that of Ru surfaces. However, it is not yet understood why the direction of the NMR shift for the two hydrogen adsorption conditions is just the opposite on the two metals for a given metal dispersion. Note that the shift direction with the amount of hydrogen adsorption is the same for Rh (24) as that for Ru.

Pt-Cu and Pt-Ag Bimetallics

Pt-Cu bimetallics are expected to form an ordered alloy with a strong segregation of copper to the surfaces while Pt-Ag bimetallics will form a random alloy with an even stronger segregation of silver to the surfaces, according to results from Monte Carlo simulations (34). The overall segregation effect is due to an interplay of cohesive energy differences and mixing energies.

The strong hydrogen chemisorption data shown in Figure 12 for the Pt-Cu and Pt-Ag bimetallic catalysts prepared by the same method (ion exchange) indicates more adsorption of hydrogen on Pt-Cu than on Pt-Ag at the same atomic percent of Group Ib elemert. If one assumes that hydrogen adsorption will measure the total number of surface Pt in the Pt-Cu bimetallics, a misleading conclusion may be reached that more segregation exists in Pt-Cu than in Pt-Ag. However, in the Ru-Cu bimetallic system (39), hydrogen has been found to spill over from Ru to Cu, and actually hydrogen chemisorption measures the total number of surface Ru and Cu instead of Ru alone. Therefore, it is likely that hydrogen would spill over from Pt to Cu in the Pt-Cu bimetallic system by the same mechanism, i.e., through surface diffusion and exchange. Thus, hydrogen chemisorption measures really the total number of surface Pt and Cu atoms. In fact, the capacity for hydrogen chemisorption remained constant up to 40 at.% Cu

before it decreased, indicating spillover of hydrogen onto copper. The decrease in hydrogen chemisorption capacity at high Cu loadings simply means that larger Pt-Cu bimetallic particles are formed.

Evidence of interaction between Pt and Cu can be seen from the variation of the upfield shift with Cu loading (see Figure 21 and Table 6). The direction of the shift is the same as that for Ru-Cu bimetallics, i.e., downfield with increasing Cu loading. At high Cu loadings, the lineshift values tend to level off, indicating complete masking of the Pt surfaces by copper. Copper islands are expected to form at these high Cu loadings. In fact, a downfield resonance corresponding to hydrogen adsorbed on pure copper has been observed at 70 at.% Cu (see Figure 19).

The upfield shift values have been obtained from the relatively less mobile, strongly bound hydrogen instead of the fast-exchanging weakly bound hydrogen, as in the case of Ru-Cu bimetallics (39). However, to a first approximation, the same linear relation between the observed shift and the surface composition used in the Ru-Cu bimetallic system was employed here for the Pt-Cu bimetallics to obtain a rough estimate of surface composition. The calculated value for the surface fraction of Pt can then be multiplied by the H/Pt ratio from the irreversible hydrogen chemisorption to obtain the fractional Pt dispersion of the Pt-Cu bimetallics. The

results are plotted in Figure 22 along with the data from the strong hydrogen chemisorption (assuming hydrogen adsorbs only on the Pt) and the calculated values from an ideal monolayer masking of Pt particles by copper. As shown in the figure, the values computed from the NMR shift (diamonds) are almost identical to those from monolayer assumption (circles) in the range of 0 to 30 at.% Cu. This result indicates intimate contact between the two elements and strong segregation of copper to the surface of the particles. The data from hydrogen chemisorption in fact represents the ratio between the total number of surface Pt and Cu atoms and the total number of bulk Pt atoms in the bimetallic catalysts because of hydrogen spillover from Pt to Cu.

Chemisorption data from the irreversible hydrogen (see Figure 12 and Tables 3 and 4) on the three series of Pt-Ag bimetallic catalysts indicate very different trends with the silver content. The 4% Pt-Ag/SiO_2 series shows virtually no decrease in hydrogen chemisorption capacity while the 5% Pt-Ag/SiO_2 (ion exchange) series indicates a notable decrease. The reason for the discrepancy is in the different methods of catalyst preparation. The 4% Pt-Ag/SiO_2 series was prepared by ion exchange for platinum but impregnation for silver. Therefore, after hydrogen reduction, Pt and Ag are likely to form separate Pt and Ag particles since platinum is highly dispersed but silver is not in this case. For the 5% Pt-

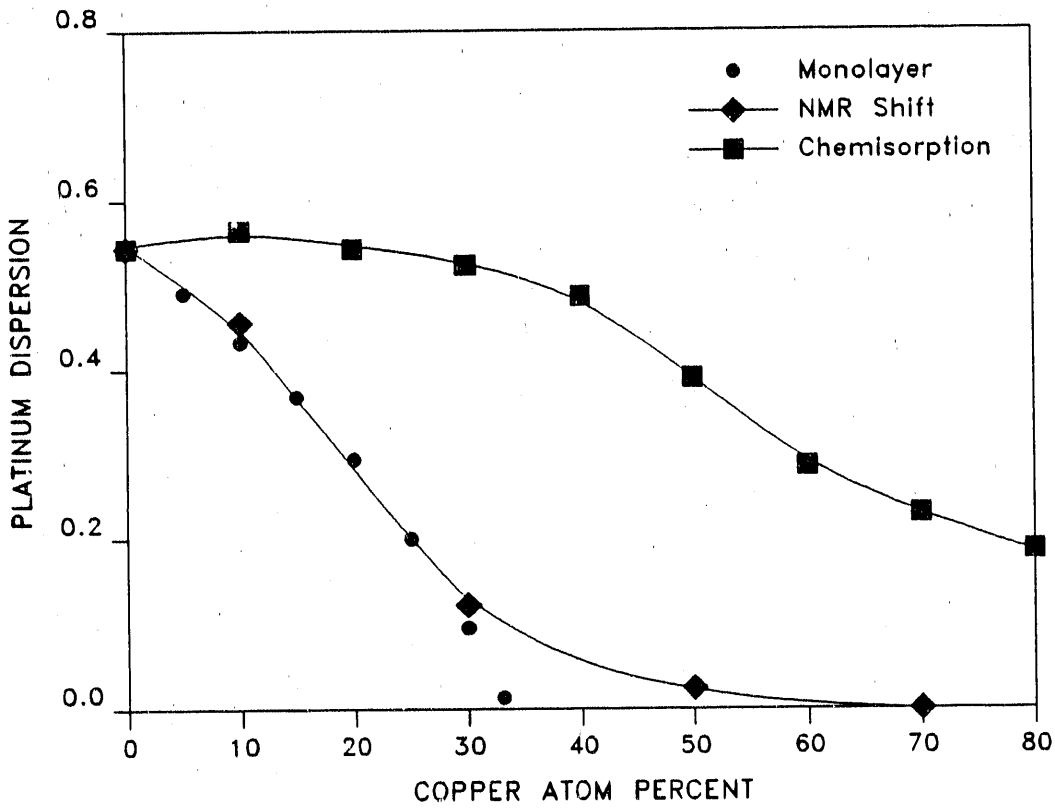

Figure 22. Plot of platinum dispersion versus copper content for a series of 5% Pt-Cu/SiO_2 catalysts. Results from hydrogen chemisorption and NMR lineshift are shown. Also, the calculated values from assuming a monolayer blocking of surface platinum atoms by copper atoms are plotted together for comparison

Ag/SiO_2 series made from only the ion exchange method, both metals are highly dispersed and more bimetallic particles are expected to form. Since hydrogen is not expected to spill over from Pt onto Ag, as seen in the Ru-Ag bimetallics (56), a decrease in the hydrogen chemisorption capacity should be observed. For the $Pt-Ag/SiO_2$ series made from the sequential impregnation, the extend of this decrease is even stronger. This is caused by the low Pt dispersion, which requires less amount of silver to cover the same fraction of Pt surfaces.

Figure 23 compares the fractional Pt dispersion, defined as the ratio between the number of surface Pt and the total number of Pt in the bimetallics, for both the Pt-Cu and Pt-Ag bimetallic series as well as for the calculated values from a monolayer assumption. All values have been normalized to the dispersion for the pure Pt catalyst. As indicated in the figure, copper is in intimate contact with the platinum preferentially enriching to the bimetallic surfaces. At copper loadings greater than 50 at.% Cu, the entire Pt surface is masked by copper. The additional Cu will form three-dimensional islands and separate copper particles, as indicated by the emerging downfield peak at high Cu contents in Figure 19, corresponding to hydrogen adsorbed on Cu. Silver does not interact as strongly with Pt as does Cu. There is a tendency for silver to form islands or separate particles before completely covering the platinum surfaces.

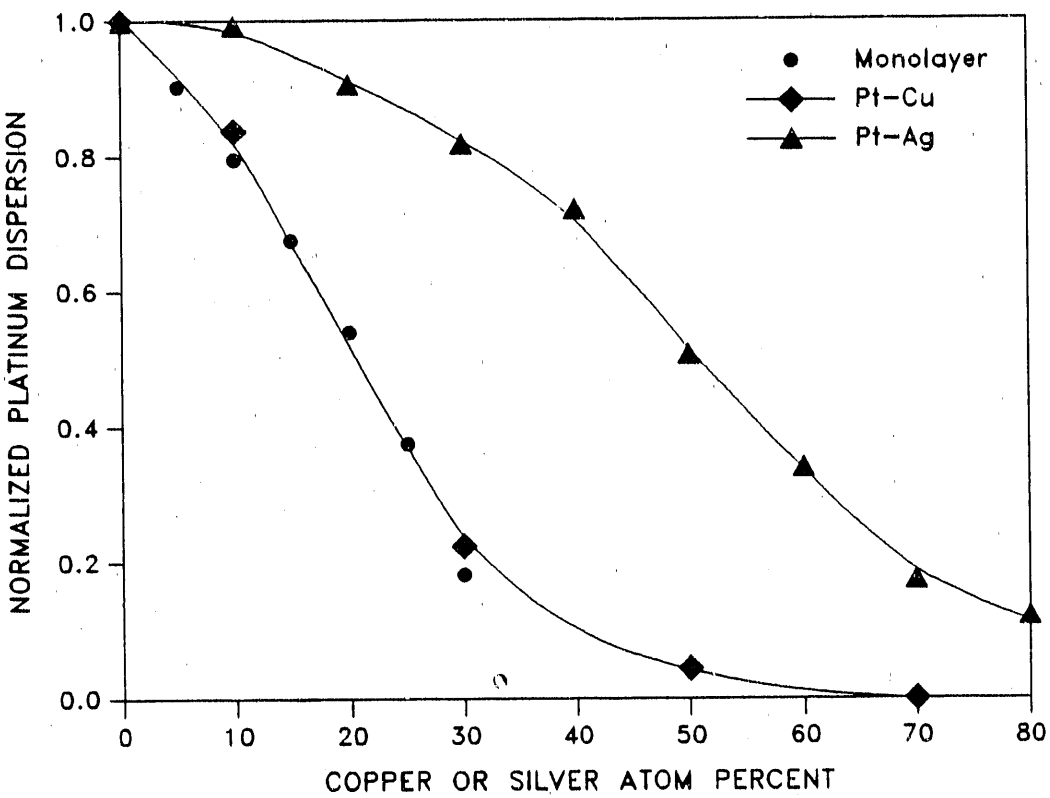

Figure 23. Normalized platinum dispersion versus copper or silver content for a series of 5% Pt-Cu/SiO_2 and a series of 5% Pt-Ag/SiO_2 bimetallic catalysts. The platinum dispersion was normalized to that of the pure Pt/SiO_2 catalyst. Also, the calculated values from an assumption of monolayer blocking of surface platinum atoms by copper or silver atoms are plotted for comparison

CONCLUSIONS

NMR of hydrogen adsorbed on Pt surfaces can be used to probe the local environment of Pt particles. Considerable change in the NMR shift with Pt dispersion has been observed due to either change in magnetic susceptibility of platinum particles or the local electronic environment on the platinum surfaces. Two adsorbed states of hydrogen, irreversibly and reversibly adsorbed hydrogen, exist on the Pt surfaces. The presence of different adsorbed states of hydrogen has a significant influence on the electronic state of the platinum particles.

Both hydrogen chemisorption and proton NMR have clearly indicated that copper is capable of adsorbing hydrogen at ambient temperature. A low saturation hydrogen coverage of 0.2 has been observed. A slow hydrogen-deuterium exchange experiment indicates that the hydrogen adsorbs on copper atomically rather than molecularly. Also, the NMR lineshift variation with Cu dispersion reveals change of electronic environment of Cu surfaces with Cu particle size.

A deuteration technique has been applied to the Pt/SiO_2 and $Pt\text{-}Cu/SiO_2$ catalysts to improve the detectability of the hydrogen adsorbed on metal(s) by NMR. Change in the NMR shift indicates interaction between Pt and Cu, and the shift variation has been used to estimate surface composition of the Pt-Cu bimetallics. Hydrogen chemisorption cannot be

used to measure the fraction of Pt exposed at the surfaces of Pt-Cu bimetallics because of hydrogen spillover to copper. On the Pt-Ag bimetallics, hydrogen chemisorption indicates different trends for catalysts prepared by different methods. The effect of Ag is to decrease the hydrogen chemisorption capacity of the Pt-Ag bimetallics to an extent depending on the dispersed state of catalyst precursors. By comparison, platinum and copper interact much more strongly with each other than platinum and silver. Consequently, silver tends to segregate more strongly to the platinum surfaces than copper.

ACKNOWLEDGMENT

This work was fully supported by the U. S. Department of Energy, Office of Basic Energy Science, Contract No. W-7405-ENG-82. The support of the Engineering Research Institute of Iowa State University is also acknowledged.

REFERENCES

1. Anderson, J. R., Structure of Metallic Catalysts (Academic Press, New York/London, 1975).

2. Benesi, H. A., Curtis, R. M., and Studer, H. P., J. Catal. 10, 328 (1968).

3. O'Rear, D. J., Loffler, D. G., and Boudart, M., J. Catal. 121, 131 (1990).

4. Sermon, P. A., and Bond, G. C., Catal. Rev. 8, 211 (1973).

5. Conner, W. C., Jr., Pajonk, G. M., and Teichner, S. J., in Advances in Catalysis, edited by D. D. Eley, P. W. Selwood, and Paul B. Weisz. (Academic Press, New York, 1986), Vol. 34, pp. 1-79.

6. Christmann, K., Ertl, G., and Pignet, T., Surf. Sci. 54, 365 (1976).

7. Baro, A. M., Ibach, H., and Bruchmann, H. D., Surf. Sci. 88, 384 (1979).

8. Baro, A. M., and Ibach, H., Surf. Sci. 92, 237 (1980).

9. Bernasek, S. L., and Somorjai, G. A., J. Chem. Phys. 62, 3149 (1975).

10. Poelsema, B., Mechtersheimer, G., and Comsa, G., Surf. Sci. 111, 519 (1981).

11. Salmeron, M., Gale, R. J., and Somorjai, G. A., J. Chem. Phys. 67, 5324 (1977).

12. Salmeron, M., Gale, R. J., and Somorjai, G. A., J. Chem. Phys. 70, 2807 (1979).

13. Paal, Z., and Menon, P. G., Catal. Rev. Sci. Eng. 25, 229 (1983).

14. Tsuchiya, S., Amenomiya, Y., and Cvetanovic, R. J., J. Catal. 19, 245 (1970).

15. Eley, D. D., Moran, D. M., and Rochester, C. H., Trans. Faraday Soc. 64, 2168 (1968).

16. Primet, M., Basset, J. M., Mathieu, M. V., and Prettre, M., J. Catal. 28, 368 (1973).

17. Primet, M., Basset, J. M., and Mathieu, M. V., J. Chem. Soc. Faraday Trans. I 70, 293 (1974).

18. Candy, J. P., Fouilloux, P., and Primet, M., Surf. Sci. 72, 167 (1978).

19. Dixon, L. T., Barth, R., and Fryder, T. W., J. Catal. 37, 368 (1975).

20. Szilagyi, T., J. Catal. 121, 223 (1990).

21. Ito, T., Kadowaki, T., and Toya, T., Japan. J. Appl. Phys. 2, 257 (1974).

22. De Menorval, L. C., and Fraissard, J. P., Chem. Phys. Lett. 77, 309 (1981).

23. Sheng, T. C., and Gay, I. D., J. Catal. 71, 119 (1981).

24. Sheng, T. C., and Gay, I. D., J. Catal. 77, 53 (1982).

25. Lenz, D. H., Conner, W. C., Jr., and Fraissard, J. P., J. Catal. 117, 281 (1989).

26. Balooch, M., Cardillo, M. J., Miller, D. R., and Stickney, R. E., Surf. Sci. 46, 358 (1974).

27. Greuter, F., and Plummer, E. W., Solid State Commun. 48, 37 (1983).

28. Shield, L. S., and Russell, W. W., J. Phys. Chem. 64, 1592 (1960).

29. Rossington, D. R., and Holden, S. J., Nature (London) 199, 589 (1963).

30. Alexander, C. S., and Pritchard, J., J. Chem. Soc. Faraday Trans. I 68, 202 (1972).

31. Pritchard, J., Nature 205, 1208 (1965).

32. Ito, T., and Kadowaki, T., Japan. J. Appl. Phys. 14, 1673 (1975).

30. Hansen, M., Constitution of Binary Alloys, 2nd ed. (McGraw-Hill, New York, 1958).

34. Strohl, J. K., and King, T. S., J. Catal. 116, 540 (1989).

35. Anderson, J. H., Jr., Conn, P. J., and Brandenberger, S. G., J. Catal. 16, 326 (1970).

36. Botman, M. J. P., de Jongste, H. C., and Ponec, V., J. Catal. 68, 9 (1981).

37. Meitzner, G., Via, G. H., Lytle, F. W., and Sinfelt, J. H., J. Chem. Phys. 83, 353 (1985).

38. Liao, P. C., Carberry, J. J., Fleisch, T. H., and Wolf, E. E., J. Catal. 74, 307 (1982).

39. Liao, P. C., Fleisch, T. H., and Wolf, E. E., J. Catal. 75, 396 (1982).

40. Toolenaar, F. J. C. M., Stoop, F., and Ponec, V., J. Catal. 82, 1 (1983).

41. Wu, X., Gerstein, B. C., and King, T. S., J. Catal. 121, 271 (1990).

42. De Jong, K. P., Bongenaar-Schlenter, B. E., Meima, G. R., Verkerk, R. C., Lammers, M. J. J., and Geus, J. W., J. Catal. 81, 67 (1983).

43. De Jong, K. P., Meima, G. R., and Geus, J. W., J. Catal. 14, 73 (1982).

44. Sachtler, J. W. A., and Somorjai, G. A., J. Catal. 81, 77 (1983).

45. O'Cinneide, A., and Gault, F. G., J. Catal. 37, 311 (1975).

46. Clarke, J. K. A., Manninger, I., and Baird, T., J. Catal. 54, 230 (1978).

47. Van Der Burg, A., Doornbos, J., Kos, N. J., Ultee, W. J., and Ponec, V., J. Catal. 54, 243 (1978).

48. Clarke, J. K. A., Kane, A. F., and Baird, T., J. Catal. 64, 200 (1980).

49. De Jongste, H. C., and Ponec, V., J. Catal. 64, 228 (1980).

50. Sachdev, A., and Schwank, J., J. Catal. 120, 353 (1989).

51. Balakrishnan, K., Sachdev, A., and Schwank, J., J. Catal. 121, 441 (1990).

52. Bassi, I. W., Lytle, F. W., and Parravano, G., J. Catal. 42, 139 (1976).

53. Cheung, T. T. P., Worthington, L. E., Murphy, P. D. B., and Gerstein, B. C., J. Magn. Reson. 41, 158 (1980).

54. Fry, C. G., Iwamiya, J. H., Apple, T. M., and Gerstein, B. C., J. Magn. Reson. 63, 214 (1985).

55. Stoll, M. E., "A Fast Recovery, Low Noise Receiver-Amplifier for Pulsed NMR Experiments," SAND80-8797 (Sandia National Laboratory, Livermore, Ca., 1980).

56. King, T. S., Goretzke, W. J., and Gerstein, B. C., J. Catal. 107, 583 (1987).

57. Wu, X., Gerstein, B. C., and King, T. S., J. Catal. 118, 238 (1989).

58. Wu, X., Gerstein, B. C., and King, T. S., J. Catal. 123, 43 (1990).

59. Tirendi, C. F., Mills, G. A., and Dybowski, C. R., J. Phys. Chem. 93, 3282 (1989).

SECTION VI

INVESTIGATIONS OF SUPPORTED PT-RE BIMETALLIC CATALYSTS BY HYDROGEN CHEMISORPTION, PROTON NMR, AND CATALYTIC DEHYDROGENATION OF CYCLOHEXANE

INVESTIGATIONS OF SUPPORTED PT-RE BIMETALLIC CATALYSTS BY HYDROGEN CHEMISORPTION, PROTON NMR, AND CATALYTIC DEHYDROGENATION OF CYCLOHEXANE

Xi Wu[1]

Bernard C. Gerstein[2]

Terry S. King[1]

[1]Department of Chemical Engineering and Ames Laboratory

231 Sweeney Hall

Iowa State University

Ames, Iowa 50011

[2]Department of Chemistry and Ames Laboratory

229 Spedding Hall

Iowa State University

Ames, Iowa 50011

ABSTRACT

Prior to ^1H NMR experiments and a reaction study, the reducibility of the $HReO_4$ precursor was first investigated by thermogravimetric analysis. TGA data indicated an incomplete reduction of both Re/SiO_2 and Re/Al_2O_3 catalysts after they were reduced in hydrogen at 400°C. The Pt/SiO_2 and Pt/Al_2O_3 catalysts were fully reduced by hydrogen. The calculated values of the average Re oxidation state from the TGA data indicated a near complete reduction of the $HReO_4$ precursor in the $Pt-Re/SiO_2$ and the $Pt-Re/Al_2O_3$ bimetallic catalysts. Rhenium showed very little hydrogen chemisorption capacity and the small amount of hydrogen adsorbed on Re cannot be detected by ^1H NMR. Hydrogen chemisorption capacity for the Pt catalysts was higher than for Pt-Re bimetallic catalysts. Deuteration of both the silica and the alumina support made possible a clear detection of the strongly bound hydrogen on Pt and Pt-Re surfaces by ^1H NMR. Large NMR lineshift changes for both the strongly and weakly bound hydrogen on platinum were observed with addition of rhenium, indicating alloying and electronic interaction between the two metals. Results from both ^1H NMR and a reaction study clearly showed that the Pt-Re bimetallic catalysts were more active in cyclohexane dehydrogenation than the pure Pt catalysts. This enhanced activity may be a result of less carbon residue deposition on the platinum-rich bimetallic surfaces caused by alloying.

INTRODUCTION

The advantages of alumina supported Pt-Re bimetallic catalysts over P' monometallic catalysts for reforming of the naphtha fraction in petroleum refining were first reported in the late 1960s (1, 2). The greater stability and higher average reformate yield for the Pt-Re/Al_2O_3 compared to the Pt/Al_2O_3 catalysts are certainly beneficial to the production of high-octane gasoline. However, the exact role of rhenium in the Pt-Re bimetallic catalysts is still poorly understood today and remains the subject of considerable debate.

Since the discovery of the Pt-Re/Al_2O_3 bimetallic reforming catalyst, a large number of early studies (3-14) have produced conflicting evidence as to whether in the reduced catalyst the rhenium exists mainly as an alloy with platinum or a reduced or unreduced separate entity. The most notable controversy concerns the valence state of rhenium after hydrogen reduction. Evidence for both zero valence and 4+ state for rhenium has been presented in the literature. Experimental methods include the use of conventional chemical probes, such as temperature program reduction (TPR) (3, 5, 6, 9, 13, 15-18) and hydrogen-oxygen titration (11, 12, 19-22), and advanced instrumental techniques, such as infrared spectroscopy (8, 10, 12, 14) and extended x-ray absorption fine structure (EXAFS) (23-26). The EXAFS technique was also applied to examine the bimetallic Pt-Re/Al_2O_3 catalysts in

the drying and calcination stage of preparation (27-28).

Perrhenic acid $HReO_4$, made by dissolving Re_2O_7 in water, is a common source of Re for catalyst preparation. It has been found that the degree of drying of the high-area alumina support after impregnation has a considerable effect on the reducibility of the Pt-Re/Al_2O_3 catalyst. When the water formed during hydrogen reduction is not removed, rhenium is thermodynamically favored to be reduced only to the 4+ state (3, 4). In very dry systems where the water is continually removed, hydrogen uptake indicates complete reduction of rhenium to the zero valence state in pure Re/Al_2O_3 (5, 6) and Pt-Re/Al_2O_3 (7, 9, 13). However, a recent study (29) by x-ray photoelectron spectroscopy (XPS) showed that rhenium was predominantly reduced to Re(+4) state with hydrogen at 500°C but to Re(0) state when small amounts of water or butane were present in the hydrogen feed.

The phenomenon of platinum-catalyzed reduction of Re has be reported in several studies (7, 13, 15-18). Rhenium is generally reduced at much higher temperatures (about 600°C or higher) than platinum when supported on alumina. However, in the presence of platinum, reduction of rhenium occurs at a lower temperature and is more extensive. Two mechanisms have been proposed to explain the observations. The first involves spillover of H, activated by platinum, onto the alumina support. The spiltover hydrogen diffuses to a Re_2O_7

center and reduces it (16-17). The second mechanism involves migration of the Re_2O_7 oxide to platinum reduction centers, where reduction of the oxide is catalyzed by platinum (13, 15).

TPR results (15, 18) have indicated a strong retarding effect of drying on the reduction of Pt-Re/Al_2O_3 bimetallic catalysts. The mobility of the oxide is influenced by the presence of water; different degrees of hydration of Re_2O_7 results in varying mobility of the oxide. It is concluded that a substantial fraction of Re_2O_7 is still partially hydrated at drying temperatures of 500°C or less and able to migrate to platinum centers to be reduced. Spectroscopic studies (6, 30-35) have suggested that treatment of catalysts at 500°C causes a strong interaction between rhenium oxide and the alumina support. The formation of this rhenium oxide surface complex inhibits the migration of rhenium. Under such a condition, the presence of platinum has no catalytic effect on the reduction of rhenium. On the other hand, water will hydrolyze this surface complex, allowing the rhenium oxide to migrate and be reduced around platinum particles at lower temperatures. Thus, the second reduction mechanism seems to be more reasonable. But a combined mechanism of reduction under a hydration condition is still possible.

A few advanced physical characterization techniques have been used to probe the valence state of rhenium. X-ray

absorption spectroscopy applied to the Re L_{III} edge showed evidence of a mixture of valence states (23-24). Two more recent x-ray absorption studies examined both the same edge and the associated extended fine structure (EXAFS) reported contradictory results. Short et al. (25) concluded that Re is in the 4+ state in the reduced Pt-Re/Al_2O_3 catalysts but Meitzner et al. (26) claimed that essentially all of the Re in the bimetallic catalyst has an oxidation state of zero after reduction in hydrogen at a temperature of 775 K. In a study by both electron spin resonance (ESR) spectroscopy and CO chemisorption, it was shown that both the Re(0) and Re(4+) oxidation state coexist on the surface of reduced Re/Al_2O_3 and Pt-Re/Al_2O_3 catalysts (36). This coexistence of rhenium species with different oxidation states may account for the discrepancy observed with EXAFS.

It is well known that Pt and Re form a miscible alloy when they are bulk metals (37). A recent study by Godbey and Somorjai (38) on metal overlayer growth of Pt on Re(0001) has shown that Pt grows layer by layer in a hcp structure. Also, x-ray photoemission spectra indicated the formation of alloys at the Re-Pt(111) interface. However, whether they still form alloys or bimetallic clusters when highly dispersed in the alumina support is another issue of extensive debate, just as the issue of rhenium valence state. In order to form an alloy or mixed cluster, both elements must be in the zero-

valent state and form a metallic bond.

Evidence of alloy formation has been presented by the results from TPR experiments (13, 18). A shift to lower temperature of hydrogen uptake corresponding to reduction of rhenium was observed in the presence of platinum. But the effect is strongly dependent of the degree of drying prior to hydrogen reduction, as remarked earlier, and may not be a definite indication of alloy formation. Hydrogen-oxygen titration has also provided evidence on Pt-Re interactions. Two recent studies by the same authors (21, 22) have shown that the hydrogen chemisorption capacity is less but the amount of titratable oxygen is more in the Pt-Re/Al_2O_3 bimetallic catalyst than that expected for no interaction between the two metals. Similar findings were reported earlier from another research group using the same technique (19). Direct evidence of a strong interaction between Pt and Re comes from the frequency shifts of chemisorbed CO on both metals with varying Re content as observed by infrared spectroscopy (8). Results from an EXAFS study (26) also suggest significant coordination of rhenium to platinum in bimetallic clusters of the two elements.

On the other hand, evidence against Pt-Re alloying in the alumina supported bimetallic catalysts has also been reported by many investigators. Infrared spectroscopy of adsorbed NO and CO as probe molecules has been applied to

both industrial and laboratory Pt-Re/Al_2O_3 catalysts (10). But no unique spectral features for the bimetallics were found that could not be represented as a combination of features observed for the monometallics. In a study by EXAFS (25), the measured interatomic distances for rhenium showed no bond lengths characteristic of metals, even after 16 hr hydrogen reduction at 758 K. The results from this study indicate that Re is neither zero valent nor significantly associated with Pt. Another study (39) by ion-scattering spectroscopy and scanning transmission electron microscopy also found that Re is widely dispersed on the surface of alumina support and not well associated with Pt. These discrepancies in Pt-Re interactions as reported by the previous researchers cannot be rationalized without some further detailed investigations.

As mentioned earlier, hydrogen spillover upon activation of gaseous hydrogen on platinum surfaces may assist reduction of rhenium oxide. The phenomenon of hydrogen spillover can still exist in a hydrogen environment at ambient temperatures after the catalysts have been completely reduced. Dowden et al. (40) and Barbier et al. (19) have recognized hydrogen spillover in the Pt-Re/Al_2O_3 catalysts and its contribution to errors in the hydrogen chemisorption measurements. The maximum amount of spillover was found at about 50 at.% Re by these researchers. A recent study on the influence of Re on

coke hydrogenation also found hydrogen spillover in the same bimetallic system (41).

Hydrogen is capable of adsorbing on single crystal (42) and polycrystalline Re surfaces (43). Temperature programmed desorption showed second order kinetics for desorption of hydrogen indicating that the adsorbed hydrogen is possibly dissociated on Re surfaces (43). However, the saturation coverage for hydrogen is less than a monolayer on rhenium. On Re/Al_2O_3 catalysts, hydrogen adsorption appears to be an activated process. A study by Freel (44) showed for the first time that the amount of chemisorbed hydrogen increased with increasing chemisorption temperature and that only a trace amount was chemisorbed at room temperature. But the Re/Al_2O_3 catalyst chemisorbed oxygen at room temperature. The low hydrogen chemisorption capacity for Re/Al_2O_3 catalyst has also been reported by some other researchers (19-22).

Godbey et al. (45) have studied ethane hydrogenolysis on Re-Pt(111) and Pt-Re(0001) single crystal surfaces. It was found that rhenium was much more active for this reaction than platinum but surfaces with a surface Re/Pt ratio of about 2:1 exhibit a maximum activity. A Pt(111) surface covered with two or more monolayers of rhenium displayed virtually the same activity as the clean Re(0001) surface. An electronic or ligand effect extending only to the first nearest neighbors was postulated by the authors to explain

the enhanced activity.

Catalytic reaction studies on Pt-Re/Al_2O_3 bimetallic catalysts have also provided valuable insight into the Pt-Re interactions and alloy formation. An early study (46) has revealed quite complex behavior of several reactions on the Pt-Re/Al_2O_3 catalysts. Activity for dehydrogenation of 1,1,3-trimethylcyclohexane declined monotonically with an increase in Re content to a level less than that obtained when the two metals were supported separately. However, catalytic activity in benzene hydrogenation, cyclopentane hydrogenolysis, butane hydrogenolysis, and benzene-deuterium exchange all had a maximum near 70% Re. This behavior was understood as the combination of the monometallic activities with an unknown electronic interaction between the metals. In another study (47), dehydrocyclization of n-hexane was reported to be more active and selective on a Pt-Re/Al_2O_3 catalyst than on a Pt/Al_2O_3 catalyst, probably due to the formation of small Pt-Re bimetallic clusters. Augustine and Sachtler (48) recently reported that the hydrogenolysis of cyclopentane is more active on the Pt-Re/Al_2O_3 bimetallic catalysts than either one of the monometallic catalyst. This was explained by the formation of certain ensembles of atoms containing both platinum and rhenium and the resulting heat of adsorption with reacting intermediates on the bimetallics somewhere in between that on either one of the monometallics.

In other words, the heat of adsorption on the bimetallics causes the reaction to move near the peak of the volcano-shaped curve. A more recent study by Botman et al. (49) presented results for the reaction of 2,2-dimethylbutane (neohexane) on both Pt-Re/Al_2O_3 and Pt-Re/SiO_2 catalysts. Maximum activity was observed at about 70 at.% Re for the two series of catalysts. They believed that rhenium is reduced and forms bimetallic clusters with Pt. They have found that isomerization prevails on both Pt and Pt-rich catalysts while hydrogenolysis is more active on Re and Re-rich catalysts. A comparative study of Pt/Al_2O_3 and Pt-Re/Al_2O_3 catalysts was carried out by Menon and Froment (50). Using a pulse reactor system, they injected n-pentane and n-hexane as reactants and found that various catalyst treatments have a much stronger effect on hydrogenolysis activity of the Pt/Al_2O_3 catalyst than that of the Pt-Re/Al_2O_3 catalyst. They suggested that most of the platinum in the bimetallic catalyst is not in a monometallic state but in close interaction or alloyed with rhenium.

The role of rhenium in Pt-Re/Al_2O_3 bimetallic catalysts for hydrocarbon conversion has been discussed extensively by various researchers (14, 41, 51-57) but is still not well understood. In his original patent (1), Kluksdahl stated that Pt-Re/Al_2O_3 produces an excessive amount of gases caused by a high hydrogenolytic activity which can be diminished by

sulfiding the catalyst with a small amount of sulfur prior to contact with naphtha. Some proposed functions of rhenium include: (a) decrease of coke deposition in the support (53); (b) effect on the extent of hydrogen spillover that may change the selectivity patterns (41); (c) anchoring of Pt particles to prevent sintering (51); (d) strong binding with sulfur species to free platinum sites and induce an ensemble size effect (14); (e) suppressed deposition of carbonaceous species on platinum or conversion of these species into graphite (54-57). The interactions of Re and S with Pt have been claimed to induce geometric and electronic effects (56). Furthermore, the beneficial effect of sulfur and chlorine on the activity maintenance and selectivity has been documented in many publications (58-64). The Pt-Re/Al_2O_3 catalysts have much higher tolerance for chlorine than for sulfur. However, excessive amounts of either of these additives will result in significant deactivation of the catalysts.

Cyclohexane dehydrogenation is one of the five major reactions in catalytic reforming (65). Studies of catalytic dehydrogenation of cyclohexane on the supported Pt and Pt-Re catalysts have been conducted by many researchers (66-69). The reaction is structure insensitive on Pt surfaces (68). Both supported platinum-containing catalysts are very active for this reaction. Activation energies of 16-20 kcal/mole were reported on Pt/Al_2O_3 catalysts at temperatures below

270°C (67-68). Activation energies for Pt-Re/Al_2O_3 catalysts were found to be 24-26 kcal/mole for temperatures above 336°C and 62 kcal/mole for temperatures below 336°C (69). Since rhenium is an active catalyst for hydrogenolysis, a different reaction path to open the cyclohexane ring and further break up the C_6 molecule is possible in addition to dehydrogenation to form benzene. However, this competing reaction seemed to be insignificant compared with the dehydrogenation reaction occurring on Pt-Re/Al_2O_3 bimetallic catalysts.

In the present study, ^1H NMR of chemisorbed hydrogen was applied for the first time to probe the metal surfaces of supported Pt-Re catalysts to elucidate the local electronic environments. The NMR data were interpreted in conjunction with the hydrogen chemisorption data. In addition, ^1H NMR of adsorbed cyclohexane and benzene was used to directly monitor dehydrogenation and hydrogenation reactions on the bimetallic catalysts. The NMR results were correlated with the results of catalytic activity for cyclohexane dehydrogenation from a reaction study employing a laboratory flow micro-reactor. Reducibility of both silica and alumina supported Re and Pt-Re catalysts was examined by thermogravimetric analysis.

EXPERIMENTAL

Catalyst Preparation

The Pt/SiO_2 catalyst was prepared by the ion exchange method using $Pt(NH_3)_4(NO_3)_2$ (Alfa) as the precursor metal salt and Cab-O-Sil HS5 (300 m^2/g) as the support material. The $Pt-Re/SiO_2$ bimetallic catalysts were prepared by the coimpregnation method using $Pt(NH_3)_4(NO_3)_2$ and $HReO_4$ (Alfa, 85% aqueous solution) as the precursors and the same support. The Re/SiO_2 catalyst was prepared by the incipient wetness impregnation method with $HReO_4$ (85% solution) or NH_4ReO_4 salt as the precursor.

About 6 ml of distilled H_2O per gram of SiO_2 was used to dissolve the metal compounds with moderate heating to ensure complete dissolution of the compounds. Then SiO_2 was soaked with the solution and stirred until a slurry was formed. The resulting material was dried for 24 hours at room temperature and 8 hours at 383 K. Two series of bimetallic catalysts were made by holding either the platinum or the rhenium loading constant at 5 wt% and varying the loading of the other metallic element. About 2.5 ml distilled water per gram of SiO_2 was needed for preparation of rhenium catalysts by the standard impregnation method.

A gamma alumina support with a surface area of 186 m^2/g (AESAR) was also used to prepare Pt, Re, and Pt-Re catalysts.

The metal compounds used and the preparation procedures are the same as described above except that 3 ml distilled water per gram of alumina was used. The platinum loading was held constant at 5 wt% with varying rhenium loading for the Pt-Re bimetallic catalysts.

Thermogravimetric Analysis

The reducibility of the Re and Pt-Re catalysts supported on both silica and alumina was examined by thermogravimetric analysis with a Perkin-Elmer TGA 7 thermogravimetric analyzer equipped with a high temperature furnace. About 40 mg of a catalyst sample was loaded into a platinum pan, which was then placed inside the high temperature furnace. Before heating the sample, argon was used to flush the analyzer to remove oxygen from the system. Then, 5 vol.% hydrogen gas diluted in argon with a total flow rate of 45 cm^3/min was allowed to enter the analyzer and pass over the sample pan. The temperature of the furnace was programmed to be raised from 313 K to 1073 K at a rate of 2 K/min. The data were recorded as weight percentage versus temperature.

Catalyst Reduction and Volumetric Adsorption

Catalyst reduction was carried out using a multiport volumetric adsorption apparatus with a high-vacuum system as described previously (70). Reduction by flowing hydrogen

was performed directly inside a Pyrex cell of the adsorption apparatus. Approximately one gram of a catalyst sample was loaded into the flow-through cell, which was then connected to one of the sample ports of the manifold. While helium gas (99.999%) was allowed to flow through the sample bed in the cell at a rate of 100 cm^3/min, the temperature of the cell was raised to 423 K. The cell was kept at that temperature and He flow rate for 30 min to remove excess moisture in the sample. Then He was switched off and replaced by H_2 (99.8%) at a flow rate of 50 cm^3/min. The temperature was then raised at 5 K/min to a final temperature of 673 K. Reduction proceeded for two hours at this final temperature before the cell was allowed to be cooled to the ambient temperature for the adsorption experiments.

Hydrogen for the volumetric adsorption was purified by passing it through a catalytic hydrogen purifier (Engelhard Deoxo) in series with a gas purifier with Drierite and 5 Å molecular sieve (Alltech) to remove traces of oxygen and moisture. Hydrogen adsorption experiments were performed at room temperature (294 ± 1 K). The total hydrogen adsorption isotherm was measured in the pressure range of 0 - 30 Torr. The reversible hydrogen adsorption isotherm was collected under the same conditions after a 10 min evacuation period to 10^{-6} Torr following the total adsorption. The irreversible hydrogen uptake was obtained by taking the difference between

values of the total and the reversible adsorption isotherms extrapolated to zero pressure. An equilibration time of 1 hour was used for the initial dose and 20 min for subsequent doses.

Support Deuteration

Deuteration can effectively reduce the intense resonance associated with the hydroxyl proton in both the silica and the alumina support and hence improve spectral resolution for resonances of interest. Before deuteration, a catalyst was reduced in flowing hydrogen as described earlier. Then the catalyst was soaked in a 26 wt% $ND_3 \cdot D_2O$ solution in D_2O for at least two hours and dried at 383 K. This process was repeated three times. Finally, the catalyst was reduced in flowing deuterium gas for one hour inside an NMR tube before being dosed with hydrogen at liquid nitrogen temperature. To prevent exchange of the adsorbed hydrogen with the OD group in the silica support, the catalyst sample was always evacuated for 10 min to a pressure of 10^{-6} Torr at room temperature after dosing with hydrogen. In some experiments, cyclohexane or benzene with or without gaseous hydrogen was also condensed into the catalyst sample at liquid nitrogen temperature.

Sample Treatment and NMR Experiment

Sample treatment for the NMR experiment was carried out inside a 5-mm NMR tube by either a flow or a static hydrogen reduction method. In the flow reduction, fresh, unreduced catalysts were used, while only previously reduced catalysts were used in the static reduction method. Both methods yield virtually the same results.

Reduction by flowing hydrogen was carried out using a needle-bellows assembly (70). About 60 mg of catalyst sample was loaded inside the NMR tube and He then H_2 gas was allowed to flow through the needle and the catalyst sample. The reduction procedure was essentially the same as previously described for the volumetric adsorption experiment, but with a hydrogen flow rate of 15 cm^3/min. After reduction, the needle was lifted out of the sample, and evacuation proceeded for two hours at reduction temperature before the sample was allowed to cool to ambient temperature.

Reduction by static hydrogen was performed by a repeated cycle of reduction and evacuation. First, the sample inside the NMR tube was heated to the reduction temperature and was dosed with about 100 Torr hydrogen. Then, when the hydrogen consumption or the pressure decrease ceased, the sample was evacuated for about 5 min. The sample was dosed again with hydrogen gas up to 760 Torr and further reduction proceeded for 30 min before another five-minute evacuation. At least

three such cycles were performed on each catalyst for a complete reduction. Finally, the catalyst was evacuated for two hours at the reduction temperature before being cooled to ambient temperature.

Purified hydrogen was then dosed to the catalyst sample and the system was allowed to equilibrate for one hour. The NMR tube containing the sample was then immersed in a water bath and sealed off with a micro-torch. For catalysts dosed with hydrocarbons, the NMR tube containing the sample was first immersed in liquid nitrogen and then an appropriate amount of either cyclohexane or benzene vapor was allowed to condense in the sample tube. In the case of benzene, gaseous hydrogen was also dosed. Finally, the NMR tube was sealed off with the sample still immersed in liquid nitrogen.

The home-built NMR spectrometer (71) used for the NMR experiments was operated at 220 MHz for proton resonance. A proton-free probe with a doubly wound coil (72) was used for all the NMR measurements. The probe quality factor Q was set at about 100 to obtain the optimal values of sensitivity and ring-down time for a fixed pulse power. Description of the spectrometer's rapid-recovery receiving system has been published elsewhere (73).

All NMR spectra were collected under a repetitive 90° single-pulse sequence. For catalyst samples adsorbed with hydrogen, the recycle time between rf pulses was set at 0.2s

to selectively suppress the intense signal associated with protons in the silanol group in the catalyst support, which has a relatively long spin-lattice relaxation time T_1 (on the order of seconds). The above repetition rate avoids T_1 saturation of resonances corresponding to hydrogen adsorbed on pure platinum and platinum-rhenium bimetallics. The total number of scans for data acquisition on each catalyst sample was 10,000. For catalysts adsorbed with either cyclohexane or benzene, a single scan was sufficient to obtained the NMR spectra. A pure water sample was used as the reference standard for the observed lineshifts. All NMR measurements were taken at ambient temperature.

Reaction Study

The catalytic activity of one Pt/SiO_2 catalyst and three $Pt-Re/SiO_2$ bimetallic catalysts with a constant 5% Pt loading and varying rhenium loadings was tested for the reaction of cyclohexane dehydrogenation using a laboratory differential tubular micro-reactor described elsewhere (74). A catalyst powder sample (5-30 mg) was diluted with (100-200 mesh) crystalline silica to a volume of 3.0 cm^3 and placed in the isothermal region of the tubular reactor. Prior to reaction, the catalyst was reduced for two hours inside the reactor in flowing hydrogen at a flow rate of 200 cm^3/min at a reduction temperature of 673 K. The reactor was then allowed to cool

to the desired reaction temperature (523-573 K). After reduction, cyclohexane (Aldrich, HPLC grade) in the form of liquid was pumped into the reactor system at a feed rate of 0.1 ml/min by a high precision HPLC solvent delivery system (Kratos, Spectroflow 400). The cyclohexane feed was first vaporized by heating the feed line with heating tapes to a temperature of 413 K . A hydrogen-to-cyclohexane molar ratio of 9 to 1 and a total pressure of 1 atm was maintained during measurements of activation energy. The volumetric space velocity inside the reactor was around 4,000 hr^{-1} (STP) for all the runs. The total conversion was maintained below 10% to ensure isothermal condition inside the catalyst bed. The product line was also heated with heating tapes to prevent condensation of effluents from the reactor.

The composition of the reaction products were analyzed by a flame ionization detector (FID) in a Varian 3700 gas chromatograph. The product stream was introduced via an automatic sampling valve (Valco) into a glass capillary column (60 meter in length and 0.75 mm in diameter) that is coated with polymethylsiloxane (Alltech) and placed inside the gas chromatograph. Upon sampling, the column oven was held at 348 K for 2 min and the temperature was raised at 25 K/min to a temperature of 398 K. Commercial software on an IBM personal computer was used for automatic data acquisition and analysis of the FID signals.

RESULTS

Thermogravimetric Analysis

The reducibility of the Re precursor compounds $HReO_4$ (aqueous solution) and NH_4ReO_4 (powder) was examined by TGA in an argon-diluted hydrogen environment. As shown in Figure 1, the TGA curve for the NH_4ReO_4 compound displayed a sharp weight loss in the temperature range from 180°C to 230°C and no change in weight from 230°C up to 800°C. The percentage of sample weight in the constant region is at 69.9% of the initial weight. For the $HReO_4$ precursor, a sharp weight loss occurred at the beginning of the experiment due to loss of water vapor from the aqueous solution. In the temperature range from 120°C to 200°C, two distinct stages of weight loss were clearly observed. The first one occurred between 120°C and 160°C and the second one between 160°C and 200°C. The sample weight remained unchanged from 200°C up to 800°C at 44.7% of the initial weight.

Figure 2 compares two TGA curves obtained from the same 5% Re/SiO_2 catalyst (prepared with NH_4ReO_4) in Ar only and in a H_2/Ar gas mixture. The initial weight loss in both cases was due to loss of moisture from the catalysts. Under Ar alone, sample weight loss was observed from about 100°C to 180°C and only a gradual loss afterward. However, when hydrogen was present, a more significant loss of sample

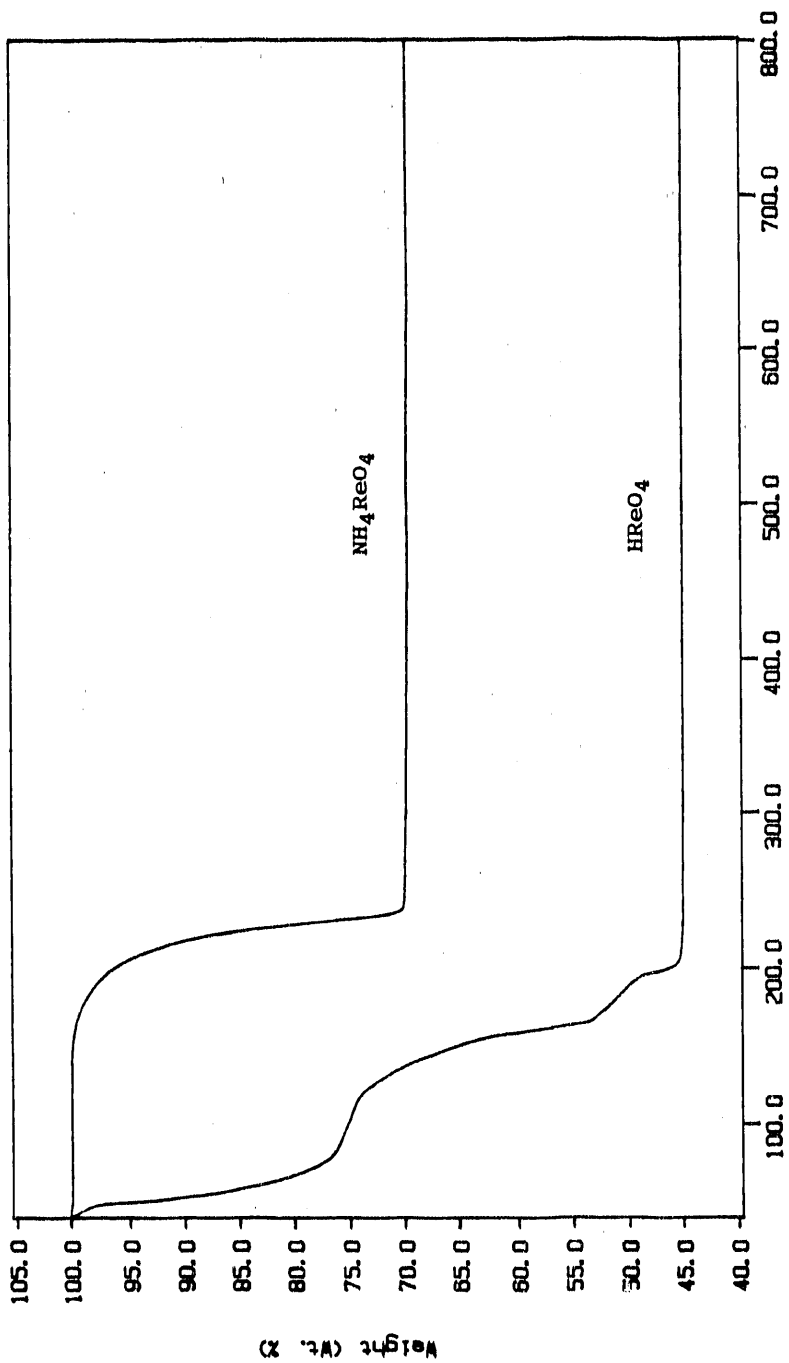

Figure 1. TGA data showing weight percent versus temperature for catalyst precursor compounds NH_4ReO_4 and $HReO_4$ (aqueous solution). The initial sample weight was used as the basis for weight percentage

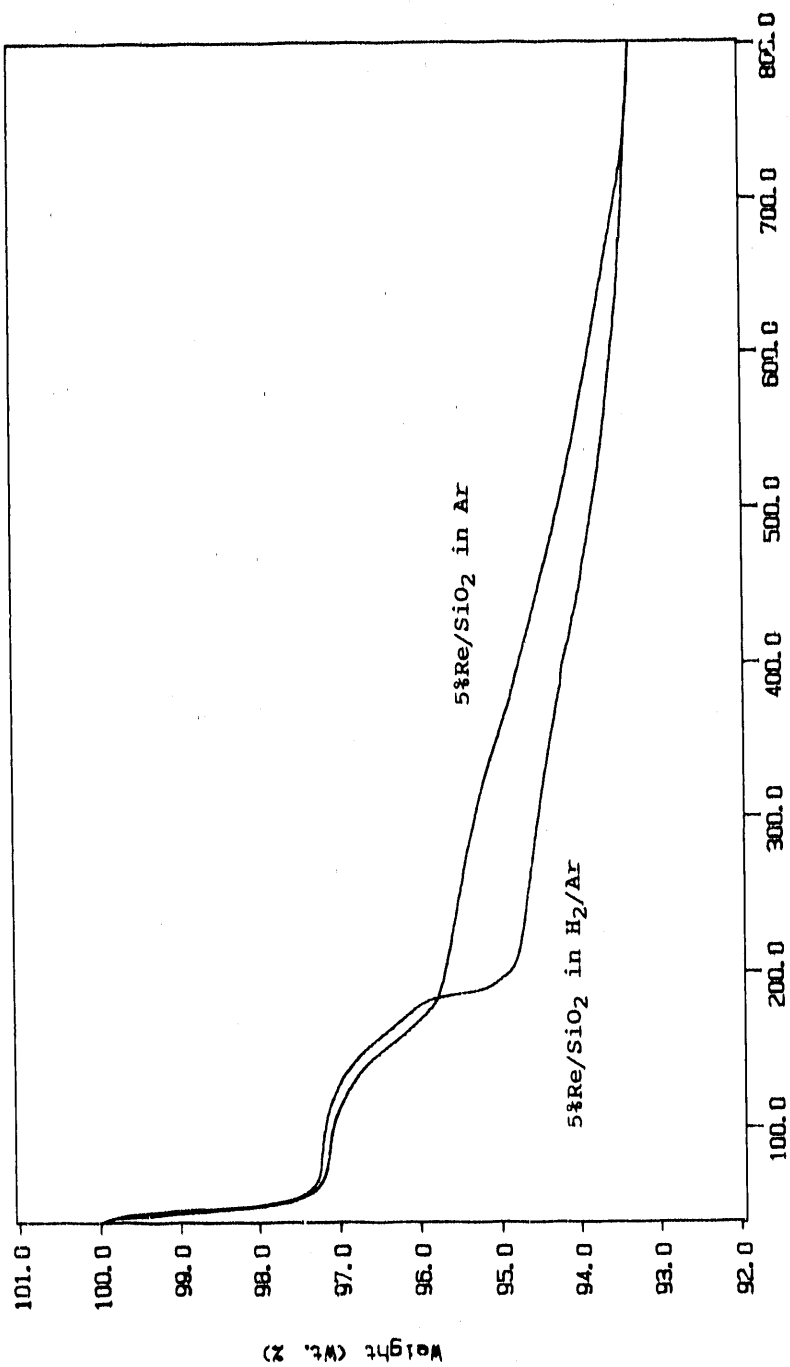

Figure 2. TGA data showing weight percent versus temperature for a 5% Re/SiO_2 catalyst. The catalyst precursor was NH_4ReO_4. Data obtained under Ar and H_2/Ar gas mixture are shown

weight occurred from 100°C to 190°C in two stages, with a sharp weight decrease between 180°C and 190°C. After 190°C, the weight loss became more gradual than under Ar alone and the two TGA curves merged into one after 750°C.

In Figure 3, two TGA curves are shown for a 5% Re/SiO_2 catalyst (prepared with $HReO_4$) under flowing Ar and H_2/Ar gas mixture, respectively. The initial weight decrease was due to loss of moisture from the catalysts. Under Ar alone, no distinct loss of weight due to decomposition of the catalyst precursor was observed after about 65°C. The weight decrease was very gradual between 65°C to 800°C. Under the H_2/Ar gas mixture, however, a rapid weight decrease occurred in the temperature range between 100°C and 140°C, with a mild trend of weight decrease after 140°C. Obviously, the weight loss was greater in the presence of hydrogen.

The TGA curves for a 5% Pt/SiO_2 and a 5% Pt-5% Re/SiO_2 catalyst are shown in Figure 4. Both samples were monitored under a flowing mixture of H_2/Ar. Again, the initial weight loss was due to evaporation of moisture from the catalysts. The subsequent weight loss occurred between 100°C and 170°C for the 5% Pt/SiO_2 catalyst and between 100°C and 220°C for the 5% Pt-5% Re/SiO_2 catalyst. The TGA curve for the 5% Pt/SiO_2 catalyst seemed to consist of two close stages with slightly different rates of weight decrease. For the 5% Pt-5% Re/SiO_2 catalyst, two distinct stages of weight loss were

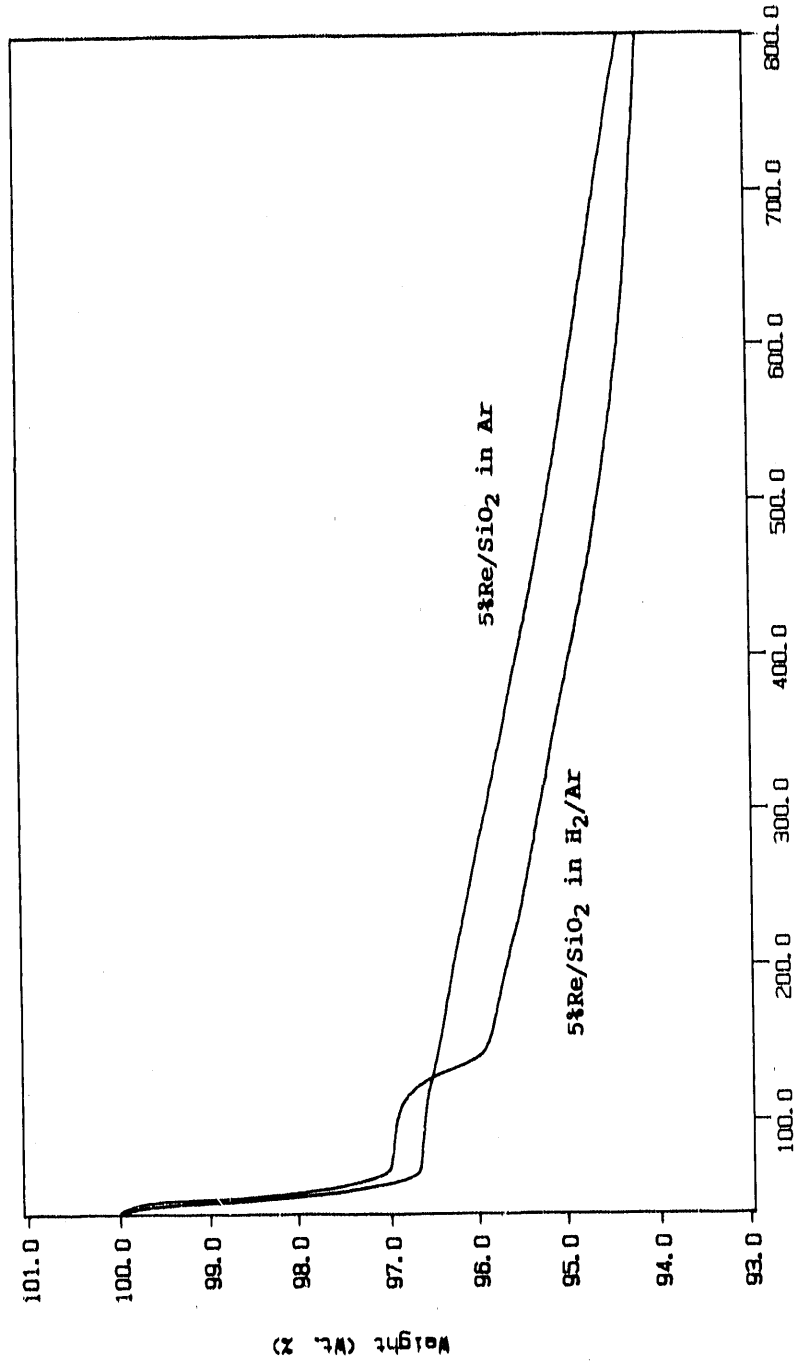

Figure 3. TGA data showing weight percent versus temperature for a 5% Re/SiO_2 catalyst. The catalyst precursor was $HReO_4$. Data obtained under both Ar and H_2/Ar gas mixture are shown

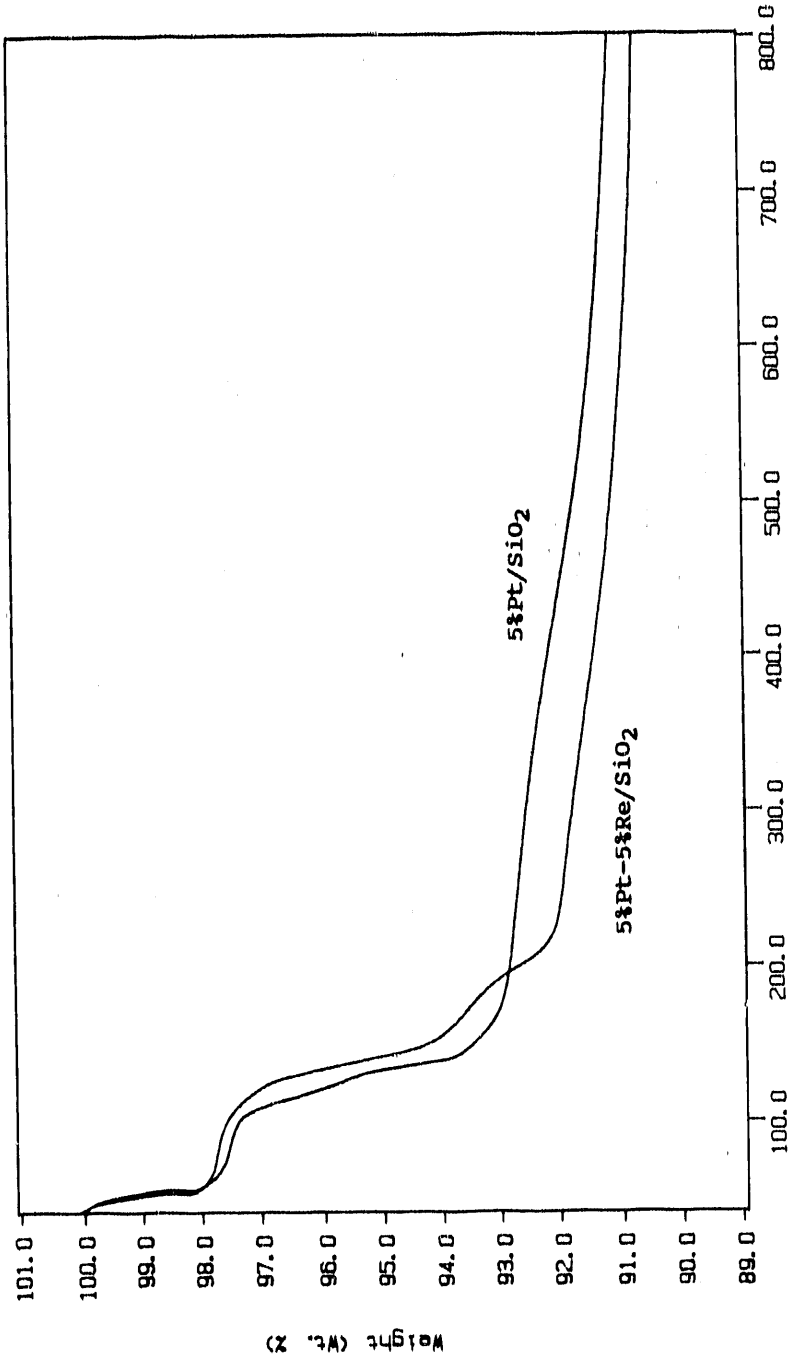

Figure 4. TGA data showing weight percent versus temperature for a 5% Pt/SiO_2 and a 5% Pt-5% Re/SiO_2 catalyst. The catalyst label is indicated in the figure

observed from the TGA curve. After 220°C, the trend for the weight loss was gradual and similar for both catalysts. As one might expect, there was a greater weight loss for the 5% Pt-5% Re/SiO_2 catalyst than for the 5% Pt/SiO_2 catalyst.

Two TGA curves obtained on the same 5% Re/Al_2O_3 catalyst in Ar alone and in a H_2/Ar gas mixture are shown in Figure 5. Strikingly different results were observed under these two conditions. Initially, both TGA curves showed a smooth and gradual weight loss characteristic of the alumina support. This smooth trend continued under the condition of Ar only until a temperature of 755°C, where a sharp loss of sample weight occurred. No further weight loss was observed up to 900°C. However, under the condition of a H_2/Ar mixture, the sample began to lose weight rapidly at about 210°C with only a gradual weight loss after 220°C.

Figure 6 shows two TGA curves for a 5% Pt/Al_2O_3 catalyst and a 5% Pt-5% Re/Al_2O_3 catalyst obtained in a flowing H_2/Ar mixture. The trend for weight loss was identical initially, but the two TGA curves split at about 70°C. They followed quite a different trend between 100°C and 150°C. For the 5% Pt/Al_2O_3 catalyst, two distinct stages of weight loss were observed at about 100°C and 138°C. For the 5% Pt-5% Re/Al_2O_3 catalyst, only one stage of weight loss was observed at about 127°C. At temperatures higher than 150°C, both TGA curves followed basically the same trend. As expected, the overall

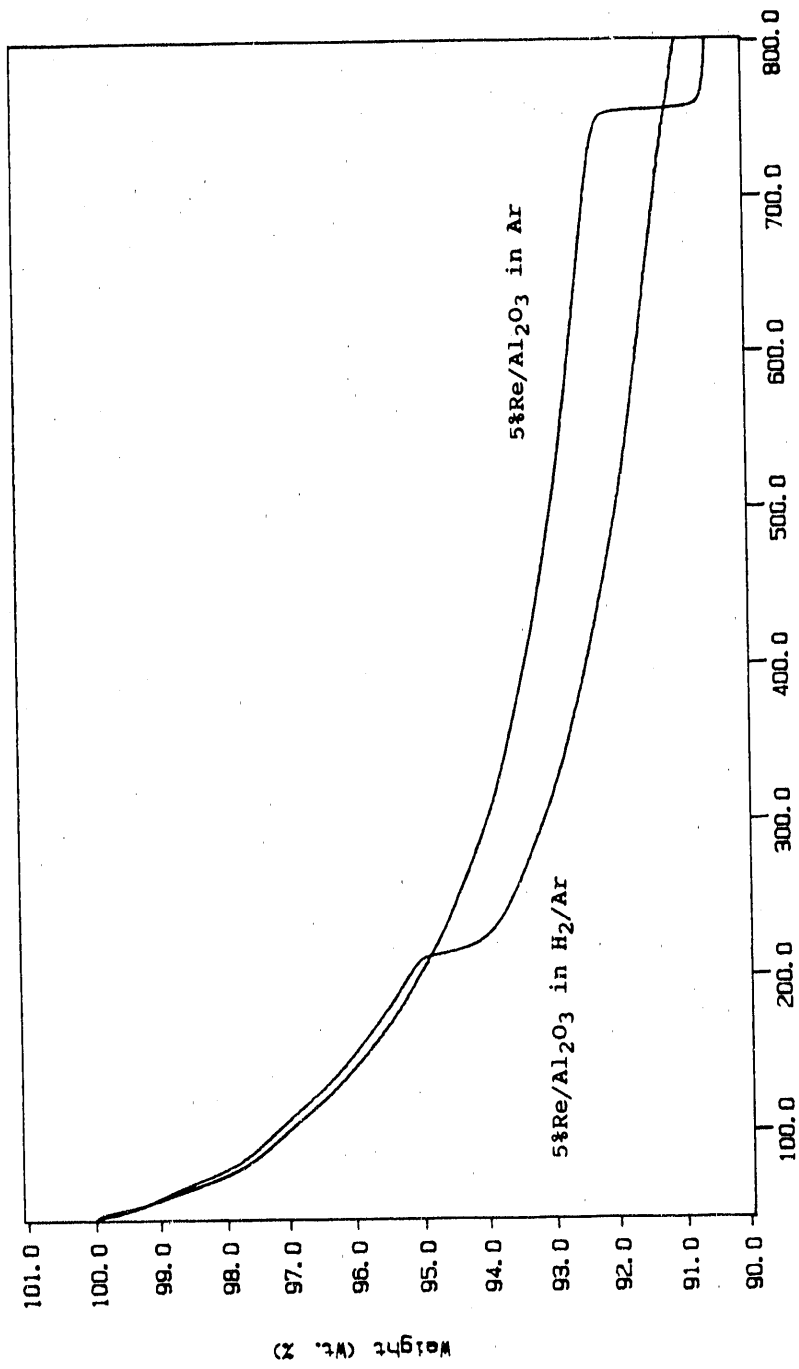

Figure 5. TGA data showing weight percent versus temperature for a 5% Re/Al_2O_3 catalyst. Data obtained under Ar only and H_2/Ar gas mixture are shown

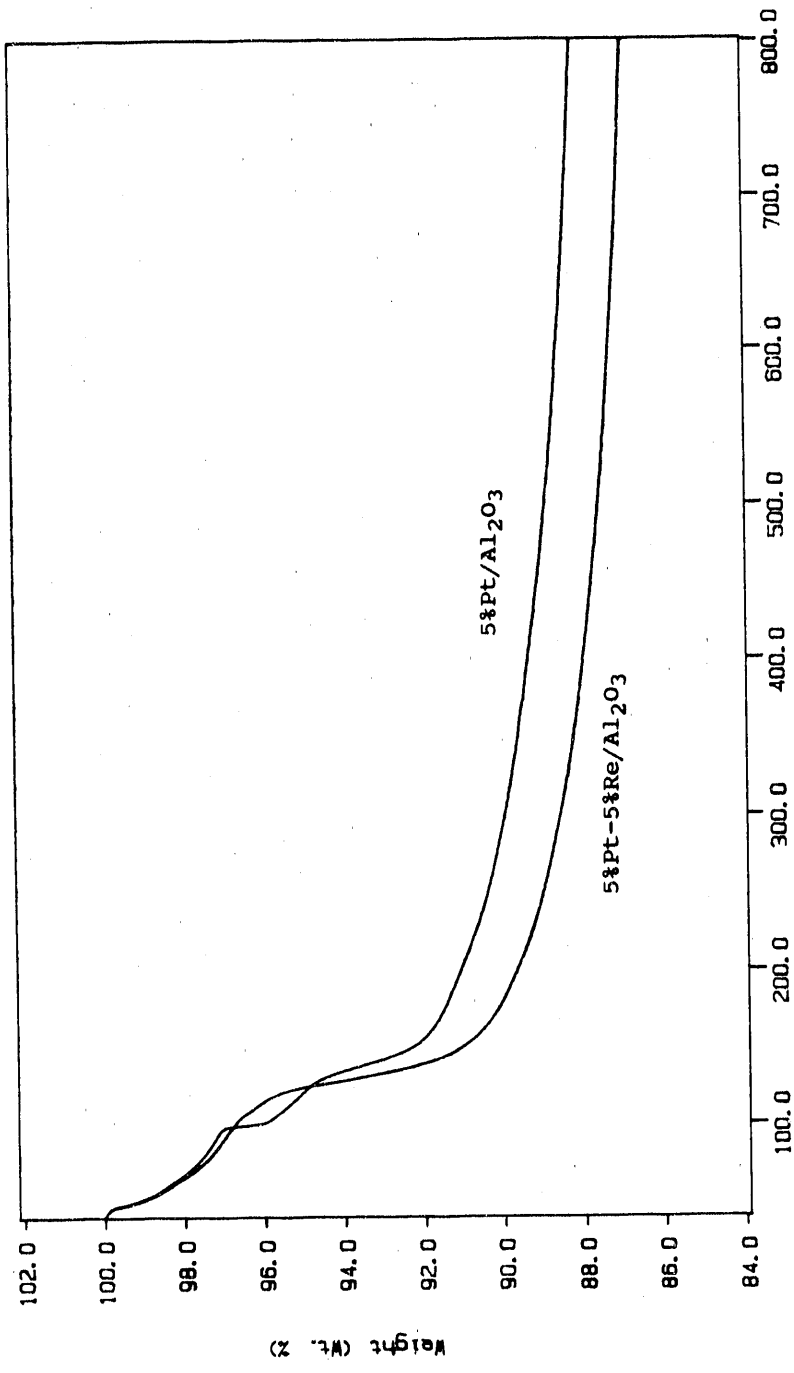

Figure 6. TGA data showing weight percent versus temperature for both a 5% Pt/Al_2O_3 and a 5% Pt-5% Re/Al_2O_3 catalyst. The catalyst label is indicated in the figure

weight loss for the 5% Pt-5% Re/Al_2O_3 catalyst was more than that for the 5% Pt/Al_2O_3 catalyst.

Hydrogen Chemisorption

Volumetric chemisorption data for a 5% Pt-5% Re/SiO_2 and a 1% Pt-5% Re/SiO_2 catalyst are shown in Figure 7 as H/Pt ratios versus hydrogen pressure. Both the total and the weak hydrogen adsorption isotherms were plotted for these two catalysts. As can be seen, all adsorption isotherms are near straight lines in the pressure range from 10 to 30 Torr, and the amounts of hydrogen adsorption increased only moderately with increasing hydrogen pressure. The H/Pt ratio for the total adsorption on the 5% Pt-5% Re/SiO_2 catalyst was 0.32, and that on the 1% Pt-5% Re/SiO_2 catalyst was 0.40, as taken by extrapolating the isotherms to zero hydrogen pressure. The reversible H/Pt ratios for the two catalysts were about the same at 0.10. The irreversible H/Pt ratio can readily be obtained by taking the difference between these two H/Pt ratios.

The adsorption isotherms for a 5% Pt/Al_2O_3 and a 5% Pt-5% Re/Al_2O_3 catalyst are shown in Figure 8 as H/Pt ratios versus hydrogen pressure. For the 5% Pt/Al_2O_3 catalyst, both the total and the reversible adsorption isotherms were straight lines in the hydrogen pressure range from 3 to 25 Torr. Portions of the isotherms below 3 Torr were curved

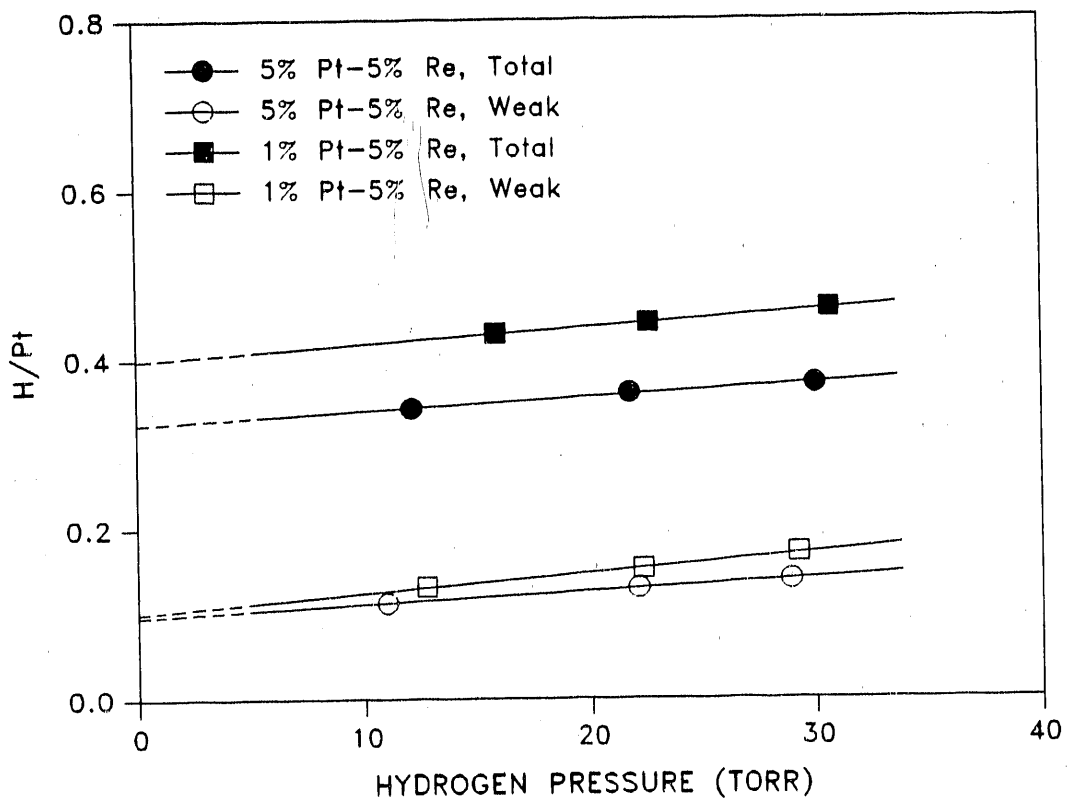

Figure 7. Hydrogen chemisorption isotherms for a 5% Pt-5% Re/SiO_2 and a 1% Pt-5% Re/SiO_2 catalyst prepared by coimpregnation method. Both the total and the reversible isotherms are shown in the figure

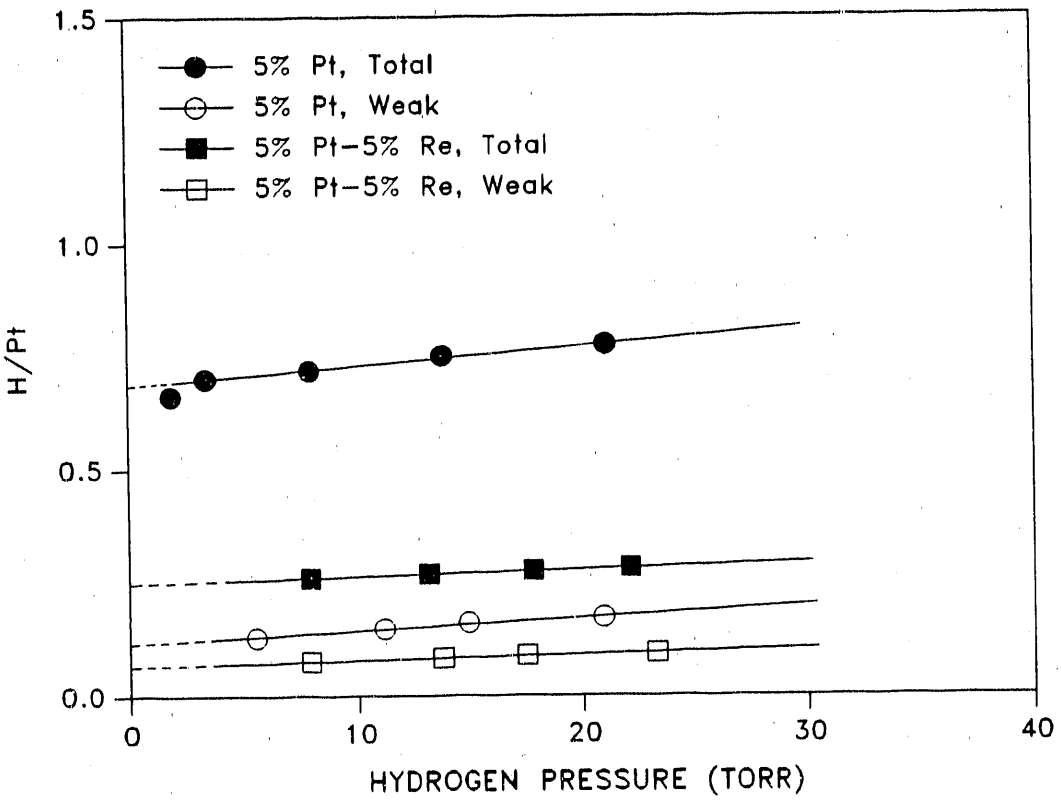

Figure 8. Hydrogen chemisorption isotherms for a 5% Pt/Al_2O_3 and a 5% Pt-5% Re/Al_2O_3 catalyst. Both the total and the reversible isotherms are shown in the same figure

downward due to kinetic limitations at these low pressures. Only the linear portion of the isotherms were extrapolated to zero hydrogen pressure to obtain the H/Pt ratio. Similar features for the adsorption isotherms were found on the 5% Pt-5% Re/Al_2O_3 catalyst. But the slopes of the isotherms were smaller than those of the 5% Pt/Al_2O_3 catalyst. This indicates less pressure dependency of hydrogen adsorption for the bimetallic catalyst. It is interesting to note that the alumina supported catalysts exhibited a stronger dependency of hydrogen adsorption on the hydrogen pressure than the silica-supported catalysts.

Chemisorption data for the total, the reversible, and the irreversible hydrogen adsorption are shown in Table 1 for one Pt/SiO_2, one Re/SiO_2, and six Pt-Re/SiO_2 catalysts. As clearly indicated, the Pt/SiO_2 catalyst has the highest H/Pt ratios while the Re/SiO_2 catalyst has the lowest H/Pt ratios. This observed low hydrogen chemisorption capacity is in good agreement with previously reported results (19-22, 44). The Re/SiO_2 catalyst did adsorb considerable amount of oxygen (O/Re = 0.083), but the amount was less than those reported by other researchers.

The amounts of hydrogen adsorption for the bimetallic catalysts were roughly half the amount for the pure Pt/SiO_2 catalyst. Bimetallic catalysts with lower Pt or Re loading showed slightly higher hydrogen chemisorption capacity, as

Table 1. Hydrogen chemisorption results for silica-supported Pt, Re, and Pt-Re catalysts

Catalyst	Total H/Pt	Weak H/Pt	Strong H/Pt
5% Pt	0.657	0.113	0.544
5% Pt-1% Re	0.374	0.094	0.280
5% Pt-3% Re	0.372	0.105	0.267
5% Pt-5% Re	0.323	0.096	0.227
1% Pt-5% Re	0.398	0.101	0.297
3% Pt-5% Re	0.311	0.097	0.214
7% Pt-5% Re	0.230	0.070	0.160
5% Re[a]	0.020	0.004	0.016

[a]Values represent the H/Re ratio.

one might expect that they have a smaller average metal particle size. For a constant Re loading of 5 wt%, the H/Pt ratio increased noticeably from 7% Pt to 1% Pt. However, at a constant Pt loading at 5 wt%, the H/Pt ratio remained almost unchanged with varying Re loading. Alternatively, one may wish to express the hydrogen chemisorption capacity for the bimetallics in the H/M ratio, where M includes both Pt and Re. Then, the values for the H/M ratios will be much smaller than the H/Pt ratios, and the results will not be as

Table 2. Hydrogen adsorption results for alumina supported Pt and Pt-Re catalysts

Catalyst	Total H/Pt	Weak H/Pt	Strong H/Pt
5% Pt	0.686	0.115	0.571
5% Pt-1% Re	0.429	0.094	0.335
5% Pt-5% Re	0.247	0.065	0.182

meaningful since the platinum-rich catalysts have much higher H/M ratios than the rhenium-rich catalysts for the same total metal loadings.

The hydrogen chemisorption results for one Pt/Al_2O_3 and two $Pt\text{-}Re/SiO_2$ catalysts are shown in Table 2 with all values expressed as H/Pt ratios. The data clearly indicated a much higher chemisorption capacity for the pure Pt/Al_2O_3 catalyst than for the bimetallic catalysts. All the H/Pt ratios decreased with an increase in the total metal loading as expected from an increase in the average metal particle size. Compared with silica-supported catalysts with the same metal loadings, the 5% Pt/Al_2O_3 catalyst and the 5% Pt-1% Re/Al_2O_3 catalyst showed slightly higher H/Pt ratios while the 5% Pt-5% Re/Al_2O_3 catalyst indicated a slightly lower H/Pt ratio.

NMR of Adsorbed Hydrogen

A set of ^1H NMR spectra for a 5% Re/SiO_2 catalyst and four $Pt-Re/SiO_2$ catalysts with a constant 5% Re loading and varying Pt loadings are shown in Figure 9. All catalysts were dosed with 5 Torr hydrogen. On the 5% Re/SiO_2 catalyst, only one resonance was observed at about 3 ppm corresponding to the silanol proton in the silica support. However, on all the bimetallic catalysts, a second resonance appeared as a shoulder peak downfield to the intense silanol peak. There was also a broad feature underneath the silanol peak. The lineshift for the downfield peak moved in the direction of upfield from -29.3 ppm to -18.8 ppm as the platinum loading increased from 1% to 7%. For the 1% Pt-5% Re/SiO_2 and the 3% Pt-5% Re/SiO_2 catalyst, the downfield peak appeared as a sharp and narrow resonance with a linewidth of about 1.7 kHz. As the platinum loading was further increased, the downfield peak became broader and appeared as a shoulder to the silanol peak.

Figure 10 shows ^1H NMR spectra for the same bimetallic catalysts already shown in the previous figure but under a different condition of hydrogen adsorption. The catalysts were first dosed with 5 Torr hydrogen and then evacuated to a pressure of 10^{-6} Torr for 10 min. In this case, the weakly bound hydrogen was removed by evacuation. As can be seen in Figure 10, the downfield peak was markedly attenuated by

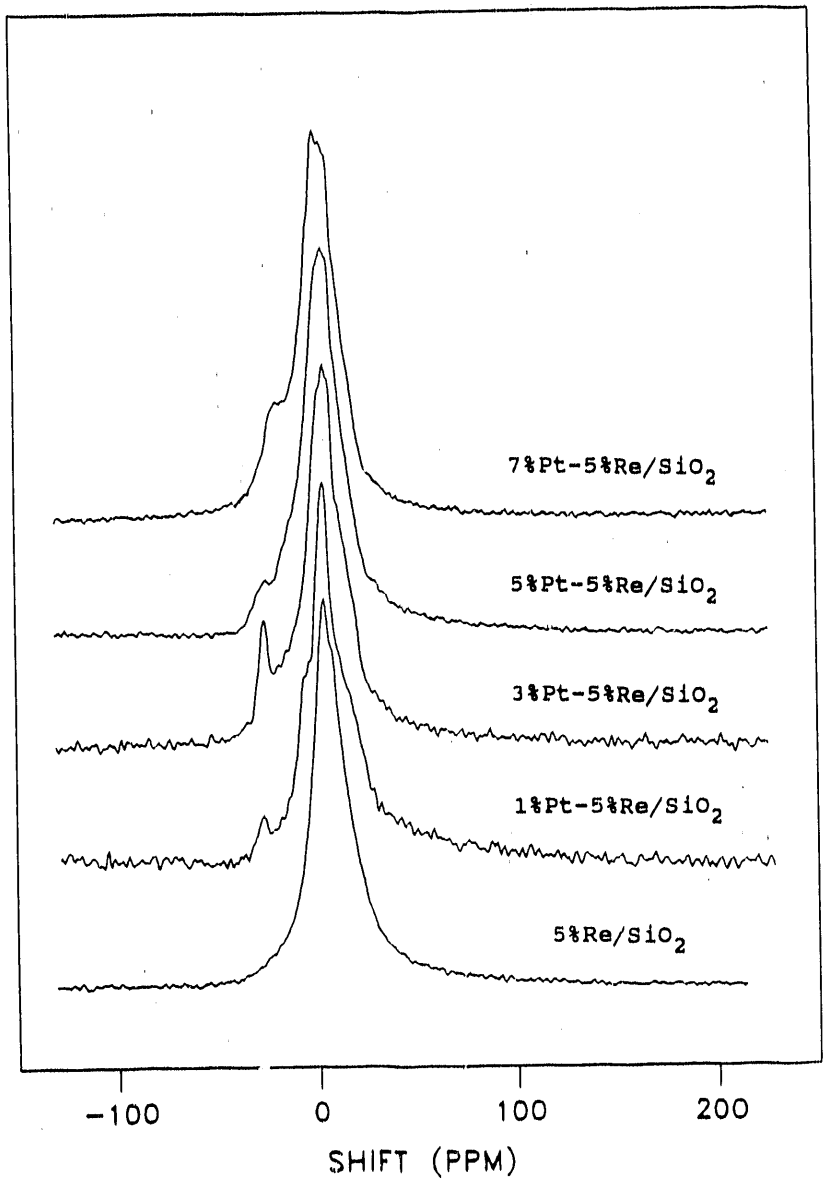

Figure 9. ^{1}H NMR spectra on a series of Pt-Re/SiO_2 catalysts under 5 Torr hydrogen. The rhenium loading was kept at 5% and the platinum loading varied from 0% to 7%. Each catalyst label is shown in the figure for the corresponding NMR spectrum

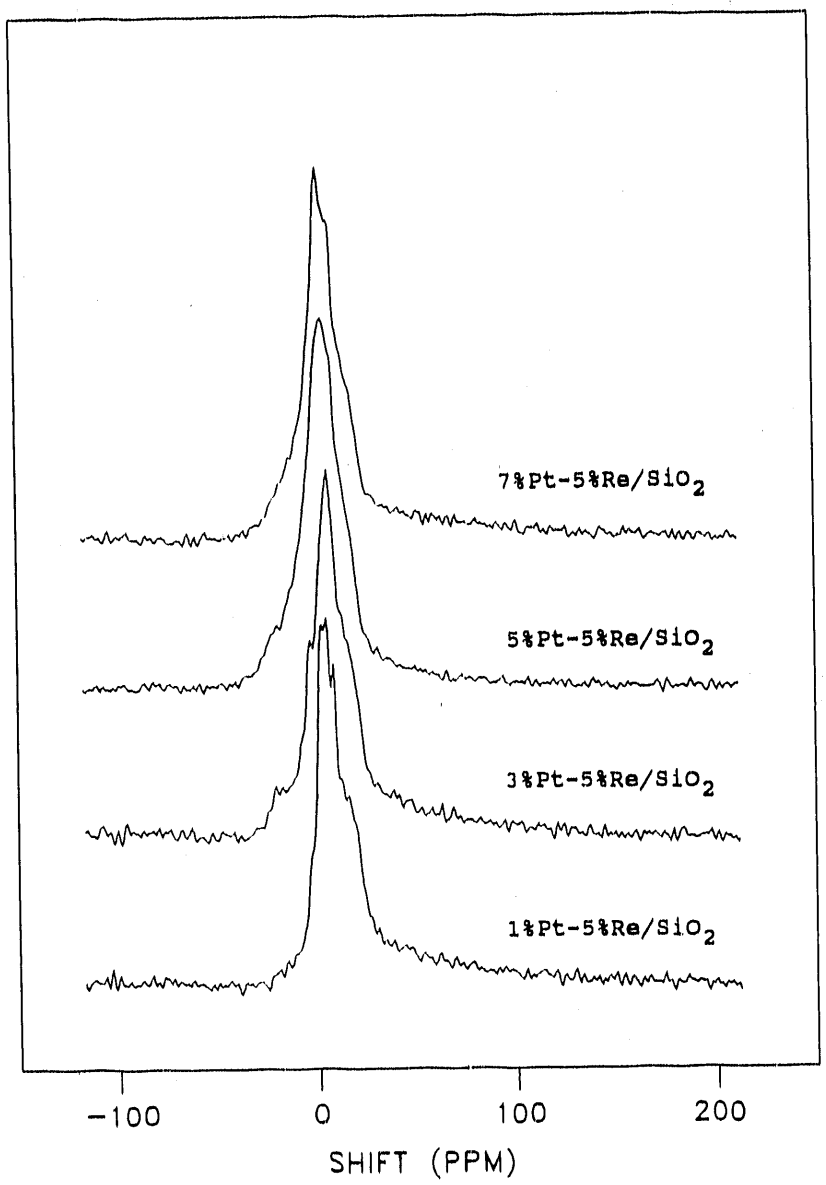

Figure 10. ^{1}H NMR spectra on a set of Pt-Re/SiO_2 catalysts under evacuation condition following adsorption with 5 Torr hydrogen. The rhenium loading was kept at 5% and the platinum loading varied from 1% to 7%. Each catalyst label is shown in the figure for the corresponding NMR spectrum

evacuation, but the broad feature under the silanol peak remained. In addition, a shoulder peak appeared upfield to the silanol peak in all the spectra.

Another set of ^1H NMR spectra are shown in Figure 11 for one 5% Pt/SiO_2 and three $Pt-Re/SiO_2$ catalysts with a constant 5% Pt loading and different Re loadings. All catalysts were dosed with 5 Torr hydrogen. For the 5% Pt/SiO_2 and the 5% Pt-1% Re/SiO_2 catalyst, the hydrogen-on-metal resonance was obscured entirely by the intense silanol peak. However, as will be seen later for a deuterated sample, the hydrogen-on-platinum peak should appear upfield to the silanol peak. For the 5% Pt-3% Re/SiO_2 and the 5% Pt-5% Re/SiO_2 catalyst, a downfield resonance was observed at -17.5 ppm and -18.8 ppm, respectively. It appeared that the hydrogen-on-metal peak was shifted from upfield to downfield relative to the silanol peak as the rhenium loading in the Pt-Re bimetallic catalyst was increased from 0% to 5%.

For the same Pt/SiO_2 and $Pt-Re/SiO_2$ catalysts shown in Figure 11, evacuation after adsorption in 5 Torr hydrogen produced the ^1H NMR spectra shown in Figure 12. Compared with Figure 11, the previously observed downfield peak was absent in all the spectra. Similar to what was observed in Figure 10, an upfield shoulder peak appeared near the silanol peak in most of the spectra under the evacuation condition. The feature was most pronounced on the 5% Pt/SiO_2 catalyst.

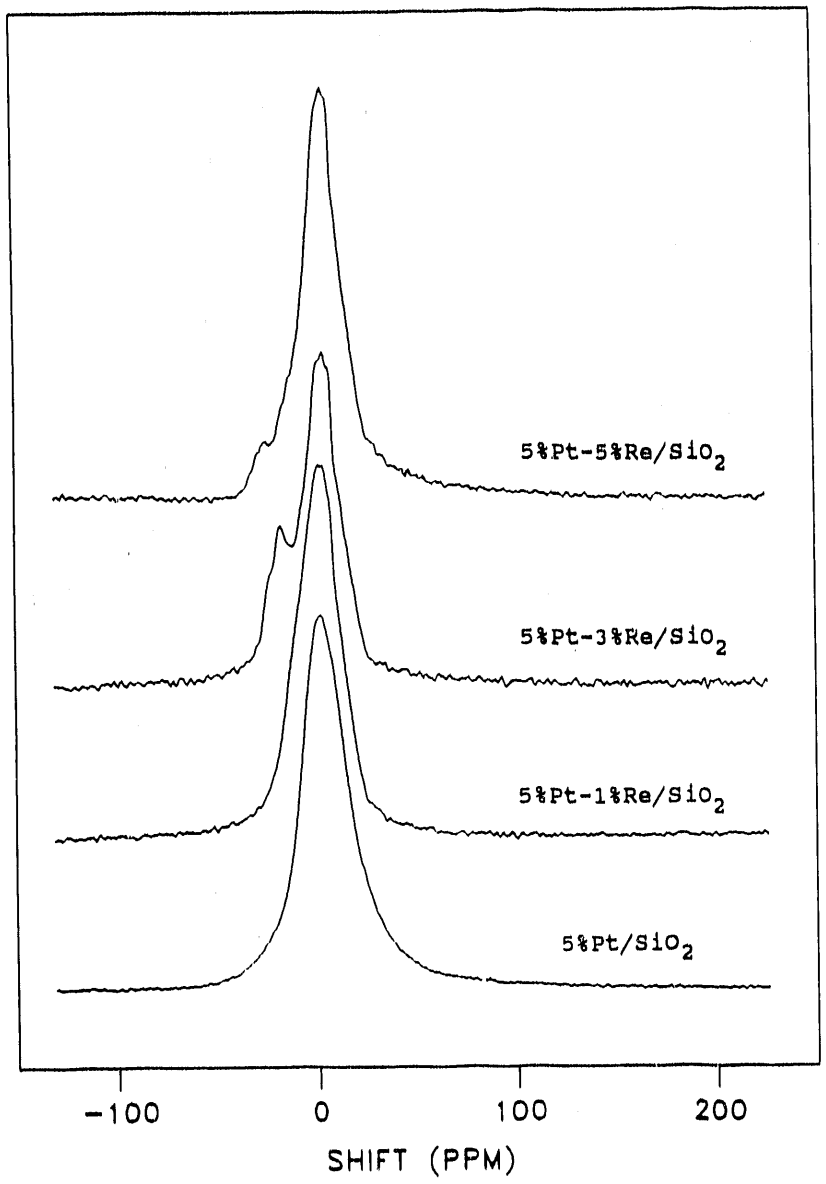

Figure 11. ^{1}H NMR spectra obtained on a series of Pt-Re/SiO_2 catalysts under 5 Torr hydrogen. The platinum loading was kept at 5% and the rhenium loading varied from 0% to 5%. The catalyst label appears in the figure for the corresponding NMR spectrum

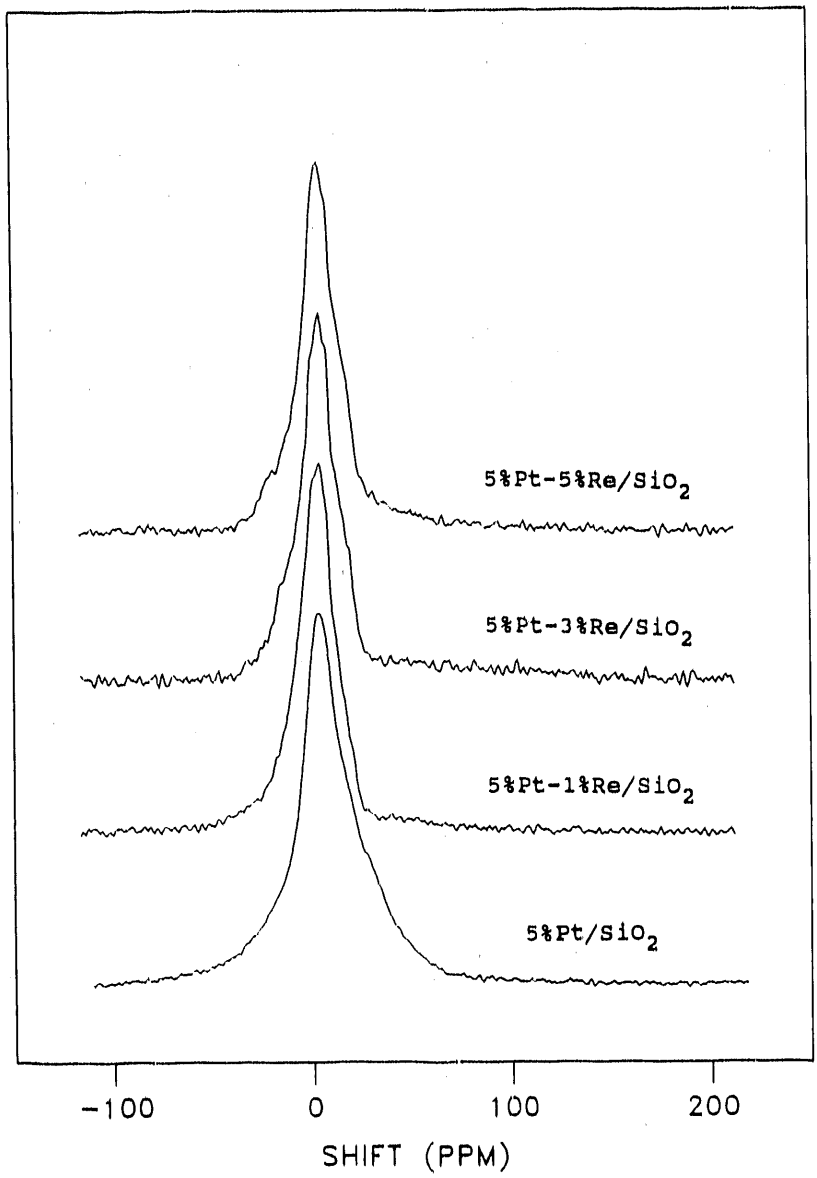

Figure 12. ^{1}H NMR spectra obtained on a series of Pt-Re/SiO_2 catalysts under an evacuation condition following adsorption under 5 Torr hydrogen. The platinum loading was kept at 5% and the rhenium loading varied from 0% to 5%. The catalyst label appears in the figure for the corresponding NMR spectrum

Deuteration of the silica support was carried out on the same 5% Pt/SiO_2 and 5% Pt-5% Re/SiO_2 catalysts as described earlier. Figure 13 shows the ^1H NMR spectra on these two catalysts after adsorption and then evacuation to leave only the irreversibly bound hydrogen. In both cases, the silanol intensity was reduced significantly and the hydrogen-on-metal resonances could be clearly observed. It is interesting to note that deuteration not only reduced the NMR resonance intensity from the silanol proton but also made the silanol peak much narrower. The observed linewidth of 2 kHz for the silanol resonance was about 2 kHz narrower than that of an undeuterated catalyst. For the 5% Pt/SiO_2 catalyst, the upfield peak was well separated from the silanol peak, and the lineshift for this peak was at 33 ppm with a linewidth of about 7.5 kHz. This resonance was assigned to the strongly bound hydrogen on Pt. For the 5% Pt-5% Re/SiO_2 catalyst, the observed upfield peak appeared as a pronounced shoulder peak next to the silanol peak, and its lineshift was at about 19 ppm. This resonance may be assigned to the strongly bound hydrogen on the Pt-Re bimetallic surfaces.

The lineshift values for the downfield peak shown in both Figure 9 and Figure 11 are tabulated in Table 3 as a function of Re atomic percent. Obviously, a larger upfield shift was seen on the bimetallic catalyst with a lower bulk rhenium composition and a more downfield shift on ones with

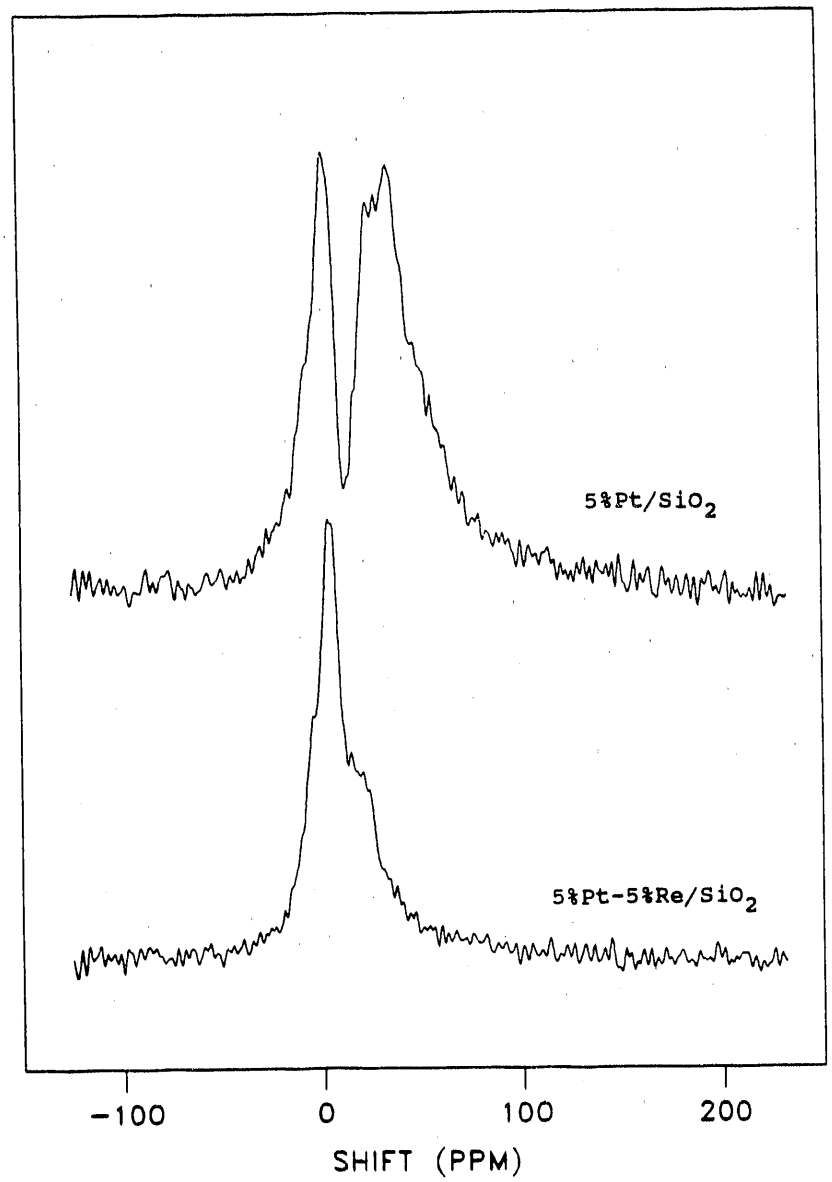

Figure 13. ^{1}H NMR spectra on a 5% Pt/SiO_2 and a 5% Pt-5% Re/SiO_2 catalyst under an evacuation condition following adsorption under 5 Torr hydrogen. The silica support in both catalysts was deuterated prior to hydrogen adsorption

Table 3. NMR lineshift values for the downfield peak on $Pt-Re/SiO_2$ bimetallic catalysts

Catalyst	Atomic % Re	Shift (ppm)
5% Pt-3% Re	38.6	-17.5
7% Pt-5% Re	42.8	-18.8
5% Pt-5% Re	51.2	-24.6
3% Pt-5% Re	63.6	-26.0
1% Pt-5% Re	84.0	-29.3

higher bulk rhenium composition. The change in the downfield peak lineshift was rather significant, a total of almost 12 ppm between bulk compositions of 39 at.% and 84 at.% rhenium.

A set of ^1H NMR spectra are shown in Figure 14 for one Pt/Al_2O_3 and two $Pt-Re/Al_2O_3$ catalysts under the adsorption condition of 5 Torr hydrogen. Resonances in all three NMR spectra exhibited excessive line broadening with resonance linewidths as wide as 17 kHz. For the 5% Pt/Al_2O_3 catalyst, the resonance was a broad Lorentzian-like line. For the bimetallic catalysts, some broad features appeared upfield of the resonance assigned with the hydroxyl proton in the Al_2O_3 support. This excessive line broadening may be in part due to the high iron content in the alumina support. Atomic

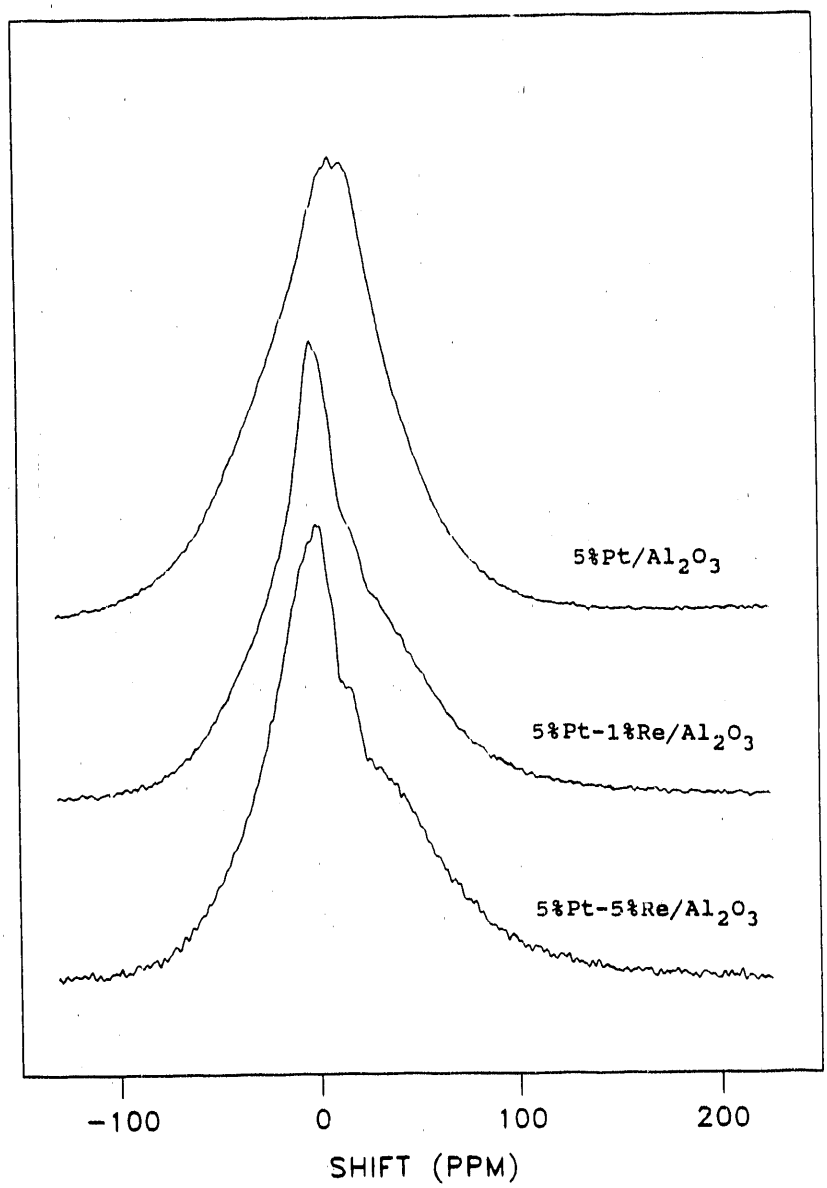

Figure 14. ^{1}H NMR spectra obtained on one Pt/Al_2O_3 and three $Pt\text{-}Re/Al_2O_3$ catalysts under 5 Torr hydrogen. The catalyst label is shown in the figure for the corresponding NMR spectrum

absorption analysis of an alumina sample indicated an iron content of 114 ppm. Under these circumstances, it is very difficult to extract any useful information from the NMR spectra.

Figure 15 displays two ^{1}H NMR spectra for the same 5% Pt/Al_2O_3 and 5% Pt-5% Re/Al_2O_3 catalyst (previously shown in Figure 14) under an evacuation condition following adsorption under 5 Torr hydrogen. The alumina support in both catalysts was deuterated prior to hydrogen adsorption. Obviously, the hydroxyl proton intensity from alumina support was diminished considerably. Although the resonances were still broadened by the iron impurity, reduction of the hydroxyl proton peak enabled us to observe the hydrogen-on-metal peaks. For the 5% Pt/Al_2O_3 catalyst, an upfield peak at about 20 ppm was barely separated from the hydroxyl peak, corresponding to the strongly adsorbed hydrogen on platinum. For the 5% Pt-5% Re/Al_2O_3 catalyst, only a broad upfield shoulder on the hydroxyl peak could be observed, possibly due to strongly bound hydrogen on the Pt-Re bimetallic surfaces.

Dehydrogenation of Cyclohexane

Catalytic dehydrogenation of cyclohexane over a 5% Pt/SiO_2 catalyst and three 5% Pt-Re/SiO_2 bimetallic catalysts with various rhenium loadings was examined in a tubular flow micro-reactor. The activity for each catalyst was calculated

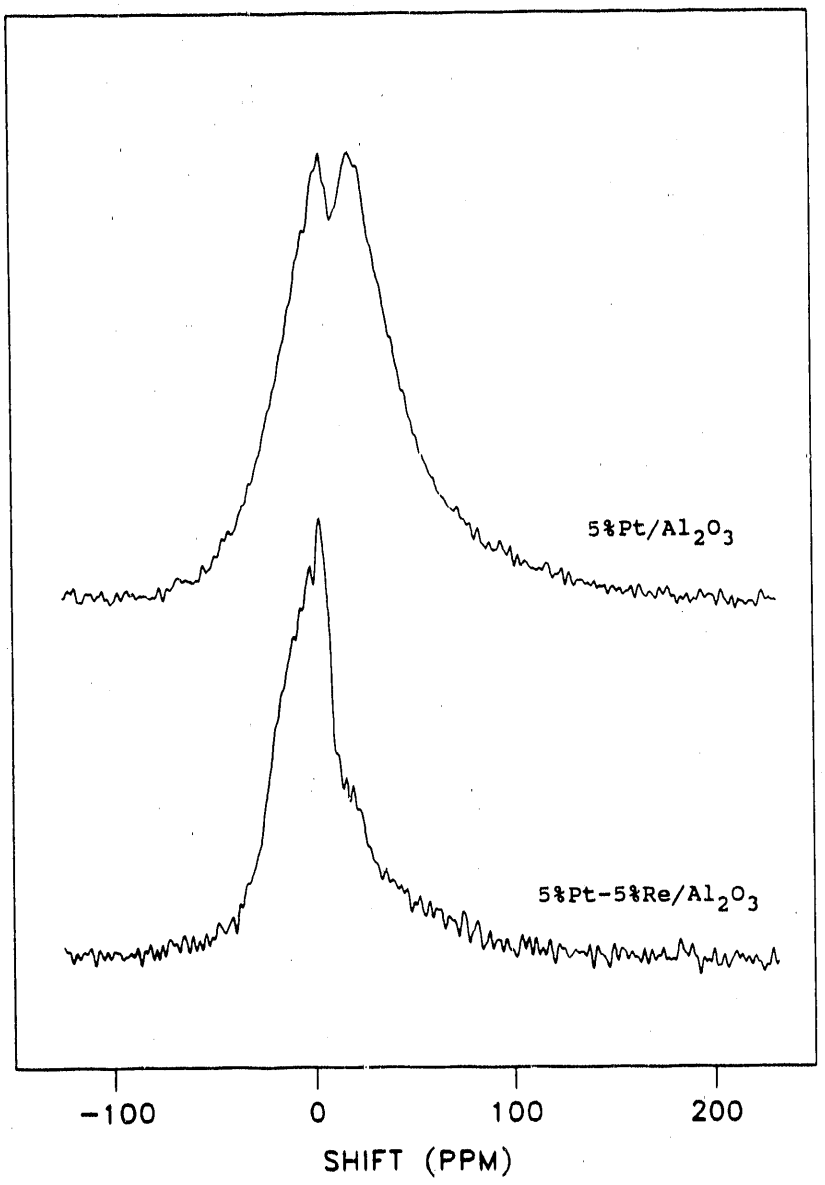

Figure 15. ^{1}H NMR spectra for a 5% Pt/Al_2O_3 and a 5% Pt-5% Re/Al_2O_3 catalyst under an evacuation condition after adsorption under 5 Torr hydrogen. Prior to adsorption, the alumina support in the catalysts were deuterated to reduce the hydroxyl intensity

based on the feed rate, the conversion, and the weight of the catalyst sample in the reactor. Figure 16 shows a plot of activity versus time for a 5% Pt/SiO_2 and a 5% Pt-5% Re/SiO_2 catalyst at a temperature of 300°C. The reaction took place at 1 atm pressure with a molar ratio $C_6H_{12}:H_2$ = 1:9 in the feed stream. The activity was expressed as the number of cyclohexane molecules reacted per bulk platinum atom per second. As clearly shown in the figure, the Pt-Re/SiO_2 bimetallic catalyst was about three times as active as the pure Pt/SiO_2 catalyst. The activity for the two catalysts was very stable and did not change appreciably over a period of six hours. Benzene was the only measurable product for the reaction. A test of the 5% Re/SiO_2 catalyst did not indicate any activity for the cyclohexane dehydrogenation reaction.

The activation energy for each catalyst was measured over a temperature range from 250°C to 300°C. The activity data were fitted by the Arrhenius rate expression

$$k = A \exp(- E_a/RT)$$

where k is the rate constant, A the preexponential factor, and E_a the activation energy. Figure 17 shows the Arrhenius plots for the four catalysts with a natural logarithmic scale for the activity. The activation energy for each catalyst

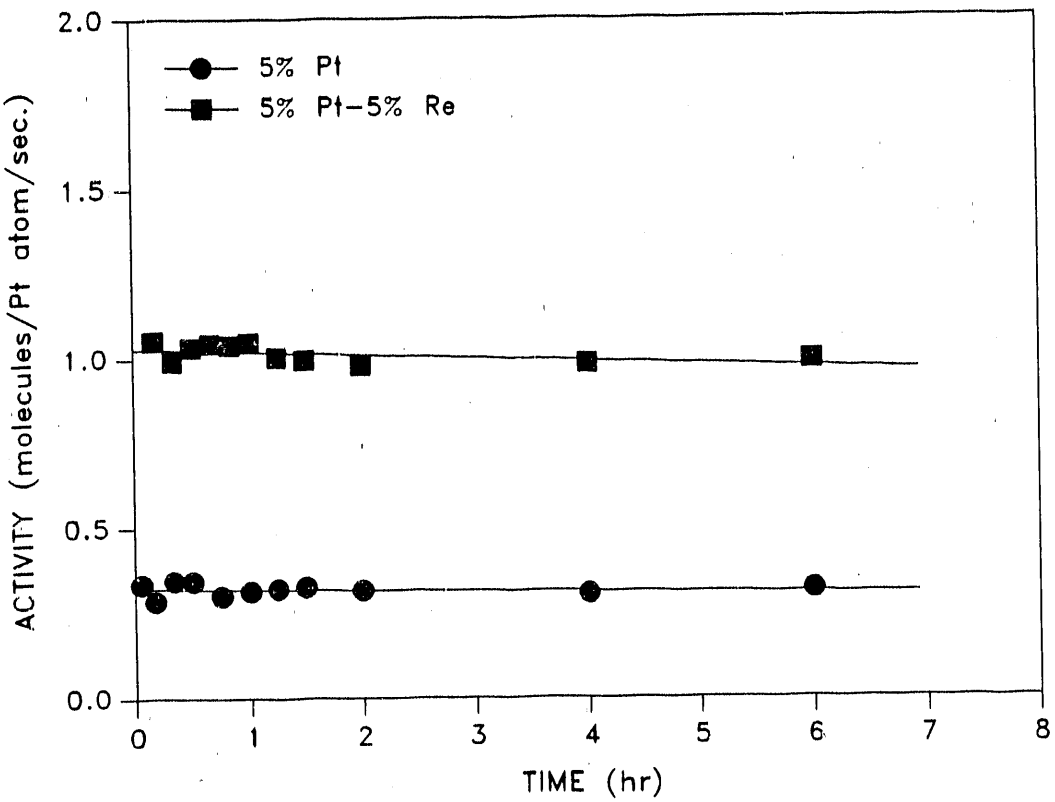

Figure 16. Activity of cyclohexane dehydrogenation reaction as a function of time for a 5% Pt/SiO_2 and a 5% Pt-5% Re/SiO_2 catalyst. The C_6H_{12} : H_2 molar ratio was 1 : 9 and reaction temperature 300°C

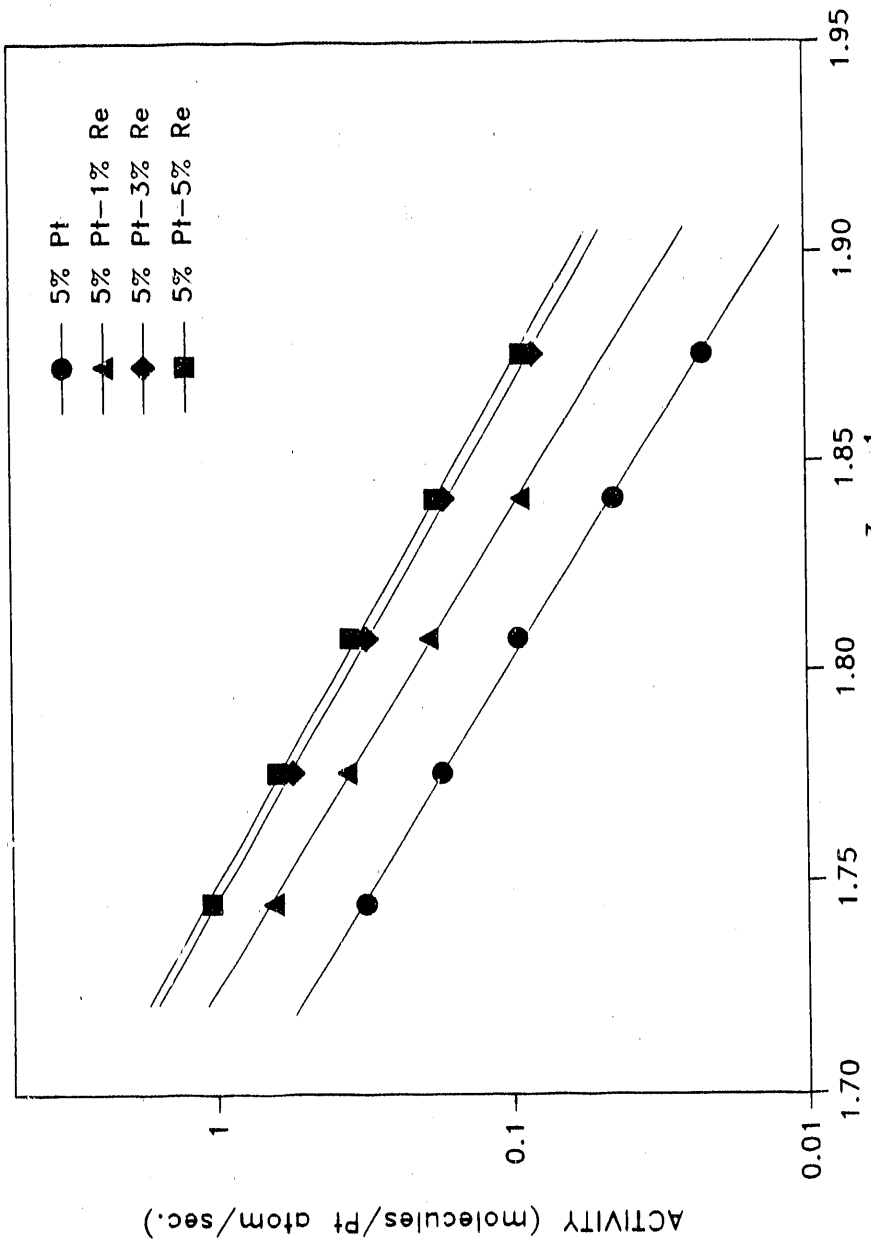

Figure 17. Arrhenius plots of activity versus reciprocal absolute temperature for a 5% Pt/SiO_2 and three 5% Pt-5% Re/SiO_2 catalysts

Table 4. Activity parameters for cyclohexane dehydrogenation on Pt/SiO_2 and $Pt-Re/SiO_2$ catalysts

Catalyst (wt%)	Preexponential factor (molecules/Pt atom/sec.)	Activation energy (kcal/mole)
5% Pt	9.1×10^{14}	40.5 ± 2
5% Pt-1% Re	1.6×10^{15}	40.3 ± 2
5% Pt-3% Re	2.4×10^{14}	37.7 ± 2
5% Pt-5% Re	1.7×10^{14}	37.2 ± 2

was obtained from the slope of the Arrhenius plot and the preexponential factor from the intercept. The data shown in the figure fell very close to a straight line for each of the catalysts and the line from each catalyst was nearly parallel to each other. It is interesting to note that at a given temperature the catalyst activity increased with increasing rhenium loading.

The preexponential factor and the activation energy for each of the four catalysts are listed in Table 4. For these four catalysts, the preexponential factor remained fairly constant between about 10^{14} and 10^{15} molecules per Pt atom per second. Also, the activation energy for each catalyst did not vary significantly and remained between 37 and 41

kcal/mole. However, it appeared that the activation energy decreased slightly with an increase in the rhenium loading. But the maximum difference in the measured activation energy between the 5% Pt/SiO_2 and the 5% Pt-5% Re/SiO_2 was 3.3 kcal/mole, which was still within the estimated experimental error ± 2 kcal/mole. Therefore, it is unclear whether the variation in activation energy is due to experimental errors or the addition of rhenium.

The activity will have a more direct physical meaning when it is expressed in number of molecules per surface site per second, or the turnover frequency. For the Pt/SiO_2 and the $Pt-Re/SiO_2$ catalysts, the turnover frequency was obtained by dividing the activity by the corresponding irreversible H/Pt ratio shown earlier in Table 1. Thus, the number of metal sites that are capable of adsorbing the irreversible hydrogen is used as the measure for the number of catalytic sites. Note that if only surface Pt atoms are active for the cyclohexane dehydrogenation reaction but surface Re atoms in a bimetallic particle are capable of irreversibly adsorbing hydrogen, the number of catalytic sites may be overcounted. The Arrhenius plot for each of the four catalysts is shown in Figure 18 with the activity expressed in turnover frequency in a natural logarithmic scale. Clearly, turnover frequency for cyclohexane dehydrogenation reaction is higher when the catalyst contains more rhenium.

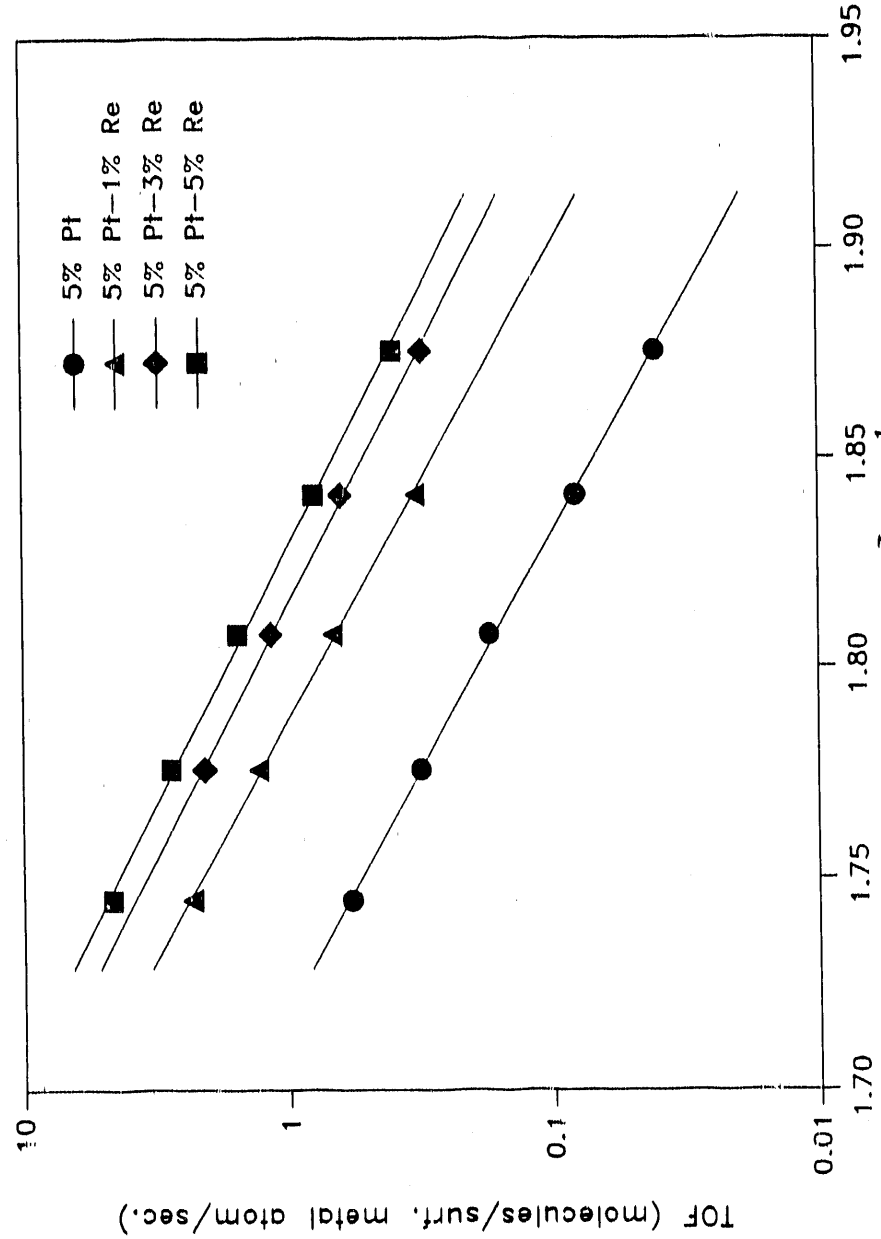

Figure 18. Arrhenius plots of the turnover frequency (TOF) versus reciprocal absolute temperature for one 5% Pt/SiO_2 and three 5% Pt-5% Re/SiO_2 catalysts

NMR of Adsorbed Hydrocarbons

The deuteration process described earlier can reduce the amount of hydroxyl protons significantly and makes possible the direct observation of hydrocarbons adsorbed on a catalyst without strong interference from the silanol proton. All the NMR spectra shown in this section were obtained on deuterated catalyst samples dosed with appropriate amount of cyclohexane or benzene. Since the hydroxyl proton in a silica or alumina support could only be deuterated to a limited extent in the present study, minor interferences from the hydroxyl proton cannot be eliminated completely.

Figure 19 shows a set of ^{1}H NMR spectra taken on a 5% Pt/SiO_2 catalyst dosed with cyclohexane at 670 Torr and room temperature. The sealed sample was heated progressively from 150°C up to 400°C for 15 min at each temperature. A ^{1}H NMR spectrum was obtained after heating at each temperature. At room temperature, only a single sharp peak at 4.5 ppm was observed, corresponding to adsorbed cyclohexane on the catalyst. A second peak at -1.0 ppm began to emerge at 150°C due to conversion of cyclohexane to benzene. This conversion became significant at 250°C and beyond, as indicated by the growth of the benzene peak. At 400°C, a considerable amount of cyclohexane was converted to benzene.

The very same experiment was performed on a 5% Pt-5% Re/SiO_2 catalyst. As shown in Figure 20, the benzene peak

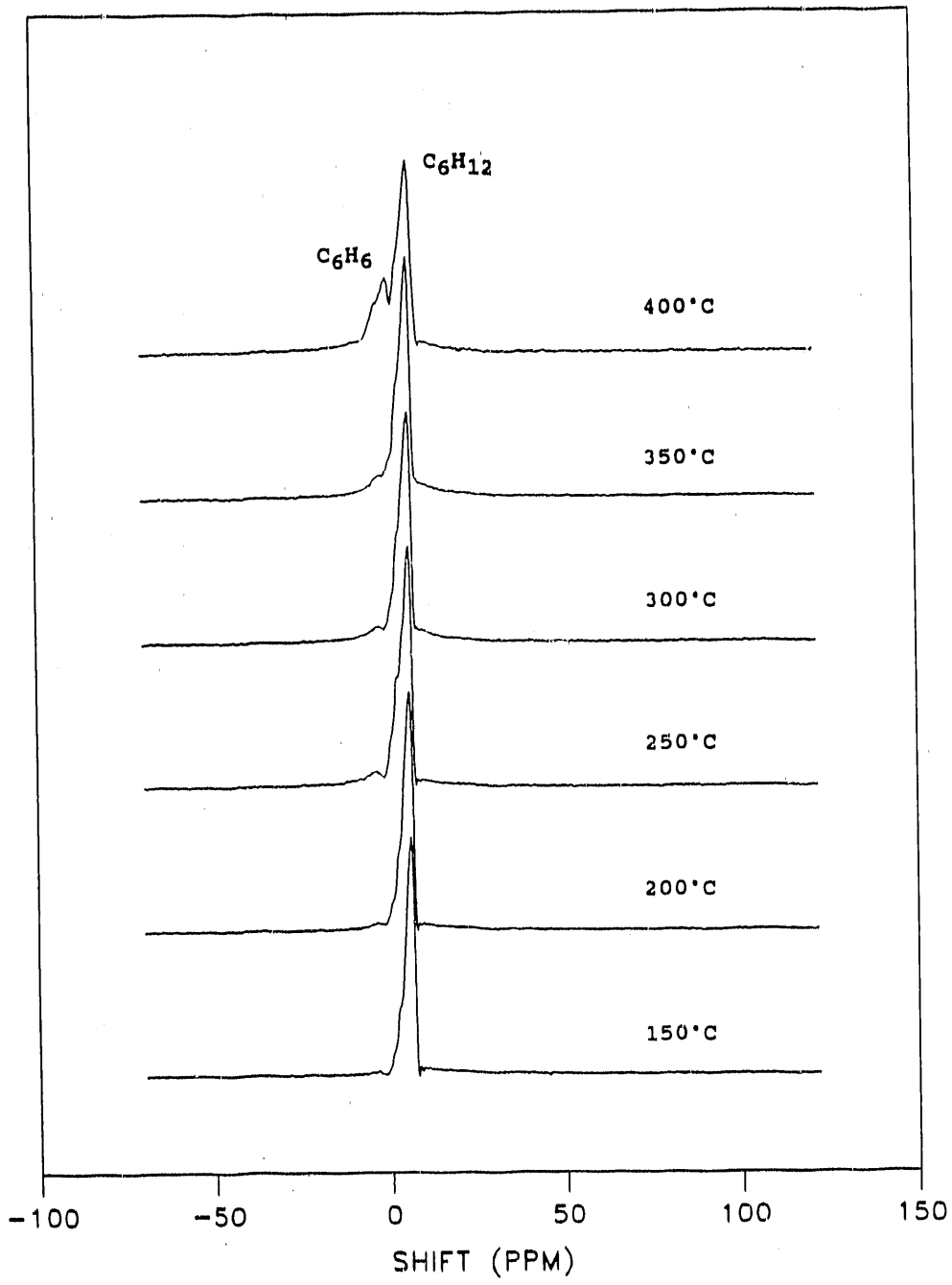

Figure 19. ^1H NMR of cyclohexane adsorbed on a 5% Pt/SiO_2 catalyst showing conversion to benzene when heated at various temperatures for 15 min. The catalyst support was deuterated before dosing with cyclohexane and no gaseous hydrogen was added

exhibited a faster growth with increasing temperature of sample heating on the Pt-Re bimetallic catalyst than on the pure Pt catalyst. Also, the benzene conversion on the Pt-Re bimetallic catalyst was much higher at temperatures beyond 250°C.

The equilibrium conversion from cyclohexane to benzene was calculated from thermodynamic data and the corresponding equilibrium constant. The calculated conversion for this reaction under the experimental conditions is tabulated in Table 5 along with the measured conversion from the ^1H NMR spectra for both the 5% Pt/SiO_2 and the 5% Pt-5% Re/SiO_2 catalyst. At temperatures below 250°C, the experimental values are in good agreement with the calculated values. However, the experimental values for both catalysts were much lower than the calculated ones at temperatures above 250°C. These discrepancies were due to occurrence of the reverse reaction, i.e., benzene hydrogenation at room temperature, during the brief time period after sample heating and before the NMR measurements. This point will be discussed in more detail later.

The same experiment was performed on a 5% Pt/Al_2O_3 and a 5% Pt-5% Re/Al_2O_3 catalyst as well. As shown in Figure 21, both catalysts catalyzed the cyclohexane dehydrogenation at 300°C. On the alumina support, protons in cyclohexane showed a single resonance at 3.6 ppm while protons in benzene showed

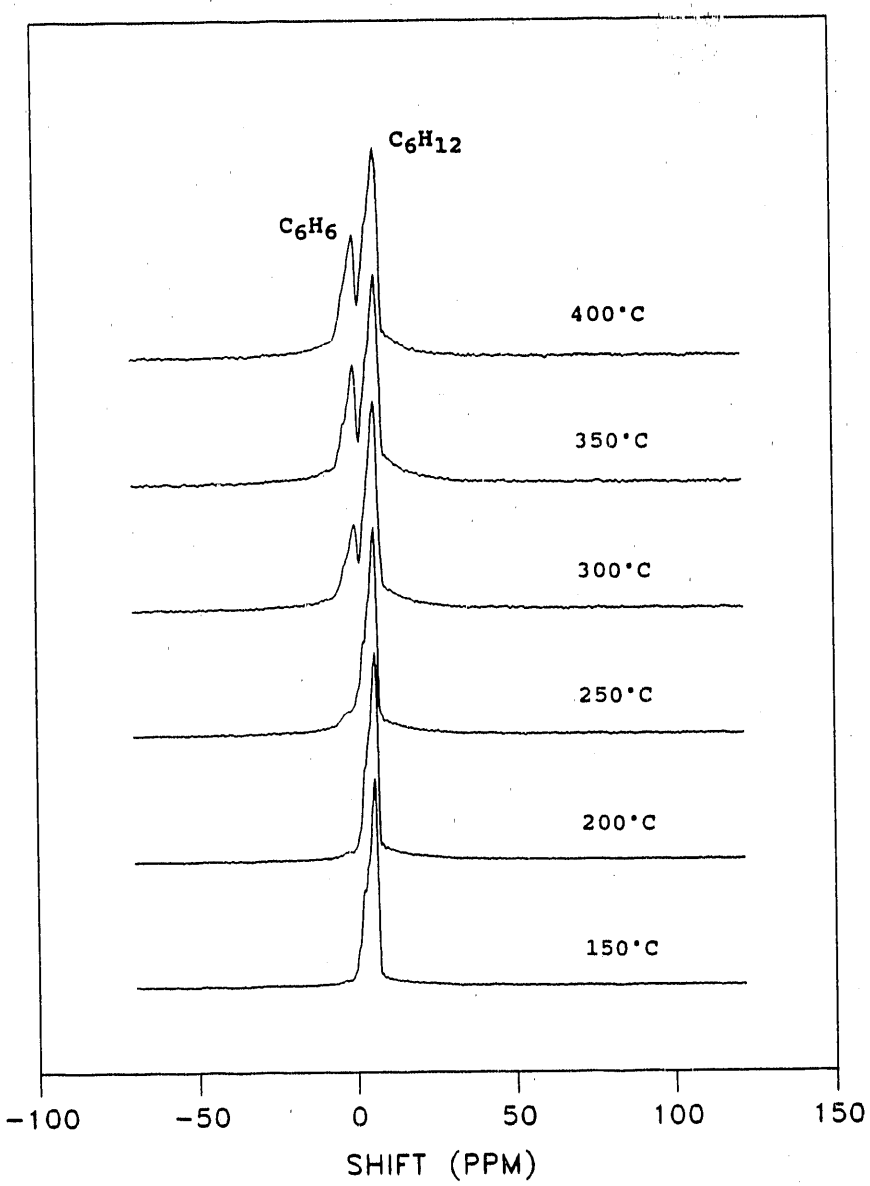

Figure 20. ^1H NMR of cyclohexane adsorbed on a 5% Pt-5% Re/SiO_2 catalyst showing conversion to benzene when heated at various temperatures for 15 min. The catalyst support was deuterated before dosing with cyclohexane and no gaseous hydrogen was added to the sample

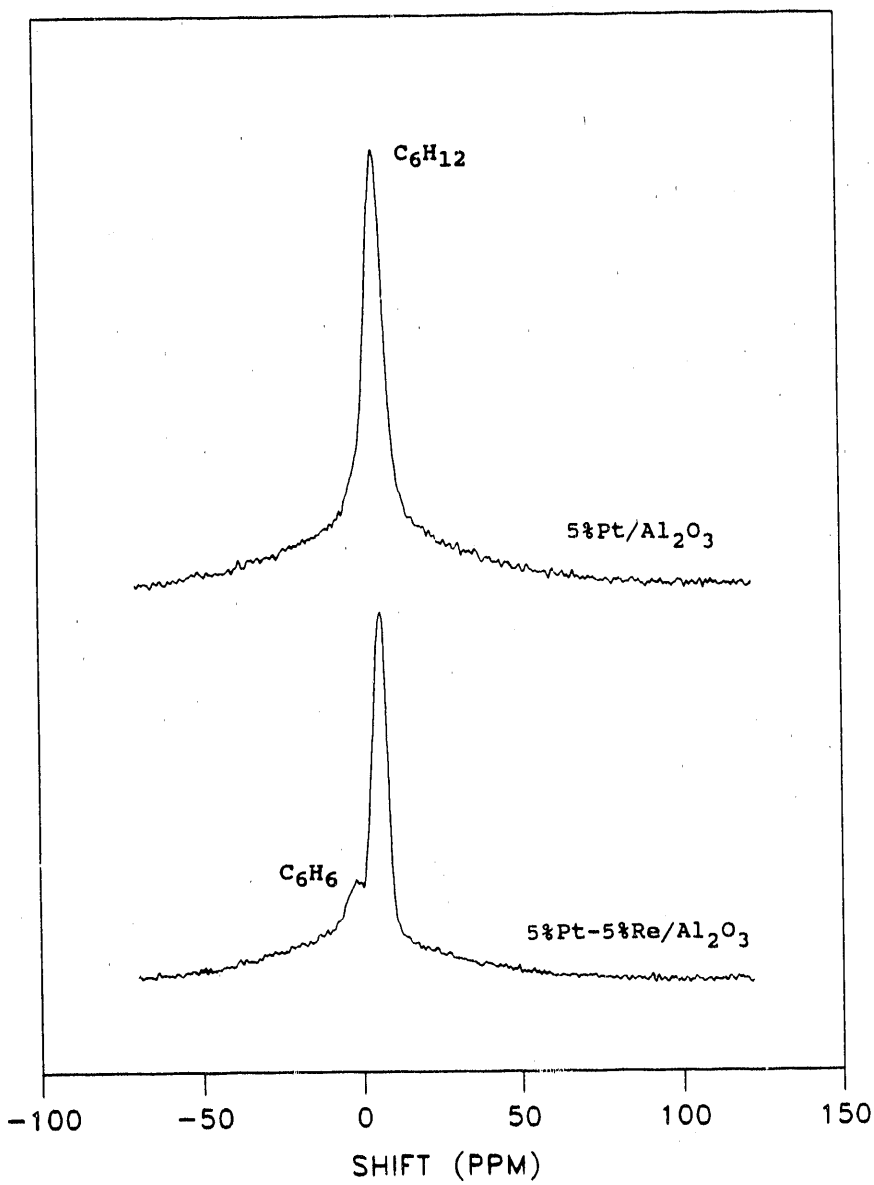

Figure 21. ^1H NMR spectra of cyclohexane adsorbed on a 5% Pt/Al_2O_3 and a 5% Pt-5% Re/Al_2O_3 catalyst showing conversion to benzene when heated at 300°C for 15 min. The catalyst support was deuterated before cyclohexane dosage and no gaseous hydrogen was added to the sample

Table 5. Experimental and theoretical conversion for the reaction of cyclohexane dehydrogenation on a 5% Pt/SiO_2 and a 5% Pt-5% Re/SiO_2 catalyst

Temperature (°C)	Pt/SiO_2 (^1H NMR)	$Pt\text{-}Re/SiO_2$ (^1H NMR)	Equilibrium conversion
150	0.008	0.010	0.007
200	0.024	0.034	0.033
250	0.094	0.110	0.112
300	0.185	0.280	0.296
350	0.213	0.474	0.608
400	0.467	0.526	0.901

one at -2.0 ppm. Conversion of cyclohexane to benzene was more efficient on the $Pt\text{-}Re/Al_2O_3$ catalyst than on the pure Pt/Al_2O_3 catalyst, as indicated by the stronger benzene peak. Note that the broad resonance line under the narrow peaks was from the hydroxyl proton in the alumina support. Due to the presence of iron impurity in the alumina support, the peaks corresponding to the adsorbed cyclohexane and benzene were broader than those observed on silica-supported catalysts. This line broadening caused considerable overlap between the cyclohexane peak and the benzene peak. As the

heating temperature was raised to 350°C, benzene conversion increased for both catalysts, as displayed by the stronger benzene peak in Figure 22. Again, conversion of cyclohexane to benzene was more efficient on the Pt-Re catalyst than on the pure Pt catalyst.

The reverse reaction, i.e., benzene hydrogenation, was also studied by ^{1}H NMR on the 5% Pt/SiO_2 and the 5% Pt-5% Re/SiO_2 catalyst. Initially, benzene and hydrogen gas were dosed onto the catalyst samples and the samples were sealed off and stored in liquid nitrogen for 20 min prior to NMR experiments at room temperature. Unexpectedly, the reaction already proceeded to a considerable extent at liquid nitrogen temperature (-196°C). As shown in Figure 23, some benzene adsorbed on the 5% Pt/SiO_2 catalyst was already converted to cyclohexane after 1 min at room temperature. After 10 min, the reaction seemed to have ceased and the system reached an equilibrium, as indicated by the invariant peak intensities with time. On the 5% Pt-5% Re/SiO_2 catalyst, this process was even faster. As can been seen in Figure 24, the benzene hydrogenation was almost completed at the beginning of the NMR experiment and reached equilibrium shortly afterwards.

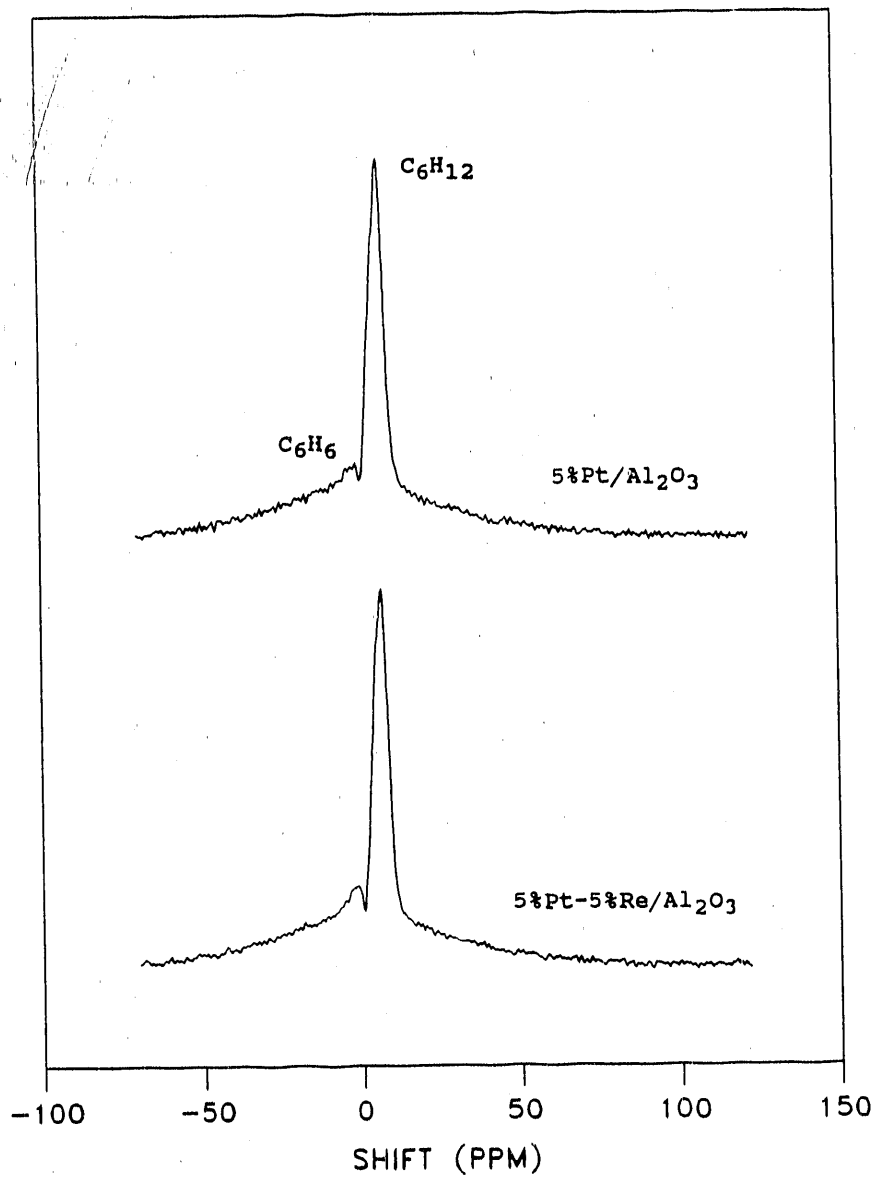

Figure 22. ^1H NMR spectra of cyclohexane adsorbed on a 5% Pt/Al_2O_3 and a 5% Pt-5% Re/Al_2O_3 catalyst showing conversion to benzene when heated at 350°C for 15 min. The catalyst support was deuterated before cyclohexane dosage and no gaseous hydrogen was added to the sample

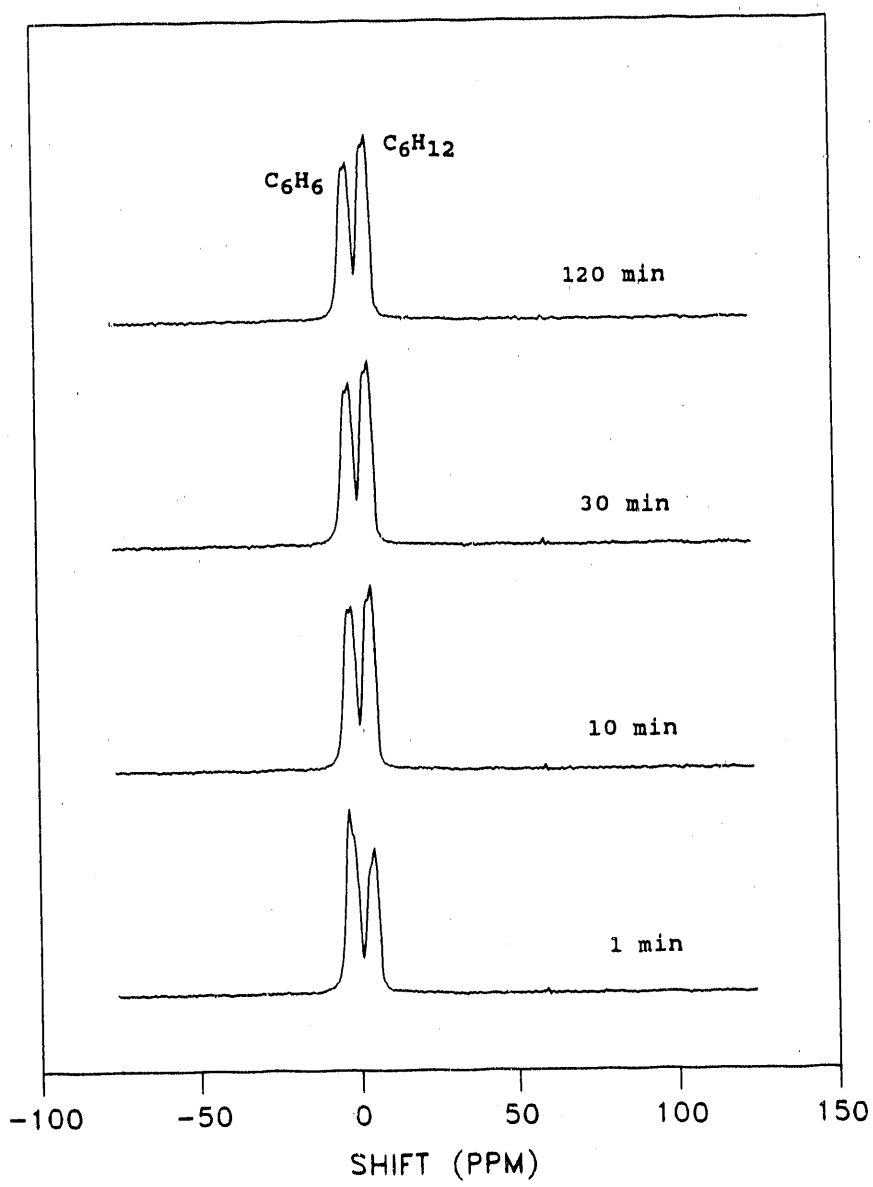

Figure 23. ^1H NMR spectra of benzene and gaseous hydrogen adsorbed on a 5% Pt/SiO_2 catalyst showing the evolution the cyclohexane peak with time at room temperature (296 K). The catalyst support was deuterated and both benzene and hydrogen were dosed and stored in liquid nitrogen prior to the NMR experiment

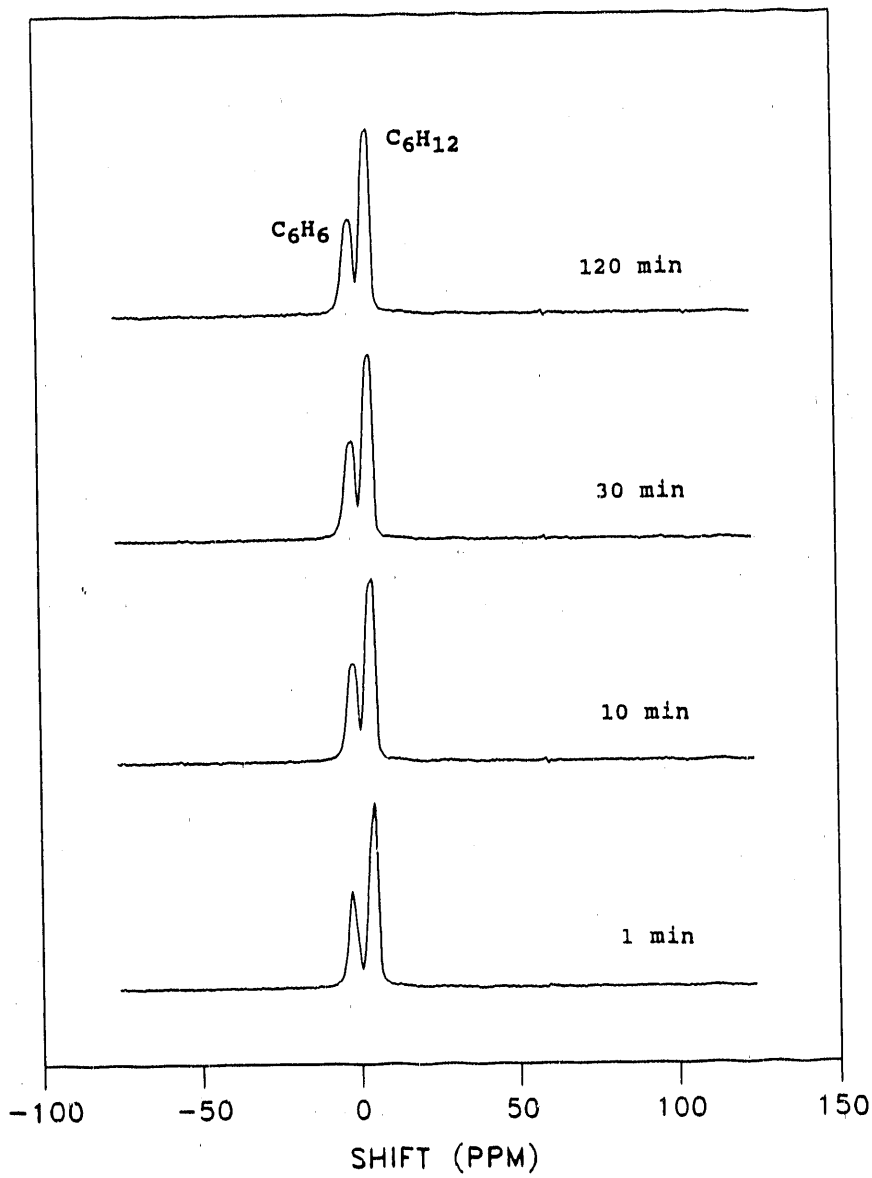

Figure 24. ^1H NMR spectra of benzene and gaseous hydrogen adsorbed on a 5% Pt-5% Re/SiO_2 catalyst showing conversion to cyclohexane at various time at room temperature (296 K). The catalyst support was deuterated and both benzene and hydrogen were dosed and stored in liquid nitrogen prior to the NMR experiment

DISCUSSION

Reducibility of Re and Pt-Re Catalysts

Complete reduction of the precursor compounds NH_4ReO_4 and $HReO_4$ by hydrogen was clearly indicated in Figure 1 by the flat portions of the two TGA curves at temperatures above 230°C and 200°C, respectively. For the NH_4ReO_4 compound, the experimental value of 69.5 wt% from TGA after reduction was in very good agreement with the theoretical value of 69.4% as calculated from the compound stoichiometry. In the case of $HReO_4$, TGA data indicated decomposition of the compound to rhenium dioxide ReO_2 prior to complete reduction to metallic rhenium, as shown by the second stage of weight loss on the TGA curve. Complete dehydration of $HReO_4$ aqueous solution was shown on the TGA curve by the inflection point in the first stage. Obviously, the perrhenic acid is easier to reduce than the pure ammonium perrhenate.

Reduction of the two 5% Re/SiO_2 catalysts was clearly shown by the TGA data in Figures 2 and 3. The weight loss under argon at the low temperature end of the TGA curves is likely due to decomposition of the precursor compounds. When supported on silica, $HReO_4$ seemed to be more difficult to decompose than NH_4ReO_4, as evidenced from the TGA curves. Under a H_2/Ar gas mixture, the extent of reduction can be evaluated from the rapid weight decrease due to reduction,

neglecting the small weight decrease due to dehydroxylation of silica in the narrow temperature range for reduction. The results indicated a complete reduction of NH_4ReO_4 precursor to zero-valent metallic rhenium but only partial reduction of $HReO_4$ to ReO_x with an average rhenium oxidation state of +2.8 as calculated from the percentage of weight loss. One can infer from these results that the more acidic $HReO_4$ precursor interacts much more strongly with the silica support (very likely with the silanol group) than the NH_4ReO_4 compound.

Similar calculations on the 5% Pt/SiO_2 based on the TGA data indicated a complete reduction of the $Pt(NH_3)_4(NO_3)_2$ precursor to metallic platinum. The extent of reduction for the $HReO_4$ compound in the 5% Pt-5% Re/SiO_2 catalyst can also be evaluated if one assumes that the platinum precursor is completely reduced. An average rhenium oxidation state of +0.6 was obtained for the bimetallic catalyst based on the corresponding TGA data shown in Figure 4.

Evidence of a strong precursor-alumina interaction was observed on the 5% Re/Al_2O_3 catalyst in the present study, in agreement with results from previous studies (30-35). As shown in Figure 5, no decomposition of $HReO_4$ in argon was detected until the temperature was raised to about 755°C. At this temperature, the precursor was decomposed to metallic rhenium as computed from the percentage of weight decrease. Note that the weight loss at lower temperatures was due to

dehydroxylation of the alumina support since a Al_2O_3 sample showed the exact same trend. In the presence of hydrogen, rapid weight loss of the catalyst occurred at a much lower temperature (210°C). But reduction at this temperature was incomplete. From the TGA data, an average oxidation state of +2.1 for rhenium was obtained on this catalyst.

On the 5% Pt/Al_2O_3 catalyst, TGA data (see Figure 6) indicated complete reduction of the precursor $Pt(NH_3)_4(NO_3)_2$ to metallic platinum at a temperature of only about 170°C. It is therefore reasonable to assume that Pt is completely reduced in the 5% Pt-5% Re/Al_2O_3 bimetallic catalyst as well. With this assumption, an average oxidation state of +0.7 for rhenium was calculated from the TGA data.

Table 6 lists the values of the oxygen number x in ReO_x and the average oxidation state for all the supported Re and Pt-Re catalysts as calculated from the TGA data. The rhenium oxidation state was computed assuming the oxidation state of -2 for oxygen. With the exception of the 5% Re/SiO_2 catalyst made from NH_4ReO_4, all catalysts listed showed some extent of incomplete reduction with an average oxidation state ranging from +0.1 to +2.8. A much higher oxidation state for rhenium was observed in the monometallic Re catalysts than in the Pt-Re bimetallic catalysts. Also, higher values of Re oxidation state seemed to be correlated with higher atomic percentage of rhenium in the Pt-Re bimetallics. From these results, one

Table 6. Values of rhenium oxidation state calculated from TGA data for Re and Pt-Re catalysts

Catalyst	Re at.%	Oxygen number[a]	Oxidation state[b]
5% Pt-1% Re/SiO_2	17.3	0.07	+0.1
5% Pt-3% Re/SiO_2	38.6	0.76	+1.5
7% Pt-5% Re/SiO_2	42.8	0.25	+0.5
5% Pt-5% Re/SiO_2	51.2	0.32	+0.6
3% Pt-5% Re/SiO_2	63.6	0.97	+1.9
1% Pt-5% Re/SiO_2	84.0	0.56	+1.1
5% Re/SiO_2	100.0	1.38	+2.8
5% Re/SiO_2[c]	100.0	0.00	0.0
5% Pt-1% Re/Al_2O_3	17.3	0.20	+0.4
5% Pt-5% Re/Al_2O_3	51.2	0.35	+0.7
5% Re/Al_2O_3	100.0	1.07	+2.1

[a]The average oxygen number x was calculated assuming that the rhenium precursor was reduced to ReO_x by hydrogen.

[b]The number represents the average oxidation state for rhenium assuming an oxidation state of -2 for oxygen.

[c]The rhenium precursor was NH_4ReO_4. For all the other Re and Pt-Re catalysts, the rhenium precursor was $HReO_4$.

may conclude that platinum assists the reduction of rhenium. This observation agrees with the previous findings of other researchers using the TPR technique (7, 13, 15-18).

The low valence oxidation states for rhenium include 0, +2, +3, and +4. This means that the observed average values for the rhenium oxidation state represents a mixture of Re, ReO, Re_2O_3, and ReO_2 with appropriate amounts. However, since the rhenium dioxide ReO_2 is the most stable oxide among the three, it is most likely that the supported Re and Pt-Re catalysts contain a mixture of Re and ReO_2 after reduction. This is consistent with the results reported by Nacheff et al. (36).

NMR of Chemisorbed Hydrogen

Two states of chemisorbed hydrogen, i.e., strongly and weakly bound hydrogen, were present on the surfaces of metal particles in the Pt/SiO_2 and $Pt-Re/SiO_2$ catalysts as shown by ^1H NMR spectra of these catalysts under different conditions of hydrogen adsorption (see Figures 9-13). Two adsorbed states of hydrogen were also measured by volumetric hydrogen chemisorption. However, the weakly bound hydrogen determined by the volumetric technique should include both the hydrogen weakly adsorbed on the metal(s) and the hydrogen spiltover to the support. The spillover phenomenon in the pure Pt/SiO_2 catalysts has been well documented (19, 40, 75-77). The

spillover hydrogen cannot be observed directly from the ^1H NMR spectra because of its minute quantity and interference from the strong silanol intensity. But its existence may be inferred by measuring the spin-lattice relaxation time T_1 of the silanol proton as a function of hydrogen pressure (70, 77). As a result of spectral interference from the silanol resonance, quantitative measurements on the NMR resonance corresponding to hydrogen adsorbed on the metal(s) could not be obtained with acceptable accuracy. Thus, a comparison of the amount of adsorbed hydrogen measured by ^1H NMR with that measured from volumetric hydrogen chemisorption was not possible in this study.

Although the hydrogen reversibly adsorbed on platinum was obscured by the silanol peak, the weakly bound hydrogen on the Pt-Re/SiO_2 catalysts exhibited considerable downfield shifts away from the silanol resonance (see Figures 9 and 11). Thus, the lineshifts for this downfield resonance could be determined accurately (see Table 3). The assignment of this new downfield peak is still uncertain. It is unlikely that the peak represent hydrogen adsorbed on pure rhenium metal surfaces or on rhenium oxides because metallic rhenium adsorbs very little hydrogen and rhenium oxides are not active for hydrogen adsorption at room temperature (3). The fact that this downfield resonance intensity increases with platinum content indicates that the resonance is mainly

associated with the metallic platinum. But it does not rule out the possibility of a hydrogen species adsorbed on the surfaces of bimetallic Pt-Re particles.

The relatively large values for the downfield resonance compared with normal values for chemical shift suggests that the resonance is caused by a Knight shift interaction between the adsorbed hydrogen and the metal (most likely platinum) conduction electrons. It has been established that Knight shift interactions between the adsorbed hydrogen and noble transition metals gives rise to an upfield proton resonance due to bonding with d valence electrons (77, 78), and that Knight shift interactions with 4s valence electrons results in a far downfield (-93 ppm) proton resonance (79, 80). The observed Knight shift on the Pt-Re bimetallics is between these two extremes. There are two plausible interpretations for the observed downfield Knight shift. First, the adsorbed hydrogen moves rapidly between Pt and Re sites on surfaces of Pt-Re bimetallics and gives rise to a peak intermediate to the resonances due to the two adsorption sites. Secondly, the observed downfield resonance is due to hydrogen adsorbed on surface platinum which is influenced electronically by substrates of rhenium or an anchoring rhenium oxide species, or both.

The fact that the downfield resonance shift moved in the downfield direction with increasing rhenium content and

that no resonance was observed on the downfield side of the NMR spectrum on the Re/SiO_2 catalyst suggested that the second explanation was more reasonable than the first one. Since a majority of rhenium was reduced to the zero-valent state as indicated by the calculated average oxidation state of rhenium from the TGA data, platinum and rhenium are likely to form alloys. The difference in the heat of sublimation for these two elements suggests that platinum will tend to segregate to the alloy surface and platinum-rich surfaces are expected on the Pt-Re bimetallic particles. It is possible that the 5d valence orbitals of rhenium atoms draws electrons from the platinum 5d orbitals and limits the ability for the platinum 5d electrons to chemisorb hydrogen. Thus, the spin polarization effect from either the more restricted platinum 5d electrons or the platinum 6s electrons is responsible for the downfield shift of the weakly bound hydrogen on the Pt-Re bimetallics. Since a small fraction of the rhenium is still in the form of an oxide, as inferred from the TGA data, Pt atoms being anchored by rhenium oxide which is bound to the silica support may coexist with Pt-Re bimetallic particles in the catalysts. This scheme of rhenium oxide as an anchor for platinum has been proposed by Yermakov and Kuznetsov et al. (51). The electronic state of the anchored platinum could be greatly influenced by the rhenium oxide.

Through partial deuteration of the silica support, the

strongly bound hydrogen on Pt and Pt-Re surfaces was clearly observed by ^1H NMR (see Figure 13). The broad line features of the resonance indicate limited mobility of this adsorbed state. It is interesting to note that the strongly adsorbed hydrogen on the Pt-Re bimetallics resonates upfield instead of downfield relative to silanol protons, as seen for the weakly bound hydrogen. However, when compared to the pure Pt catalyst, addition of rhenium to platinum moved the upfield resonance downfield by as much as 14 ppm. Since the values of magnetic susceptibility for Re and ReO_2 are only 1/3 or less of that for Pt with the same sign, and since higher Pt loading has an opposite and less pronounced effect on the upfield peak shift (see Figure 18 in Chapter V), the observed downfield shift of the upfield peak due to the presence of rhenium must be predominantly caused by an electronic effect between Pt and Re atoms, as discussed earlier for the weakly bound hydrogen. In this case, proton Knight shift is still due to the valence d electrons from the metals. This would suggest an intimate alloying between Pt and Re by sharing of the 5d valence electrons.

For the alumina supported catalysts, deuteration allowed detection of the strongly adsorbed hydrogen on Pt and Pt-Re catalysts as well (see Figure 15), although the resonances were broadened by the iron impurity in the catalysts. A downfield shift of the upfield peak appears to exist with

addition of Re to Pt, as in the case with silica support. This also indicates alloying and electronic interaction between Pt and Re when supported on alumina.

Catalytic Activity of Pt-Re Bimetallics

Test results from the reaction study showed that all three Pt-Re/SiO_2 bimetallic catalysts were more active in cyclohexane dehydrogenation than the Pt/SiO_2 monometallic catalyst. The Re/SiO_2 monometallic catalyst was not active for this reaction. For all the catalysts tested, no products resulting from hydrogenolysis was detected by the GC and the selectivity of cyclohexane dehydrogenation to benzene was 100%. For this reaction, both the activity per Pt atom and the turnover frequency increase with increasing Re content at a constant platinum loading of 5% (see Figures 17 and 18). The increases were by a factor between 2 and 8. The increase in activity is perhaps due to a subtle electronic interaction between Pt and Re that decreases the activation energy for the reaction occurring on Pt. Indeed, a small decrease in the activation energy with an increase in the rhenium content was measured for the reaction (see Table 4). In fact, the increase in activity can be accounted for by the difference in activation energy if one assumes the same preexponential factor in the Arrhenius rate expression. Among the four catalysts, the maximum difference in the activation energy

(3.3 kcal/mole) is nontrivial. But an estimated experimental error of ± 2 kcal/mole for each measured value of activation energy brings considerable uncertainty to the measurements. Thus, activation energy measurements alone cannot indicate definitively an electronic effect between the two elements.

The higher activity for cyclohexane dehydrogenation on the Pt-Re/SiO_2 bimetallic catalysts was confirmed by ^1H NMR experiments. The conversion of cyclohexane to benzene was indeed higher on the Pt-Re bimetallics than on the pure Pt catalyst at the same reaction temperature (see Figures 19-22). At high conversions, the conversion values measured by ^1H NMR were considerably lower than values for equilibrium conversion (see Table 5). This was due to the reaction of benzene hydrogenation (the reverse reaction) at ambient temperature prior to the ^1H NMR measurements. In fact, the hydrogenation of benzene in the presence of gaseous hydrogen may have occurred even at liquid nitrogen temperature (see Figures 23 and 24). This reaction is exothermic with a very low activation energy on platinum (8 kcal/mole) and a higher one on Re (11 kcal/mole) (81). The Pt activity for this reaction is about two orders of magnitude higher than the Re activity. The fact that higher conversion of benzene to cyclohexane on the Pt-Re bimetallic catalyst was observed than on the pure Pt catalyst under identical conditions may indicate a lower activation energy on the bimetallics due to

a change of electronic state of surface Pt atoms by Re.

As shown in Figure 16, the activity for both the Pt and the Pt-Re catalyst remained unchanged over a short period of six hours. A better stability for the Pt-Re bimetallics over Pt in the actual reforming process was evidenced over a much longer period of time (1, 2). This improved stability may be due to formation of Pt-Re alloys. With platinum segregated to the surface, the rhenium-rich core in the Pt-Re bimetallic particles may play a role of dispersing and stabilizing the platinum atoms.

Microscopic Reaction Model

A mechanistic model for cyclohexane dehydrogenation to benzene has been proposed by Ruiz-Vizcaya et al. (82). The model was based on all-valence electron self-consistent field calculations of charge distributions on cyclohexane molecules chemisorbed on a platinum surface. A cyclohexane molecule is assumed to approach a six-atom platinum site through one of its hydrogen atoms. During the process, the positive charge on the hydrogen atom increases to a level higher than that in an isolated cyclohexane molecule. With shortening of the bond distance, the trend is gradually reversed and hydrogen acquires a negative charge while the carbon atom bonded to the hydrogen atom becomes positively charged. Ultimately, the C-H bond is weakened and then broken with the resulting

elimination of a hydrogen molecule through association with a neighboring hydrogen atom, leaving the cyclohexene molecule π-bonded to the site. The π-bond is then transformed into a σ-bond and the process of eliminating a hydrogen molecule is repeated, forming a π-bonded cyclohexadiene. Elimination of an additional hydrogen molecule after another π-σ bond shift results in the formation of benzene. This entire process may be represented as follows:

$$A \Longleftrightarrow A\sigma \Longleftrightarrow E\pi \Longleftrightarrow E\sigma \Longleftrightarrow D\pi \Longleftrightarrow D\sigma \Longleftrightarrow B\pi \Longleftrightarrow B$$

Every step in the process is reversible. Thus, the scheme can be adopted to the benzene hydrogenation reaction. The authors also proposed that the $E\pi$-to-$E\sigma$ bond shift is rate determining. Ayo and Susu (69) also developed detailed rate expressions for both the forward and reverse reactions based on this model.

An FT-IR study (83) has presented indirect evidence for the formation of carbon residue on Pt/Al_2O_3 upon adsorption of cyclohexane followed by vacuum heating of the adsorbate. The carbon residue retains the six-membered cyclic structure of the adsorbate. Cyclohexane dehydrogenates on Pt/Al_2O_3 at 300 K to form a π-bonded benzene and a dissociated σ-bonded benzene. While benzene added to a clean Pt surface forms only a π-bonded benzene, benzene added to the Pt catalyst

with ordered carbon residues forms both π- and σ-bonded benzenes. Hydrogen reacts with any of the π- or σ-bonded benzene or the carbon residue to form cyclohexane at 300 K. In addition, the σ-bonded species exchange H from the surface OH groups of the alumina support more readily than does the π-bonded benzene.

Experimental data obtained from the present study were insufficient to either prove or disprove the reaction model. However, both π-bonded and σ-bonded species seem to exist on the platinum surfaces during cyclohexane dehydrogenation, as indicated by IR spectroscopy (83). ^1H NMR of chemisorbed cyclohexane and benzene can yield only limited information on the reactions because of limited resolution for the adsorbed species. Reaction intermediates such as π- and σ-bonded cyclohexene and cyclohexadiene have much lower concentrations on the metal surfaces than the weakly interacting cyclohexane and benzene. Also, the $-CH_2$ and the $=CH-$ proton resonances would appear under the same resonances for protons from the cyclohexane and the benzene molecules, respectively. But ^1H NMR can indicate clearly the relative amounts of cyclohexane and benzene at any point during the reaction.

For the reaction of cyclohexane dehydrogenation, carbon residue formation is likely on the Pt and Pt-Re surfaces. The reaction requires a much higher temperature than benzene hydrogenation. The formation of carbon residue is possibly

due to excessive dehydrogenation of the cyclohexane molecules first in contact with the clean metal surfaces. On the platinum catalyst, the entire surface of platinum particles may be deposited with a carbonaceous layer which serves as a substrate for the reaction. However, on the Pt-Re bimetallic catalysts, bimetallic particles are platinum-rich at the surface, but the surface Pt atoms are electron-deficient due to interaction of the valence 5d electrons with the core rhenium atoms, as shown by NMR of strongly adsorbed hydrogen. Consequently, the Pt-C bonding is relatively weak on the Pt-Re bimetallic surfaces and carbon residue deposition may not be as severe and may cover only a fraction of the surfaces. It is very likely that the hydrocarbons and hydrogen will adsorb and desorb more rapidly on the open surfaces than on a layer of carbon residue. In addition, various σ- and π-bonded reaction intermediates can transfer or exchange very rapidly between the carbonaceous layer and the adjacent open surface on top of the bimetallic particles. The net result is an enhanced reaction rate for both the forward and the reverse reactions with a small decrease in the activation energy.

CONCLUSIONS

Hydrogen treatment at 400°C on both the Re/SiO_2 and the Re/Al_2O_3 catalysts resulted in only partial reduction of the $HReO_4$ precursor compound as indicated by thermogravimetric analysis. The reduced rhenium catalysts consisted of about equal amounts of metallic Re and Re (4+) in oxide form. The Pt/SiO_2 and Pt/Al_2O_3 catalysts were completely reduced by hydrogen. Platinum assists reduction of the $HReO_4$ precursor in both $Pt-Re/SiO_2$ and $Pt-Re/Al_2O_3$ bimetallic catalysts and results in a near complete reduction of the precursor as indicated by low values of the average Re oxidation state calculated from the TGA data. The $HReO_4$ precursor interacts much more strongly with alumina than with silica.

^1H NMR of chemisorbed hydrogen revealed two adsorbed states of hydrogen on both Pt and Pt-Re surfaces: strongly and weakly adsorbed hydrogen. The hydrogen chemisorption capacity was higher on the Pt catalysts than on the Pt-Re bimetallic catalysts. The Re/SiO_2 catalyst adsorbed only minute amount of hydrogen and no hydrogen adsorbed on Re was observed by ^1H NMR. Addition of rhenium to platinum caused a significant downfield shift of both the strongly and weakly bound hydrogen on platinum surfaces. The large NMR shifts clearly indicate an electronic interaction between metallic Pt and Re with alloy formation. Platinum is very likely to segregate to the surfaces of a Pt-Re bimetallic particle or

cluster with most of the rhenium remaining in the core of the bimetallic particle. The surface platinum atoms on the Pt-Re bimetallic particles are more electron-deficient than those on the pure platinum particles.

Results from studies of cyclohexane dehydrogenation in a laboratory reactor and by ^{1}H NMR in an NMR sample tube both indicate that the addition of rhenium to platinum enhances significantly the activity of the reaction. Measurements from the reaction study suggested a small decrease in the activation energy for the reaction with an increase in the Re content. This decrease in activation energy may be caused by rhenium modification of the platinum active sites through electronic interactions, in agreement with the proton NMR observations. ^{1}H NMR also showed that benzene hydrogenation reaction was more active on Pt-Re bimetallic catalysts than on pure Pt catalysts. These enhanced activities for the two reactions may be due to less carbon residue deposition on the platinum-rich bimetallic surfaces as a consequence of the electronic interaction between platinum and rhenium.

ACKNOWLEDGMENT

This work was fully supported by the U. S. Department of Energy, Office of Basic Energy Science, Contract No. W-7405-ENG-82. The support of the Engineering Research Institute of Iowa State University is also acknowledged.

REFERENCES

1. Klucksdahl, H. E., U.S. Patent 3,415,737, December 10, 1968.

2. Jacobson, R. L., Klucksdahl, H. E., Davis, R. W., and McCoy, C. S., in Proceedings 34th Mid-year Mtg. Div. Refin., (American Petroleum Institute, Washington, DC, 1969), pp. 504-521.

3. Johnson, M. F. L., and LeRoy, V. M., J. Catal. 35, 434 (1974).

4. Johnson, M. F. L., J. Catal. 39, 487 (1975).

5. Webb, A. N., J. Catal. 39, 485 (1975).

6. Yao, H. C., and Shelef, M., J. Catal. 44, 392 (1975).

7. Bolivar, C., Charcosset, H., Frety, R., Primet, M., and Tournayan, L., J. Catal. 39, 249 (1975).

8. Bolivar, C., Charcosset, H., Frety, R., Primet, M., and Tournayan, L., J. Catal. 45, 163 (1976).

9. McNicol, B. D., J. Catal. 46, 438 (1977).

10. Peri, J. B., J. Catal. 52, 144 (1978).

11. Charcosset, H., Platinum Met. Rev. 23, 18 (1979).

12. Charcosset, H., Frety, R., Leclercq, G., Mendes, E., Primet, M., and Tournayan, L., J. Catal. 56, 468 (1979).

13. Wagstaff, N, and Prins, R., J. Catal. 59, 434 (1979).

14. Biloen, P., Helle, J. N., Verbeek, H., Dautzenberg, F. M., and Sachtler, W. M. H., J. Catal. 63, 112 (1980).

15. Isaacs, B. H., and Petersen, E. E., J. Catal. 77, 43 (1982).

16. Mieville, R. L., J. Catal. 87, 437 (1984).

17. Malet, P., Munuera, G., and Caballero, A., J. Catal. 115, 567 (1989).

18. Augustine, S. M., and Sachtler, W. M. H., J. Catal. 116, 184 (1989).

19. Barbier, J., Charcosset, H., De Periera, G., and Riviere, J., Appl. Catal. 1, 71 (1981).

20. Eskinazi, V., Appl. Catal. 4, 37 (1982).

21. Isaacs, B. H., and Petersen, E. E., J. Catal. 85, 1 (1984).

22. Isaacs, B. H., and Petersen, E. E., J. Catal. 85, 8 (1984).

23. Yermakov, Yu. I., Kuznetsov, B. N., Ovsyannikova, I. A., Startsev, A. N., Erenburg, S. B., and Sheromov, M. A., React. Kinet. Catal. Lett. 7, 309 (1977).

24. Yermakov, Yu. I., Kuznetsov, B. N., Ovsyannikova, I. A., Startsev, A. N., Erenburg, S. B., and Sheromov, M. A., React. Kinet. Catal. Lett. 8, 377 (1978).

25. Short, D. R., Khalid, S. M., and Katzer, J. R., J. Catal. 72, 288 (1981).

26. Meitzner, G., Via, G. H., Lytle, F. W., and Sinfelt, J. H., J. Chem. Phys. 87, 6354 (1987).

27. Dexpert, H., Lagarde, P., and Bournonville, J. P., J. Mol. Catal. 25, 347 (1984).

28. Bazin, D., Dexpert, H., Lagarde, P., and Bournonville, J. P., J. Catal. 110, 209 (1988).

29. Kirlin, P. S., Strohmeier, B. R., and Gates, B. C., J. Catal. 98, 308 (1986).

30. Olsthoorn, A. A., and Boelhouwer, C., J. Catal. 44, 197 (1976).

31. Shpiro, E. S., Avaev, V. I., Antoshin, G. V., Rayashentseva, M. A., and Minachev, Kh. M., J. Catal. 55, 402 (1978).

32. Kerkhof, F. P. J. M., Moulijn, J. A., and Thomas, R., J. Catal. 56, 279 (1979).

33. Wang, L., and Hall, W. K., J. Catal. 82, 177 (1983).

34. Arnoldy, P., van Oers, E. M., Bruinsma, O. S. L., de Beer, V. H. J., and Moulijn, J. A., J. Catal. 93, 231 (1985).

35. Edreva-Kardjieva, R. M., and Andreev, A. A., J. Catal. 94, 97 (1985).

36. Nacheff, M. S., Kraus, L. S., Ichikawa, M., Hoffman, B. M., Butt, J. B., and Sachtler, W. M. H., J. Catal. 106, 263 (1987).

37. Hansen, M., Constitution of Binary Alloys, 2nd ed. (McGraw-Hill, New York, 1958).

38. Godbey, D. J., and Somorjai, G. A., Surf. Sci. 202, 204 (1988).

39. Kelley, M. J., Freed, R. L., and Swartzfager, D. G., J. Catal. 78, 445 (1982).

40. Dowden, D. A., Haining, I. H. B., Irving, J. D. N., and Whan, D. A., J. Chem. Soc. - Chem. Commun. 18, 631 (1977).

41. Traffano, E. M., and Parera, J. M., Appl. Catal. 28, 193 (1986).

42. Gasser, R. P. H., Morris, G., and Szczepura, Surf. Sci. 36, 494 (1973).

43. Ducros, R., Ehrhardt, J. J., Alnot, M., and Cassuto, A. Surf. Sci. 55, 509 (1976).

44. Freel, J., Prepr. Amer. Chem. Soc. Div. Petrol. Chem. 18, 10 (1973).

45. Godbey, D. J., Garin, F., and Somorjai, G. A., J. Catal. 117, 144 (1989).

46. Betizeau, C., Leclercq, G., and Maurel, R., Bolivar, C. Charcosset, H., Frety, R., and Tournayan, L., J. Catal. 45, 179 (1976).

47. Margitfalvi, J., Hegedus, M., Szabo, S., and Nagy, F., React. Kinet. Catal. Lett. 18, 175 (1981).

48. Augustine, S. M., and Sachtler, W. M. H., J. Phys. Chem. 91, 5953 (1987).

49. Botman, M. J. P., De Vreugd, K., Zandbergen, H. W., De Block, R., and Ponec, V., J. Catal. 116, 467 (1989).

50. Menon, P. G., and Froment, G. F., J. Mol. Catal. 25, 59 (1984).

51. Yermakov, Y. I., and Kuznetsov, B. N., J. Mol. Catal. 9, 13 (1980).

52. Margitfalvi, J., Gobolos, S., Kwaysser, E., Hegedus, M., Nagy, F., and Koltai, L., React. Kinet. Catal. Lett. 24, 315 (1984).

53. Barbier, J., Corro, G., and Zhang, Y., Appl. Catal. 16, 169 (1985).

54. Shum, V. K., Butt, J. B., and Sachtler, W. M. H., J. Catal. 96, 371 (1985).

55. Shum, V. K., Butt, J. B., and Sachtler, W. M. H., J. Catal. 99, 126, (1986).

56. Parera, J. M., Beltramini, J. N., Querini, C. A., Martinelli, E. E., Churin, E. J., Aloe, P. E., and Figoli, N. S., J. Catal. 99, 39 (1986).

57. Augustine, S. M., Alameddin, G. N., and Sachtler, W. M. H., J. Catal. 115, 217 (1989).

58. Pacheco, M. A., and Petersen, E. E., J. Catal. 96, 499 (1985).

59. Pacheco, M. A., and Petersen, E. E., J. Catal. 96, 507 (1985).

60. Verderone, R. J., Pieck, C. L., Sad, M. R., and Parera, J. M., Appl. Catal. 21, 239 (1986).

61. Shum, V. K., Sachtler, W. M. H., and Butt, J. B., Ind. Eng. Chem. Res. 26, 1280 (1987).

62. den Hartog, A. J., Rek, P. J. M., Botman, M. J. P., de Vreugd, C., and Ponec, V., Langmuir 4, 1100 (1988).

63. Malet, P., Munuera, G., and Caballero, A., J. Catal. 115, 567 (1989).

64. Rek, P. J. M., Den Hartog, A. J., and Ponec, V., Appl. Catal. 46, 213 (1989).

65. Sinfelt, J. H., Advan. Chem. Eng. 5, 37 (1964).

66. Figueras, F., Mencier, B., De Mourgues, L., Naccache, C., and Trambouze, Y., J. Catal. 19, 315 (1970).

67. Haro, J., Gomez, R., and Ferreira, J. M., J. Catal. 45, 326 (1976).

68. Guenin, M., Breysse, M., Frety, R., Tifouti, K., Marecot, P., and Barbier, J., J. Catal. 105, 144 (1987).

69. Ayo, D. B., Susu, A. A., Appl. Catal. 40, 1 (1988).

70. Wu, X., Gerstein, B. C., and King, T. S., J. Catal. 118, 238 (1989).

71. Cheung, T. T. P., Worthington, L. E., Murphy, P. D. B., and Gerstein, B. C., J. Magn. Reson. 41, 158 (1980).

72. Fry, C. G., Iwamiya, J. H., Apple, T. M., and Gerstein, B. C., J. Magn. Reson. 63, 214 (1985).

73. Stoll, M. E., "A Fast Recovery, Low Noise Receiver-Amplifier for Pulsed NMR Experiments," SAND80-8797 (Sandia National Laboratory, Livermore, Ca., 1980).

74. Smale, M. W., and King, T. S., J. Catal. 119, 441 (1989).

75. Sermon, P. A., and Bond, G. C., Catal. Rev. 8, 211 (1973).

76. Conner, W. C., Jr., Pajonk, G. M., and Teichner, S. J., in Advances in Catalysis, edited by D. D. Eley, P. W. Selwood, and Paul B. Weisz. (Academic Press, New York, 1986), Vol. 34, pp. 1-79.

77. Sheng, T. C., and Gay, I. D., J. Catal. 71, 119 (1981).

78. Sheng, T. C., and Gay, I. D., J. Catal. 77, 53 (1982).

79. Ito, T., and Kadowaki, T., Japan. J. Appl. Phys. 14, 1673 (1975).

80. Wu, X., Gerstein, B. C., and King, T. S., J. Catal. 121, 271 (1990).

81. Kubicka, H., J. Catal. 12, 233 (1968).

82. Ruiz-Vizcaya, M. E., Novaro, O., Ferreira, J. M., and Gomez, R., J. Catal. 51, 108 (1978).

83. Haaland, D. M., Surf. Sci. 111, 555 (1981).

SUMMARY AND RECOMMENDATIONS

Summary of Work on Ru Monometallic Catalysts

The following conclusions can be drawn from work on clean and chlorine-contaminated Ru/SiO_2 catalysts as detailed in Section I and Section IV:

1. Proton NMR shows two adsorbed states of hydrogen, irreversible and reversible hydrogen, exist on the clean Ru surfaces at room temperature. The irreversibly adsorbed hydrogen is bound more strongly to the Ru surfaces and has less mobility than the reversibly adsorbed hydrogen.

2. Proton NMR and volumetric hydrogen chemisorption measure the same amount of irreversibly adsorbed hydrogen on ruthenium. The irreversible hydrogen adsorption should be used to measure the ruthenium dispersion.

3. The amount of reversibly adsorbed hydrogen measured by volumetric hydrogen chemisorption is larger than that by proton NMR due to hydrogen spillover from Ru to the silica support. The total amount of hydrogen adsorption should not be used to measure the ruthenium dispersion because of errors resulting from the hydrogen spillover.

4. The reversibly adsorbed hydrogen on ruthenium tends to spill over to the silica support and undergoes a slow exchange with the silanol proton at room temperature. The strongly adsorbed hydrogen alone does not spill over to the

silica support.

5. The relative amount of the reversibly bound hydrogen on Ru increases with increasing dispersion due to multiple hydrogen adsorption on the increased number of defect-like Ru sites. The Ru-H chemisorptive bond is stronger on smaller Ru particles.

6. Chlorine inhibits hydrogen chemisorption on Ru and reduces hydrogen spillover from Ru to the silica support by reducing the amount of the reversibly adsorbed hydrogen.

7. Surface chlorine not only physically blocks the Ru sites but also weakens the Ru-H chemisorptive bond via an indirect electronic effect involving the ruthenium valence electrons.

Summary of Work on Ru-Group Ib Bimetallic Catalysts

The following conclusions can be drawn from work on the $Ru-Cu/SiO_2$, $Ru-Ag/SiO_2$, and $Ru-Au/SiO_2$ bimetallic catalysts as presented in detail in Sections II, III, and IV:

1. Adsorbed hydrogen spills over from Ru to adjacent Cu sites at room temperature on Ru-Cu bimetallic particles. The chemisorptive behavior of Cu associated with Ru is modified by Ru via a small electronic perturbation.

2. Both the irreversibly and the reversibly adsorbed hydrogen exist on the Ru-Cu bimetallic surfaces. The former state of hydrogen is bound very strongly to both Ru and Cu

associated with Ru. The reversibly adsorbed hydrogen is free to move on the bimetallic surfaces and exchanges very rapidly between the two adsorption sites.

3. Volumetric measurements of hydrogen chemisorption presents errors in titrating the amount of Ru in the Ru-Cu bimetallic catalysts due to hydrogen spillover from Ru to Cu. The method measures the total number of both Ru and Cu sites instead of only Ru sites.

4. The extent of hydrogen spillover from Ru to the silica support is not affected by the addition of Cu to Ru. The strong hydrogen adsorption instead of the total hydrogen adsorption should be employed to measure the total metal dispersion in the Ru-Cu bimetallic catalysts.

5. Variation in NMR resonance shift of the hydrogen reversibly adsorbed on the Ru-Cu bimetallic surfaces can be used to measure the overall surface composition of the Ru-Cu bimetallic catalysts.

6. At low Cu contents, Cu segregates preferentially to the Ru surfaces covering the surface in a monolayer fashion. At high Cu contents, Cu forms three-dimensional islands on surfaces of Ru particles as well as separate Cu particles.

7. Addition of Ag to Ru decreases hydrogen chemisorption capacity to a greater extent than that of Au. Silver tends to segregate to the Ru surfaces and cover the defect-like Ru sites in the Ru-Ag bimetallic catalysts. Ru and Au do not

associate with each other appreciably in the Ru-Au bimetallic catalysts.

8. Hydrogen does not spill over from Ru to either Ag or Au on the bimetallic Ru-Ag and Ru-Au particles. Addition of Ag to Ru reduces the amount of reversible hydrogen adsorption to a greater extent than that of Au. Consequently, hydrogen spillover from Ru-Ag bimetallics to the silica support is less than that from the Ru-Au bimetallics.

9. Copper has the strongest tendency among the three Group Ib elements to associate with Ru to form bimetallic particles.

10. Chlorine contamination reduces the capacity for hydrogen chemisorption by the Ru-Cu/SiO_2 bimetallic catalysts but does not inhibits spillover of hydrogen from Ru to Cu.

Summary of Work on Pt and Pt-Group Ib Catalysts

The following conclusions can be reached based on the work on Pt/SiO_2 monometallic catalysts and Pt-Cu/SiO_2 and Pt-Ag/SiO_2 bimetallic catalysts as detailed in Section V:

1. Pt/SiO_2 monometallic catalysts and Pt-Cu/SiO_2 and Pt-Ag/SiO_2 bimetallic catalysts can be completely reduced by hydrogen at a temperature of 400°C.

2. Both the irreversibly and reversibly chemisorbed states of hydrogen exist on the platinum surfaces. These two chemisorbed states of hydrogen produce very different NMR

resonance shifts due to variation of electronic environments at the Pt surfaces upon adsorption of these hydrogen species.

3. In the presence of the reversibly adsorbed hydrogen, hydrogen spillover from Pt onto the silica support is very likely. Volumetric measurements of the irreversible hydrogen instead of the total hydrogen adsorption should be used to obtain the Pt dispersion.

4. NMR resonance shifts corresponding to hydrogen bound to Pt surfaces are sensitive to the Pt particle size as well as the state of the adsorbed hydrogen.

5. The hydrogen chemisorption capacity for the Pt-Cu bimetallic catalysts is much more than that for the Pt-Ag bimetallic catalysts at the same atomic percent of Cu or Ag. Hydrogen spillover from Pt to adjacent Cu associated with Pt occurs in the Pt-Cu bimetallics.

6. Silver forms bimetallic particles with platinum and reduces the hydrogen chemisorption capacity of platinum by simple site blocking. The extent of Pt-Ag interaction is dependent of the method of catalyst preparation and the resulting metal dispersion. Less association between Pt and Ag with formation of more separate Pt and Ag particles occurs on catalysts with higher metal dispersion.

7. Hydrogen adsorbed on highly dispersed Pt, Pt-Cu, and Pt-Ag catalysts tends to resonate close to the intense NMR resonance of the silanol proton from the silica support and

its resonance is obscured. However, partial deuteration of this silanol proton reduces its NMR intensity and allows clear detection of the hydrogen strongly adsorbed on Pt and Pt-Cu surfaces.

8. The NMR resonance shift for the irreversibly adsorbed hydrogen on Pt-Cu varies with Cu content. This NMR shift variation can be used to estimate the surface composition of the Pt-Cu bimetallic particles.

9. Both copper and silver segregate very strongly to the surfaces of platinum. The experimental results are in good agreement with results from a Monte Carlo simulation.

Summary of Work on Pt-Re Bimetallic Catalysts

The following conclusions are drawn from the work on both Pt-Re/SiO_2 and Pt-Re/Al_2O_3 bimetallic catalysts as shown in detail in Section VI:

1. Platinum assists the reduction of the precursor Re compound ($HReO_4$). A majority of rhenium is reduced under treatment in hydrogen at 400°C. But a small fraction of the rhenium is only partially reduced and remains in the 4+ oxidation state (very likely in the form of ReO_2).

2. Platinum and rhenium form alloys upon reduction by hydrogen. The Pt-Re bimetallic particles coexists with a small fraction of ReO_2 in the reduced catalysts.

3. The hydrogen chemisorption capacity of platinum is

reduced upon addition of rhenium. Both the irreversibly and reversibly bound hydrogen exist on Pt and Pt-Re catalysts.

4. Deuteration of the supports allows clear observation by proton NMR of the strongly adsorbed hydrogen on both Pt and Pt-Re sites.

5. The addition of rhenium to platinum makes a striking downfield shift of the NMR resonances corresponding to both the reversible and the irreversible hydrogen. The large shift is a clear indication of electronic interaction between platinum and rhenium.

6. Platinum tends to segregate to the surface of rhenium and forms platinum-rich surfaces over rhenium-rich cores. The alloyed rhenium partially draws valence 5d electrons from the surface platinum and causes the surface platinum sites to be electron-deficient.

7. Both the model reaction study and NMR of adsorbed hydrocarbons indicate that the Pt-Re bimetallic catalysts are much more active in cyclohexane dehydrogenation than the Pt catalysts under identical reaction conditions. The activity increases with increasing rhenium content up to about 50 at.% Re. The reverse reaction, i.e., benzene hydrogenation, is also more active on the Pt-Re bimetallic catalysts. The reason for the enhanced activity is likely due to less carbon residue on the electron-deficient Pt-Re bimetallic surfaces.

Summary of Work on Cu and Re Monometallic Catalysts

The following conclusions can be drawn from work on the Cu/SiO_2 catalysts (Sections II and V) and the Re/SiO_2 and Re/Al_2O_3 catalysts (Section VI):

1. Both volumetric hydrogen chemisorption and proton NMR indicate that Cu is capable of adsorbing hydrogen at room temperature. The saturation coverage of hydrogen on Cu is about 20% and does not vary much with Cu dispersion.

2. Two adsorbed states of hydrogen are also found on Cu, i.e., the strongly and the weakly adsorbed hydrogen. In the presence of both adsorbed hydrogen species, the adsorbed hydrogen slowly exchanges with silanol proton in the silica support.

3. The proton NMR shift varies significantly with a change in the Cu dispersion due to varying electronic states at the Cu surfaces.

4. The $HReO_4$ precursor compound can only be partially reduced in hydrogen at 400°C. A mixture of about equal amount of metallic Re and unreduced ReO_2 coexists in the reduced silica- and alumina-supported Re catalysts.

5. The Re catalysts are capable of adsorbing oxygen but adsorb very little hydrogen.

Summary of Work on Applications of Proton NMR

It has been demonstrated throughout this dissertation that proton NMR is a powerful technique in characterization and fundamental investigations of supported monometallic and bimetallic catalysts. The following specific points can be made on the application of proton NMR:

1. Proton NMR can be used to probe various adsorbed states of hydrogen on monometallic and bimetallic surfaces.

2. Proton NMR can be used to probe effectively subtle changes in electronic environments at the surfaces of metal particles due to changes in particle size or structure, the state of adsorbed hydrogen, and the presence of coadsorbate or surface contaminant.

3. Proton NMR can be used to detect and monitor the motional behavior of the adsorbed hydrogen on metal surfaces and the exchange process between the adsorbed hydrogen and the proton from the support.

4. Proton NMR can provide quantitative information about the amount of hydrogen adsorbed directly on the surfaces of metallic particles.

5. Proton NMR can be used to measure surface composition of certain bimetallic systems when both metallic elements adsorb hydrogen with considerably different shifts in the NMR spectra.

6. Proton NMR can also be used to monitor the progress

of chemical reactions occurring on the surfaces of metallic particles.

Recommendations for Future Work

The author would like to make some recommendations on the possible extension of the experimental work presented in this dissertation. The experimental methods used in this work may continue to be applied to some other mono- and bimetallic systems, or they can be improved and applied on the same catalysts.

Considerable attention has been directed to the carbon-metal surface interactions or carbon-carbon bonding on the metallic surfaces in the literature. The role of hydrogen in the process of hydrocarbon conversion has received less attention until recently (12). In the author's opinion, the hydrogen-metal interactions and the C-H formation or cleavage are just as important as the ones for carbon. Some of the catalytic reactions such as ethane hydrogenolysis (4, 13) are strongly dependent of hydrogen pressure. In fact, hydrogen inhibits this reaction to some extent possibly by occupying the Ru sites at the surfaces (4). It is therefore desirable to know the actual hydrogen coverage on metal surfaces under the reaction conditions.

The author has calculated the equilibrium hydrogen coverages on both Ru and Pt bare surfaces as functions of

temperature by extrapolating the kinetic data obtained from single crystal studies (14, 15) to high temperatures and pressures (see Appendix). The calculations can be repeated on any metal surfaces provided that sufficient kinetic data are available.

It is possible to perform high-temperature proton NMR experiments with a suitable device to measure the actual hydrogen coverages on Ru/SiO_2 and Pt/SiO_2 catalysts and make comparison of the results with the calculated ones. Clearly, the advantage of high-temperature proton NMR will be a much narrower resonance for the adsorbed hydrogen on the metal surfaces due to increased motion of the adsorbed hydrogen. But a poorer signal-to-noise ratio is expected due to the decreased Boltzmann factor. In addition, a much faster hydrogen exchange between the adsorbed hydrogen and the silanol proton will take place and may influence the observed proton NMR spectrum. If the experiments are successful, new kinetic and thermodynamic data may be extracted from the NMR observations.

The high-temperature proton NMR experiments may also be carried out on the bimetallic catalysts such as $Pt\text{-}Rh/SiO_2$ or $Pt\text{-}Ru/SiO_2$, where the proton resonances for the chemisorbed hydrogen are relatively far away from the silanol resonance and the proton resonances on the two metals are reasonably far apart. High temperatures will facilitate fast exchange

between the two adsorption sites and a single resonance is expected to be observed. One should be able to obtain the surface composition on these bimetallic catalysts from the NMR lineshift variations.

Additional work on the supported Re catalysts is needed to better understand chemisorptive and catalytic properties of these catalysts. The catalysts can be completely reduced possibly at a higher reduction temperature (e.g., 600°C). The adsorption of hydrogen on Re may be very similar to that on Cu with a low saturation coverage. It will be interesting to find out where the hydrogen adsorbed on Re will resonate on a highly dispersed Re catalyst. The reduction temperature for the supported Pt-Re bimetallic catalysts can also be raised to 500°C to achieve a more complete reduction of ReO_x.

Reaction studies employing benzene hydrogenation can be carried out on the same supported Pt and Pt-Re catalysts to better understand the catalytic properties of these metal catalysts. In order to verify whether carbon residue has less tendency to deposit on the Pt-Re bimetallic surfaces than on the Pt surfaces, NMR of adsorbed hydrogen may be used to probe the open metal surfaces on the Pt-Re bimetallic catalysts already used for the hydrogenation of benzene. Of course, ^{13}C NMR can also be used to observe directly the carbon residue in this case.

It is highly possible that extensive deuteration of the

silica and alumina support will completely eliminate the OH group resonance from the proton NMR spectra. This should open up the possibilities for numerous experiments previously not possible. Many conceivable experiments can be performed to observe adsorbed hydrogen or hydrocarbons on completely deuterated supported mono- and bimetallic catalysts.

ADDITIONAL LITERATURE CITED

1. Sinfelt, J. H., Bimetallic Catalysts - Discoveries, Concepts, and Applications (Wiley, New YorK, 1983).

2. Carter, J. L., McVicker, G. B., Weissman, W., Kmak, W. S., and Sinfelt, J. H., Appl. Catal. 3, 327 (1982).

3. Hansen, M., Constitution of Binary Alloys, 2nd ed. (McGraw-Hill, New York, 1958).

4. Smale, M. W., Ph.D. dissertation. Iowa State University, 1989.

5. Wu, X., Gerstein, B. C., and King, T. S., J. Catal. 121, 271 (1990).

6. Anderson, J. R., Structure of Metallic Catalysts (Academic Press, New York/London, 1975).

7. Delgass, W. N., Haller, G. L., Kellerman, R., and Lunsford, J. H., Spectroscopy in Heterogeneous Catalysis (Academic Press, New York/London, 1979).

8. Gerstein, B. C., and Dybowski, C., Transient Techniques in NMR of Solids (Academic Press, New York/London, 1985).

9. Slichter, C. P., Principles of Magnetic Resonance, 2nd ed. (Springer, New York, 1982).

10. Duncan, T. M., and Dybowski, C., Surf. Sci. Rep. 1, 157 (1981).

11. Slichter, C. P., Ann. Rev. Phys. Chem. 37, 25 (1986).

12. Paal Z., and Menon, P. G., Hydrogen Effects in Catalysis - Fundamentals and Practical Applications (Marcel Dekker, New York, 1988).

13. Boudart, M., and Djega-Mariadassou, G., Kinetics of Heterogeneous Catalytic Reactions (Princeton University Press, Princeton, New Jersey, 1984).

14. Feulner, P., and Menzel, D., Surf. Sci. 154, 465 (1985).

15. Christmann, K., Ertl, G., and Pignet, T., Surf. Sci. 54, 365 (1976).

16. McCabe, R. W., and Schmidt, L. D., Surf. Sci. 65, 189 (1977).

ACKNOWLEDGMENTS

I would like to express my gratitude and appreciation to Professor Terry S. King for his encouragement, suggestions, and stimulating discussions throughout this project. I would also like to thank Professor Bernard C. Gerstein for making valuable comments and sharing his knowledge and expertise in solid state NMR. Without their proper guidance, the success of this project would not have been possible. My thanks are also due to Dr. Po-Jen Chu for his helpful suggestions in NMR experiments in the early stage of this project.

This work was performed at Ames Laboratory under contract no. W-7405-ENG-82 with the U. S. Department of Energy. The United States government has assigned the DOE Report number IS-T 1441 to this dissertation.

APPENDIX

Equilibrium Hydrogen Coverage

The hydrogen adsorption-desorption equilibrium process on a noble metal surface can be expressed as follows:

$$H_2 + * * \longleftrightarrows H\text{-}* \; *\text{-}H$$

where the adsorption is a dissociative process.

The adsorption rate v_a is proportional to the collision rate of hydrogen molecules on the metal surface v_c

$$v_a = s(\theta)\, v_c \tag{1}$$

where $s(\theta)$ is the sticking coefficient for hydrogen the value of which depends on the hydrogen coverage θ. According to the gas kinetic theory (13), the rate of collision is given by

$$v_c = n \left(\frac{k\,T}{2\pi m}\right)^{1/2} = n \left(\frac{R\,T}{2\pi M}\right)^{1/2} \tag{2}$$

where T is the absolute temperature, R the gas constant, and M the molar mass. The number density of gas molecules n can be expressed in terms of pressure and temperature by the ideal gas law as

$$n = \frac{P\ N_o}{R\ T} \tag{3}$$

where N_o is the Avogadro constant.

The rate for the second-order desorption of hydrogen v_d can be written as

$$v_d = -\frac{d\sigma}{dt} = k_d\ \sigma^2 = k_d\ L^2\ \theta^2 \tag{4}$$

where σ is the surface density for adsorbed hydrogen atoms, L the surface density of metal adsorption sites, and k_d the rate constant for desorption. The desorption rate constant is given by the Arrhenius rate expression:

$$k_d = A_d\ \exp(-\ E_d/RT) \tag{5}$$

where E_d is the activation energy for desorption and A_d is the corresponding preexponential factor.

At equilibrium, the rate of adsorption equals the rate of desorption and the final combined expression is

$$N_o P s(\theta)/(2\pi MRT)^{1/2} = A_d \exp(-\ E_d/RT) L^2 \theta^2 \tag{6}$$

The hydrogen coverage is an implicit function of pressure and

temperature. One can easily make numerical calculations for the hydrogen coverage from Equation (6) at any given pressure and temperature provided that the kinetic data on $s(\theta)$, A_d, and E_d are known. Note that A_d and E_d may also depend on the hydrogen coverage.

Figure 1 presents the results of numerical calculations of hydrogen coverage on the Ru(0001) single crystal surface versus temperature at various hydrogen pressures. Kinetic data for the adsorbed hydrogen on Ru(0001) were obtained from the work by Feulner and Menzel (14).

Figure 2 shows the similar calculated isobars on the Pt(111) single crystal surface. Kinetic data for hydrogen on Pt(111) were based on the work by Christmann et al. (15) and that by McCabe and Schmidt (16).

Since reliable kinetic data on surfaces of clean, small metal particles are not available in the literature, data from single crystal surfaces must suffice for the purpose of estimation on supported metal catalysts. The structure and even the size of a metal particle may have an influence on the kinetic parameters for both adsorption and desorption of hydrogen, especially when a metal particle contains as few as tens to hundreds of metal atoms. Proton NMR performed on supported metal catalysts at various temperature will provide direct quantitative measurements for hydrogen coverages at much higher pressures than those for single crystal studies.

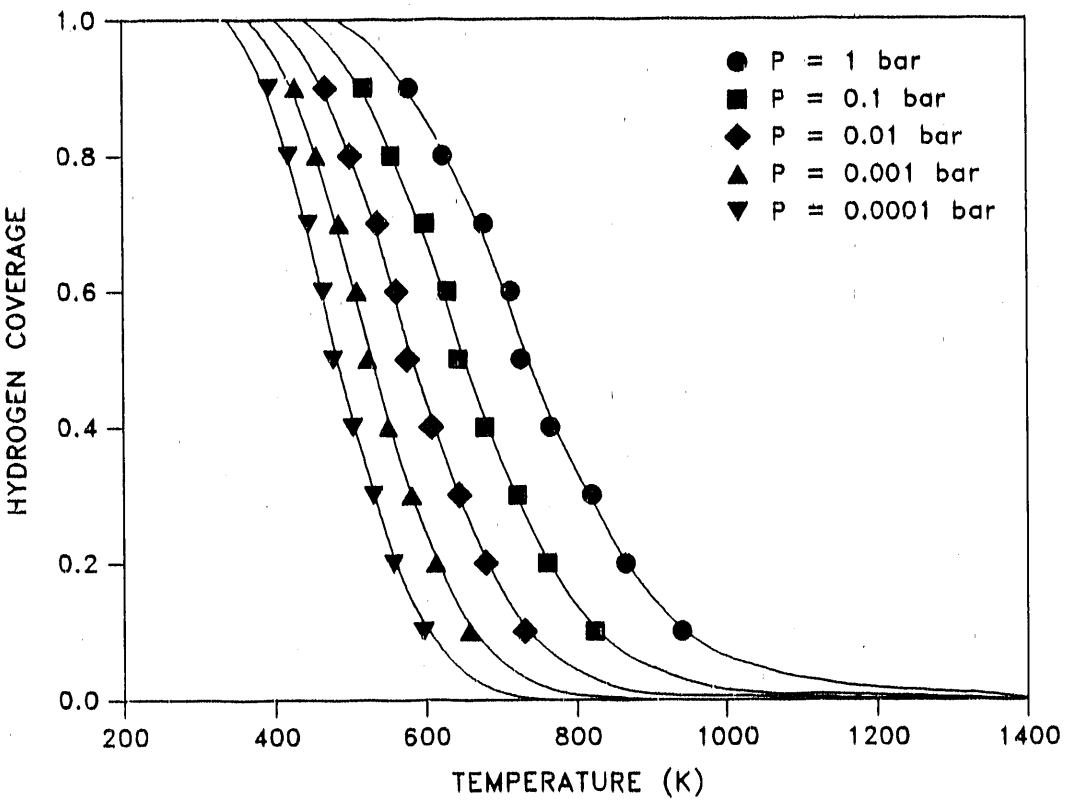

Figure 1. Plots of equilibrium hydrogen coverage versus temperature at various hydrogen pressures on a Ru surface. The calculated values were based on data from single crystal Ru(0001).

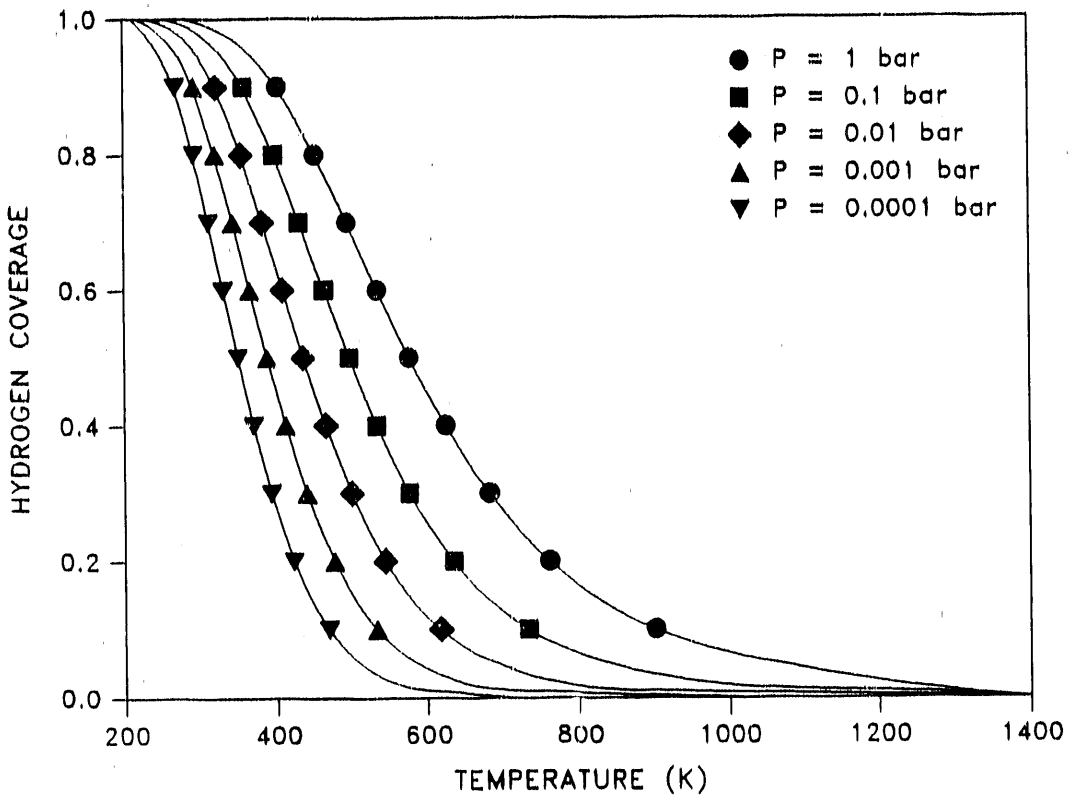

Figure 2. Plots of equilibrium hydrogen coverage versus temperature at various hydrogen pressures on a Pt surface. The calculated values were based on data from single crystal Pt(111).

The proton NMR measurements may produce average kinetic parameters for a supported metal catalyst by fitting the NMR data with Equation (6).

The true significance of plots such as those shown in Figures 1 and 2 is to reveal the exact role of chemisorbed hydrogen on metal surfaces during a catalytic reaction. As can be seen in the figures, rapid drops of hydrogen coverage occur in a range of temperature typically used in various reactions. It is highly possible that hydrogen will compete or even block the metal surface sites during a reaction when the bonding of the reactant molecules with the metal is less favorable than with hydrogen.

END

DATE FILMED

11 / 15 / 90